RESERVOIR CHARACTERIZATION AND MODELLING OF
POTASH MINE INJECTION WELLS IN SASKATCHEWAN

A Thesis Submitted to the
College of Graduate and Postdoctoral Studies
In Partial Fulfillment of the Requirements
For the Degree of Master of Science
In the Department of Civil, Geological and Environmental Engineering
University of Saskatchewan
Saskatoon

By

DAVID PHILLIPS

PERMISSION TO USE

In presenting this thesis/dissertation in partial fulfillment of the requirements for a Postgraduate degree from the University of Saskatchewan, I agree that the Libraries of this University may make it freely available for inspection. I further agree that permission for copying of this thesis/dissertation in any manner, in whole or in part, for scholarly purposes may be granted by the professor or professors who supervised my thesis/dissertation work or, in their absence, by the Head of the Department or the Dean of the College in which my thesis work was done. It is understood that any copying or publication or use of this thesis/dissertation or parts thereof for financial gain shall not be allowed without my written permission. It is also understood that due recognition shall be given to me and to the University of Saskatchewan in any scholarly use which may be made of any material in my thesis/dissertation.

Requests for permission to copy or to make other uses of materials in this thesis/dissertation in whole or part should be addressed to:

> Head of the Department of Civil, Geological and Environmental Engineering
> University of Saskatchewan
> 57 Campus Drive,
> Saskatoon, Saskatchewan, S7N 5A9, Canada
>
> OR
>
> Dean
> College of Graduate and Postdoctoral Studies
> University of Saskatchewan
> 116 Thorvaldson Building, 110 Science Place
> Saskatoon, Saskatchewan, S7N 5C9, Canada

ABSTRACT

In the Saskatchewan potash mining industry vast quantities of brine wastewater are generated from potash processing and mine inflow water. As treatment of such waste is prohibitively expensive, disposal in deep saline aquifers is the only readily available option. However, the effects that such injection activities have on the subsurface conditions of the targeted aquifers are not well known. Additionally, the reservoir characteristics of the targeted aquifers are not well understood. The aim of my dissertation is to provide a large scale reservoir characterization study to the aquifers used for subsurface waste disposal at the potash mines in Saskatchewan, the basal clastics and the Interlake Group. The second aim of this research is to use the data from the reservoir characterization study to build analytical models of the injection wells in order to study the effects that such injection activities have had on the targeted aquifers.

Characterizing deep aquifers such as the basal clastics and the Interlake Group is often difficult due to limited subsurface information available at great depths. In this investigation, available information from oil and gas exploration and development, such as geophysical logs, drill stem tests and core analysis provided valuable information on the subsurface distribution and rock characteristics (permeability) of these formations. This information allowed for a better understanding of the factors that have led to the success of injection activities at the potash mine sites and will assist future projects targeting fluid injection in the basal clastics and the Interlake Group. Through this analysis, it was found that there are great differences in the permeabilities both spatially and with respect to lithology in these aquifers, with permeability values in the Winnipeg Formation between $10^{-18.1}$-$10^{-11.8}$ m^2 and $10^{-15.9}$-$10^{-11.6}$ m^2 in the Deadwood Formation and $10^{-16.0}$-$10^{-11.5}$ in the Interlake Group obtained from the various methods of analysis. Through the information gained through the reservoir characterization study, analytical models were generated in Aqtesolv (HydroSOLVE Inc. 2016) in order to simulate the reservoir response to the injection activities. History-matching was conducted in order to generate models with simulation outputs that most closely matched the falloff test pressure data. The calibrated history-matched models were able to provide insights into the pressure response as well as the extent of the pressure propagations in the aquifers. It was found some of the potash mine sites have generated significantly higher pressure responses than others and that the injection rates and aquifer permeability played a significant role in the pressure response at each mine site.

ACKKNOWLEDGMENTS

TABLE OF CONTENTS

LIST OF TABLES

LIST OF FIGURES

LIST OF ABBREVIATIONS

<u>Nomenclature</u>

TVD= True Vertical Depth (m)
<u>Drill Stem Tests/ Falloff Tests</u>
T= Flowing time (DST) (min)
ΔT= Shut in time (min)

$TB_{Aquifer}$= Aquifer Transmissibility ($\frac{m^4*s}{kg}$)

T_P=Injection Time (s) (Falloff test)

q= Flow rate ($\frac{m^3}{s}$)

m= slope ($\frac{Pa}{cycle}$) (DST/Falloff test)

k=permeability (m^2)

μ= Formation fluid viscosity (Pa*s)

h= Net aquifer thickness (m)

B= Formation Volume Factor ($\frac{rcm}{stcm}$)

RI=Radius of Investigation (m) (DST/Falloff test)

ϕ =Porosity (fraction)

C_{bulk}=Bulk Compressibility (Pa^{-1})

P_s=Static formation pressure (kPa)

ΔT_e=Agarwal time function

V_{rec}=Volume Recovered (m^3) (DST)
<u>McKinley DST Analysis</u>

F= F Factor ($\frac{ft^3}{psi}$)

q=Flow rate ($\frac{bbl}{day}$)

C= Correction factor (dimensionless)

$T_{Aquifer}$=Aquifer Transmissibility ($\frac{mD*ft}{cp}$)

ΔP= Change in pressure during shut in period (psi)

Skin Factor for DSTs
s=skin factor (dimensionless)
p_i=Initial Static Reservoir Pressure (psi)
p_{wf}= Bottom Hole Flowing Pressure (psi)
t= Flowing Time (min)
μ=Viscosity (cp)
r_w=Wellbore Radius (ft)
Skin Factor of a Falloff Test (EPA 2002)
P_{1hr}=Pressure intercept along semi-log straight line at shut in time of 1 hr (psi)
P_{wf}=Injection Pressure Prior to Shut In (psi)
μ= Formation fluid viscosity at Reservoir Conditions (cp)
m=Slope of Semi-log Straight Line ($\frac{psi}{cycle}$)
k=Permeability (mD)
c_{bulk}=Bulk Compressibility (psi^{-1})
t_p=Injection Time (hrs)
r_w=Wellbore Radius (ft)
Formation Compressibility
c_{Pore}=Pore Volume Compressibility (Pa^{-1})
c_{solid}=Solid (Rock) Compressibility (Pa^{-1})
V_d=Poisson's ratio (dimensionless)
Δt_c=Compressional wave transit time (μs/m)
Δt_s=Shear wave transit time (μs/m)
E_d=Dynamic Young's modulus (Pa)
ρ_b=Bulk formation density (kg/m^3)
E_S=Static Young's Modulus (Pa)
K=Bulk modulus (Pa)
c_{bulk}=Bulk compressibility (Pa^{-1})= C_f=Formation compressibility (Pa^{-1})
Formation Volume Factor

B_W= Formation volume factor of water $(\frac{rcm}{stcm})$

Gas Formation Volume Factor

B_g= Formation volume factor of gas $(\frac{rcm}{stcm})$

Z=Gas compressibility factor

P_{Res}=Reservoir Pressure (kPa)

P_{PR}=Pseudo-Reduced Pressure

P_{CRIT}=Critical Pressure (kPa)

T_{PR}=Pseudo-Reduced Temperature

T_{RES}=Reservoir Temperature (°K)

T_{CRIT}=Critical Temperature (°K)

γ_g=Gas Gravity

Oil Formation Volume Factor

R_S=Solution gas ratio $(\frac{scf}{STB})$

T=Reservoir Temperature (°F)

γ_g=Gas specific gravity

API=Oil Gravity (API)

γ_{gp} =Gas Gravity Obtained at Separator Conditions

p= Separator Pressure (assumed standard conditions (14.504 psi)

T= Separator Temperature (assumed standard conditions 77°F)

C_o=Oil compressibility (psi^{-1})

T=Reservoir Temperature (°F)

 API= Oil Gravity (API)

γ_{gs}=Gas Specific Gravity at Reference Conditions (100psi)

B_O=Oil Formation Volume Factor below bubble point pressure (RB/STB)

B_{OB}= Oil Formation Volume Factor at Bubble Point Pressure (RB/STB)

p=Reservoir Pressure (psi)

p_b=Bubble Point Pressure (psi)

Density of Formation Water
ρ_w=Formation Water Density (kg/m3)
P=Pressure (Mpa)
T_{Res}= Reservoir Temperature (°K)
C=Concentration of total dissolved solids $\left(\frac{g}{L}\right)$

Oil Viscosity
μ_{OD}= Viscosity of Gas Free Oil (cp)
R_S=Solution Gas Ratio $\left(\frac{scf}{STB}\right)$
μ_{go}= Viscosity of Gas Saturated Oil (cp)
API= Oil Gravity (°API)

Gas Viscosity
μ_g=Gas Viscosity (cp)
MW_G=Molecular Weight of Gas (dimensionless)
T_{Res}= Reservoir Temperature (°K)

Permeability
k-max= Maximum horizontal permeability (m^2)
k-90= Horizontal permeability in direction perpendicular to k-max (m^2)
k-vert= Vertical permeability (m^2)

Analytical Modelling
s(t)= drawdown (or buildup) in aquifer (m)
Q= Pumping (or injection) rate $\left(\frac{m^3}{s}\right)$
$T_{Aquifer}$=Aquifer transmissivity $\frac{m^2}{s}$
K=Aquifer hydraulic conductivity $\frac{m}{s}$
b=Aquifer saturated thickness 9m)
r= Distance between pumping (or injection) well and observation well (m)
S=Storativity (dimensionless)
t_{pump}= Time since pumping started (s)
S_S=Specific Storage (m^{-1})
g= acceleration due to gravity $\left(\frac{m}{s^{2)}}\right)$
α= Aquifer skeleton compressibility (Pa^{-1})
β= Compressibility of formation water (Pa^{-1})
(Δψ)= Change in pressure head (m)
ΔP_{sim}=Aquifer pressure increase
$\Delta P_{Falloff}$=Falloff test change in aquifer pressure

1. Introduction

1.1 Background

Disposal of liquid wastes is oftentimes a problematic and expensive problem for many industries including oil and gas producers, chemical manufacturing and mining operations. Injection of such wastes in deep saline aquifers is often a cost effective and efficient option. Deep saline aquifers (i.e., porous rock formations) present in many sedimentary basins are capable of supporting large fluid injection volumes, often without the need for stimulation (Ferguson and Grasby 2014). Deep subsurface disposal of wastes offers large costs savings, up to 80% as compared to the alternative methods of landfilling wastes or chemical treatment (Lehr 1986).

In the Saskatchewan potash industry, brine wastewater from potash processing and mine inflow have been injected into deep saline aquifers since the late 1960's. The quantities of the fluids injected have been very large, dwarfing oil and gas waste disposal (Ferguson 2015), where in some potash mine injection wells tens of millions of cubic metres of wastewater have been injected over the last few decades with high injection rates (1000-10 000 m^3/day). The potash mine sites in Saskatchewan contain injection wells targeting both the Basal Clastics and Interlake Group. The mine sites targeting the Basal Clastics include the Cory, Vanscoy, Patience Lake, Allan, Colonsay, Lanigan and Belle Plaine (Figure 1-1). The mine sites that target the Interlake Group are the Mosaic K1, K2 and Potash Corp Rocanville sites.
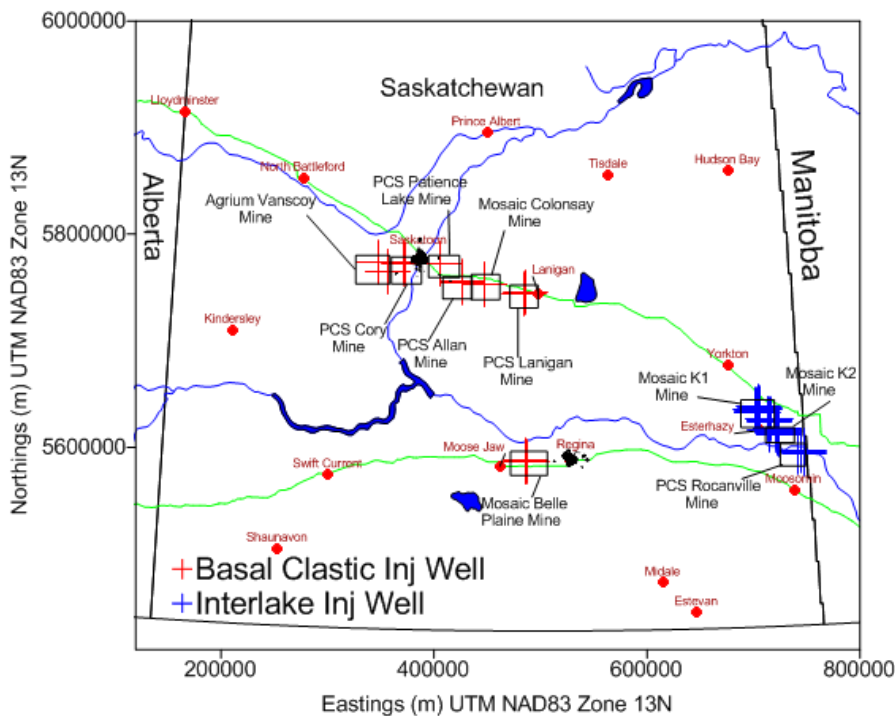
Figure 1-1: Red crosses show the Basal Clastics injection wells and blue crosses show the Interlake Group injection wells at the respective potash mine sites throughout Saskatchewan.

In order to implement large scale liquid waste injection effectively, a thorough understanding of the characteristics of these deep aquifers is essential. Permeability is a particularly important characteristic, as it will dictate the ease at which injected fluids will be accepted into the aquifer. However, the characteristics of such aquifers (including the Basal Clastics and Interlake Group) often are poorly understood, as there is limited information available at these depths due to high drilling costs (Alley et al. 2014, Tsang and Niemi 2013).

Characterizing deep aquifers requires different techniques than those applied to studying shallow aquifers. Much of the data for characterizing deep aquifers is available from oil and gas exploration. Single well tests are critical to analyzing deep aquifers, as multiple well tests that employ the use of monitoring wells (as used in shallow groundwater pumping tests) are not feasible due to the substantial expense of installing monitoring wells at these depths (Alley et al. 2014). Single well tests available in deep aquifers include drill stem tests (DSTs) and falloff tests. These tests offer valuable information on the in-situ characteristics of the formation. Core extracted from deep aquifers yields valuable porosity and permeability data, however this information is typically only available for very limited intervals of the formation and the laboratory tests conducted are not representative of the true in-situ characteristics of the formation. Geophysical logs provide valuable information on the spatial distribution of subsurface formations allowing for correlations of formations from well to well over large areas, as well as estimates of formation porosity. However, geophysical logs are unable to provide measurements of vital permeability data.

Additionally, the effects that large-scale injection of liquid wastes have on the targeted aquifers are often not well known; both in general, and at the potash mine injection sites in Saskatchewan. Injection of liquid wastes would undoubtedly result in an increase in the aquifer pressures. However, the magnitude of these increases as well as how far these pressure increases propagate through the aquifer are not well understood at most injection sites. Over pressuring an aquifer could result in harmful effects such as interference between neighbouring injection wells, damage to caprock (if fracture pressure is exceeded), as well as injection induced seismicity. Through gaining a better understanding of the how the aquifer pressures have changed over time as a result of waste injection, future injection activities at these sites could be better managed in order to mitigate over-pressuring these aquifers.

1.2 Objectives

The first goal of this dissertation was to develop a better understanding of the aquifer characteristics at the injection sites, and how these characteristics have affected injection activities. This was accomplished by conducting a large scale reservoir characterization study of the aquifers utilized for brine wastewater injection in Saskatchewan (Basal Clastics and Interlake Group), based on analysis of DSTs, falloff tests, core data and geophysical logs available in the Basal Clastics and the Interlake Group. Additionally, through mapping the permeability values of these aquifers throughout the study area, locations suitable for future injection wells were identified.

The second goal of this dissertation was to develop a better understanding of how the aquifers have responded over time to the injection volumes they were subjected. This was accomplished by creating analytical models of the injection sites, and using them to analyse the changes in aquifer pressure over time at each of the mine sites as well as how far these pressure increases propagated through the aquifer. This information could aid in future planning of injection activities at these sites in order to avoid undesirable side effects.

1.3 Thesis Structure

Chapter 2 of this dissertation covers the reservoir characterization study. In the aquifers of interest (Basal Clastics and Interlake Group) the permeabilities were examined through core data, DSTs and falloff tests. The permeability values of each of these tests were compared to the geophysical logs of the tested intervals in order to determine correlations between lithology and permeability. As well, the permeability values of each of these tests were mapped throughout the study area in order to determine any regional trends in permeability of each of these aquifers.

The analytical modelling conducted through Aqtesolv (HydroSOLVE Inc. 2016) for each of the potash mine sites is covered in chapter 3. Initial aquifer pressures at each of the sites were established using pre-injection DSTs. Typical initial aquifer pressures were between 11,000-16,500 kPa (at depths approximately 1100-1400 m TVD). Analytical models were then constructed with known injection rates from each of the wells, and aquifer parameters determined in the reservoir characterization study (permeability, compressibility, aquifer thickness). These models were able to predict the injection induced pressure response in the aquifer. These models as well provided insights into how far the pressure increases propagated away from the injection wells. The pressure response from each of these models was compared to the aquifer pressure data determined from the annual falloff tests at each of the wells. Subsequent analytical models were constructed with different values of the aquifer parameters (transmissivity, storativity) until simulation outputs were generated which most closely matched the falloff test data (history-matched model). These history-matched models were considered the best representation of the real world conditions at each of the mine sites, providing the most accurate insights into the amount of pressure change in the injected aquifers and the distances that these pressure changes propagated from the injection wells.

In chapter 4, the major findings of chapters 2 and 3 are summarized. Additionally, there are recommendations for future work that could be undertaken in order to build upon the findings of this work.

2. Reservoir Characterization of the Basal Clastics and Interlake Group

2.1 Reservoir Characterization Introduction

The basal clastic unit ("basal clastics") in Saskatchewan, which is comprised of the Winnipeg and Deadwood formations, is an example of a deep aquifer where characterization is challenging due to data scarcity. The basal clastics have been primarily used for the injection of brine wastes from potash mines located throughout the province (Ferguson 2015) (Figure 1-1). There has been minor gas production from the Deadwood Formation in southwestern Saskatchewan (Geological Systems Ltd.), and minor oil production from the Winnipeg Formation in North Dakota (Anderson, 1982) and southeastern Saskatchewan. There has been minor water production from the Deadwood Formation, with one source well in the Kindersley area operating from 1986-2005. The basal clastics have been developed for carbon sequestration in southeastern Saskatchewan at the Aquistore project (Whittaker and Worth 2011). The Deadwood and Winnipeg formations have favourable geological characteristics for carbon sequestration including the presence of continuous highly permeable sand packages as well as various seals to mitigate vertical migration of CO_2 (Rostron et al. 2014). The Winnipeg and Deadwood formations of Saskatchewan also offer the possibility of future geothermal energy development (Ferguson and Grasby 2014).

The Interlake Group carbonates are utilized for injection of potash mine liquid wastes in the Esterhazy area of eastern Saskatchewan (Figure 1-1). This unit also presents challenges for reservoir characterization as there is only limited data available from oil and gas exploration as this unit lies below the major oil producing strata in Saskatchewan. There has been only minor oil and gas production from the Interlake Group in Saskatchewan (Martindale and Larson 2003).

The basal clastics and Interlake Group have been examined in other studies including Bachu and Hitchon (1996), where the groundwater flow in these formations was interpreted, as well Benn and Rostron (1998) and Palombi and Rostron (2006) studied the geochemical characteristics of the formation waters in these formations. The distribution of permeability, which if often a limiting factor in the installation and operation of production and injection wells, has not been studied in detail over a broad geographical area for the basal clastics or the Interlake Group carbonates.

Through conducting a large scale reservoir characterization study using geophysical well logs, core data and in situ hydraulic testing in the basal clastics and Interlake Group throughout the study area (Figure 2-1) the distribution of permeability values was better understood and the factors leading to the success of injection activities at the mine sites were better comprehended. Geophysical well logs were obtained from geoScout (geoLOGIC Systems Ltd. 2016), drill stem test and fall off tests were analyzed with records obtained from IRIS (www.saskatchewan.ca/iris), and permeability and porosity data obtained from laboratory analysis on core data was obtained from geoScout (geoLOGIC Systems Ltd. 2016). The distribution of the basal clastics in the subsurface of southern Saskatchewan and Manitoba is illustrated in Figure 2-2.

Figure 2-1: Area of study in southern Saskatchewan region of Western Canada, WCSB (Western Canadian Sedimentary Basin)
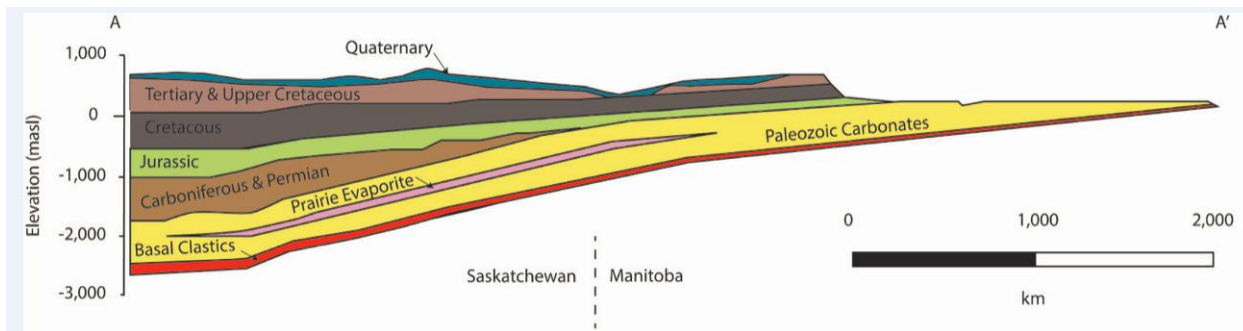
Figure 2-2: Geological cross section of sedimentary units in southern Saskatchewan and Manitoba from A-A' of Figure 2-1, illustrating distribution of the Basal Clastics in the subsurface, Prairie Evaporite unit mined for potash in Saskatchewan

2. 2 Geology of the Winnipeg, Deadwood and Interlake Formations

2.2.1 Geology of the Deadwood Formation

The Deadwood Formation, a middle Cambrian to lower Ordovician age unit (Kent 1994) is present in the subsurface of central and southern Alberta and Saskatchewan, as well as eastern

5

Manitoba. It is present in both the subsurface and outcrop in western Montana, northern Wyoming and in South Dakota (Greggs and Hein 2000).

The Deadwood Formation was deposited onto the eroding Precambrian shelf in a shallow sea that was inboard of the Laurentian passive margin in Saskatchewan (Slind et al. 1994). Further to the south in North Dakota and Montana, as well as into Alberta, the Deadwood strata were deposited in deeper water (Dixon 2008). The Deadwood Formation is primarily located within the Williston Basin (Figure 2-1). As the Williston Basin was not created until the beginning of the Arenig interval in the mid Ordovician, the Deadwood Formation cannot be considered to be deposited in the basin as the unit predates the basin formation (Greggs and Hein 2000).

Within the Deadwood Formation there is a large degree of heterogeneity, being made up of regolith (Precambrian sourced), glauconitic quartz sands, conglomerates, siltstones, shales and calcareous mudstones and limestones (Greggs and Hein 2000). This heterogeneity is readily apparent from geophysical log analysis in geoScout (geoLOGIC Systems Ltd. 2016), with large differences in log characteristics within the formation. In western Saskatchewan, the Deadwood Formation lies directly below the Ordovician carbonates and the upper portion is heavily shale dominated, grading into the sand packages of the underlying Earlie Formation. For the purposes of this study the Earlie Formation was grouped with the Deadwood Formation. Further east in the Belle Plaine area the Deadwood Formation is more sand dominated with alternating thick sand packages with thin shale layers.

Through geophysical well log analysis in geoScout (geoLOGIC Systems Ltd. 2016) it was observed the deepest areas of the Deadwood Formation were in the Estevan area where the maximum depths where 3340m TVD (True vertical depth) and -2800m subsea (Figure 2-3). In this area the Deadwood Formation is quite thin, being roughly 10m thick. The Deadwood Formation thickens to the west, reaching a maximum thickness of 600m west of Lloydminster, Alberta (Greggs and Hein 2000). Further to the east in the Saskatoon area, the formation is approximately 300m thick. The formation is considerably shallower to the north (Figure 2-3), with the shallowest depths being found at only 547m TVD and -52 m subsea in the Meadow Lake area of northern Saskatchewan.
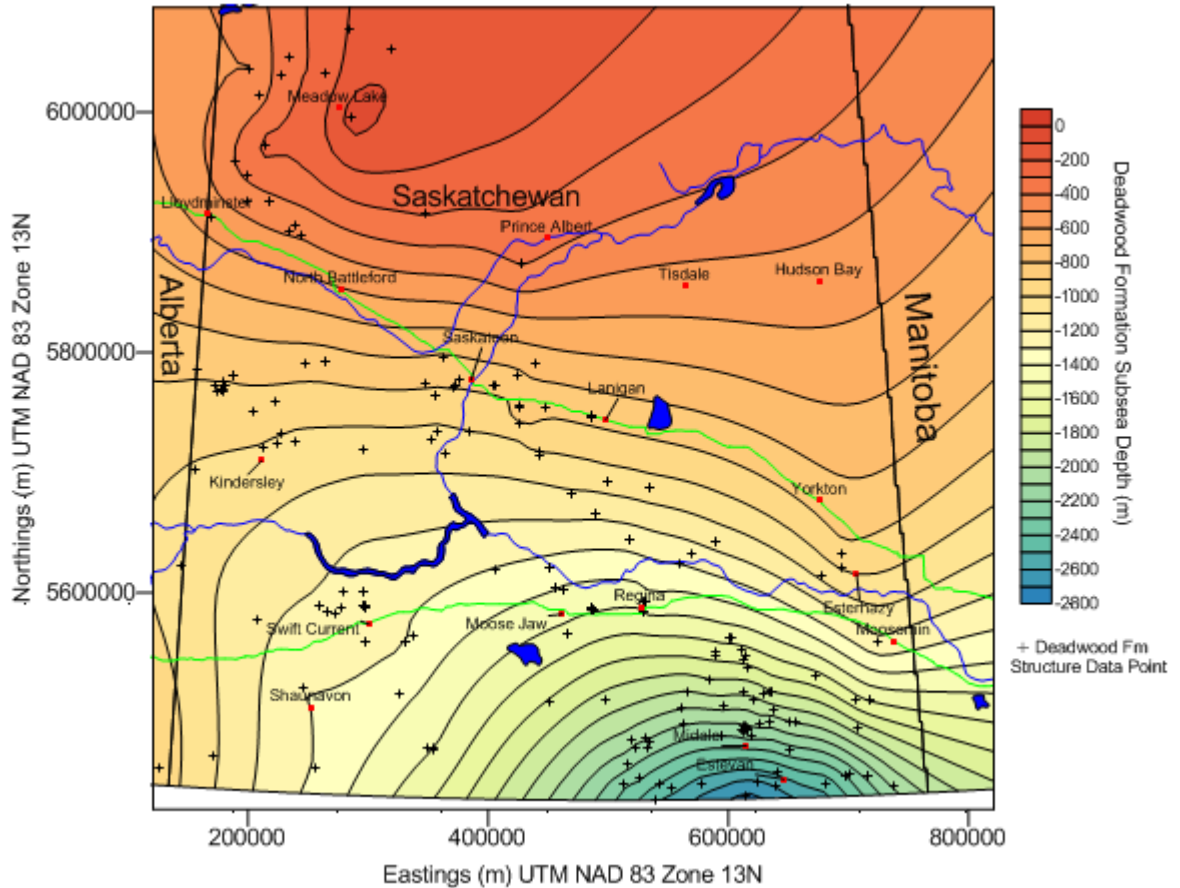
Figure 2-3: Deadwood Formation structure map of southern Saskatchewan (metres subsea), with Deadwood Formation data points from geophysical well logs

2.2.2 Geology of the Winnipeg Formation

The mid-Ordovician Winnipeg Formation makes up the upper sequence of deep Phanerozoic rocks in southern Saskatchewan (Paterson 1988). In the far southeast of Saskatchewan the formation directly overlies Precambrian metamorphic units and further west the Winnipeg Formation rests on top of the Deadwood Formation (Paterson 1988) (Figure 2-4). The Tippecanoe transgression was brought about by basin subsidence; during this time the Winnipeg Formation was deposited (Sloss 1963). The Winnipeg Formation is comprised of three different members, the Black Island, Icebox and Roughblock (Smith and Bend 2004). The lowermost Black Island Member is comprised predominantly of quartzose sands that are poorly to well sorted (Vigrass 1971; LeFever 1996; Nimegeers 2000). Geophysical logs of wells in southeastern Saskatchewan indicate this member is the target for oil and gas production within the Winnipeg Formation. Overlying the Black Island sands is the Icebox Member shale deposited as a massive flooding surface (Kessler 1991; Seibel 2002). The Roughblock Member overlying the Icebox shale is present in North Dakota but not in Saskatchewan (LeFever 1996).

7
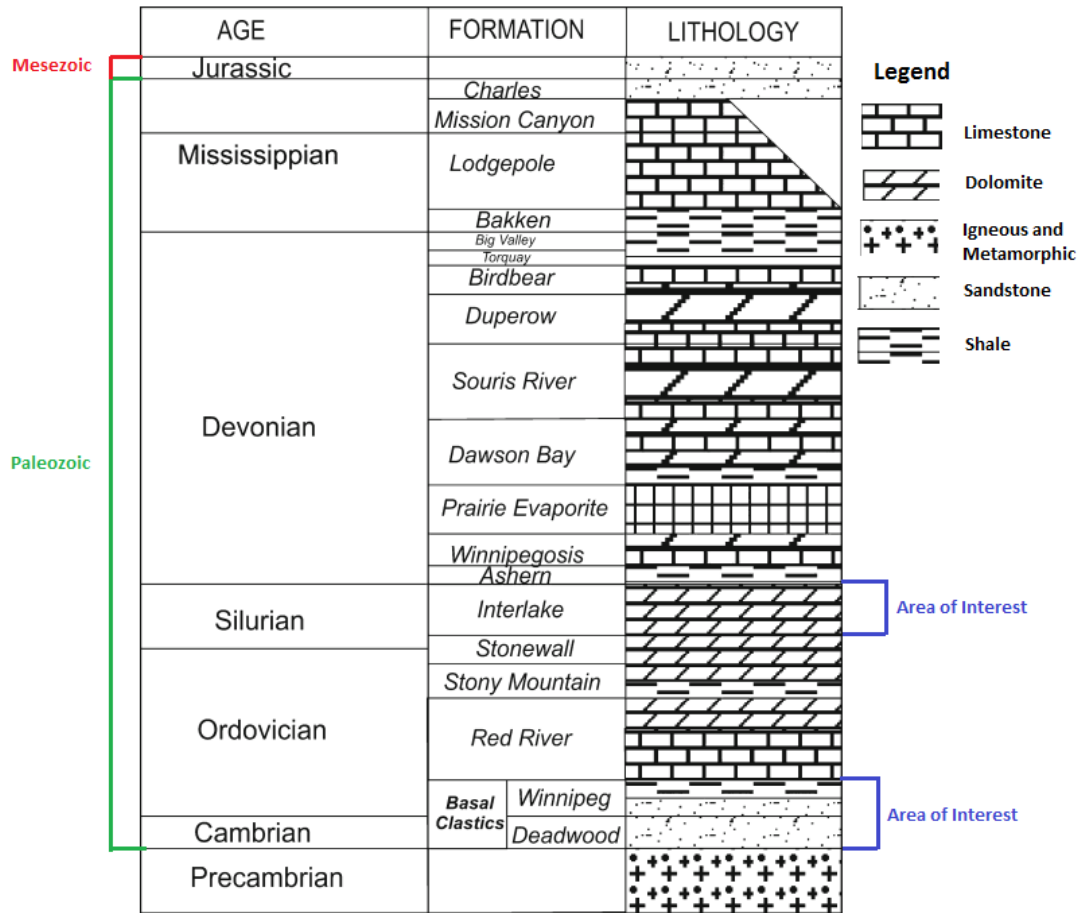
Figure 2-4: Stratigraphic succession of Paleozoic era in Saskatchewan (Saskatchewan Ministry of Energy Resources 2011; Ferguson and Grasby 2014)

As with the Deadwood Formation, the deepest areas of the Winnipeg Formation are in the southeast of Saskatchewan, near Estevan. In this area the TVD depth of the Winnipeg Formation is up to 3275m, it also exhibits the largest thickness in this area, at up to 60m. The formation thins and shallows to the north. West of the third Meridian the formation is not present and the Deadwood Formation directly underlies the upper-Ordovician age carbonates of the Red River Formation.

2.2.3 Geology of the Interlake Group

The Interlake Group represents a sequence of several distinct carbonate formations of Silurian age, the three major subgroups being the Lower, Middle and Upper Interlake (Megathan 1987). The deposition of Interlake strata occurred in the ancestral Williston Basin during the early Silurian (Megathan 1987) in a shallow low relief carbonate ramp setting (Haidl et al. 2006). The lower Interlake subgroup consists of clean limestones and dolomites alternating with shales that are laterally extensive and correlatable across the basin (Megathan 1987). The middle Interlake consist predominantly of clean dolomites. The upper Interlake was deposited in a tidal

flat environment that resulted in cyclic deposition of alternating hypersaline marine carbonates with pedogenic carbonates (Martindale and Larson 2003). The Interlake Group is conformably underlain by the Stonewall Formation and unconformably overlain by the mid-Devonian Ashern Formation (Haidl et al. 2006). There has been significant oil and gas production from the Interlake Group in North Dakota, and there is significant potential for development in Saskatchewan (Martindale and Larson 2003). Along with the basal clastics, the Interlake Group is deepest in the southeast of the study area, shallowing to the north and west (Figure 2-5).
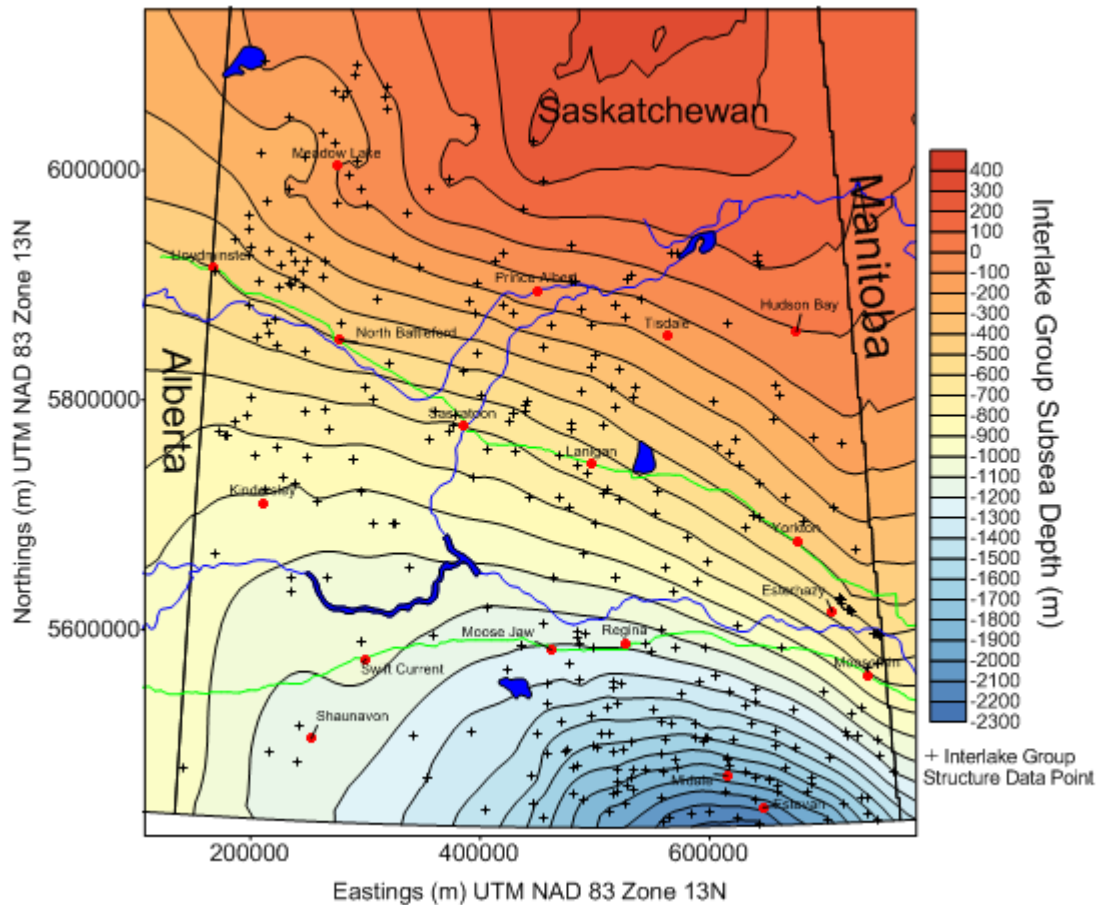
Figure 2-5: Interlake Group structure map of Saskatchewan (metres subsea), with Interlake Group top data points from geophysical logs

2.3 Literature Review

2.3.1 Drill Stem Test Analysis

Drill stem tests (DSTs) are hydrologic tests commonly employed in the oil and gas industry to provide information on the properties of the formation fluids as well as estimates of subsurface formation pressure and permeability (Bredehoeft 1965). These tests are conducted by lowering a DST string into the well to the tested interval, where packers are inflated to isolate the interval of interest. The formation is allowed to produce for a short period by opening the tester valve, this being the first flow period (Bredehoeft 1965). The tester valve is then shut in and

pressure measurements are taken at periodic intervals. The process is again repeated with a second flow and shut in period. Fluid samples are collected during the second flow period; as this period is also used to create a pressure perturbation that extends past the area of the wellbore damaged by the effects of the drilling fluid (Borah 1992). This damage can be quantified by calculating the skin effects (Appendix A). The second shut in period yields valuable information used to calculate the formation transmissibility, formation damage and the radius of investigation of the test (Borah 1992). The formation permeability, and to a lesser extent the amount of drawdown caused by the flow periods, are the primary factors that determine the length of shut in time required to achieve a complete pressure buildup in the test (Black 1956).

The wellbore pressure data recorded at periodic intervals of the shut in periods are compared to log ($\frac{T+\Delta T}{\Delta T}$) (McAlister et al. 1965) (Figure 2-6). T being the total flow time, which for the first shut in period being the length of the first flowing period and ΔT being the time since shut in began (McAlister et al. 1965). For shut in period 2 the total flow time T, is the sum of flow periods 1 and 2. In Horner DST analysis larger ΔT values correspond to the smaller $\frac{T+\Delta T}{\Delta T}$ values. A value of $\frac{T+\Delta T}{\Delta T}$ approaching 1 corresponds to an infinite shut in time, at which the aquifer would be restored to its static aquifer pressure (P_s) (Warner and Lehr 1981) (Figure 2-6). The slope of the line fit to the late time pressure recordings is taken over 1 log cycle.
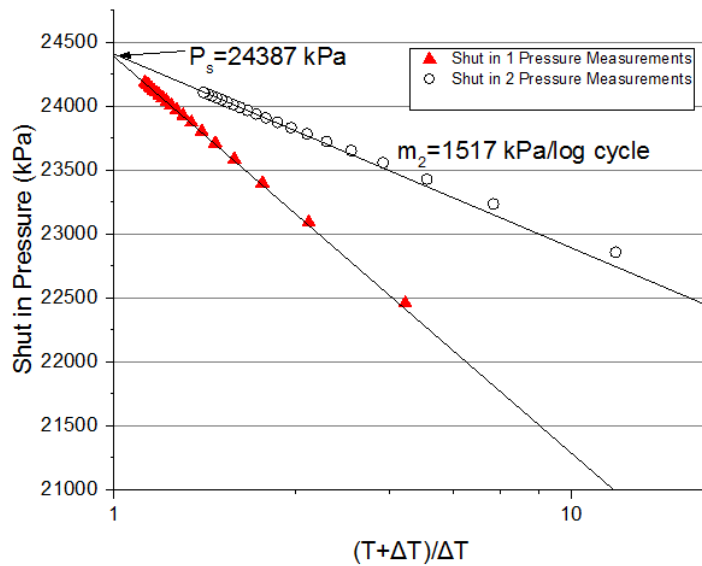
Figure 2-6: Sample DST Horner Plot with interpreted slope from shut in period 2 (m_2) and interpreted static aquifer pressure (P_s)

This slope ($\frac{Pa}{cycle}$) is used to calculate the aquifer transmissibility of the DST interval through equation 2.1 (modified from Borah 1992).

$$TB_{Aquifer} = \frac{0.1857qB}{m} \qquad (2.1)$$

where $TB_{Aquifer}$ (Aquifer transmissibility) is the flow rate achieved through an aquifer under a unit hydraulic gradient and given aquifer thickness (Brown 1953) and is measured in units of $\frac{m^4 s}{kg}$. The slope over one log cycle (Pa/cycle) is defined as m. Flow rate (q) which is the rate at which the formation fluids are flowing into the wellbore during the flow periods and is measured in $\frac{m^3}{s}$. The flow rate of the well, if not supplied in the DST report, can be calculated by relating the pressures in the initial flow period and the final flow period with the total fluid recovery (Borah 1992) using equation 2.2 to find the height of the fluid recovered during each flow period. The volume of fluids recovered can be calculated based on the inside diameters of the drill collars and drill pipe.

$$Height\ of\ Recovery\ Flow\ 1\ (m) = \frac{Final\ Flow\ 1\ P}{Final\ Flow\ 2\ P} \times Total\ Recovery\ (m) \quad (2.2)$$

A flow rate can then be calculated for each flow period based on the volume of recovered fluids (m^3) and the flow time of each flow period (T) (s) (Equation 2.3).

$$q = \frac{V_{rec}}{T} \quad (2.3)$$

The formation volume factor B is a measure of the change in volume of the fluids at reservoir conditions compared to standard conditions (surface conditions) (Dake 1978) and measured in $\frac{rcm}{stcm}$. For water recovery wells the formation volume factor can be approximated as 1, as changes in temperatures and pressures have offsetting effects from one another and the resulting change in volume is negligible (McCain 1990). For oil and gas recovery the formation volume factor needed to be calculated accordingly (Appendix B).

The permeability can be determined from equation 2.4 (modified from Mckinley et al. 1968).

$$k = \frac{TB_{Aquifer}\mu}{h} \quad (2.4)$$

where k is permeability (m^2) that describes the ability of a material to transmit a fluid (Lohman et al. 1970), μ (viscosity) ($Pa \times s$) is calculated according to the formation water salinity, in-situ temperature and pressure (Kestin et al. 1981) (Appendix C). For tests involving oil and gas recovery viscosity was estimated using methods explained in Appendix D. The formation thickness h (m) is comprised of the productive areas of the aquifer contributing to flow during the test and intervals. The permeability values calculated from DSTs are a representation of the average effective permeability for the entire interval tested (Dolan et al. 1957). In a clastic formation such intervals would be identified from gamma ray log intervals of 75 API or less, as shales due to low permeability would not contribute to flow. Within the sandstones, lower gamma ray intervals are considered clean sands (15-40 API) while higher gamma ray sands (40-75 API) would be considered dirty sands due to the higher clay and shale content (Figure 2-7).
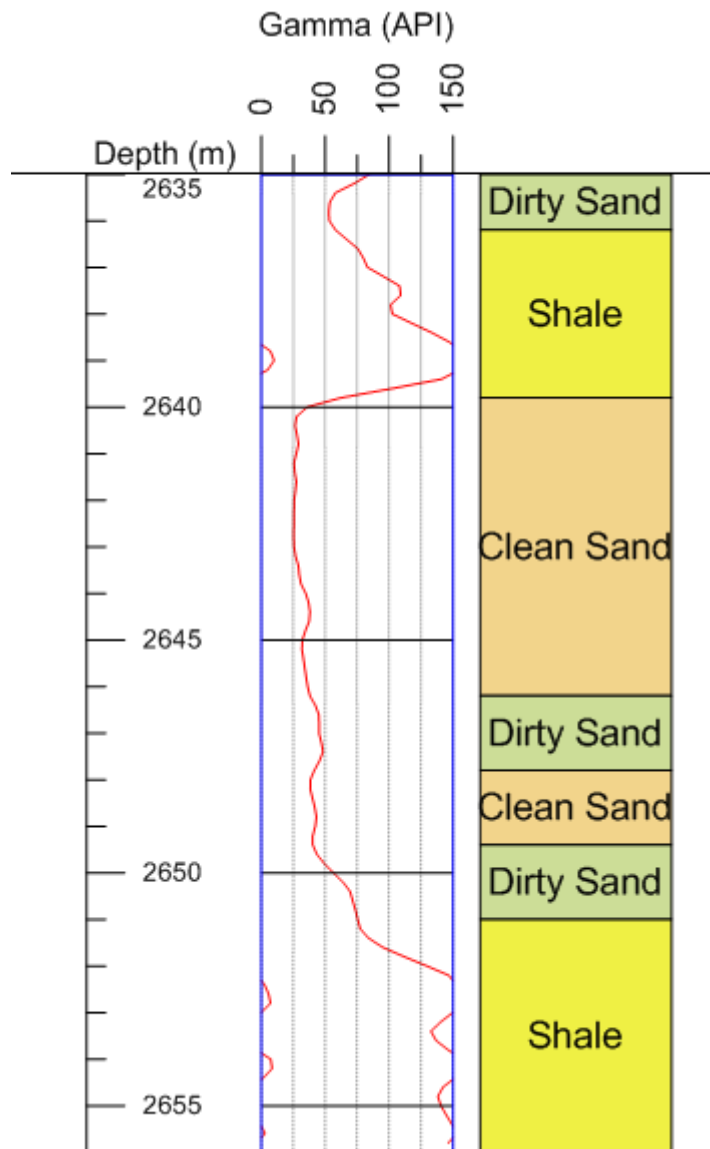
Figure 2-7: Showing sample log of dirty sand, clean sand, shale (121/15-23-009-23W2), wrap around gamma values indicate values greater than 150 API, scale becomes 150-300 API.

The radius of investigation (RI) or how far the DST is able to measure into the formation is calculated through equation 2.5 (modified from Borah 1992 and Maier 1962).

$$RI = \sqrt{\frac{kt}{\phi \mu c_{bulk}}} \qquad (2.5)$$

where porosity (ϕ) is the fraction of the void space in the rock, t is the flow time of the test (s), μ is the formation fluid viscosity (Pa×s), k is the permeability (m^2), c_{bulk} is the bulk compressibility (Pa^{-1}).

An underlying assumption of Horner analysis is radial flow conditions during the test, however if radial flow conditions were not achieved during the test either due to low permeability and insufficient test length, the shut in periods have insufficient development for Horner analysis. McKinley analysis (Crawford et al. 1977) can be undertaken in DSTs where wellbore storage effects are still dominant and provide reliable results. In McKinley analysis, type curves were developed for various flow times. The pressure buildups of the shut in periods are plotted on a plot of $\log(\Delta T)$ vs $\log(\Delta P)$. The pressure buildup plot is overlayed on the Mckinley type curve for the corresponding flow time and matched to a type curve of $(\frac{T}{F})$ for both the early time wellbore storage pressure readings and later formation pressure readings. A match point is then chosen along the type curve to obtain a value of $\frac{\Delta pF}{q}$ off the McKinley type curve underlay and a value of ΔP from the buildup pressure overlay. The F-factor $(\frac{ft^3}{psi})$ is then calculated with equation 2.6 (Crawford et al. 1977).

$$\text{F} = \frac{q\frac{\Delta PF}{q}}{C\Delta P} \tag{2.6}$$

where q is the flow rate $(\frac{bbl}{day})$, C is the flow time correction factor based of the $(\frac{T}{F})$ value of the wellbore storage period.

The transmissibility of the aquifer then calculated according to equation 2.7 (Crawford et al. 1977).

$$TB_{Aquifer} = \left(\frac{T}{F}\right) \times F \tag{2.7}$$

where TB$_{Aquifer}$ is the aquifer transmissibility $(\frac{mDft}{cp})$. From the transmissibility, the aquifer permeability can be calculated with equation 4.

2.3.2 Falloff Test Analysis

A falloff test is a well test conducted in an injection well, where the well is shut in and the pressures are monitored (either at the surface or bottom hole) over time (Kazemi et al. 1972). The pressure falloff plots constructed from the test data can be analyzed while considering the pressure rise in the well during the injection period and the pressure decline observed during shut-in (Nowak and Lester 1955). A falloff test is analogous to a production well's pressure buildup test (Kazemi et al. 1972), therefore the equations used for fluid flow analysis in production tests can be used in the case of injection wells with consideration for the fluid property differences and the difference in the flow direction (Nowak and Lester 1955). The length of time necessary to shut in a well for proper analysis will be correlated with the extent of any skin or wellbore damage (EPA 2002).

In falloff test analysis the pressure measurements taken during the shut in period are plotted against a time function (EPA 2002). This time function can be either the Miller Dyes Hutchinson (MDH) plot, Horner plot analysis, Agarwal equivalent time plot as well as the superposition time function which requires the use of well test software. Once the shut in

pressure measurements are plotted against the various time functions, line fitting is undertaken whereby a line is fitted to the late time data that is not effected by wellbore storage and skin effects (Kazemi et al. 1972), in a manner similar to Horner analysis in DSTs. The slope of this line on the semi-log plot is then taken over one log cycle, the aquifer transmissibility can be calculated in the same manner as in a DST using equation 2.8 (modified from EPA 2002).

$$TB_{Aquifer} = \frac{0.1857qB}{m} \tag{2.8}$$

where q is the injection rate prior to shut in and all other parameters are the same as previously defined.

The permeability is then calculated from the transmissibility using equation 2.4. The viscosity (μ) used is taken as that of the formation fluid rather the injected fluid (EPA 2002).

In the Horner plot line fitting, a straight line can be extrapolated to infinite shut in time (where $\frac{Tp+\Delta T}{\Delta T}=1$) in the same manner as a DST, providing an estimate of the static aquifer pressure (Nowak and Lester 1955). Where T_P is the injection time since last pressure equalization, and ΔT is the shut in time (EPA 2002).

The skin factor measured in a falloff test gives an indication of the conditions in the well, which could be affected a great deal by the injected fluid (EPA 2002). A positive skin value is indicative of formation damage that inhibits flow into the formation, while a negative skin indicates stimulation, whereby the near wellbore permeability is actually increased, enhancing injection into the host formation. The calculation for skin factor is included in Appendix A.

The radius of investigation for the falloff tests is defined as the distance into the host formation where the pressure transient is able to propagate after a rate change in the injection well (EPA 2002). The radius of investigation (RI) in metres is calculated from equation 2.9 (Modified from Matthews and Russel 1967)

$$RI = \sqrt{\frac{3.93 \times kT_p}{\phi\mu c_t}} \tag{2.9}$$

where T_p is the injection period (s), which is taken as the Agarwal equivalent time function ΔT_e for the cases where the injection period is longer than the falloff period (EPA 2002). All other parameters are the same as defined in equation 3.

2.3.3 Formation Compressibility Estimation

Formation compressibility, a vital input parameter for conducting reservoir simulations was calculated using two different methods. The first was through an empirical correlation of porosity with compressibility (Hall 1953). The second method determined compressibility through the relationship between compressional and shear wave velocities in dipole sonic logs.

2.3.3.1 Hall 1953 Compressibility Estimation

The formation compressibility needed for the calculation of the radius of investigation for DSTs and falloff tests, as well as for the calculation of aquifer storativity used in the aquifer

simulations can be estimated using a variety of methods. One such method, Hall (1953) utilizes an empirically derived relationship between formation porosity and pore volume compressibility.

The Hall (1953) empirical relationship between formation porosity and pore volume compressibility allows for an estimate of pore volume compressibility (c_{pore}) (psi^{-1}) using equation 2.10 (Hall 1953)

$$c_{pore} = \left(\frac{1.782}{\phi^{0.438}}\right) x 10^{-6} \tag{2.10}$$

where ϕ is the formation porosity (fraction).

However, the pore volume compressibility only represents the compressibility of the void spaces in the rock and is a function of the porosity of the rock. In order to calculate the overall bulk compressibility of the aquifer the porosity as well as the compressibility of the solid (rock) material (c_{solid}) (Pa^{-1}) must be taken into account. The bulk compressibility (c_{bulk}) (Pa^{-1}) of the aquifer can be calculated through the equation (Khatchikian 1996)

$$c_{bulk} = (1 - \phi)c_{solid} + \phi c_{pore} \tag{2.11}$$

Generally, the solid compressibility is considered negligible compared to the pore compressibility and as a result the first term of the equations can be ignored.

2.3.3.2 Sonic Log Formation Compressibility Estimation

The Hall (1953) method only provides a general empirical value of aquifer compressibility. In order to provide a value that is reflective of information acquired at each of the wells, available sonic logs can be analyzed to estimate aquifer compressibility. The bulk compressibility of the aquifer material can be estimated from the relationship between the shear wave (parallel to borehole) and compressional wave (perpendicular to borehole) transit times available in dipole sonic logs. This is accomplished through calculating Poisson's ratio (modified from Nygaard 2010)

$$v_d = \frac{0.5\left(\frac{\Delta t_s}{\Delta t_c}\right)^2 - 1}{\left(\frac{\Delta t_s}{\Delta t_c}\right)^2 - 1} \tag{2.12}$$

Where v_d is the Poisson's ratio, Δt_s is the shear wave transit time ($\frac{\mu s}{m}$) and Δt_c is the compressional wave transit time ($\frac{\mu s}{m}$).

With Poisson's ratio as well as the bulk density of the formation (available from the density logs) the dynamic Young's modulus (E_d) (Pa) of the material is calculated as follows (modified from Nygaard 2010)

$$E_d = 10^6 \frac{\rho_b}{\Delta t_c^2} \frac{(1-2v_d)(1+v_d)}{(1-v_d)} \tag{2.13}$$

Where ρ_b is the formation bulk density ($\frac{kg}{m^3}$) available from geophysical logs and all other parameters are the same as defined in equation 2.12.

The dynamic Young's modulus obtained from log data must be converted to static Young's modulus (E_s) (Pa) in order to reflect values at static loading conditions in situ. An empirical relationship between dynamic and static Young's modulus in brine saturated sandstones was established by Hongkui et al. 2001 as follows:

$$E_s = 0.6 \times E_d \tag{2.14}$$

The bulk modulus (K) (Pa^{-1}) of the aquifer can then be calculated from (Bansal 2010)

$$K = \frac{E}{3(1-2v_d)} \tag{2.15}$$

The bulk compressibility (c_b) (Pa^{-1}) is the inverse of the bulk modulus (White and Mohsenin 1967)

$$c_{bulk} = \frac{1}{K} \tag{2.16}$$

The compressibility obtained from the dipole sonic logs is representative of the aquifer compressibility, which is a function of both the rock compressibility and the pore volume compressibility.

2.4 Data Compilation

Throughout Saskatchewan there has been an extensive number of DSTs conducted in the basal clastics and Interlake Group, with 253 tests conducted in the Basal Clastics and 189 in the Interlake Group. The DST data for many of these wells were acquired from the Saskatchewan Ministry of the Economy. Many of the DST reports were comprehensive, including pressure measurement data throughout the flowing and shut in periods during the tests which allowed Horner analysis to be conducted. This included 32 tests in the Winnipeg Formation and 40 tests in the Deadwood and Earlie formations and 36 in the Interlake Group. However, many of the reports (especially those from older wells drilled in the 1950's and 1960's) had inadequate shut in pressure measurement data for Horner analysis to be performed and were thus culled.

2.4.1 Deadwood Formation Data

Within the Deadwood Formation there were 25 wells with core, 24 wells with DSTs (some wells with multiple tests) and 12 wells with falloff tests available for analysis throughout Saskatchewan (Table 2-1). The geographic distribution of these wells can be seen in Figure 2-8.

Table 2-1: Deadwood Formation wells analyzed for core properties, DSTs and falloff tests

Well UWI	Well #	Core	DST	Falloff	Well UWI	Well #	Core	DST	Falloff
111/16-23-002-01W2/00	42	X			121/12-03-031-20W3/00	58	X		
131/06-02-003-21W2/02	81		X		102/12-21-031-21W3/00	76		X	
101/10-03-005-08W3/00	65	x			141/04-05-035-26W3/00	59	X		
101/12-10-005-08W3/00	80		X		141/03-18-036-25W3/00	60	X		
131/11-34-006-11W2/02	66		X		101/16-36-036-25W3/00	61	X		
141/04-16-006-13W2/00	43	X			131/01-20-033-23W2/00	53		X	X
142/12-01-010-09W2/00	44	X			141/02-28-033-23W2/00	54	X	X	X
131/01-33-014-12W2/00	46	X			131/02-21-034-27W2/00	55		X	X

Location	No.	Col1	Col2	Col3	Location	No.	Col1	Col2	Col3
111/09-18-007-11W2/00	67		X		101/15-34-034-27W3/00	75	X		
131/04-01-009-13W2/02	44		X		191/14-16-034-27W2/00	70			X
121/15-23-009-23W2/00	47		X		141/13-22-034-01W3/00	71		X	X
101/02-11-015-26W2/00	50	X			111/16-28-034-01W3/00	72		X	X
131/03-08-017-19W2/00	48	X	X		121/03-21-035-08W3/00	56	X	X	X
191/04-24-017-24W2/00	49		X		191/15-16-035-08W3/00	57			X
191/08-14-017-24W2/00	69		X	X	111/13-07-036-06W3/00	51		X	X
191/04-04-018-19W2/00	68	X			111/08-13-036-07W3/00	52		X	X
101/05-07-014-10W3/00	85	X			111/10-12-036-07W3/00	73		X	X
101/09-27-014-10W3/00	79	X			111/05-15-036-09W3/00	74		X	
101/01-09-017-14W3/00	78	X			101/11-15-046-01W3/00	62	X		
101/03-10-017-14W3/00	82	X	X		121/12-30-049-27W3/00	63	X		
111/11-03-017-14W3/00	83	X			101/01-25-054-26W3/00	87	X		
121/07-09-017-14W3/00	84	X			101/12-04-058-19W3/00	88		X	
101/08-17-018-14W3/00	77		X		101/08-11-062-22W3/00	64	X		
101/13-20-030-14W3/00	86		X						
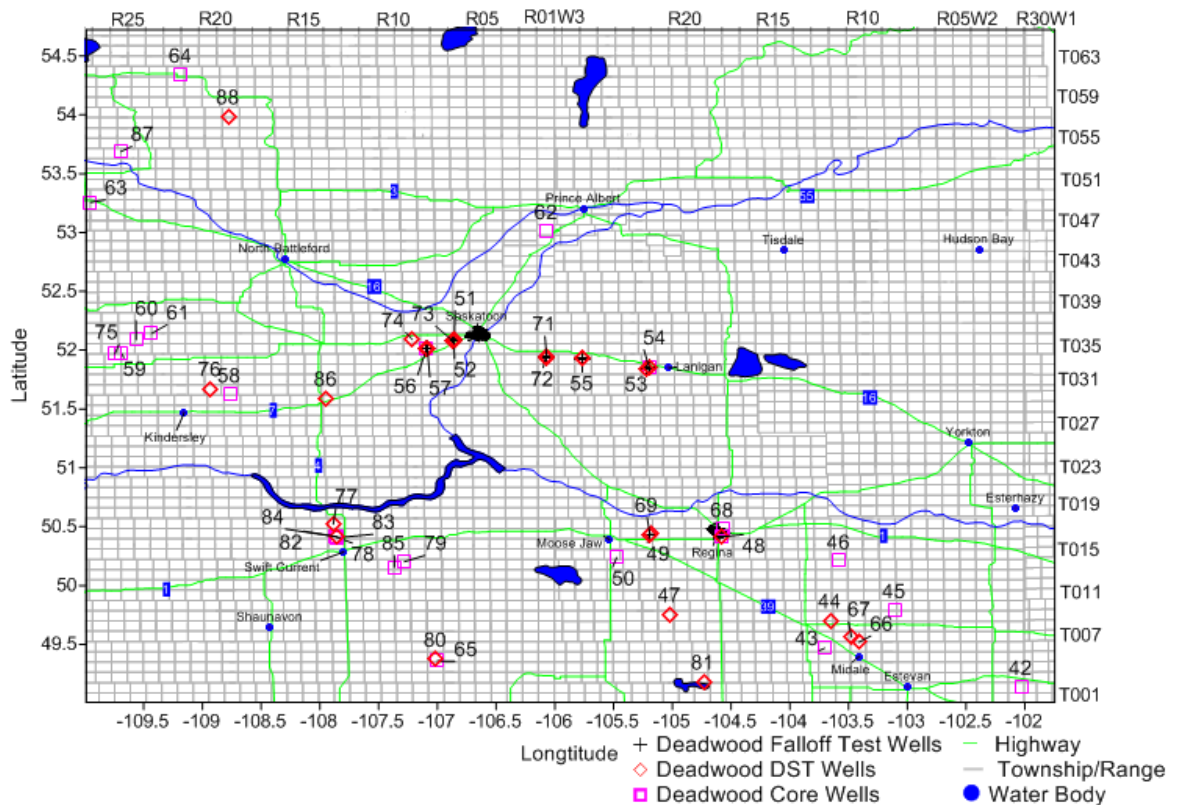
Figure 2-8: Deadwood Formation wells analyzed in this work. Wells with core, DST and falloff test data are labeled as indicated in the legend. See Table 2-1 for well number definitions.

2.4.2 Winnipeg Formation Data

Throughout Saskatchewan there were 15 wells with core, 28 with DSTs (some wells with multiple tests) and 1 with a falloff test in the Winnipeg Formation that were available for analysis in this study (Table 2-2). The locations of these wells is seen in Figure 2-9.

Table 2-2: Winnipeg Formation wells analyzed for core properties, DSTs and falloff tests

Well UWI	Well #	Core	DST	Falloff	Well UWI	Well #	Core	DST	Falloff
141/16-19-001-32W1/00	30	X			141/03-11-010-16W2/00	24		X	
101/01-06-002-04W2/00	1		X		101/03-27-011-09W2/00	11	X		
101/03-16-002-10W2/00	3		X		131/07-04-011-09W2/00	12		X	
131/06-02-003-21W2/02	20	X	X		121/06-36-012-15W2/02	25		X	
101/12-33-005-23W2/00	18		X		111/06-24-012-26W2/00	26		X	
133/03-06-005-21W2/00	19		X		101/08-02-012-27W2/00	27		X	
111/14-06-006-06W2/00	2		X		121/06-28-013-11W2/00	13		X	
131/08-16-006-11W2/02	31	X			101/16-26-013-27W2/00	14		X	
111/16-20-006-11W2/00	32	X			131/01-33-014-12W2/00	36	X		
131/08-34-006-11W2/00	4		X		101/08-36-016-06W2/00	29		X	
141/04-35-006-11W2/03	5	X			131/03-08-017-19W2/02	15		X	
121/06-20-006-13W2/00	8	X	X		191/08-14-017-24W2/00	16		X	X
121/08-06-007-15W2/05	37	X			101/08-17-023-20W2/00	17		X	
101/11-34-007-25W2/00	21		X		121/03-20-017-30W1/00	28		X	
141/07-24-008-09W2/02	6		X		121/01-14-017-30W1/00	38	X		
131/02-32-008-10W2/00	9		X		111/14-27-019-32W1/00	22		X	
131/06-18-009-06W2/00	7		X		121/10-14-020-33W1/00	40	X		
141/07-02-009-13W2/00	34	X			101/04-22-021-02W2/02	39	X		
132/07-02-010-09W2/00	35	X			101/04-10-022-32W1/00	23		X	
141/07-28-010-10W2/02	10		X		101/02-05-061-24W2/00	41	X		
191/08-06-010-15W2/02	11		X						
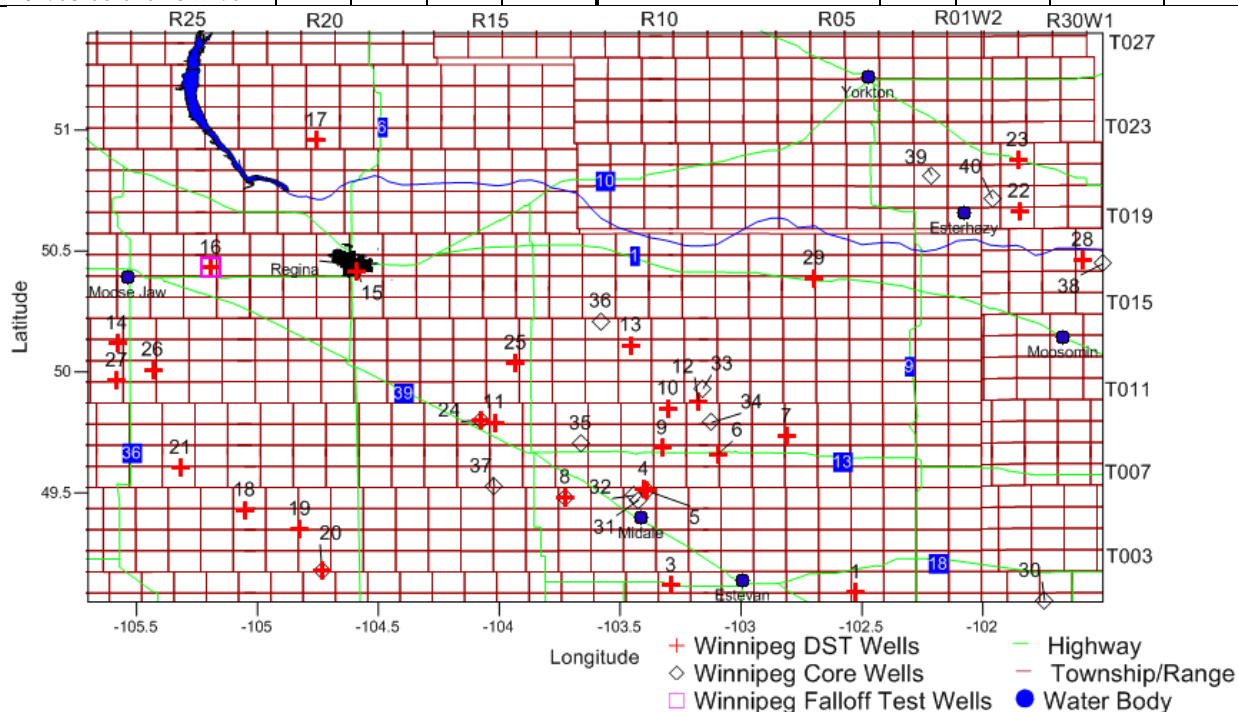
Figure 2-9: Winnipeg Formation wells analyzed in this work. Wells with core, DST and falloff test data are labeled as indicated in the legend. See Table 2-2 for well number definitions.

2.4.3 Interlake Group Data

Throughout the study area there were 12 wells with core analysis in the Interlake Group, 32 wells with DSTs (some wells with multiple tests), and 14 with falloff tests available for analysis (Table 2-3). In Figure 2-10 the geographic distribution of these wells can be seen.

Table 2-3: Interlake Group wells analyzed for core properties, DSTs and falloff tests

Well UWI	Well #	Core	DST	Falloff	Well UWI	Well #	Core	DST	Falloff
111/16-23-002-01W2/00	89		X		131/07-22-019-32W1/02	103		X	
131/09-34-003-04W2/00	122	X			131/10-22-019-32W1/02	104		X	
101/09-05-003-28W2/00	96		X		111/14-27-019-32W1/00	105		X	X
101/02-04-004-11W2/00	90		X		191/05-33-019-32W1/00	132			X
101/03-26-004-20W2/00	95		X		142/04-33-019-32W1/00	135			X
191/04-11-004-21W2/00	94		X		111/01-26-020-33W1/00	106		X	X
111/03-01-004-25W2/00	97		X		111/11-23-020-33W1/00	136			X
131/11-04-005-07W2/04	123	X			121/11-26-020-33W1/00	107		X	X
101/15-05-005-07W2/00	124	X			141/13-26-020-33W1/00	108		X	X
101/12-10-005-08W3/00	116		X		121/16-26-020-33W1/00	109		X	X
101/11-34-007-25W2/00	98		X		121/10-14-020-33W1/00	133			X
101/14-19-008-32W1/00	125	X			101/08-17-023-20W2/00	112		X	
101/08-30-008-33W1/00	126	X			101/01-32-027-11W3/00	117		X	
111/03-27-008-13W2/00	91		X		121/03-24-028-08W2/00	110		X	
131/06-32-008-16W2/00	127	X			101/13-22-030-16W2/00	113		X	
101/12-12-010-14W2/00	92		X		101/13-20-030-14W3/00	118		X	
192/08-06-010-15W2/00	93		X		101/09-21-033-15W3/00	119		X	
131/01-32-014-30W1/00	99		X		191/01-27-035-09W2/00	111		X	
141/08-20-014-31W1/00	100		X		121/03-21-035-08W3/00	121		X	
121/01-14-017-30W1/00	102	X	X	X	101/07-02-038-01W3/00	120		X	
121/03-20-017-30W1/00	139			X	101/15-12-042-22W2/00	114		X	
121/12-22-017-30W1/00	130			X	101/16-09-043-21W2/00	115		X	
141/06-23-017-30W1/00	134			X	101/01-32-047-19W2/00	128	X		
131/11-27-019-32W1/00	131			X					
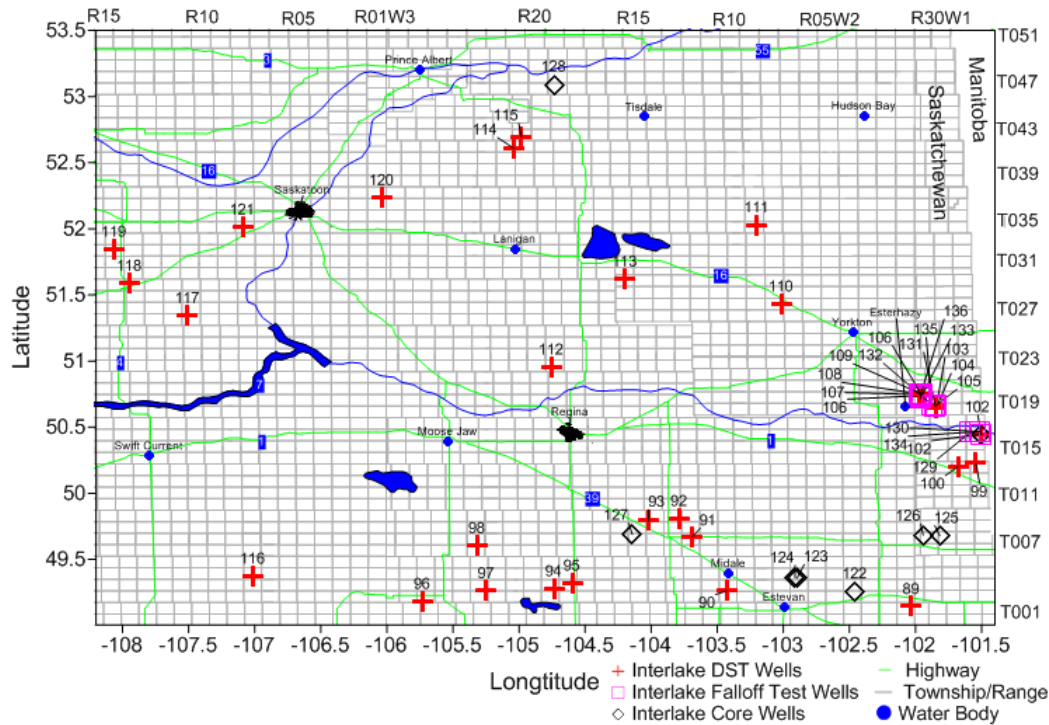
Figure 2-10: Interlake Group wells analyzed in this work. Wells with core, DST and falloff test data are labeled as indicated in the legend. See Table 2-3 for well number definitions.

2.5. Methods and Sample Calculations

2.5.1 Core and Geophysical Log Data

Porosity and permeability data obtained from laboratory analysis of core in the Winnipeg and Deadwood formations from wells throughout Saskatchewan was reported in geoSCOUT (geoLOGIC Systems Ltd. 2016). The permeability data extracted from geoSCOUT included the maximum horizontal permeability (k-max), the horizontal permeability in a direction perpendicular to the k-max (k-90), and the vertical permeability (k-vert). Porosity and permeability values were available for discreet intervals (10-50 cm typically) of each core.

The cored intervals were examined through analysis of geophysical logs available in geoSCOUT (geoLOGIC Systems Ltd. 2016). The sand and shale distributions within these intervals were identified using a gamma-ray log cut-off of 75 API units. Gamma-ray values less than 75 API were considered sand. The effective permeabilities were taken as the discreet values associated with the sand intervals in the gamma-ray logs. These values were arithmetically averaged in order to determine an effective k-max for each cored interval. The effective k-max derived from this analysis allows for a better comparison of permeability values obtained from other tests including DSTs and falloff tests.

2.5.2 DST Analysis

The DST records obtained from the Saskatchewan government IRIS database (www.saskatchewan.ca/iris) were digitized in order to be analyzed using Horner analysis

20

(Bredehoeft 1965) in order to calculate formation permeability, radius of investigation, wellbore skin effects and static formation pressure.

2.5.2.1 Horner plot line fitting confidence rating and sensitivity analysis

In DST Horner analysis there are often various interpretations that can be taken when line fitting to the data. These different interpretations often result in fit lines with significantly different slopes, thereby affecting the transmissibility and hence calculated permeability for each test. In each of the tests included in this study a confidence rating of low, medium or high was assigned. High confidence plots displayed neatly plotted pressure vs Horner time measurements with little variation in possible line fitting. Medium confidence plots often had somewhat erratic pressure measurements and often had to use shut in period 1 for Horner Analysis as shut in 2 pressure measurements were flat as a result of flow being choked out in the main flow period. Low confidence plots often had few pressure measurements with erratic values due to problems encountered during testing operations. Many of these low confidence tests were discarded; however some low confidence tests were able to be analyzed using the less favourable first shut in period.

In each of the DSTs a sensitivity analysis was undertaken with the line fitting whereby the maximum and minimum permeability values that could be interpreted from the tests based on the reasonable maximum and minimum slopes that could be interpreted from the Horner plot.

2.5.2.2 High Confidence Horner Plot with Sample Calculations

DST 2 from well 51 111/13-07-036-06W3 (a Potash Corp Cory mine injection well) was conducted in dirty sands in the Deadwood Formation. In this test, 1260m of formation fluid was recovered in the drill string; 143.4m of this in the 72 mm diameter drill collars and the remaining 1116.6m in the 97.2 mm diameter drill pipe for a total fluid recovery of 8.87 m^3. This formation fluid was recovered during the first and second flow periods that totalled 12 minutes. The flow rate for the first and second shut in periods were calculated separately based on the recovery recorder pressure measurements. The recovery recorder sits directly above the shut in valve thus is able to measure the hydrostatic weight of the recovered fluids throughout the entire test. Thus, the hydrostatic weight of flow periods 1 and 2 are able to be distinguished and subsequently separate flow rates can be established using equation 2.2.

Flow period 1

$$Height\ of\ Recovery\ Flow\ 1 = \frac{4646\ kPa}{13\ 997\ kPa} \times 1260m$$

$$Height\ of\ Recover\ Flow\ 1 = 418.2\ m$$

Flow Period 2

$$Height\ of\ Recovery\ Flow\ 2\ (m) = Total\ Recovery\ (m) - Recovery\ Flow\ 1\ (m)$$

$$Height\ of\ Recovery\ Flow\ 2 = 1260m - 418.2m$$

$$Height\ of\ Recovery\ Flow\ 2 = 841.77\ m$$

Flow Period 2 volume of recovery based on drill pipe inside diameter of 97.2 mm

$$Volume\ Recovered\ Flow\ 2 = 6.25\ m^3$$

The flow rate of flow period 2 was then calculated using equation 2.3.

$$q = \frac{6.25\ m^3}{(10\ min \times 60\ sec/\min)} = 1.04 \times 10^{-2}\frac{m^3}{s}$$

From the Horner plot of the shut in pressures vs Horner time (Figure 2-11) the late time pressure recordings (increasing time to the left) follow a smooth trend with no erratic measurements allowing for accurate line fitting. The slope (m) of the line for shut in 2 was found to be 117 $\frac{kPa}{cycle}$.
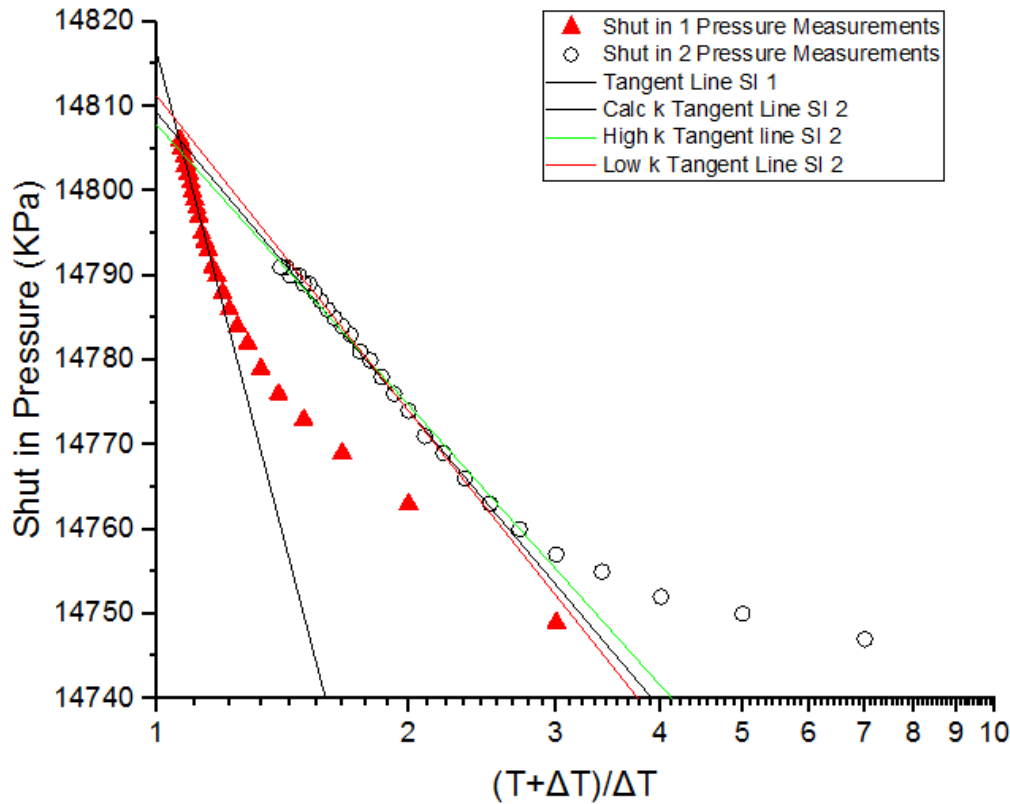
Figure 2-11: Horner Plot for DST 2 from well 51 (111/13-07-036-06W3)

Using this slope the transmissibility was calculated using equation 2.1, with a formation volume factor of 1 for water, as follows.

$$TB_{Aquifer} = \frac{0.1857 \times 1.04 \times 10^{-2}\frac{m^3}{s} \times 1.0\frac{rcm}{stcm}}{117\ 211\frac{Pa}{cycle}} = 1.65 \times 10^{-8}\frac{m^4 s}{kg}$$

A formation fluid viscosity of $1.15 \times 10^{-3} \frac{kg}{m*s}$ was estimated from Kestin et al. (1981) based on a formation temperature of 30 °C, a formation pressure of 14800 kPa estimated from shut in period 1 and a formation fluid salinity of 225 000 mg/L. The net sand thickness was 111.5m within the DST interval as identified in the gamma-ray log using a sand cut-off of 75 API (Figure 2-12).
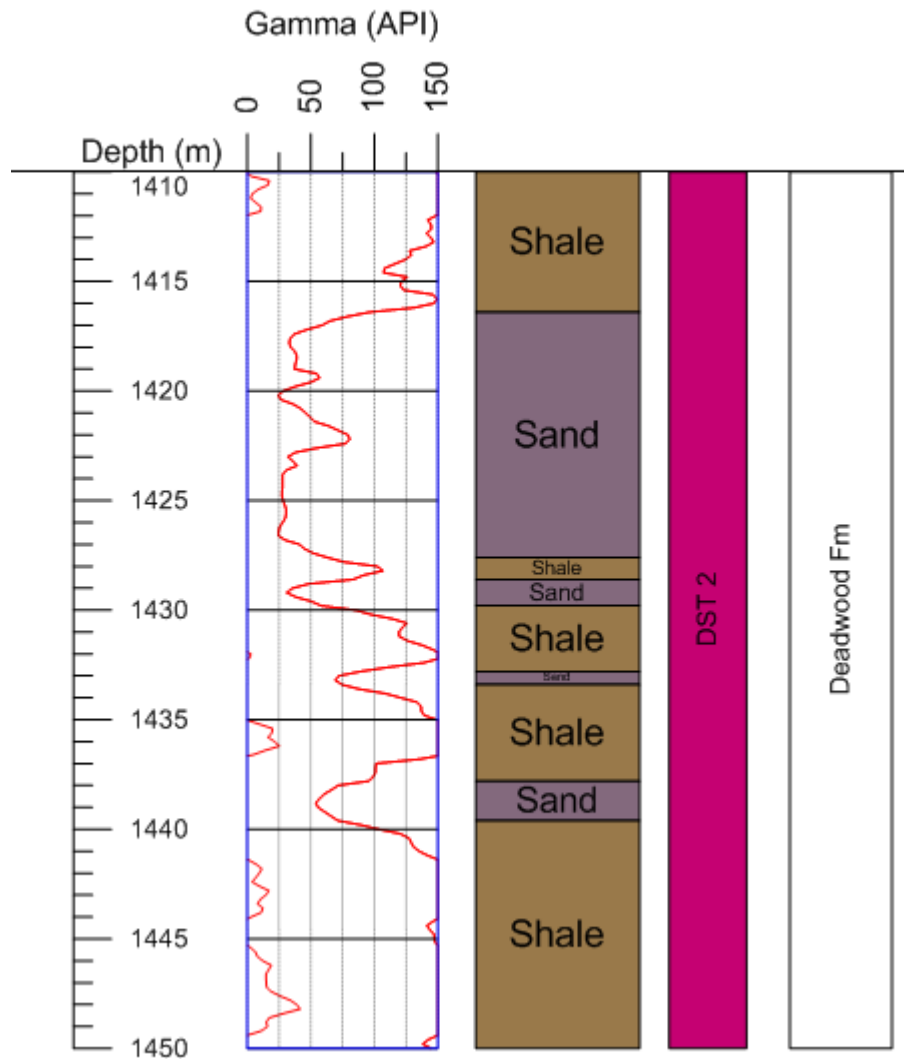
Figure 2-12: Gamma ray log for well 51 (UWI 111/13-07-036-06W3) for part of the DST 2 interval within the Deadwood Formation illustrating sand vs shale intervals using a 75 API gamma-ray cutoff, wrap around gamma values indicate values greater than 150 API, scale becomes 150-300 API.

From the calculated formation transmissibility, formation fluid viscosity and net sand thickness the formation permeability was estimated with equation 2.4.

$$k = \frac{\left(1.65 \times 10^{-8} \frac{m^4 s}{kg}\right) \times 1.15 \times 10^{-3} \frac{kg}{m \times s}}{111.5m} = 1.70 \times 10^{-13} \ m^2 = 10^{-12.8} \ m^2$$

In this DST there is little room for significant variation in line fitting with the red and green lines representing the reasonable lower and upper bound interpretations, in this case the lower bound value was only 5.6 % lower than the best fit line and the upper bound was 6.3% higher respectively. The early time data is ignored in the line fitting, as this data is most often not representative of in situ formation properties.

In this particular test only water was recovered and thus the formation permeability only pertained to the intrinsic permeability of water. In several of the wells studied there were multiple fluid phase recoveries including various combinations of water, gas, oil and condensate. For these wells, the effective permeabilities of each of these phases was calculated individually.

In order to assess the accuracy of the manual line fitting of the Horner plots, regression analysis was undertaken in Excel (Microsoft Office 2013). For DST 2 in well 51 (111/13-07-036-06W3) linear regression analysis of pressure vs $\log(\frac{T+\Delta T}{\Delta T})$ was conducted for different late time intervals. The resultant correlation (R^2) is observed in Figure 2-13. The manual line fitting which was undertaken based on shut in times ranging from 20-29.5 minutes results in an R^2 value of 0.991, while the Excel linear regression analysis conducted over the same time interval results in an R^2 of 0.996. From this it can be seen that the manual line fitting produces results that are similar to the automated line fitting.
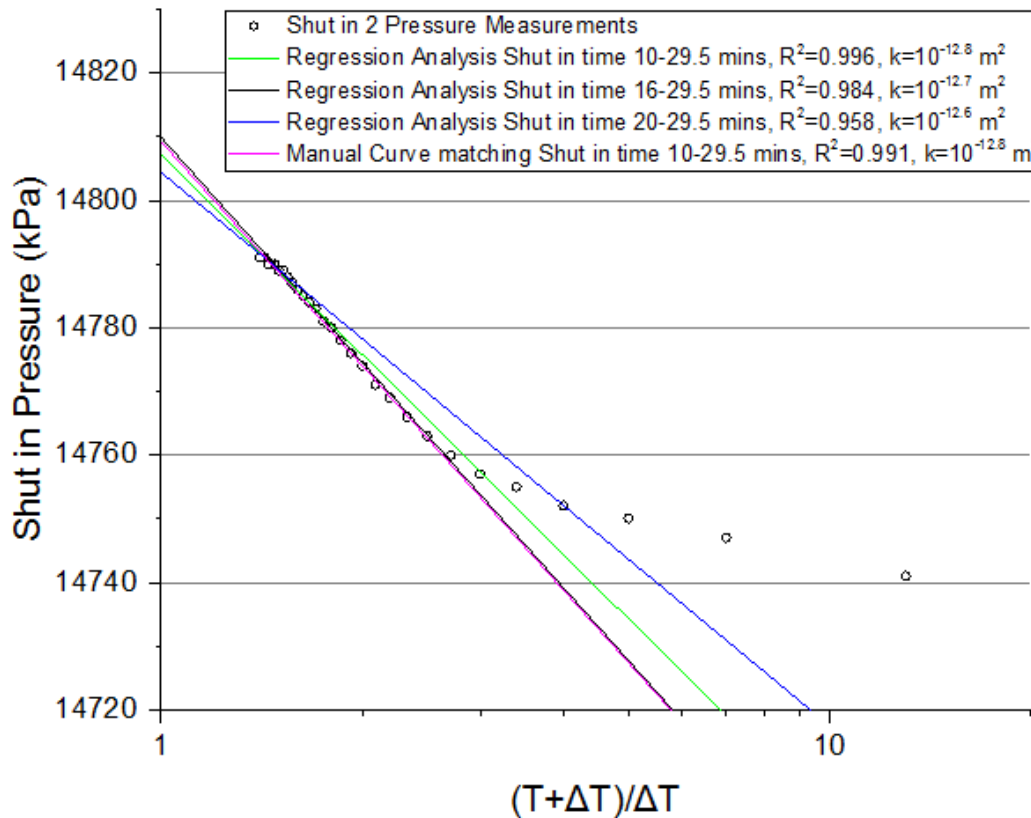
Figure 2-13: Horner Plot for well 51 111/13-07-036-06W3 DST 2, regression analysis plot with manual line fitting with corresponding R^2 values and resultant calculated permeabilities.

2.5.2.3 Medium Confidence Horner Plot

From the Horner plot of DST 3 from well 23, (UWI 133/03-06-005-21W2), which was conducted in clean Winnipeg Formation sands (Figure 2-14) it is apparent that shut in 2 pressure measurements could be interpreted in different ways. The early time data appears to be linear while the later time data has a sharp increase in pressure, possibly due to encountering boundary effects (Prasad 1975). If this is the case the later time data would not be a good representation of the formation properties and the early time data should be used for line fitting. For this analysis a moderated approach was taken between these two extremes resulting in a calculated permeability of $10^{-13.5}$ m^2. The high permeability case calculated using the early time data resulted in a permeability of $10^{-12.7}$ m^2, 531% higher. This may be the representative permeability of this well, however the moderated value was to prevent overestimation of permeability in the area. The decrease in pressure observed in shut in 1 was the result of a packer leak.
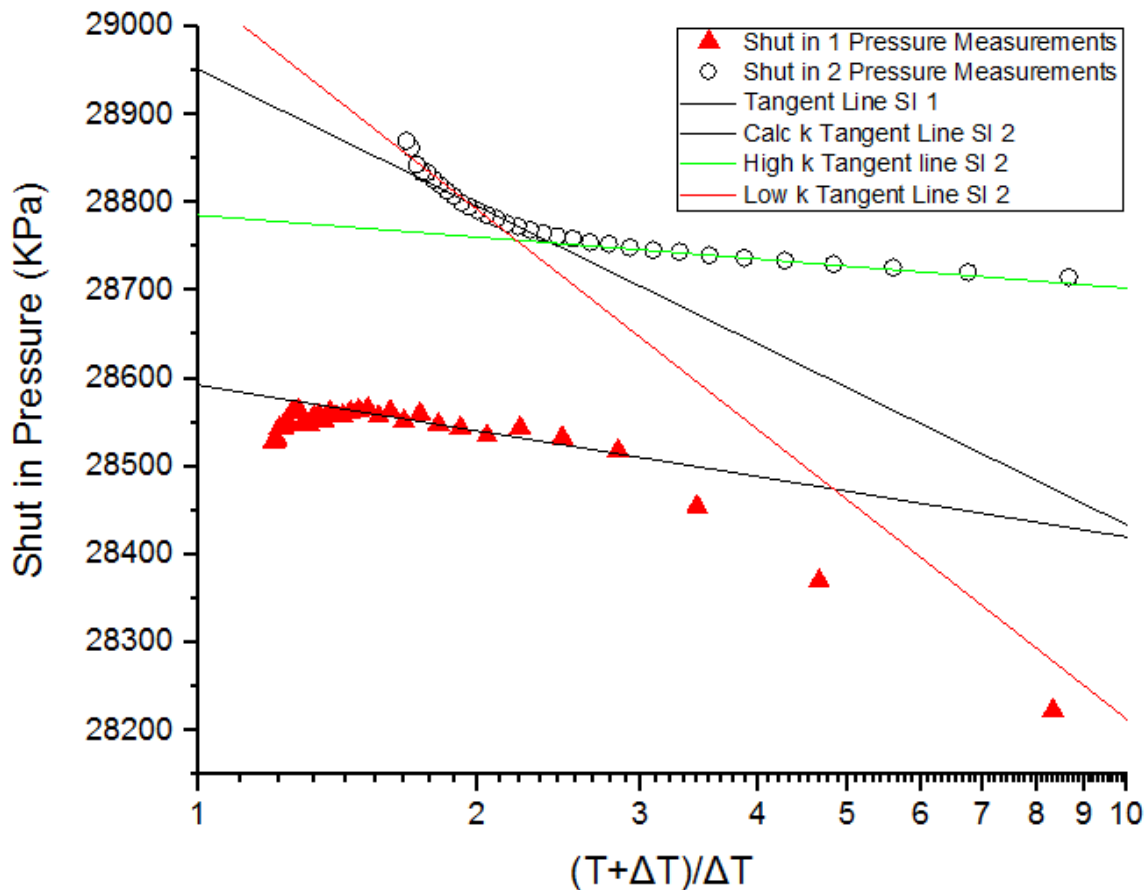
Figure 2-14: Medium confidence DST Horner plot for well 23 (133/03-06-005-21W2) DST 3 conducted in Winnipeg Formation clean sands

Regression analysis was conducted on this DST that was undertaken based on automated line fitting to several ranges of shut in pressure measurement vs time measurements (Figure 2-15). The manual line fitting based on measurements from shut in times from 38-60 minutes resulted

in an R^2 value of 0.938, which was similar to the automated regression analysis using these pressure measurements in the same time interval with an R^2 value of 0.951.
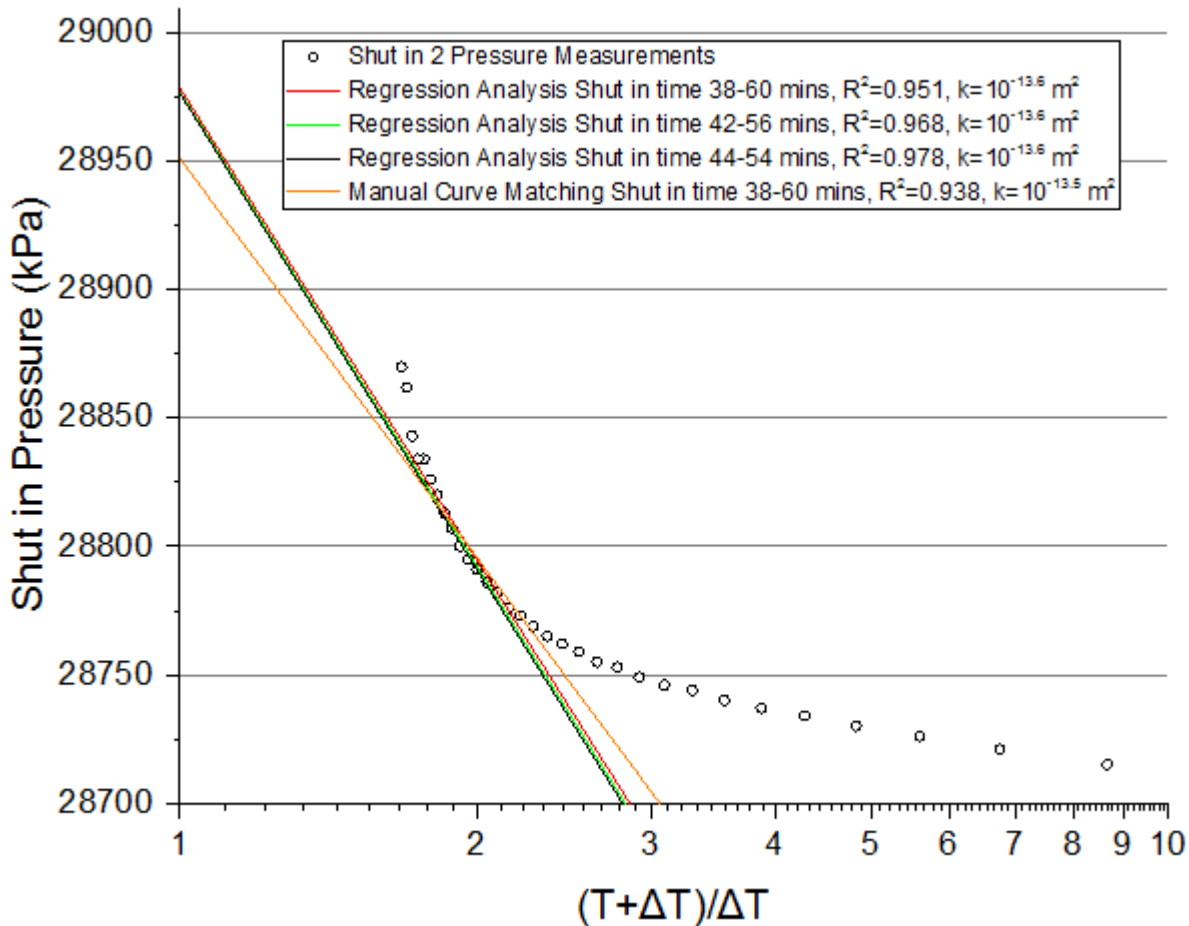
Figure 2-15: Horner plot for Well 19 (133/03-06-005-21W2) DST 3, regression analysis plot with manual line fitting and corresponding R^2 values and calculated permeabilities

2.5.2.4 Low Confidence Horner Plot

In DST 1 from well 71 (UWI 141/13-22-034-01W3) (Figure 2-16) conducted in dirty Deadwood Formation sands, the less desirable shut in 1 pressure measurements were used for the calculations as shut in 2 pressure measurements were completely flat (i.e., no variation in pressure with time). The flat measurements in shut in 2 are due to the well killing itself in the second flow, whereby the permeability in the tested zone was so high that the well was flowing so efficiently that the pressure in the wellbore became equal to the formation pressure. Thus, there was no more flow into the wellbore and the pressure measurements became flat. The late time data for shut in 1 was also flat due to the well killing itself, thus the early time data was used for interpretation. As such, the confidence in the interpretation for this test is low. The result of this was a low and high case permeability that varied by 41 and 67% from the calculated value respectively
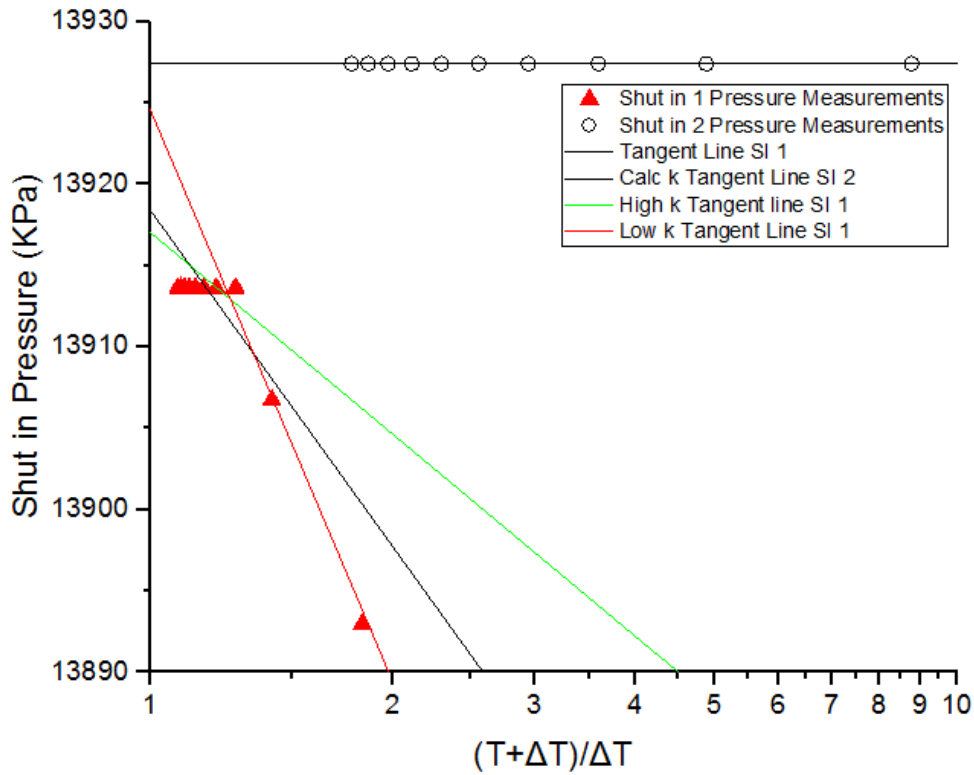
Figure 2-16: Horner plot for DST 1 from 141/13-22-034-01W3 conducted in dirty sands of the Deadwood Formation

Regression analysis (Figure 2-17) was undertaken on this well test with analysis conducted on a variety of pressure vs time measurements. In this low confidence test the line fitting is ambiguous and as a result the R^2 value of the manual line fitting from shut in time 12-24 of 0.726 is somewhat lower than the automated regression analysis value of R^2=0.89

27
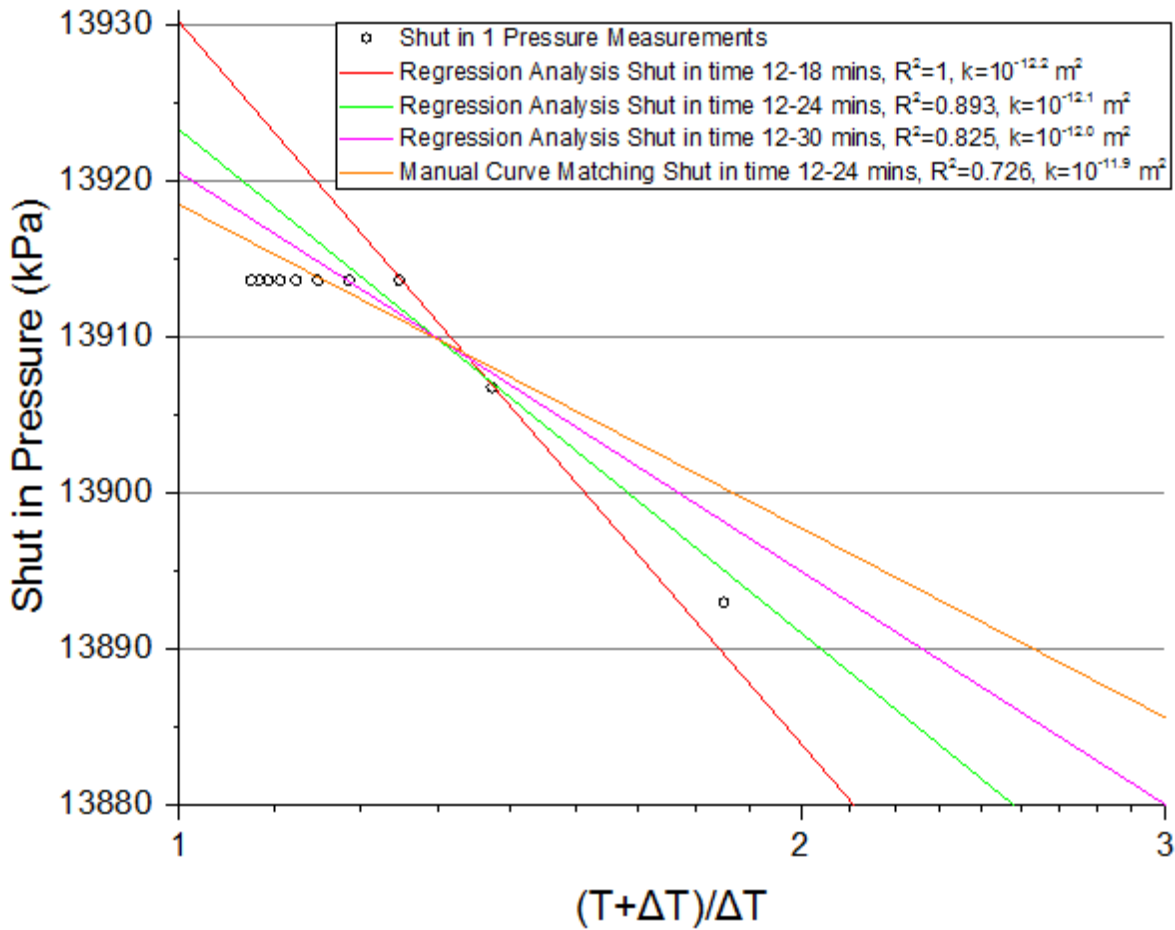
Figure 2-17: Horner plot for DST 1 from 141/13-22-034-01W3, regression analysis plot with manual line fitting with R^2 values

Through the sensitivity analysis conducted in all of the DSTs tested in the Winnipeg and Deadwood formations it was observed that there was a higher degree of variability in the low and high case permeabilities for the medium and low confidence tests than for the high confidence tests (Table 2-4). The exception to this being the medium confidence Winnipeg Formation tests, where the high sensitivity variability is higher than in the low confidence tests. However, it should be noted that the Winnipeg medium confidence tests are highly skewed from the well 19 (UWI 133/03-06-005-21W2) DST 3 test where the high end permeability interpretation was 525 % higher than the calculated permeability. If this test is omitted the medium confidence high k sensitivity is only 31%. Further examples of high, medium and low confidence DSTs are available in Appendix E.

Table 2-4: Winnipeg and Deadwood formations DST Horner Plot Sensitivity Analysis Distribution

Winnipeg Formation			Deadwood Formation		
Confidence Level	Low k Sensitivity %	High k Sensitivity %	Confidence Level	Low k Sensitivity %	High k Sensitivity
High	-10.7	14.4	High	-8.3	11.7
Medium	-16.4	50.9	Medium	-15.0	23.5
Low	-30.0	50.0	Low	-37.3	50.0

2.5.3 Falloff Test Analysis

Falloff test records for the injection wells obtained from IRIS were analyzed in order to determine formation permeability, radius of investigation of the tests, wellbore skin effects and static formation pressure (EPA 2002). In the analysis of the falloff tests the Horner, Miller Dyes Hutchinson (MDH) and Agarwal time functions were all plotted against the pressure measurements taken during the shut in period. In each of the falloff tests the three different time function methods yielded similar results. For the time function calculations, q (injection rate prior to shut in) and v_p (injection volume since last pressure equalization) are needed (EPA 2002). These values were obtained from AccuMap (IHS AccuMap 2016). A benchmark value of 400 hours or less of injection for a month or the last falloff test was considered to be the last time of pressure equalization for a particular well for calculating the volume injected since the last pressure equalization.

Annual falloff tests were generally available for each of the injection wells at each respective mine site. For the purposes of this study the first reliable falloff test since injection began was taken to calculate the permeability of the injection interval in the well. In later tests, millions of cubic metres of brine injection have likely affected the conditions of the formation. In well 51 (Potash Corp Cory mine well 111/13-07-036-06W3), the first falloff test was recorded in June 1999. The falloff pressure measurements were plotted against the Horner time function (Figure 2-18), and a resultant fitted line was matched to the late time data and extrapolated to infinite shut in time ($\frac{Tp+\Delta T}{\Delta T}$=1). The resultant slope was found to be 345 $\frac{kPa}{cycle}$.
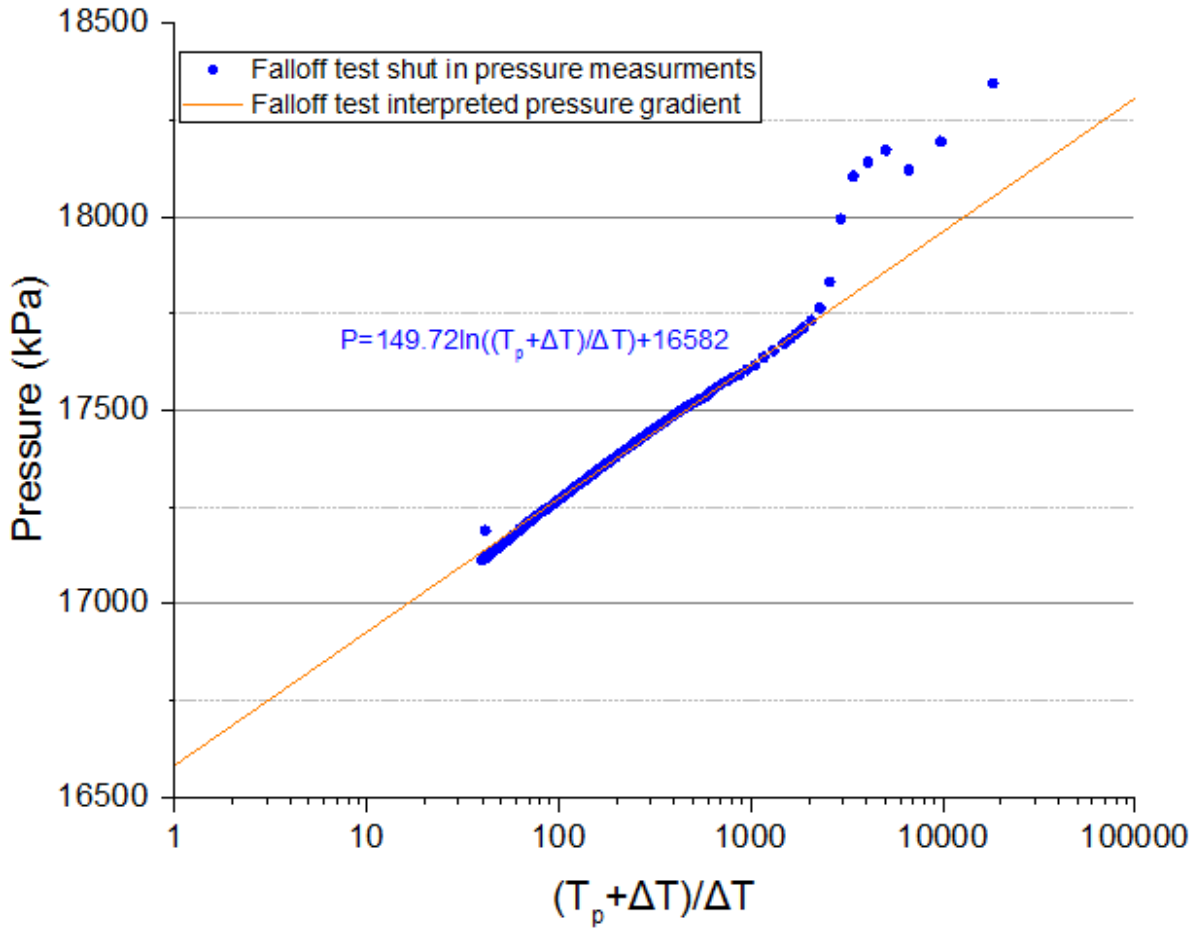
Figure 2-18: Horner plot for well 51 (111/13-07-036-06W3) 1999 falloff test data.

The flow rate (q) for this test was found in AccuMap (IHS AccuMap 2016) as the average flow rate for June 1999, which was 4385.4 $\frac{m3}{day}$ (5.08x10^{-2} $\frac{m^3}{s}$). The formation volume factor was taken as 1 $\frac{rcm}{stcm}$ for water. The transmissibility was then calculated using equation 2.8.

$$TB_{Aquifer} = \frac{0.1857 \times (5.08 \times x10^{-2} \frac{m^3}{s}) \times (1.0\frac{rcm}{stcm})}{344\ 740\frac{Pa}{cylce}} = 2.7 \times 10^{-8} \frac{m^4 s}{kg}$$

The formation water viscosity was estimated at 9.54x10^{-3} $\frac{kg}{m*s}$ using Kestin et al. (1981). This was based on the midpoint injection temperature of 42 °C (estimated from DST temperature recordings at mine site) the static formation pressure of 17405 kPa estimated from the falloff test and the salinity of the formation water (250 000 $\frac{mg}{L}$) estimated from the DST water samples in the area. The net pay injection (sand intervals with gamma-ray values <75 API) was found to be 35.9m, representing the sand thickness within the perforated injection intervals between 1556-1665m MD. From these parameters the formation permeability was estimated using equation 2.4.

$$k = \frac{2.73 \times 10^{-8} \frac{m^4 s}{kg} \times (9.54 \times 10^{-4} \frac{kg}{m \times s})}{35.9\ m} = 7.3 \times 10^{-13} m^2 = 10^{-12.1}\ m^2$$

2.5.4 Formation Compressibility Estimation

2.5.4.1 Hall 1953 Compressibility Estimation

      Porosity values obtained from neutron logs and core within the Deadwood and Winnipeg formations were used to estimate the aquifer skeleton compressibility using the Hall (1953) empirical correlation. In well 56 (PCS Cory mine injection well 121/03-21-035-08W3), core extracted from the Deadwood Formation exhibited an average porosity of 0.21. For DST 7, conducted in this well within the Deadwood Formation, the aquifer skeleton compressibility was estimated using equation 2.10 as follows.

$$c_{pore} = \left(\frac{1.782}{0.21^{0.438}}\right) \times 10^{-6} = 3.53 \times 10^{-6}\ psi^{-1} = 5.12 \times 10^{-10}\ Pa^{-1}$$

The bulk compressibility was then able to be calculated based of the pore volume compressibility and the formation porosity estimated from core data and geophysical logs. The solid compressibility component in equation 2.11 was ignored in this calculation as it is considered to be negligible compared to the pore volume compressibility.

$$c_{bulk} = (0.21)(5.12 \times 10^{-10} Pa^{-1}) = 1.08 \times 10^{-10} Pa^{-1}$$

2.5.4.2 Sonic Log Compressibility Estimation

      In the Deadwood Formation there were limited numbers of wells with dipole sonic logs available. The only wells with such logs where in the Estevan area; i.e., the Aquistore observation well 141/05-06-002-08W2 and a Husky oil well 111/05-08-006-19W2. In these wells a relationship between the compressional and shear wave transit times was established as seen in Figure 2-19. This relationship was then extrapolated to other wells in the Winnipeg and Deadwood formations, where the shear wave transit times could be estimated based on the compressional wave transit times available from the borehole compensated logs. From this estimation, the Poisson's ratio and the dynamic Young's modulus could be calculated, and from this the formation compressibility was estimated.
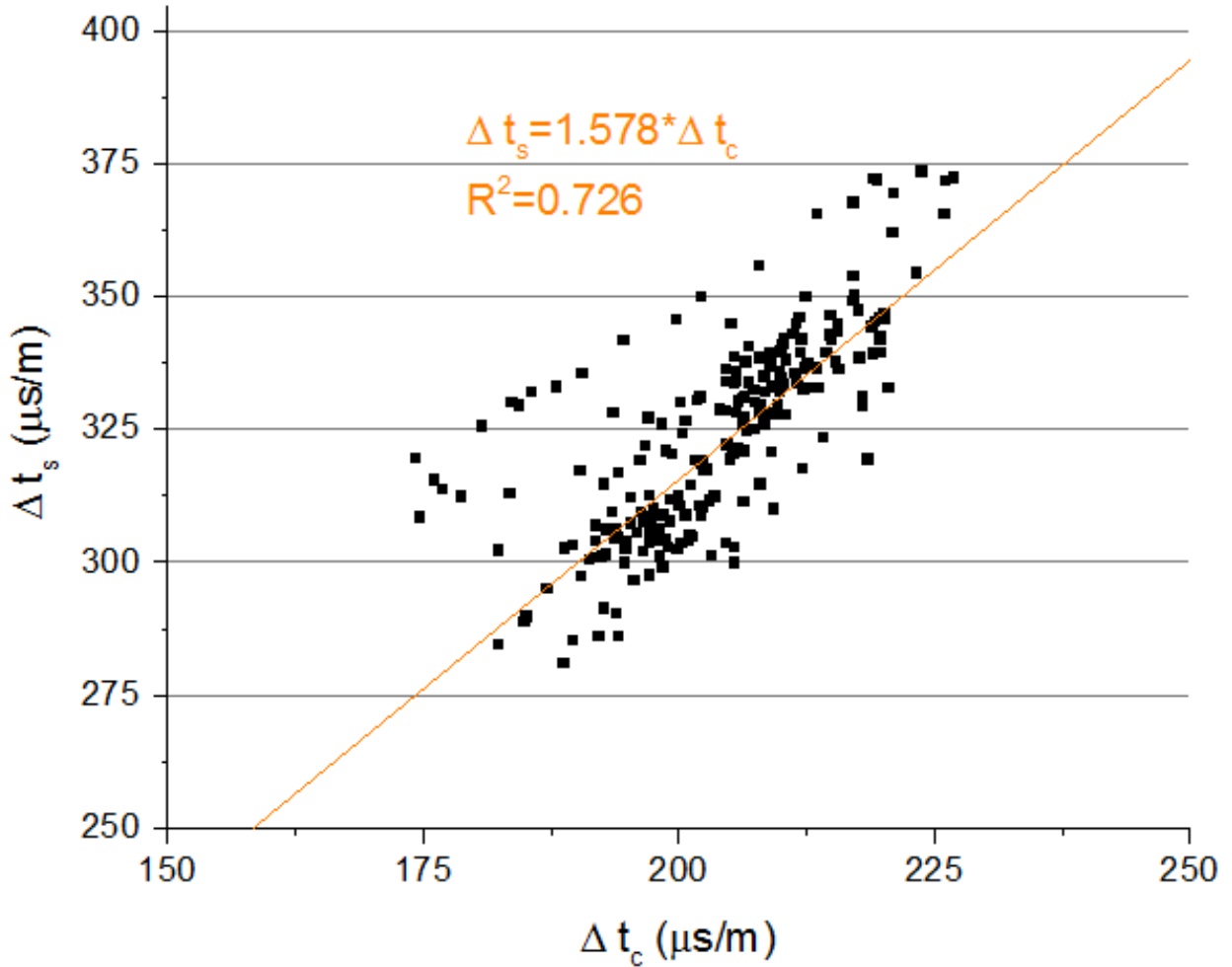
Figure 2-19: 111/05-08-006-19W2 dipole sonic log shear wave transit time (Δt_s) vs compressional wave transit time (Δt_c).

In the Cory mine well 56 (121/03-21-035-08W3) the Deadwood formation compressibility was estimated using the relationship between the shear wave and compressional wave travel times from dipole sonic logs from two wells in the Deadwood Formation in the Estevan area.

In order to calculate formation compressibility the Poisson's ratio between the shear wave and compressional wave travel times was calculated using equation 2.12, as follows:

$$v_d = \frac{0.5\left(\frac{458.97\,\frac{\mu s}{m}}{290.86\,\frac{\mu s}{m}}\right)^2 - 1}{\left(\frac{458.97\,\frac{\mu s}{m}}{290.86\,\frac{\mu s}{m}}\right)^2 - 1} = 0.16$$

From the Poisson's ratio and the bulk density from the geophysical logs the dynamic Young's modulus of the material was calculated using equation 2.13, as follows:

32

$$E_d = \frac{2264.72 \frac{kg}{m^3}}{0.00029 \frac{s}{m}} \frac{(1-2(0.1644))(1+0.1644)}{(1-0.1644)} = 2.5 \times 10^{10} Pa$$

The dynamic Young's modulus is then converted to static Young's modulus using equation 2.14:

$$E_s = 0.6 \times 2.5 \times 10^{-10} \ Pa = 1.5 \times 10^{-10} \ Pa$$

The bulk modulus of the aquifer material is calculated with equation 2.15:

$$K = \frac{1.5 \times 10^{-10} \ Pa}{3(1-2(0.1644))} = 7.5 \times 10^9 Pa$$

The formation compressibility is taken as the inverse of the bulk modulus using equation 2.16:

$$c_b = \frac{1}{7.5 \times 10^9 \ Pa} = 1.3 \times 10^{-10} \ Pa^{-1}$$

The bulk compressibility was calculated throughout the sand intervals in the wells, and then averaged to calculate a representative bulk compressibility for the formation sand. These calculations were completed using the relationship between shear and compressional wave travel times in both of the wells with dipole sonic logs. The results between the two relationships were similar, and the results were averaged to obtain the representative bulk compressibility for the well.

2.6. Reservoir Characterization Results

2.6.1 Deadwood Formation Permeability

Through extensive analysis of core, DSTs and falloff tests within the Deadwood Formation the spatial and lithological trends of the permeability characteristics of this formation were able to be established. The results from each of the individual tests is located in Appendix F.

2.6.1.1 Deadwood Formation Core Permeabilities

Through analysis of the geophysical logs of the tested intervals the Deadwood Formation core was able to subdivided into groups based on lithology with tests either being considered clean sand (15-40 gamma ray API), dirty sand (40-75 API) or shale (75 API or higher). Through this analysis it was readily apparent that the clean sand core exhibited the highest permeabilities (average $10^{-12.4}$ m^2), with lower permeabilities in the dirty sands ($10^{-13.1}$ m^2) and even lower values in the shales ($10^{-14.0}$ m^2) (Figure 2-20).
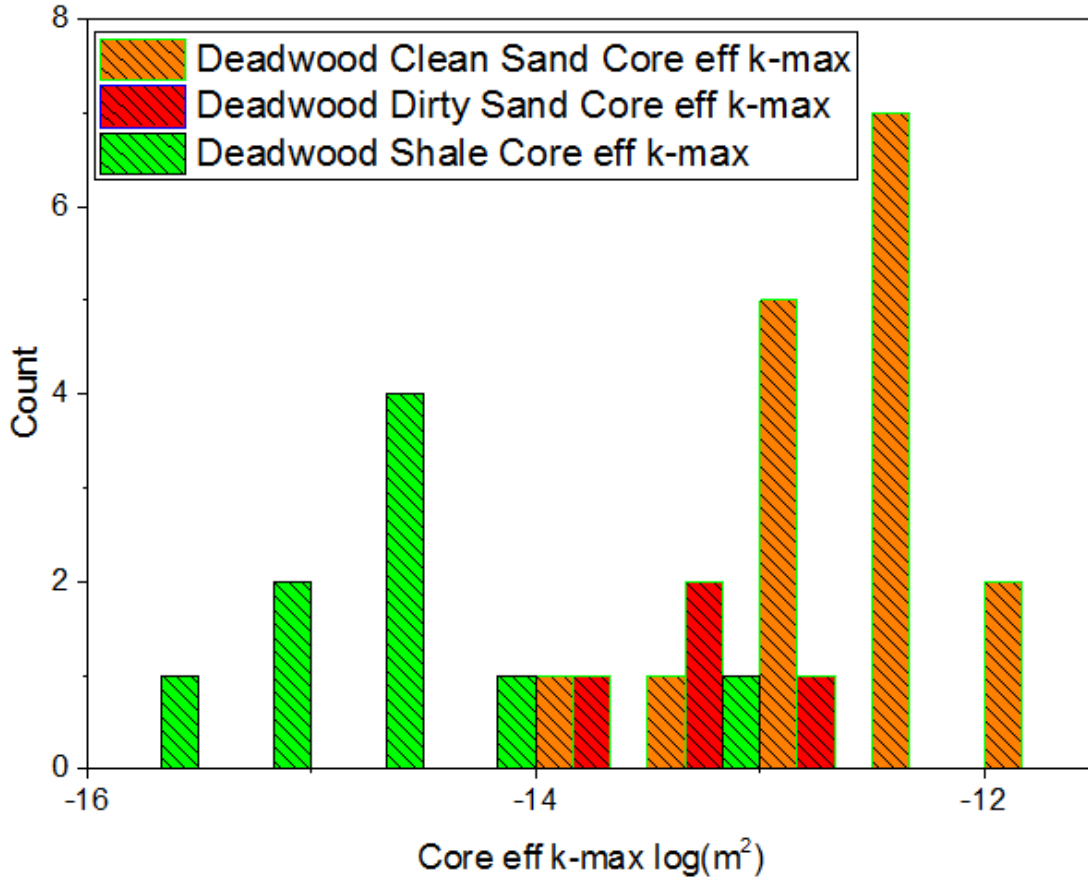
Figure 2-20: Deadwood Formation core permeability distribution

Throughout the study area there were significant spatial variations in the permeability values obtained from core (Figure 2-21). The lowest core permeabilities were observed in the Swift Current area, where the formation is more shale rich and the core was predominantly obtained from shale. An example is illustrated in Figure 2-22 for well 82 where the permeability values obtained were quite low ($10^{-14.4}$-$10^{-15.5}$ m^2).
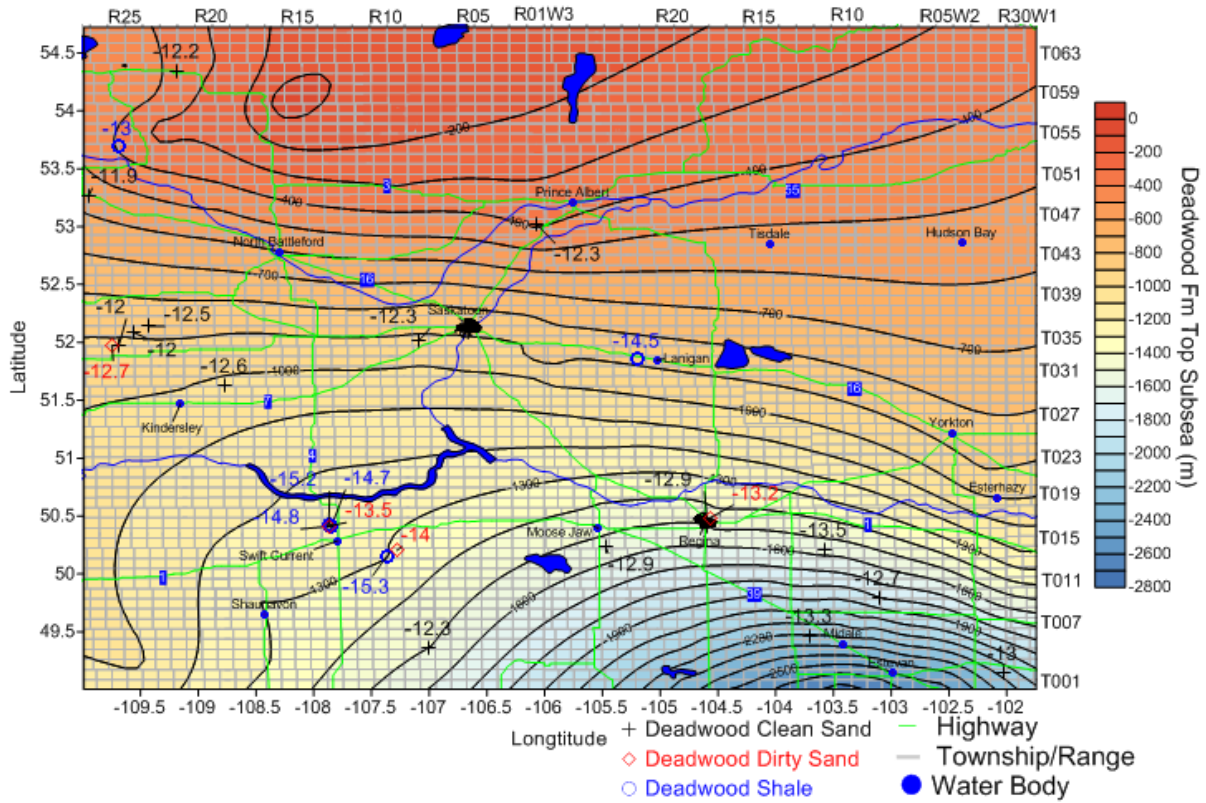
Figure 2-21: Deadwood Formation clean gamma ray and dirty gamma ray and shale core permeabilities distribution (log(m^2)), (core permeabilities were arithmetically averaged throughout each core interval) with Deadwood Formation structure (metres subsea).
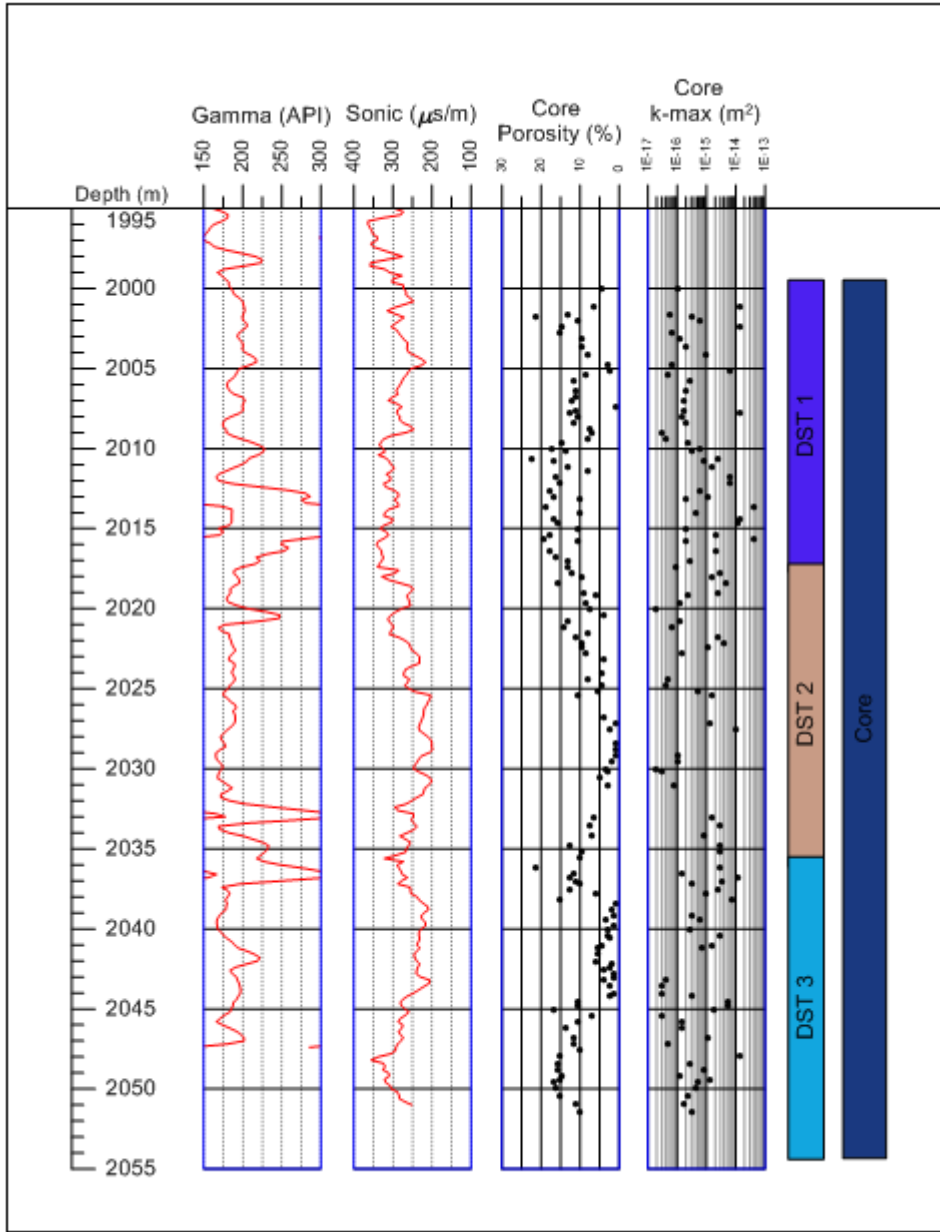
Figure 2-22: Geophysical logs for well 82, (UWI 101/03-10-017-14W3) in the Swift Current Area. Core analysis porosity and k-max permeability included. Note that the gamma-ray scale is 150-300 API units.

In other areas of the province, Deadwood Formation core exhibited relatively high permeabilities. An example from the Kindersley area in the southwest of the study area for core extracted from the Deadwood Formation sands is illustrated in Figure 2-23 (well 60). In this well, core extracted from moderately clean sands (30-50 API) exhibited an arithmetically averaged k-max of $10^{-12.0}$ m^2. Other tests in this area indicated lower permeabilities; however, these tests were primarily conducted in shales. The limited core data in the Saskatoon area also showed higher permeabilities, with a core taken from a clean sandstone having a permeability of

$10^{-12.3}$ m^2 (Figure 2-20). In the deeper areas of the basin near Estevan, the core data illustrated fairly low permeabilities ($10^{-13.4}$ - $10^{-12.7}$ m^2), despite being obtained from clean sands.
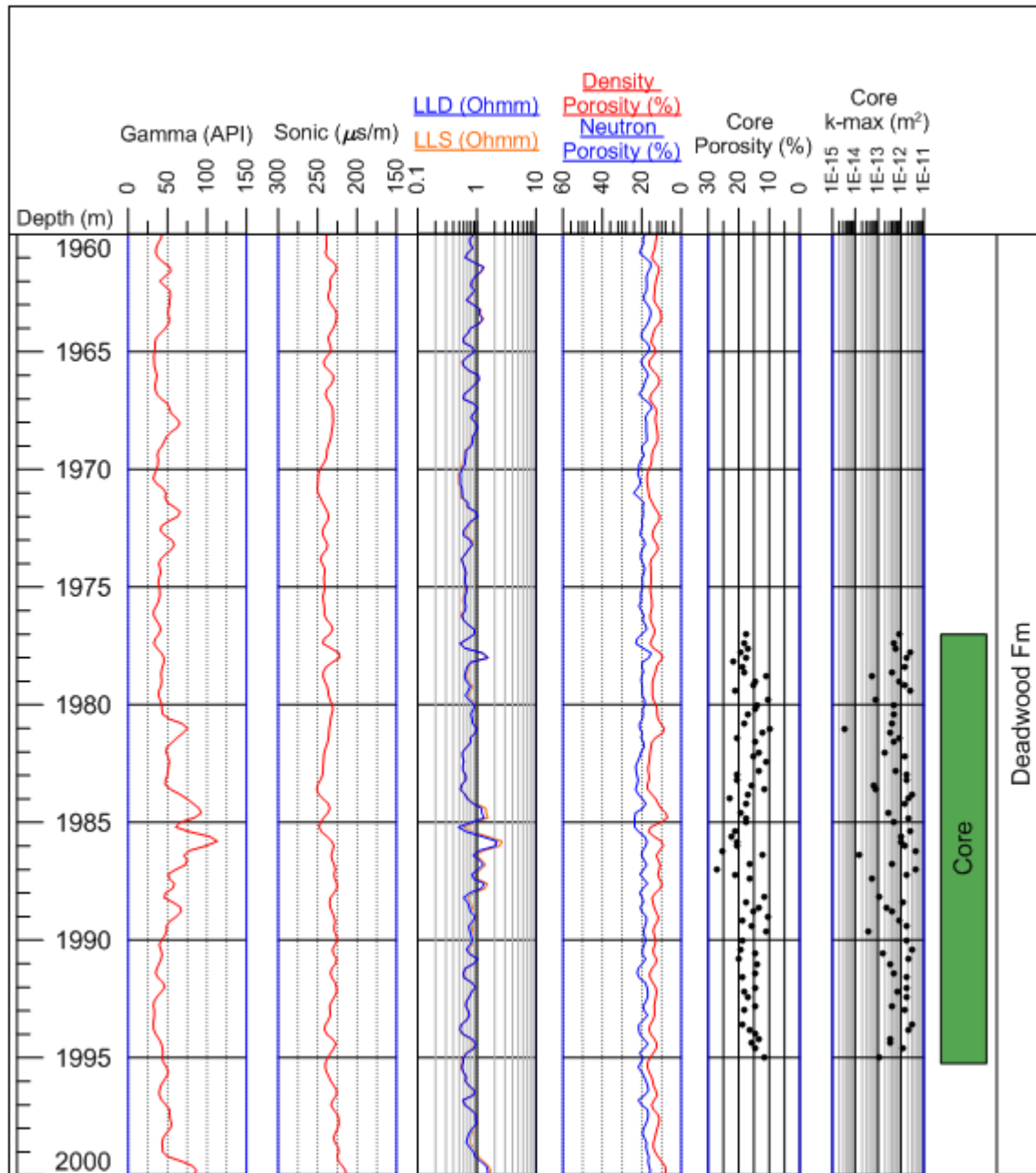
Figure 2-23: Geophysical logs for well 60, (UWI 141/03-18-036-25W3) in the Kindersley Area with core porosity and permeability (k-max)

2.6.1.2. Deadwood Formation Drill Stem Test Permeabilities

The Deadwood Formation DSTs, when subdivided into clean sand, dirty sand and shale, exhibited a permeability distribution similar to the core data, with the clean sands generally having higher permeabilities (average $10^{-11.9}$ m^2) with slightly lower values in the dirty sands

(average $10^{-12.1}$ m^2) and lower permeabilities in the shale intervals (average $10^{-13.0}$ m^2) (Figure 2-24).
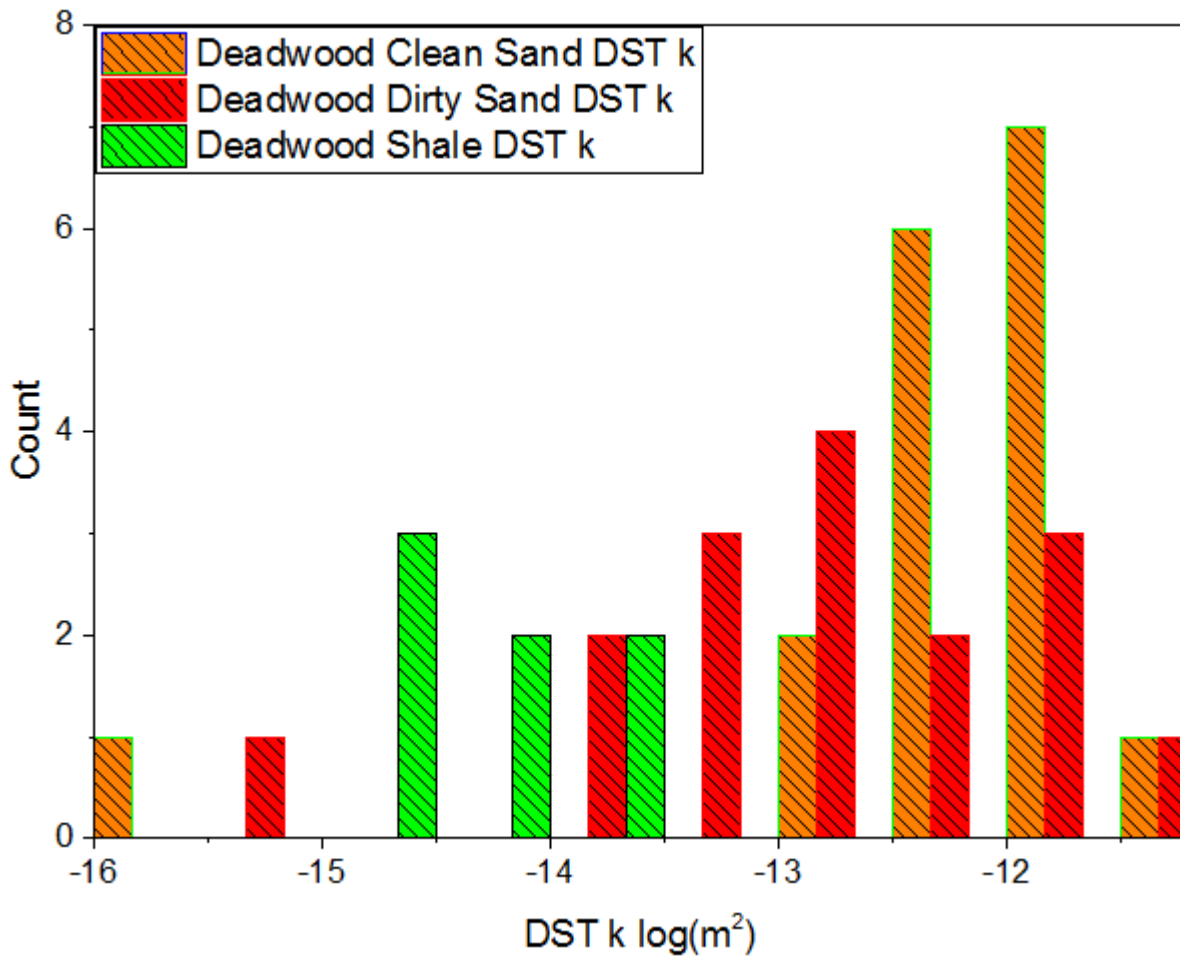
Figure 2-24: Deadwood Formation DST permeability distribution

As with the core, the DSTs exhibited significant spatial variations in permeability (Figure 2-25). The highest values occurred in the Saskatoon area, an area of extensive potash mining activity. In this area, the Deadwood Formation exhibited 30-40 API as well as 40-75 API gamma ray sands. Though these are not the cleanest sands, the permeabilities were quite high (in the range of $10^{-11.3}$-$10^{-13.3}$ m^2). The neutron porosity readings were generally quite high for the sand intervals as well (20-25%). A typical profile of a DST in this area is demonstrated in Figure 2-26 where the permeability was found to be $10^{-12.3}$ m^2 in well 56. Well 56 being an injection well, the completed intervals available for injection are shown by the perforated intervals. Only the quality sand intervals were completed for injection and not the high gamma-ray shales, as these intervals do not have adequate permeabilities to accept injected fluids.

Figure 2-25: Deadwood Formation clean and dirty sand and shale DST permeability distribution ($\log(m^2)$) with Deadwood Formation structure (metres subsea)
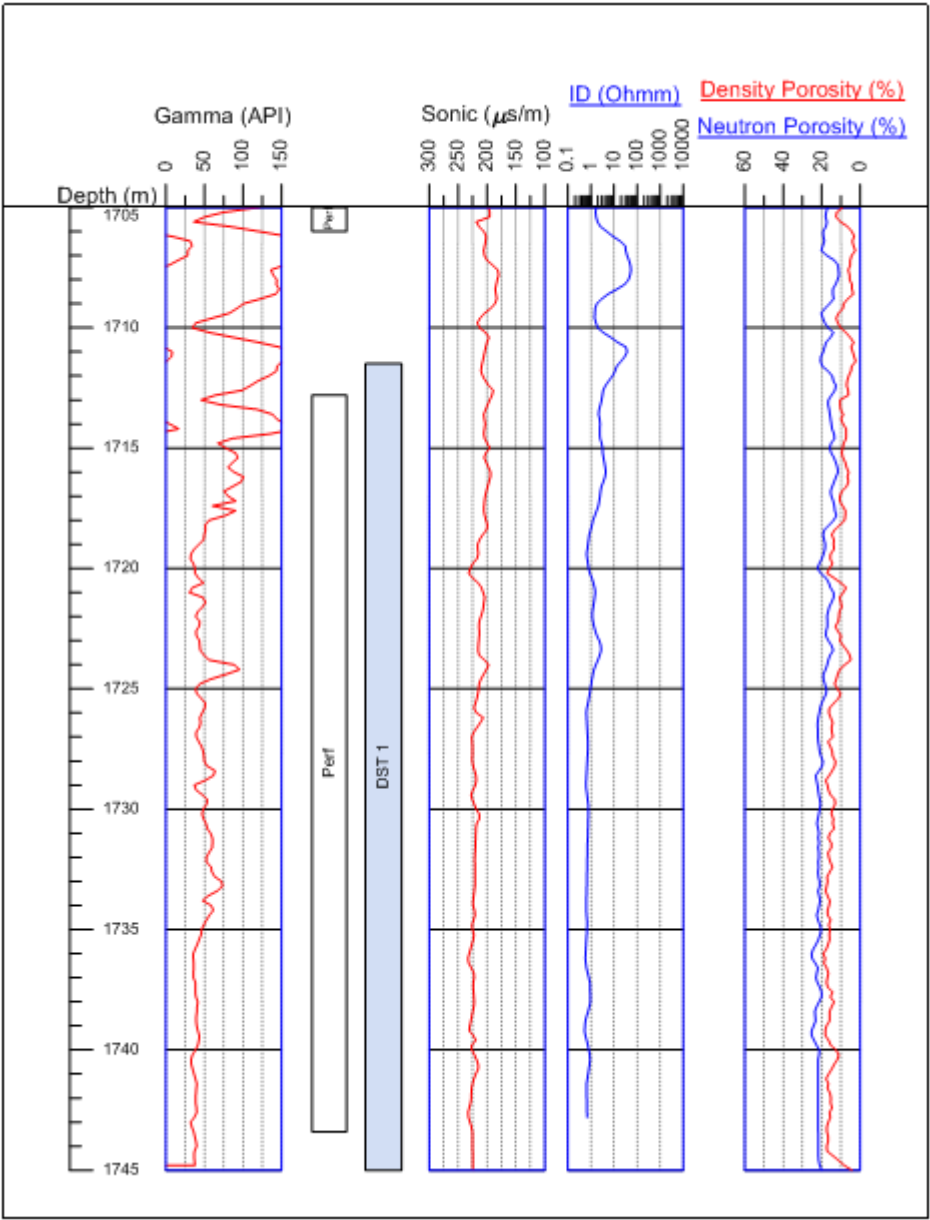
Figure 2-26: Geophysical logs for well 56, (UWI 121/03-21-035-08W3) DST 1 in the Saskatoon Area, wrap around gamma values indicate values greater than 150 API, scale becomes 150-300 API.

2.6.1.3. Deadwood Formation Falloff Test Permeabilities

The intervals tested in could not be classified as clean or dirty sands as the tests were carried out over very large intervals (in the hundreds of metres), encompassing a wide variety of lithologies in each test . The falloff tests were primarily located in the Saskatoon area (Figure 2-27), an area containing many potash properties including Potash Corp mines Cory, Allan, Lanigan and Patience Lake, the Agrium Vanscoy mine and Mosaic Colonsay mine. The falloff

test average permeabilities in this area were high at $10^{-12.1}$ m^2, therefore these tests were likely heavily influenced by the clean gamma ray sands within the injection intervals of these wells.
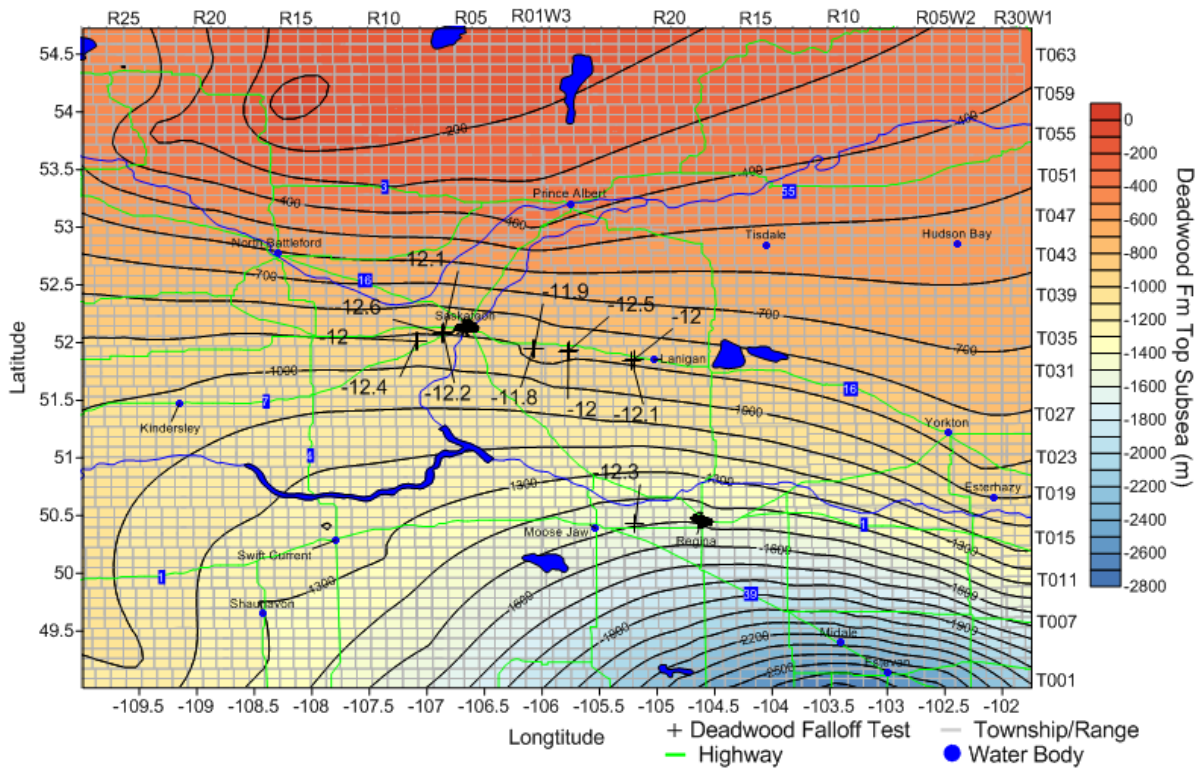
Figure 2-27: Deadwood Formation Falloff Test permeability distribution (log(m^2)) with Deadwood Formation structure (metres subsea)

2.6.1.4. Deadwood Formation Core vs DST vs Falloff test permeabilities

Overall the falloff tests exhibited higher permeabilities than those seen is DSTs or core (Figure 2-28). However, the falloff tests exhibit some bias, as the injection wells in which the tests where conducted are generally located in areas of higher permeability of the Deadwood Formation as confirmed by core and DSTs in these areas. Within the Saskatoon area, where most of the falloff tests were located, the average falloff test permeability was $10^{-12.1}$ m^2, which is in fairly close agreement with the average clean sand DST permeability of $10^{-11.8}$ m^2 in the area, and the core permeability of $10^{-12.3}$ m^2.
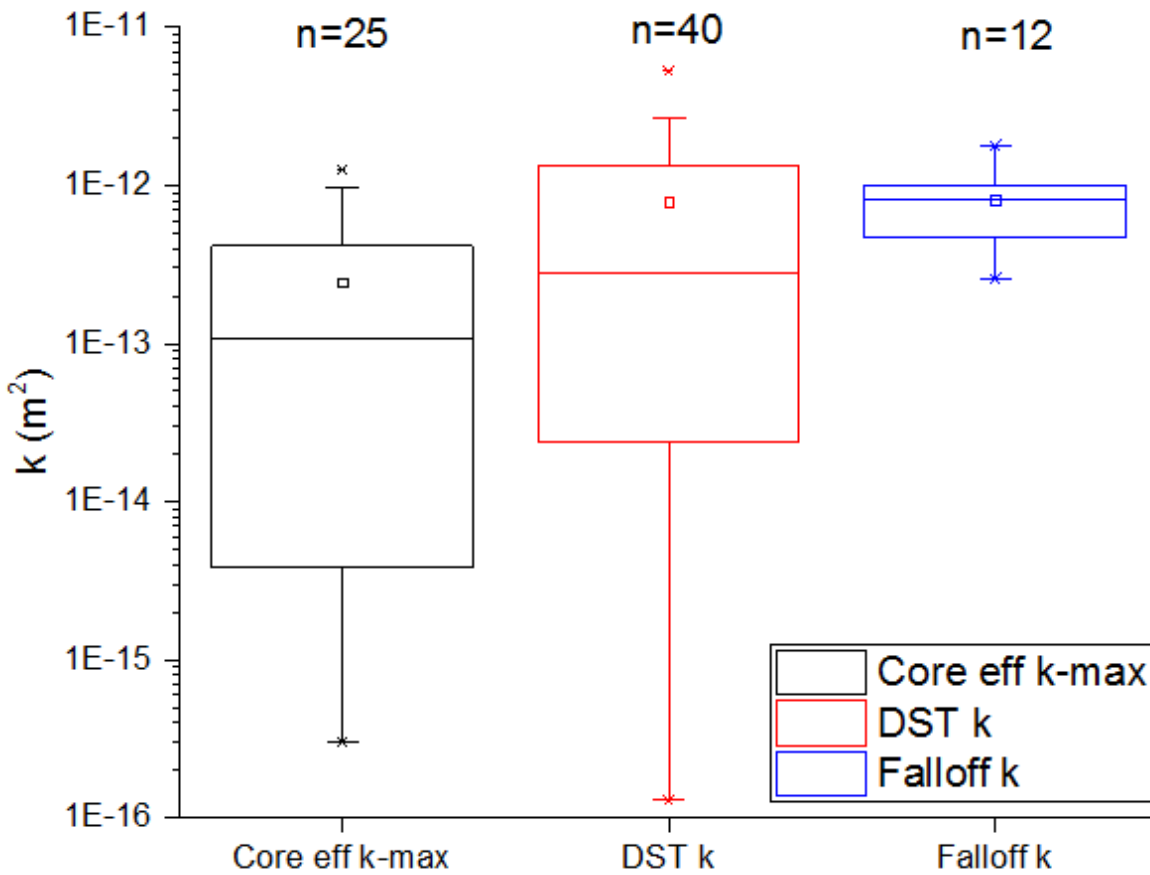
Figure 2-28: Box and whisker plot of Deadwood Formation DST, core and falloff test permeability, small middle box indicates mean, middle line indicates median, upper and lower bounds of large box indicate 25 and 75% quartiles, and whisker ends indicate 5 and 95% values

2.6.1.5 Deadwood Formation Drill Stem Test Permeability vs Radius of Investigation

   The relationship between permeability and radius of investigation of the DSTs is seen in Figure 2-29. The higher permeability values are matched with larger radii of investigation, as a higher permeability formation would more readily transmit fluids into the wellbore during a DST and fluids would be able to be drawn from a larger radius around the wellbore in the allotted time of the test. The relationship between k and RI is a power law correlation with an R^2 value of 0.397 with a P-value of 1.33×10^{-5}, providing a fairly strong correlation.
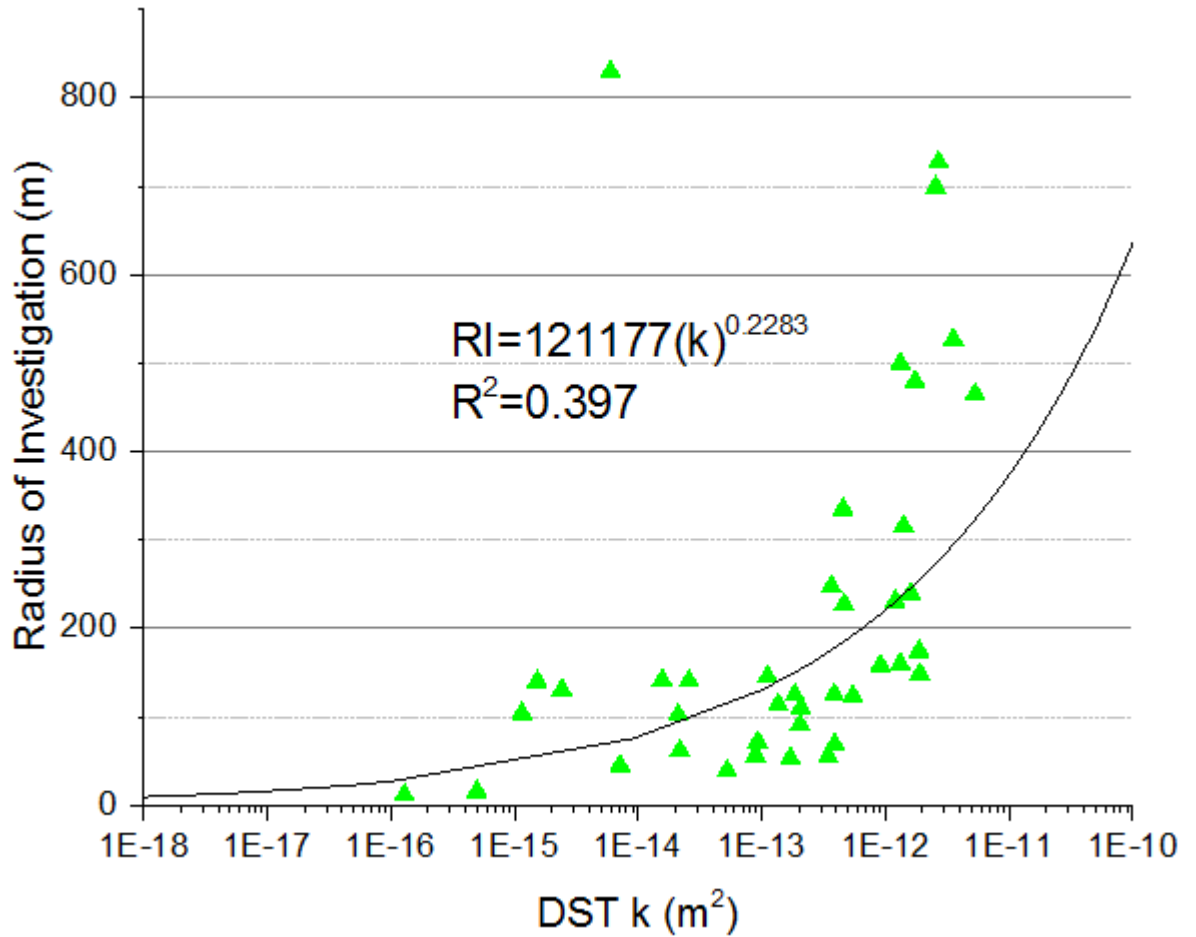
Figure 2-29: Deadwood Formation DST permeability vs radius of investigation, demonstrating a power law relationship with an R^2 value of 0.397 and a P-value of 1.33×10^{-5}, radius of investigation (RI) (m) can be calculated using inset equation $RI=121177(k)^{0.2283}$

2.6.1.6 Deadwood Formation Gamma-Ray vs Permeability

The relationships between the gamma-ray values (API) logged in the DST and cored intervals and permeability are illustrated in Figures 2-30 and 2-31. The figures show a trend of permeability decrease with gamma-ray increase. This trend is expected, as an increase in gamma-ray API means increased shale content, with a consequent decrease in permeability. The correlation is stronger for cores than DSTs. Using exponential equations shown in these figures, permeability values can be roughly estimated from observed gamma-ray API values.
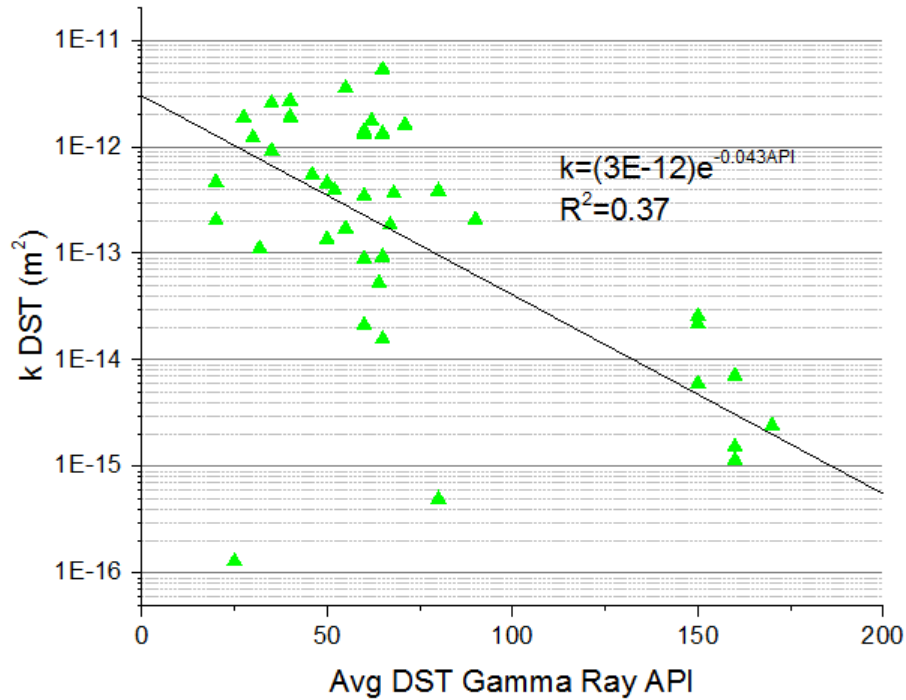
Figure 2-30: Deadwood Formation DST interval average gamma-ray API values vs DST permeability, with an R^2 value of 0.37 and P-value of 1.65×10^{-7}, indicating a significant correlation
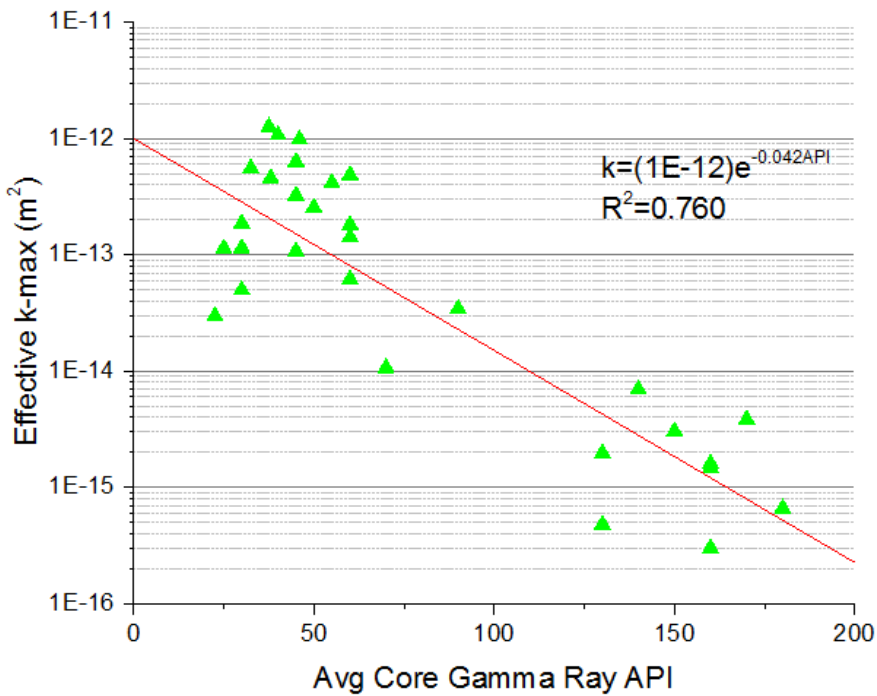
Figure 2-31: Deadwood Formation core average gamma-ray vs effective k-max permeability, exhibiting an exponential relationship with an R^2 value of 0.76 and a P-value of 7.3×10^{-10} indicating a strong relationship

2.6.1.7 Deadwood Formation Compressibility vs Depth

The Deadwood Formation bulk compressibilities calculated using sonic logs exhibited significant spatial variability throughout the province (Figure 2-32). It can be seen that the compressibilities are generally lower in the deeper parts of the basin in southeastern part of the study area. This is due to the increased overburden at these greater depths, resulting in higher compaction and lithification of the formation and thereby lower compressibilities. The compressibilities are significantly higher in the shallower areas of the basin including the Saskatoon area, the Esterhazy area and northwestern corner of the study area. The lower compressibilities observed in the Kindersley area can be accounted for by the fact that the Deadwood Formation sands (upon which the compressibility calculations are based) occur at significantly greater depths than indicated by the Deadwood Formation top, as the upper part of the formation is shale dominated in this area.
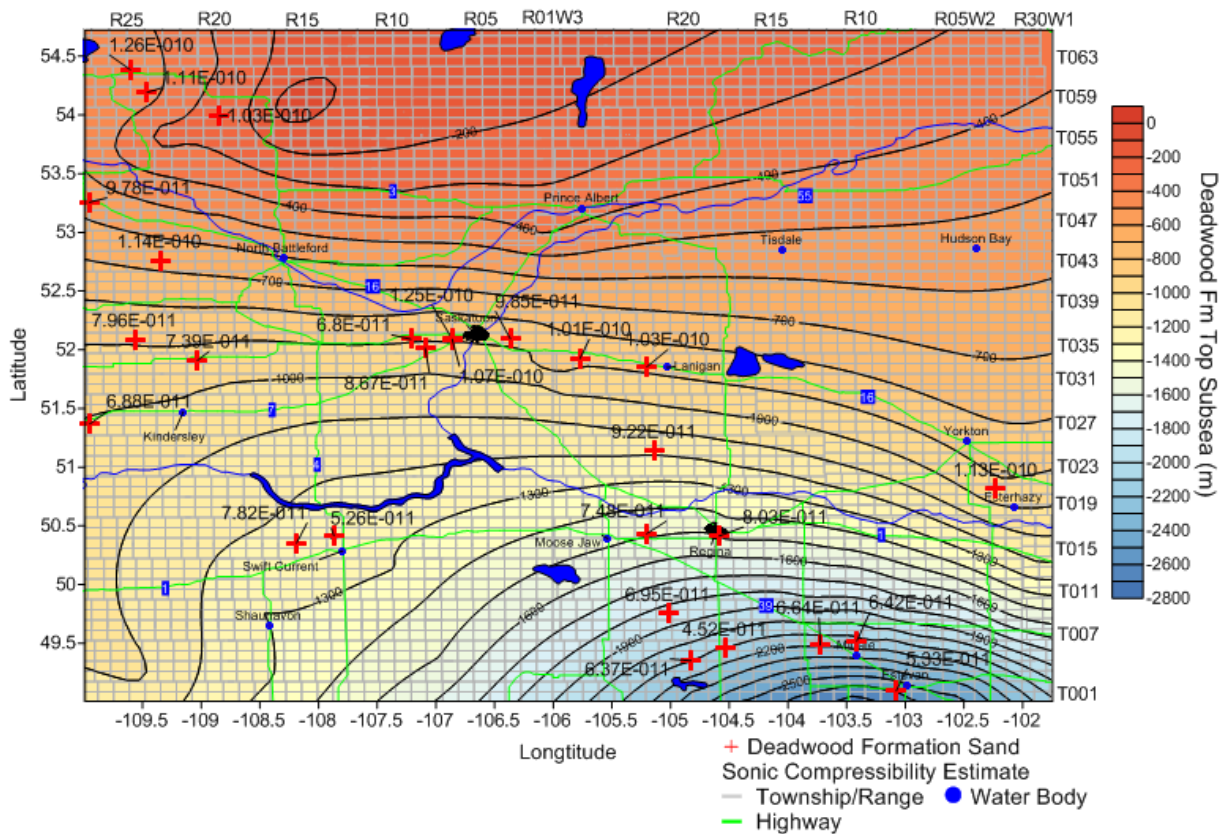
Figure 2-32: Deadwood Formation bulk compressibilities (Pa^{-1}) calculated from sonic logs with Deadwood Formation structure (metres subsea)

Figure 2-33, suggests a linear trend of decreasing compressibility with depth based on the sonic log measurements throughout the study area. From this relationship, an estimation of the Deadwood Formation bulk compressibility can be made based on subsea depth.
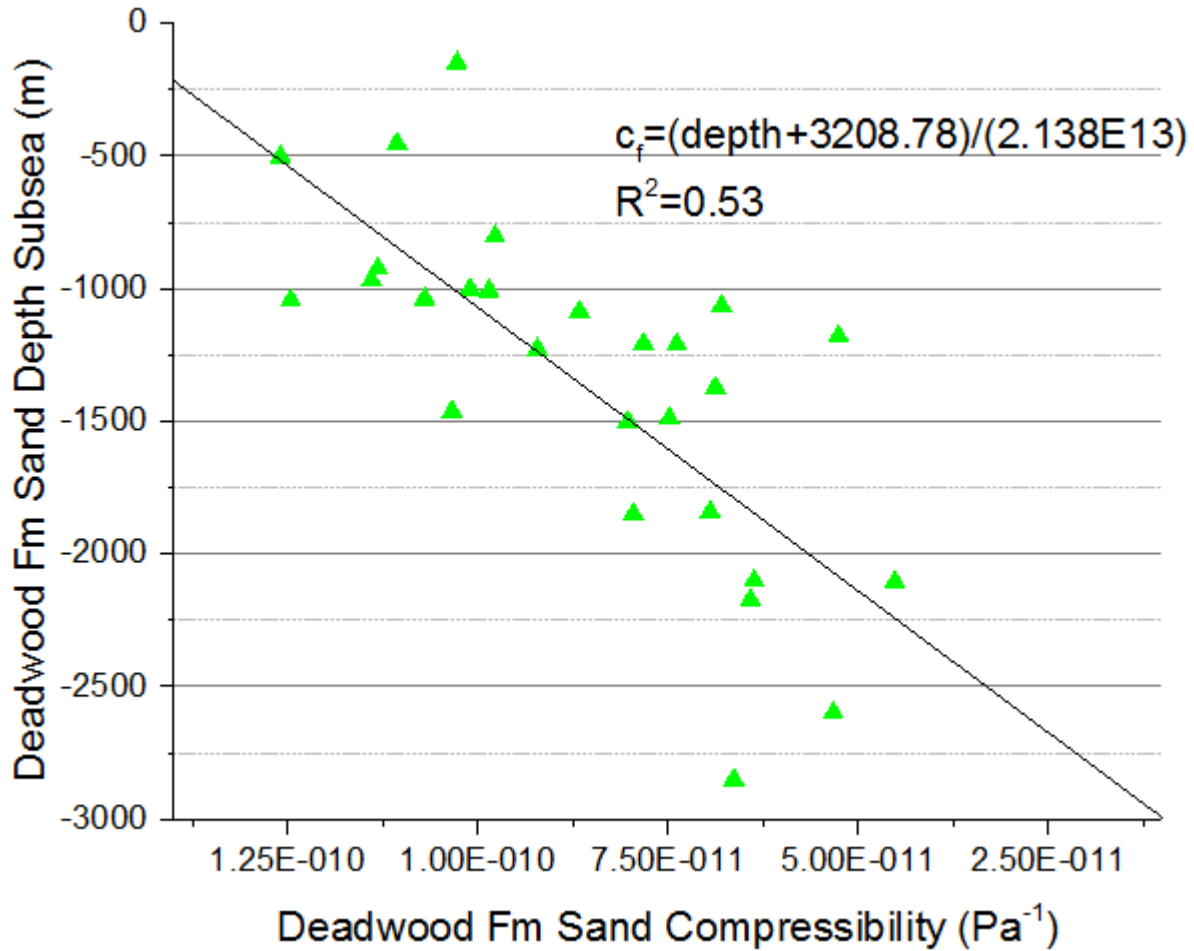
Figure 2-33: Deadwood Formation sonic log derived sand aquifer compressibility vs formation sand depth subsea (m) with an R^2 value of 0.53 and a P-value of 1.0×10^{-4}, a fairly strong correlation

2.6.2 Winnipeg Formation Permeability

The Winnipeg Formation in Saskatchewan was studied in detail through DSTs, core analysis and limited falloff test analysis throughout the province. The results from the core and DST analysis of the individual wells is located in Appendix G.

2.6.2.1 Winnipeg Formation Core Permeabilities

The limited core data available within the Winnipeg Formation indicated low permeabilities with an average of $10^{-13.0}\,m^2$. The lowest core permeabilities were observed in the southeast of the study area, near Estevan (Figure 2-34). Despite being extracted from clean sands the permeabilities were low ($10^{-15.0}$-$10^{-13.1}\,m^2$). As a result, the clean sand core permeability distribution is heavily skewed to lower values (Figure 2-35) with the clean sand core having a lower average permeability than the dirty sand core ($10^{-13.4}$ vs $10^{-12.4}\,m^2$ respectively).
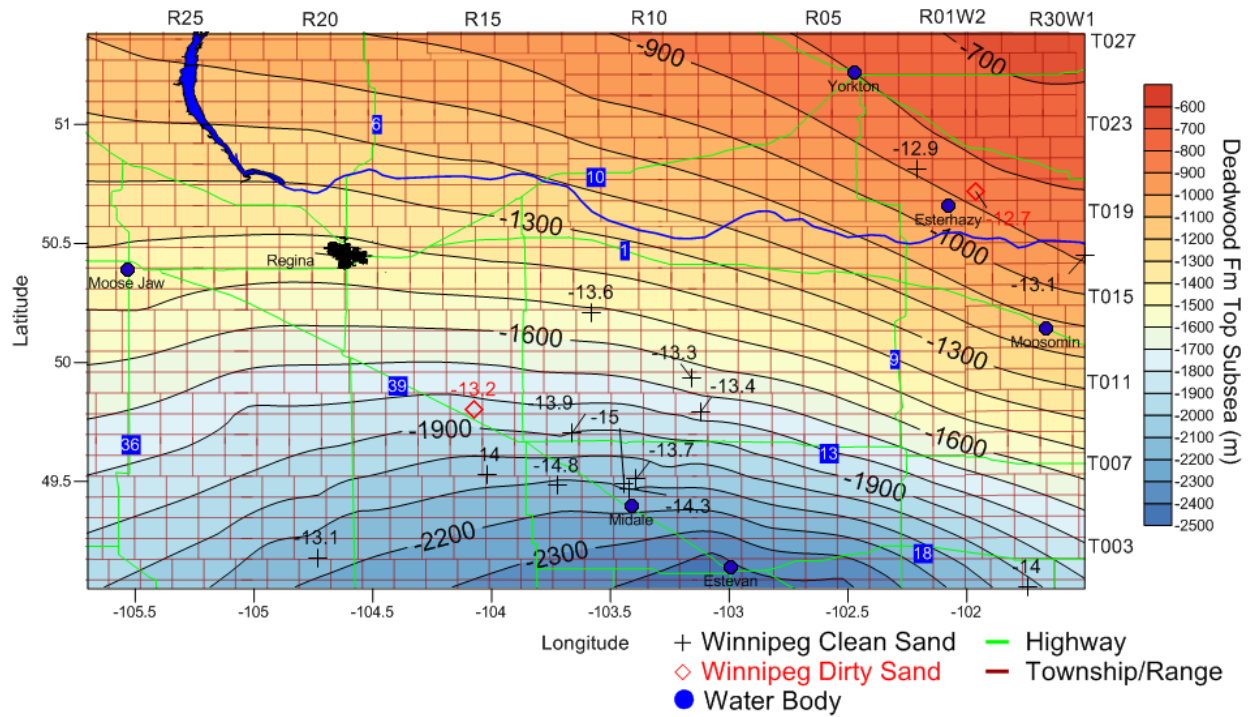
Figure 2-34: Winnipeg Formation core permeabilities (log (m^2)), (arithmetically averaged over cored intervals) with Winnipeg Formation structure (metres subsea)
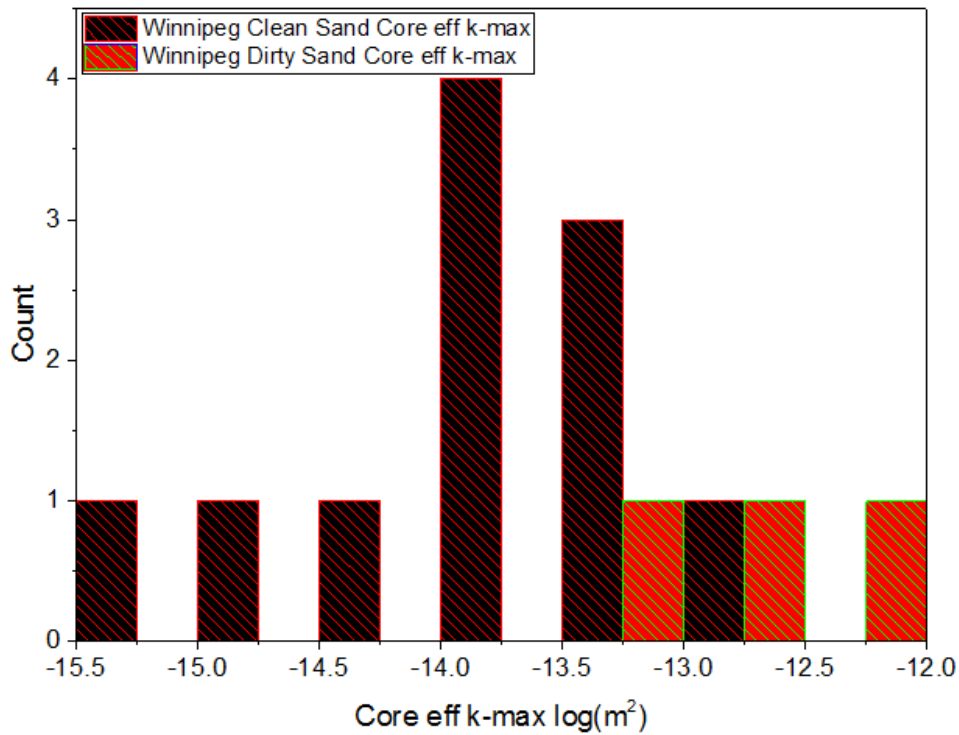
Figure 2-35: Winnipeg Formation Core Permeability Distribution

2.6.2.2 Winnipeg Formation Drill Stem Test Permeabilities

The Winnipeg Formation DSTs conducted throughout the study area exhibited a large range of permeabilities (Figure 2-36). As with the core, the DSTs in the Winnipeg Formation indicated a significant number of low permeability tests ($10^{-18.0}$- $10^{-13.4}$ m^2) conducted in clean sands in the Estevan area (Figure 2-37).
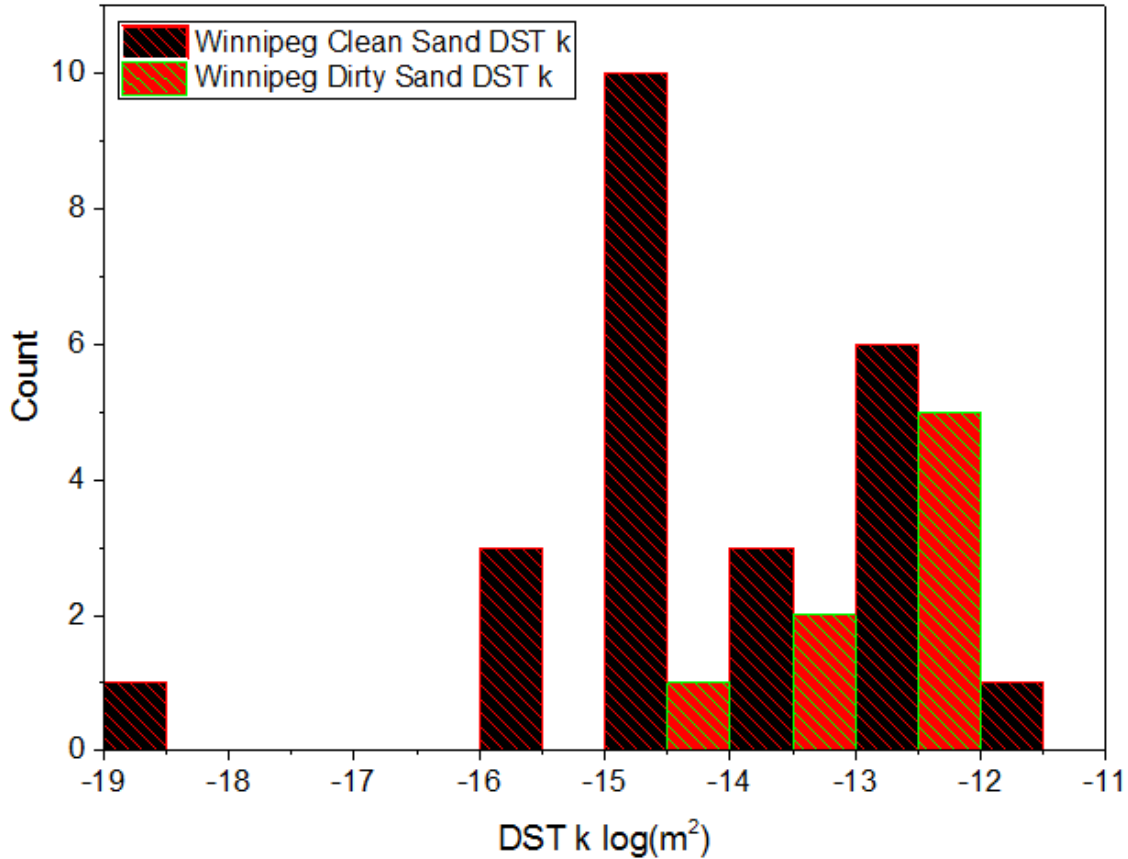
Figure 2-36: Winnipeg Formation DST permeability distribution
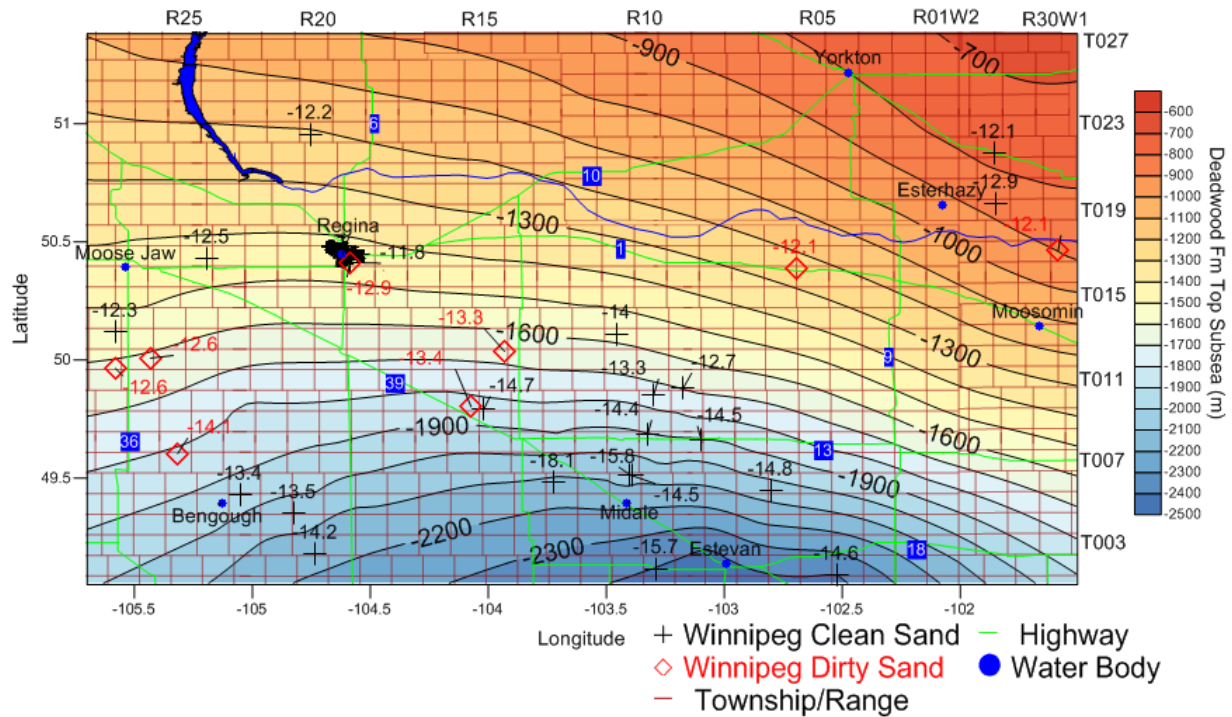
Figure 2-37: Winnipeg Formation clean and dirty sand DST permeability distribution ($\log(m^2)$)) with Winnipeg Formation structure (metres subsea).

In well 13 in the Estevan area, DST 1 (Figure 2-38) was conducted in a clean sand (25 gamma ray API), (shale interval not included in net pay), with approximately 15% neutron porosity, however the permeability was found to be only $10^{-14.0}$ m^2, quite low for a clean sand. There are likely lithological factors present in the formation in this area that are precluding permeability not readily apparent in the geophysical logs, such as quartz overgrowth cements.
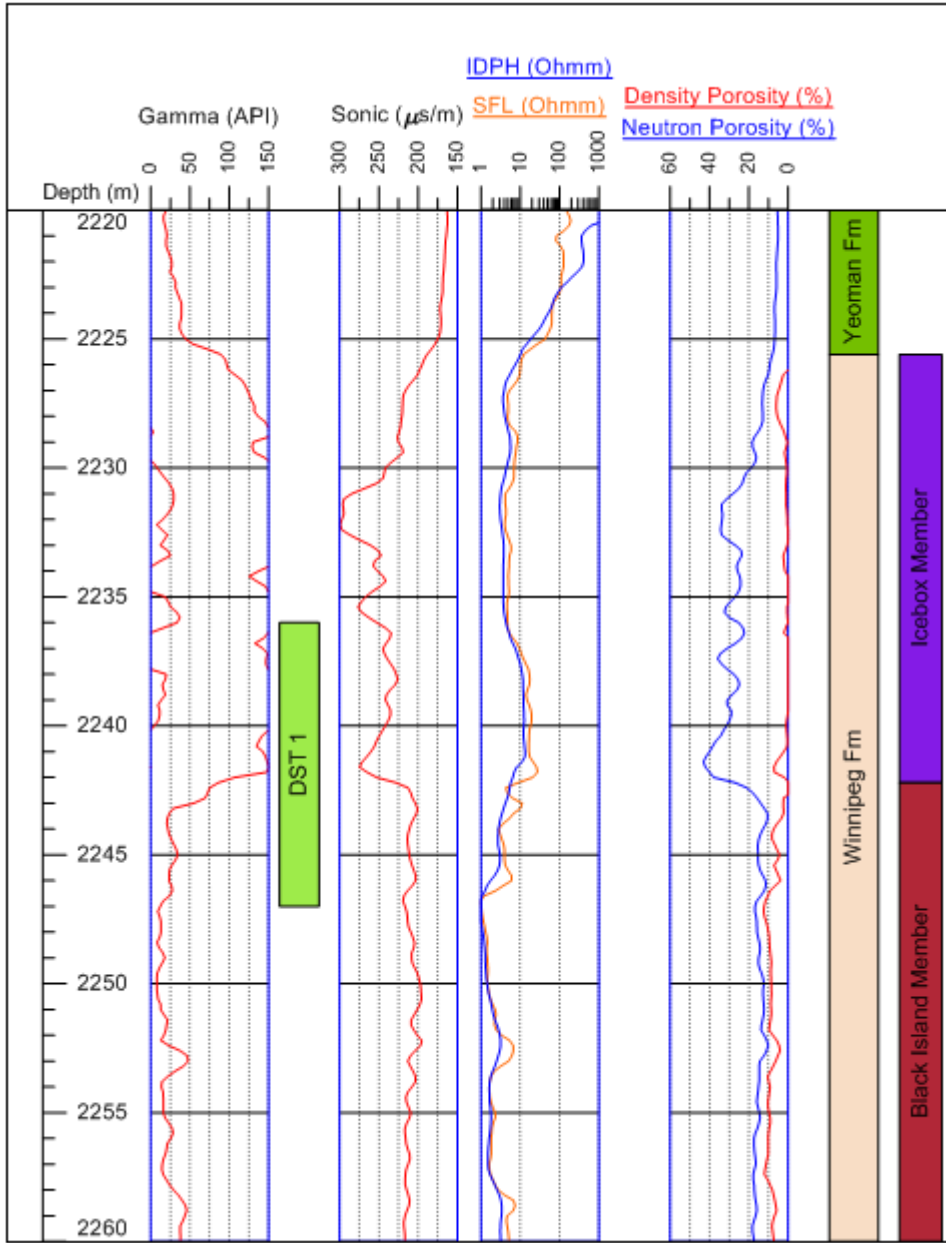
Figure 2-38: Geophysical logs for well 13, (UWI 121/06-28-013-11W2) DST 1, in the Estevan Area, wrap around gamma values indicate values greater than 150 API, scale becomes 150-300 API.

In the Bengough area (Fig 2-37), the log characteristics of the DST intervals were quite similar to those seen in the Estevan area; however, the permeability values were higher. In well 19 DST 3 (Figure 2-39) which was tested primarily in clean sands (20 gamma ray API), the calculated permeability was $10^{-13.5}\,m^2$, significantly higher than the values seen in the Estevan area. In the Bengough area there is likely not the same lithological factors precluding permeability as are present in the Estevan area.
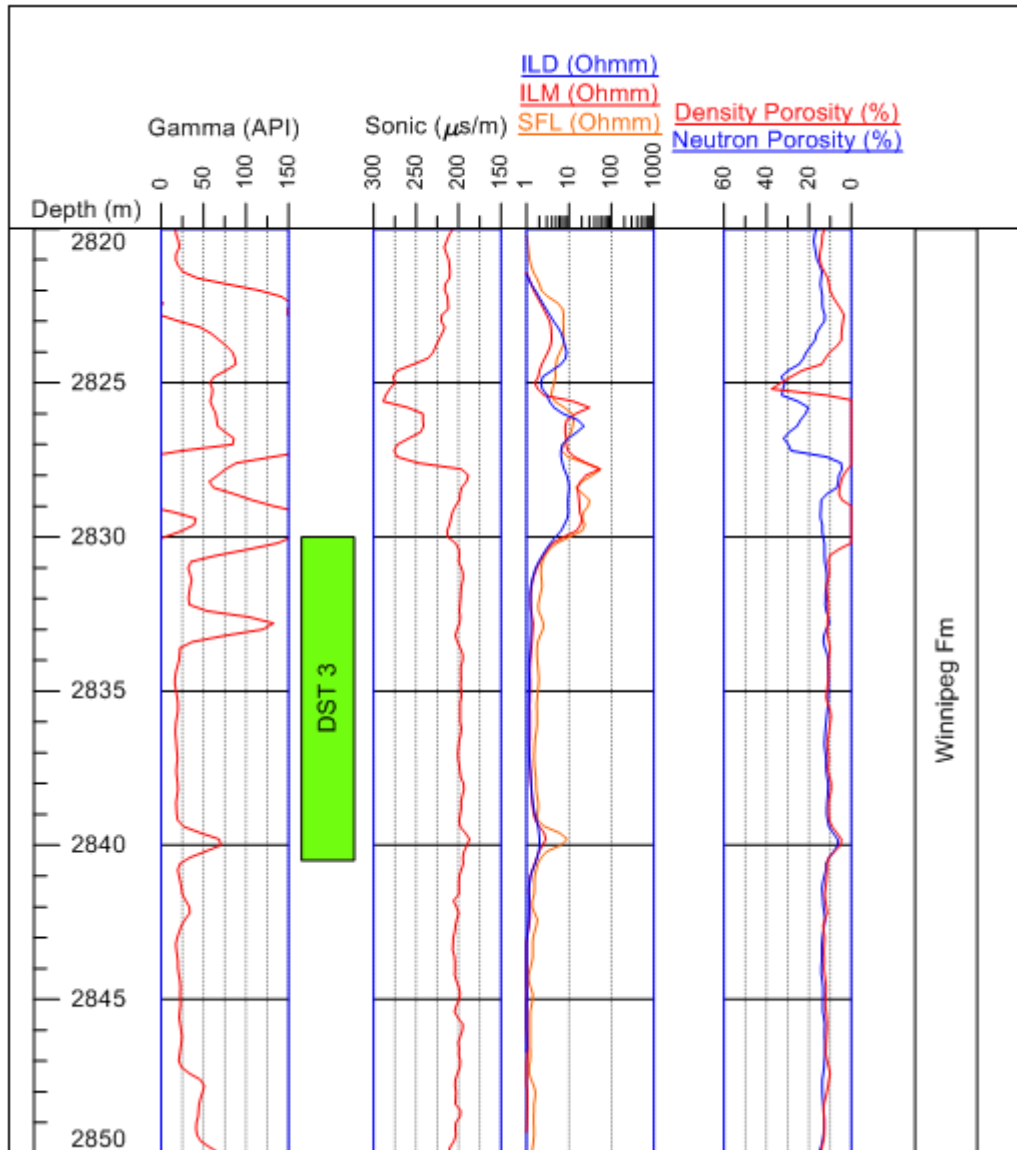
Figure 2-39: Geophysical logs for well 19, (UWI 133/03-06-005-21W2) DST 3 in the Bengough Area, wrap around gamma values indicate values greater than 150 API, scale becomes 150-300 API.

The Winnipeg Formation DST permeabilities are largely controlled by lithological factors. Generally, if the tests were conducted in clean (15-30 gamma ray API) sands the permeabilities were higher than those in dirtier sands that contain higher amounts of shales that would impede permeability. The exception being the tests taken in the southeast of the study area near Estevan, where tests conducted in clean sands exhibited low permeability values, the lowest values seen throughout the study area. The highest DST permeabilities were in the Belle Plaine area northwest of Regina and to a lesser extent the Esterhazy area.

Excluding the Estevan area tests the DST permeability distribution is skewed to higher values from tests conducted in both clean and dirty sand (Figure 2-40) with an average of $10^{-12.5}$ m^2 for clean sand intervals compared to $10^{-12.6}$ m^2 in dirty sand intervals.
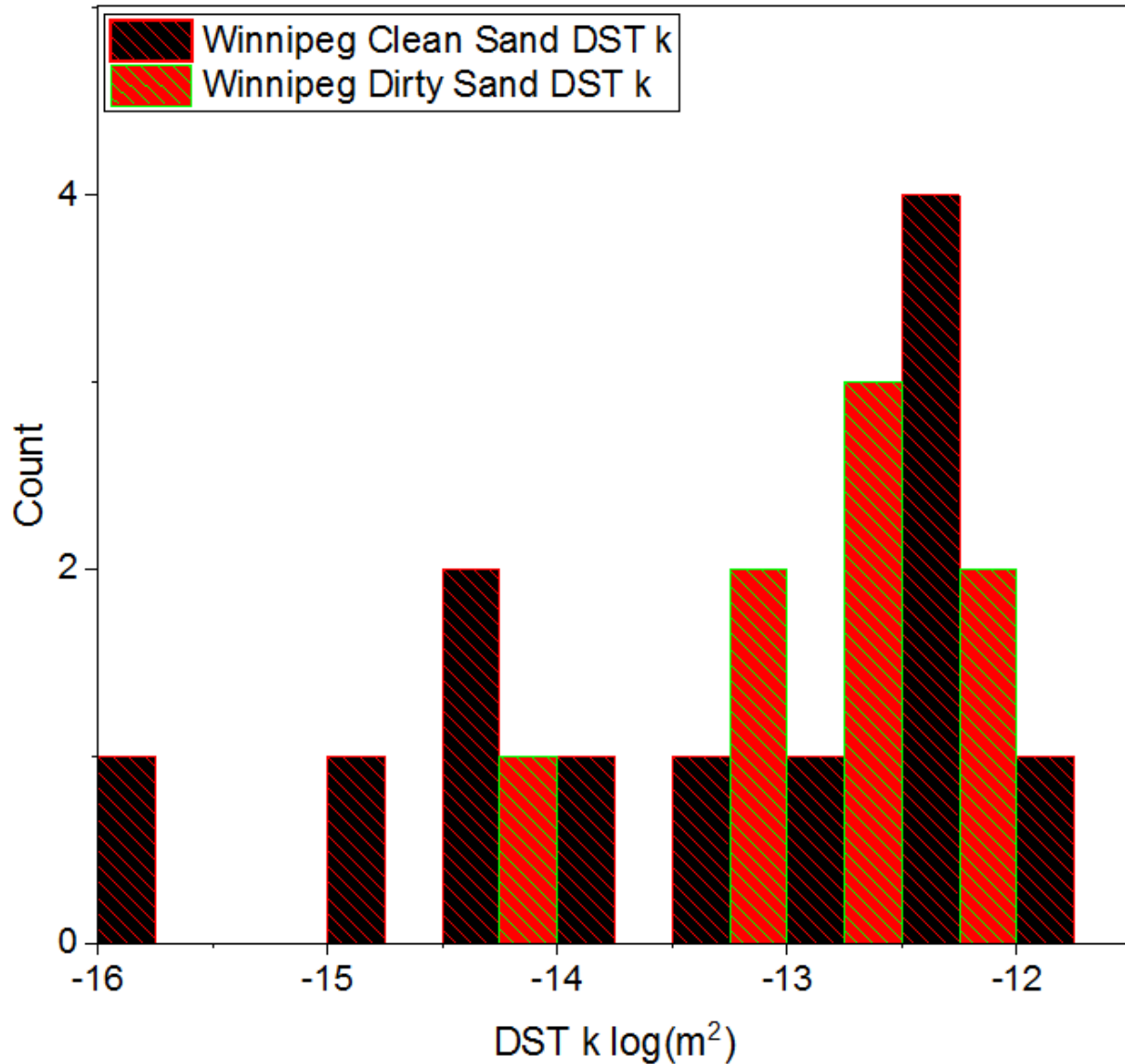
Figure 2-40: Winnipeg Formation DST permeability distribution excluding tests from the Estevan area

The lithological effects on permeability are observed in well 15 where DST 1 conducted primarily in dirty sands (Figure 2-41) was found to have a permeability of $10^{-12.9}$ m^2, whereas DST 2 carried out predominantly in clean sands, the permeability was considerably higher at $10^{-11.8}$ m^2. Both DST intervals have shale portions present, these shales would not contribute to flow during the test, thus are not included in the net pay of the tested interval, thereby not lowering the calculated permeability of the test.
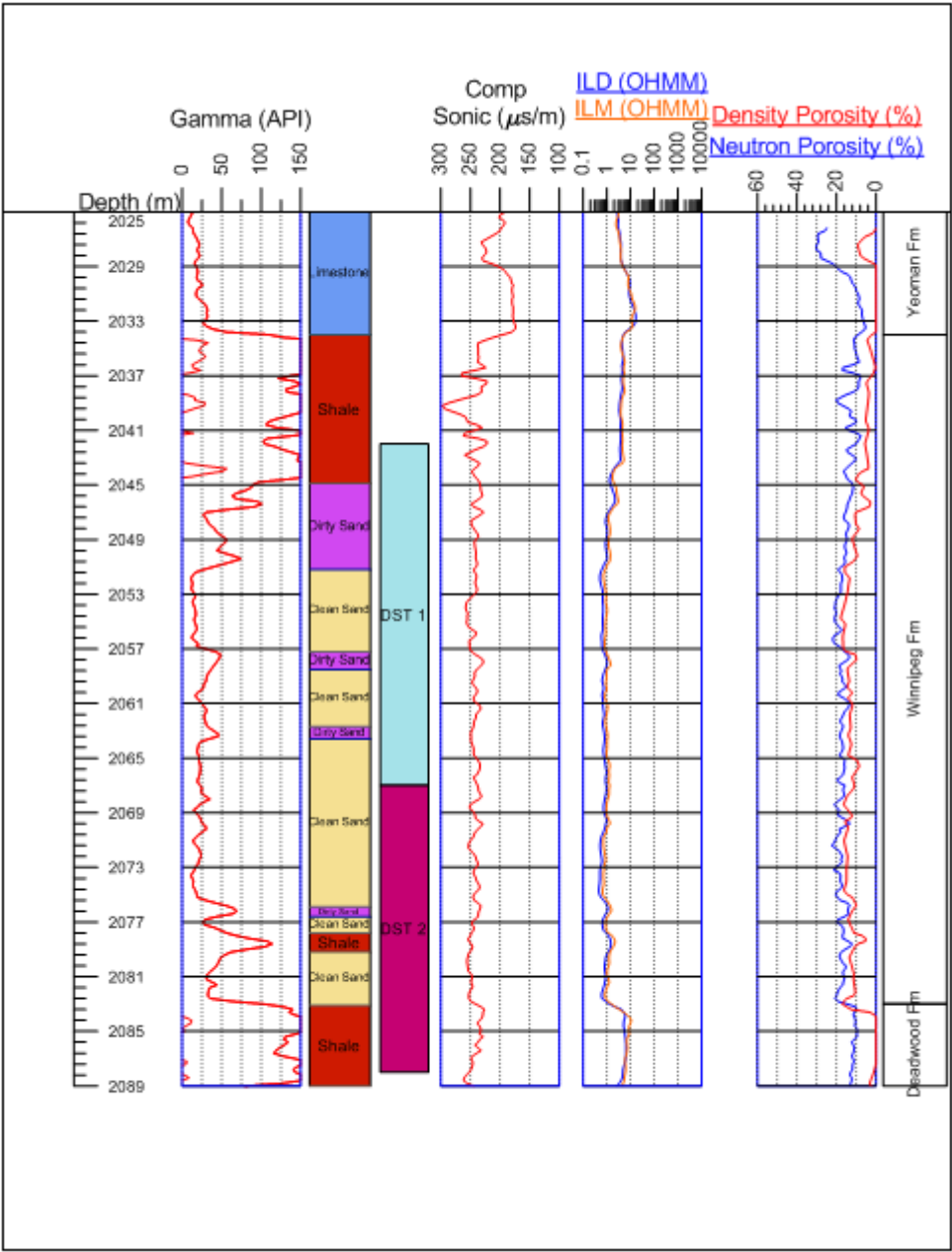
Figure 2-41: Geophysical logs for well 15, (UWI 131/03-08-017-19W2/02) DST 1 and 2, in Belle Plaine Area, wrap around gamma values indicate values greater than 150 API, scale becomes 150-300 API.

2.6.2.3 Winnipeg Formation Core vs Drill Stem Test Permeability

Permeabilities measured from core and DSTs in the Winnipeg Formation indicated similar median values, however the core values exhibited much less variability (Figure 2-42). The average permeability of the DSTs was higher than that of the core ($10^{-12.7}$ vs $10^{-13.0}$ m^2 respectively). Excluding the Estevan area tests (where many of the Winnipeg Formation DSTs were conducted in) the average DST permeability was $10^{-12.5}$ m^2.
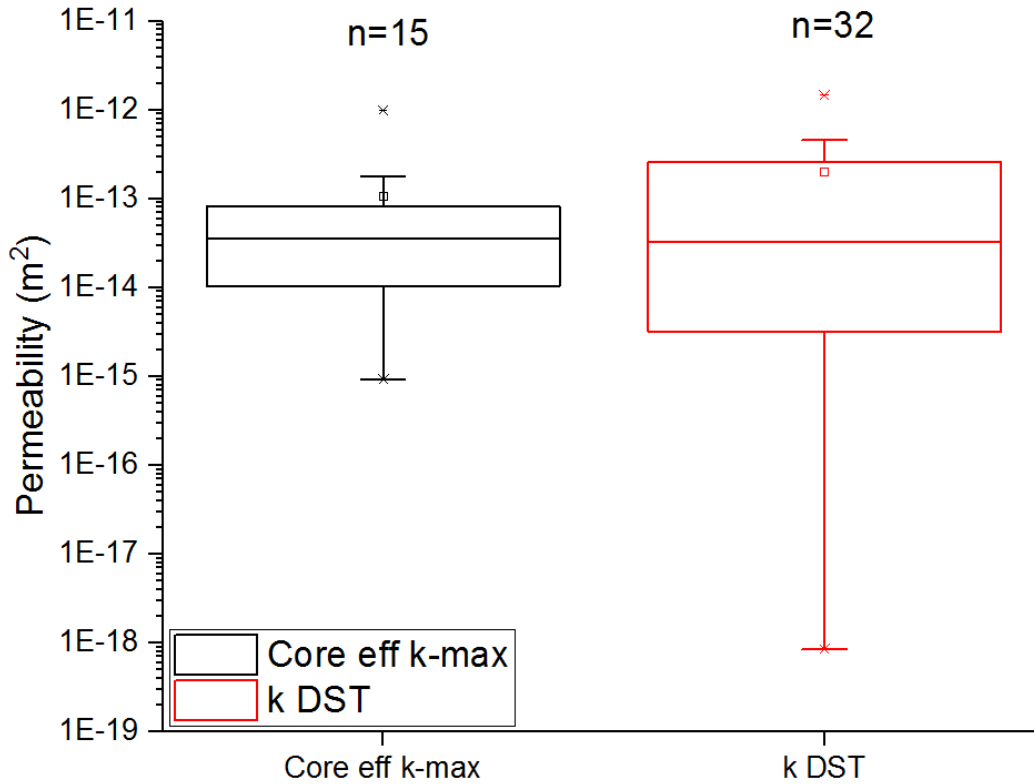
Figure 2-42: Winnipeg Formation DST, core and falloff test permeability, small middle box indicates mean, middle line indicates median, upper and lower bounds of large box indicate 25 and 75% quartiles, and whisker ends indicate 5 and 95% values

2.6.2.4 Winnipeg Formation Drill Stem Test Permeability vs Radius of Investigation

The relationship between permeability and radii of investigation in the Winnipeg Formation DSTs is illustrated in Figure 2-43. As with the Deadwood Formation, larger permeability values correlated with a larger radii of investigation. The relationship between DST k and RI is a power law relationship with an R^2 value of 0.696 and a P-value of 6.90×10^{-9}, a strong correlation.
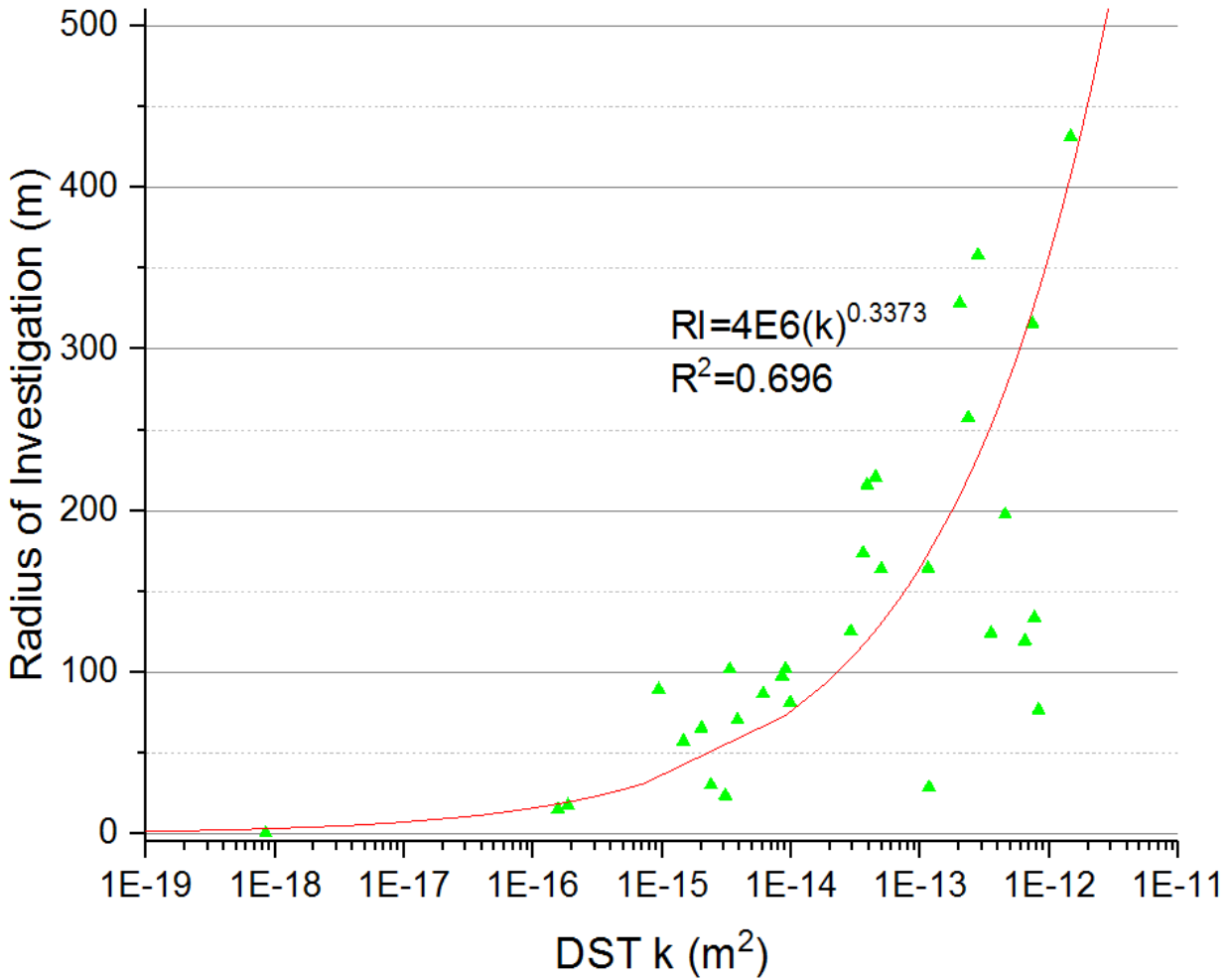
Figure 2-43: Winnipeg Formation DST permeability vs radius of investigation, exhibits a power law relationship with an R^2 of 0.696 and P-value of 6.90×10^{-9}, radius of investigation (RI) (m) can be calculated using inset equation RI=4E6(k)$^{0.3373}$

2.6.2.5 Winnipeg Formation Compressibility vs Depth

As with the Deadwood Formation, the sonic derived bulk compressibilities of the Winnipeg Formation were lowest in the deeper parts of the basin in south-east of the study area, with higher compressibilities in the shallower areas of the formation such as in the Esterhazy area and to the north of Regina (Figure 2-44).

Figure 2-44: Winnipeg Formation sonic calculated bulk compressibilities (Pa^{-1}) with Winnipeg Formation structure (metres subsea)

A linear relationship was observed between sonic derived bulk compressibilities vs subsea formation depth in the Winnipeg Formation (Figure 2-45). From this relationship, Winnipeg Formation bulk compressibilities can be estimated based on formation depth throughout the study area.

Figure 2-45: Winnipeg Formation Sand sonic derived formation compressibility vs subsea formation depth (m) with an R^2 value of 0.733 and a P-value of 4.98×10^{-6}

2.6.3 Interlake Group Permeability

The Interlake Group in Saskatchewan was studied through DSTs, core analysis and limited falloff test analysis throughout the province. The results from the core and DST analysis of the individual wells is located in Appendix H.

2.6.3.1 Interlake Group Core Permeabilities

Within the core extracted from the Interlake Group, the permeabilities exhibited a fair degree of variation (Figure 2-46), with an average value of $10^{-13.0}$ m^2. Unlike the basal clastics, there are no readily apparent regional trends in core permeabilities observed throughout the study area in the Interlake Group (Figure 2-47), however with the limited sample size of the core available regional trends in permeability cannot be discounted. Through analysis of the geophysical logs of the cored intervals it is apparent that there are correlations with permeability and the log characteristics. In the PCS disposal well 102 (UWI 121/01-14-017-30W1) the high permeability values obtained from core analysis are associated with the high neutron porosity readings indicated in the geophysical logs (Figure 2-48). The lower permeability values obtained from this core were observed in the tighter low neutron porosity intervals.
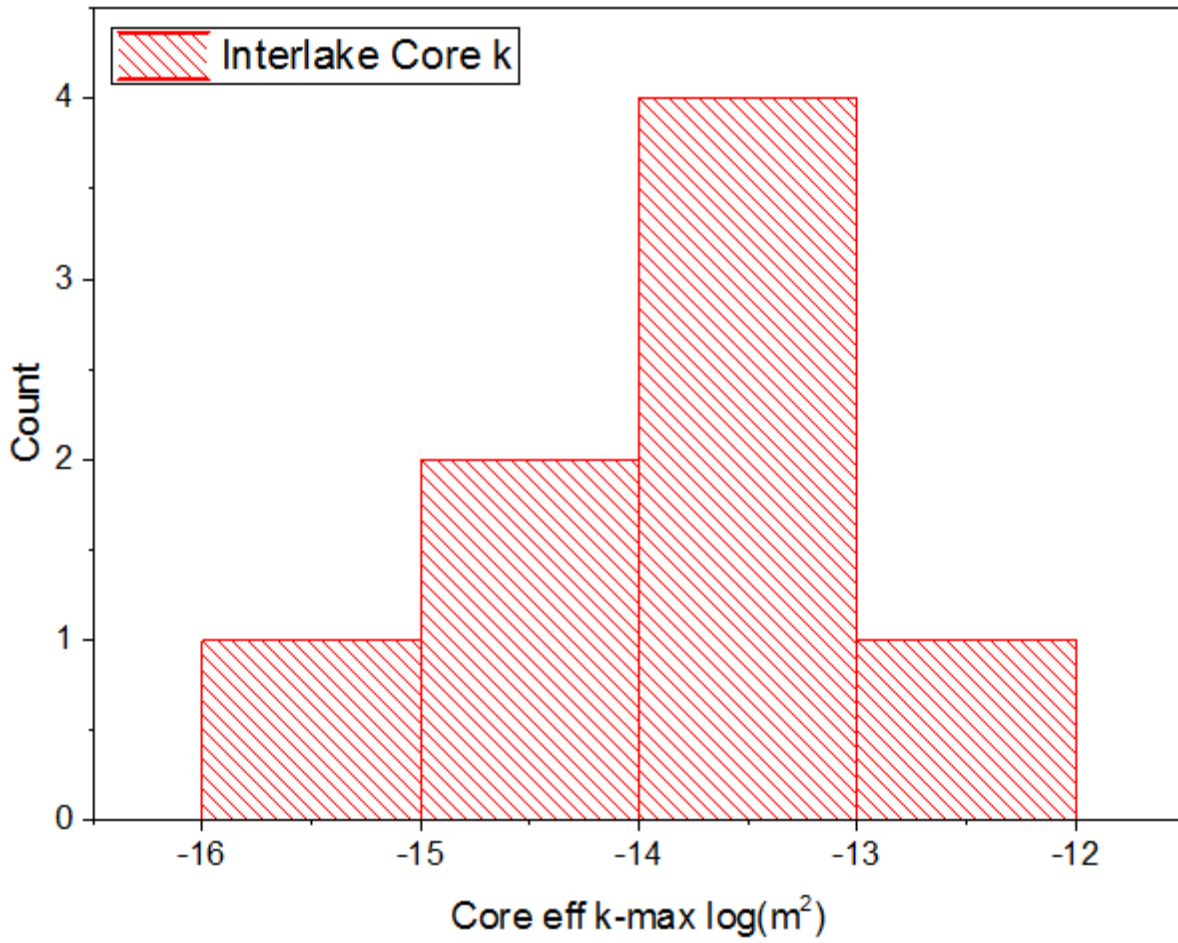
Figure 2-46: Interlake Group core permeability distribution
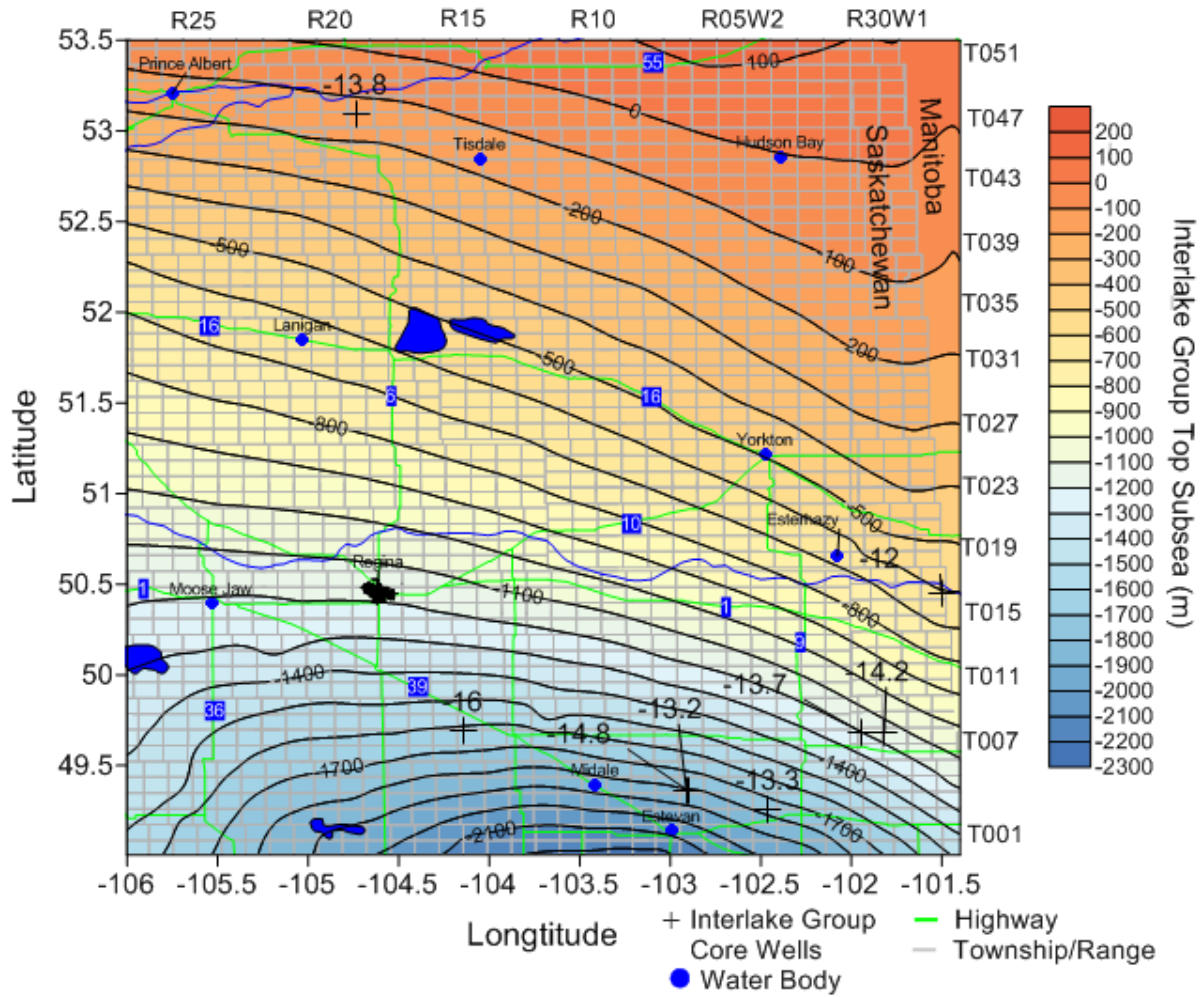
Figure 2-47: Interlake Group core permeabilities distribution (log (m^2), arithmetically averaged over each core interval, with Interlake Group structure (metres subsea)
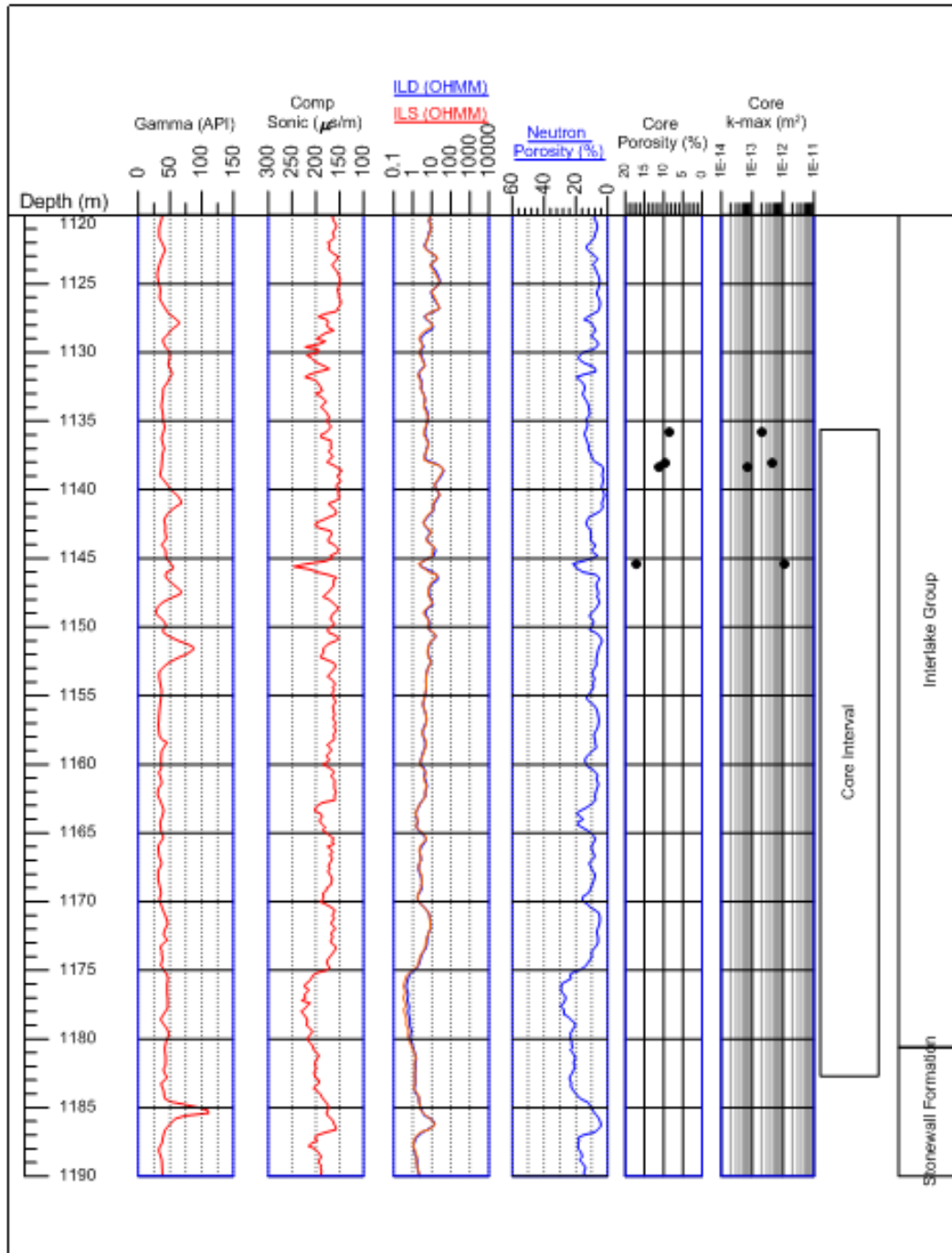
Figure 2-48: Geophysical logs for well 102 (UWI 121/01-14-017-30W1) an injection well from PCS Rocanville site, with core extracted from the Interlake Group along with core analysis porosity and permeability values

2.6.3.2 Interlake Group Drill Stem Test Permeabilities

DSTs were analyzed throughout the study area with a large number of tests available in the Esterhazy area (Figure 2-49) where the Interlake Group is utilized for brine injection. A large

variation in permeability values was observed through this analysis (Figure 2-50) that is somewhat normally distributed with an average of $10^{-12.6}$ m^2. Similar to the core in the Interlake Group there are no recognizable spatial trends in the DST permeability distribution (Figure 50).
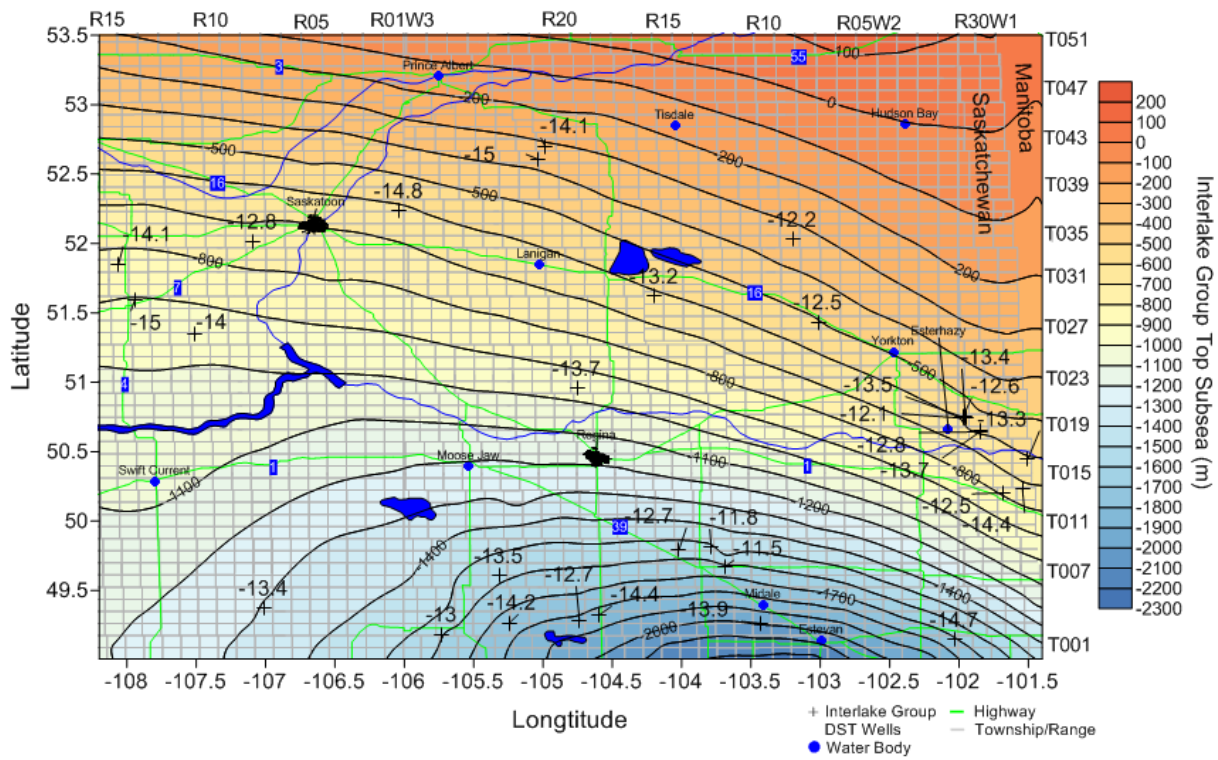
Figure 2-49: Interlake Group DST permeability distribution (log (m^2) with Interlake Group structure (metres subsea)
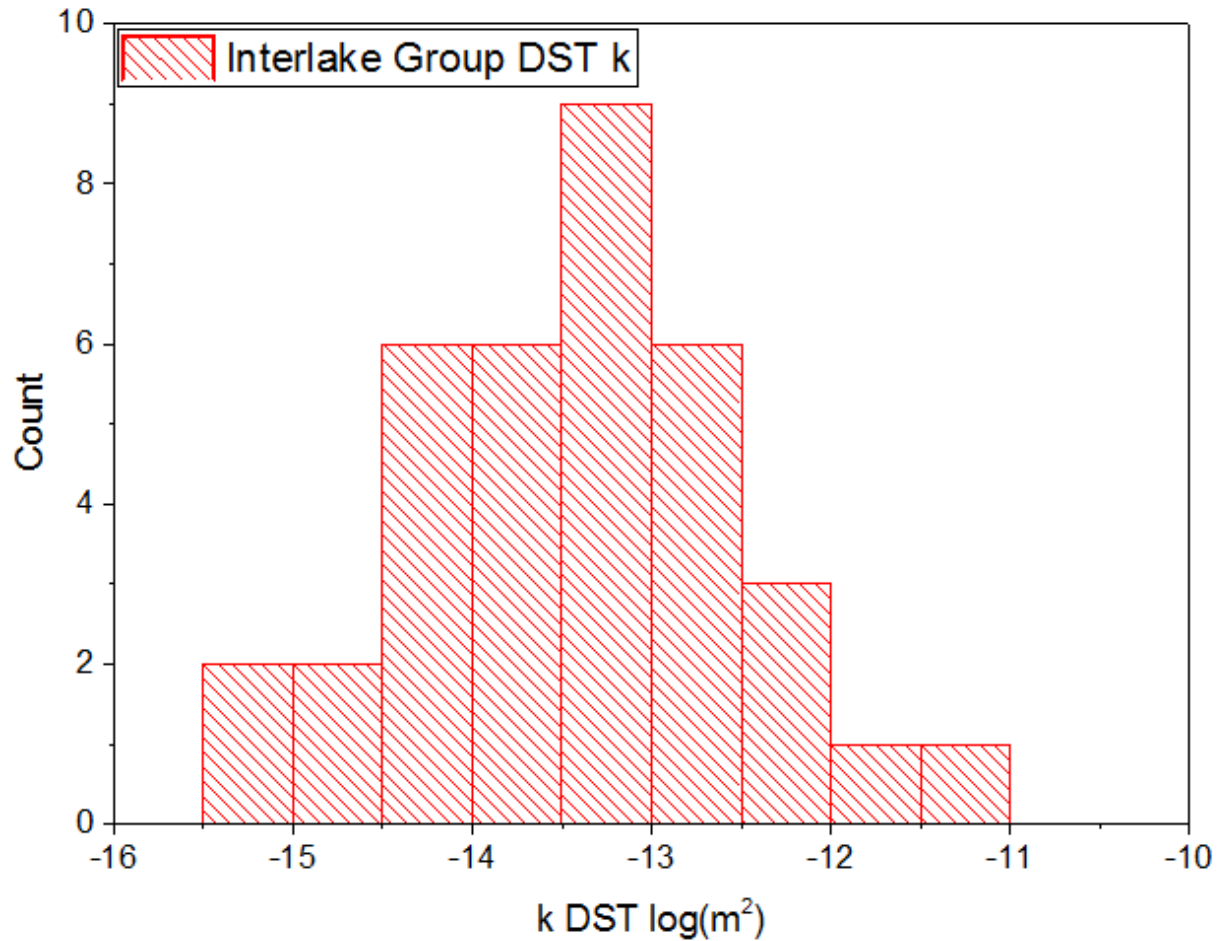
Figure 2-50: Interlake Group DST permeability distribution

Through analysis of the geophysical logs of the DST intervals, definitive correlations between the log parameters and permeabilities were observed. The high permeability tests were generally conducted in high porosity intervals of the Interlake group characterized by high neutron porosity intervals. This is seen in the Mosaic K2 injection well 105 (UWI 111/14-27-019-32W1) (Figure 2-51) where within the DST 1 interval from 1111.6-1165.9m MD, fairly high neutron porosity readings are indicated with an average of 13.5%. This high porosity interval of the formation yielded a DST calculated permeability of $10^{-13.1}$ m^2, a fairly high permeability.
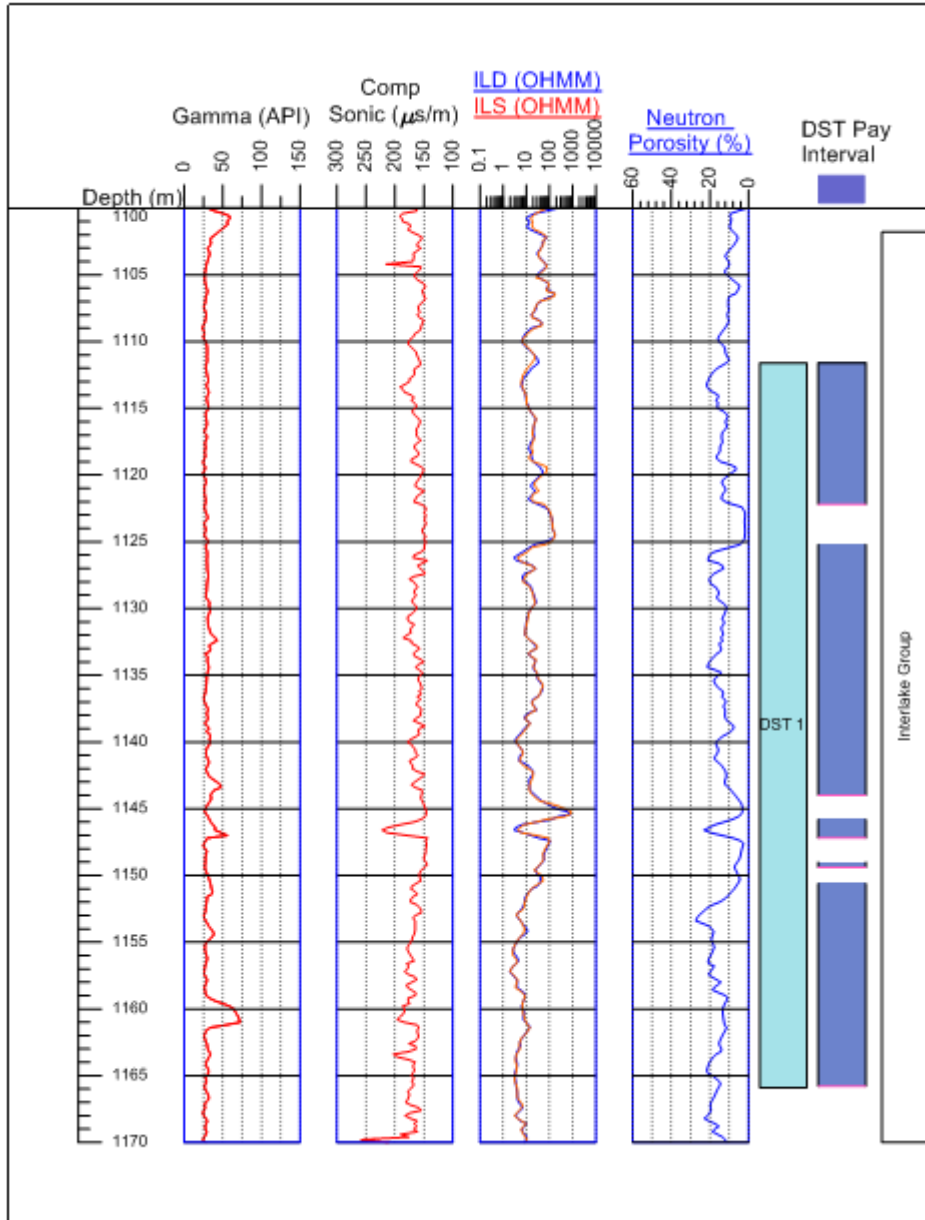
Figure 2-51: Geophysical logs for well 105 (UWI 111/14-27-019-32W1) DST 1, illustrating high neutron porosity readings within the DST interval, DST net pay noted for regions with greater than 6% neutron porosity readings

The low permeability DST tests were generally conducted in tighter intervals indicated by low neutron porosity readings. DST 5 from well 90 (UWI 101/02-04-004-11W2) conducted from 2686.8-2709.7m in the Interlake Group carbonates had very low neutron porosity readings (average of 3.18%), indicating a tight formation not readily available to flow (Figure 2-52). This DST had a permeability of $10^{-13.9}$ m^2, quite a low permeability.
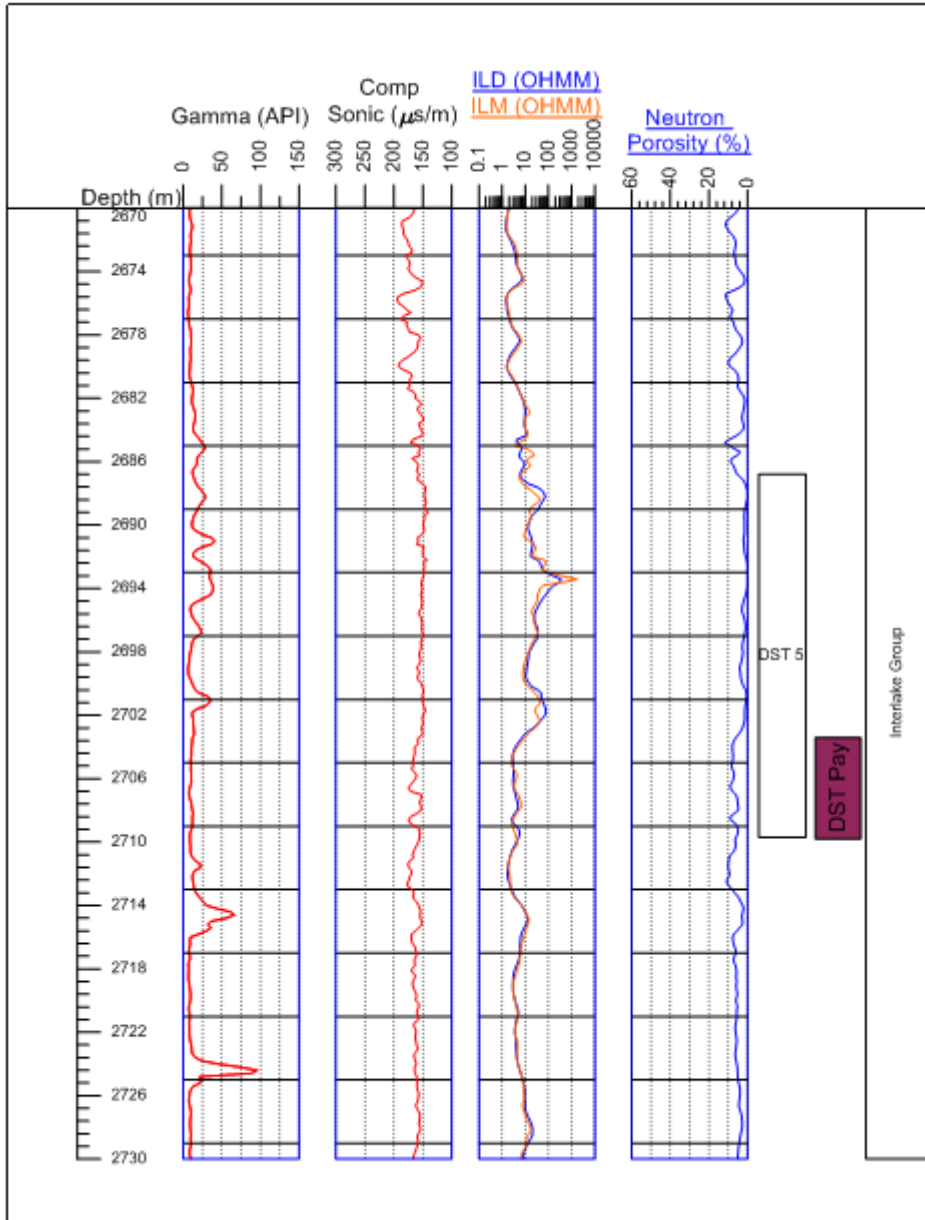
Figure 2-52: Geophysical Logs for well 90 (UWI 101/02-04-004-11W2) DST 5 conducted in low neutron porosity interval, DST net pay noted as interval with greater than 6% neutron porosity

2.6.3.3 Interlake Group Falloff Test Permeabilities

Falloff tests in the Interlake Group where available in 14 wells in the Esterhazy area at the Potash Corp Rocanville mine site and the Mosaic K1 and K2 sites (Figure 2-53). The first reliable falloff test was used to infer permeability at each well as in later tests the wellbore conditions were affected by large scale fluid injection. The range of permeabilities in the falloff tests was significantly less than those seen in the Interlake Group core and DSTs (Figure 2-54)

with the falloff test values being between $10^{-13.4}$ m^2 – $10^{-12.6}$ m^2 with an average permeability of $10^{-12.9}$ m^2.
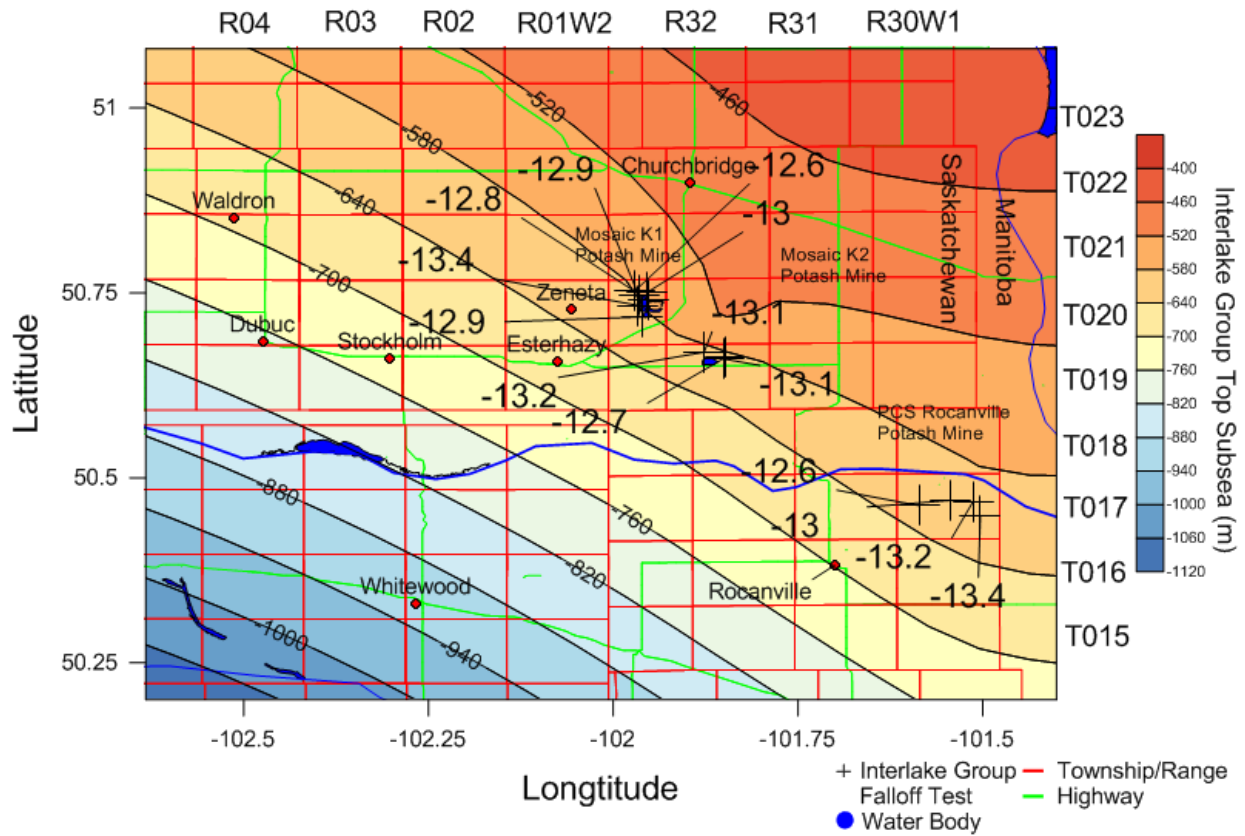
Figure 2-53: Interlake Group falloff test permeability distribution (log (m^2) with Interlake Group structure (metres subsea)
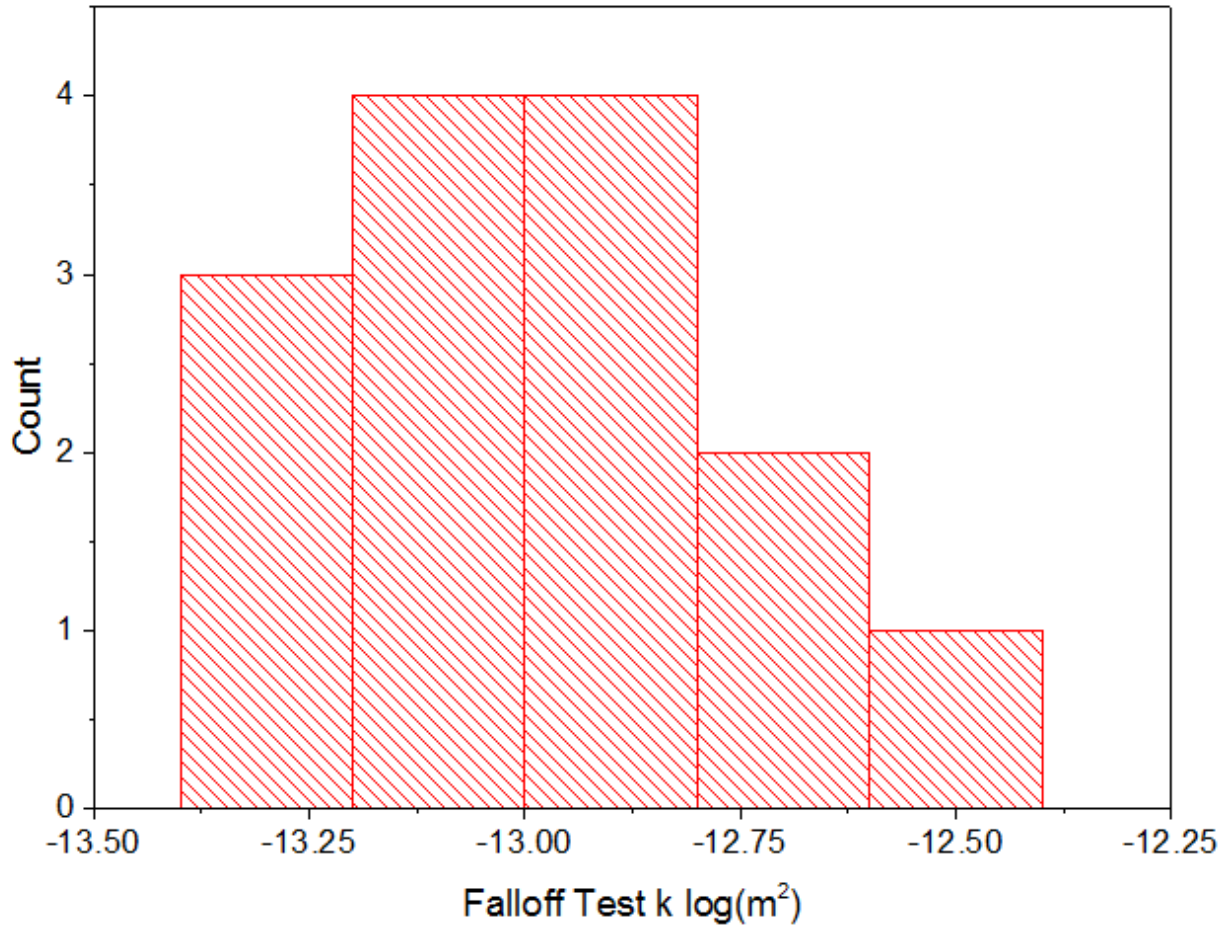
Figure 2-54: Interlake Group falloff test permeability distribution

2.6.3.4 Interlake Group Core vs DST vs Falloff Test Permeability

As was observed in the basal clastics, within the Interlake Group the falloff tests exhibited the largest permeabilities, followed by DSTs and core with the smallest permeabilities (Figure 2-55). However, with the limited sample size of the core available in the Interlake Group a great deal of confidence cannot be assigned to the core permeability distribution.
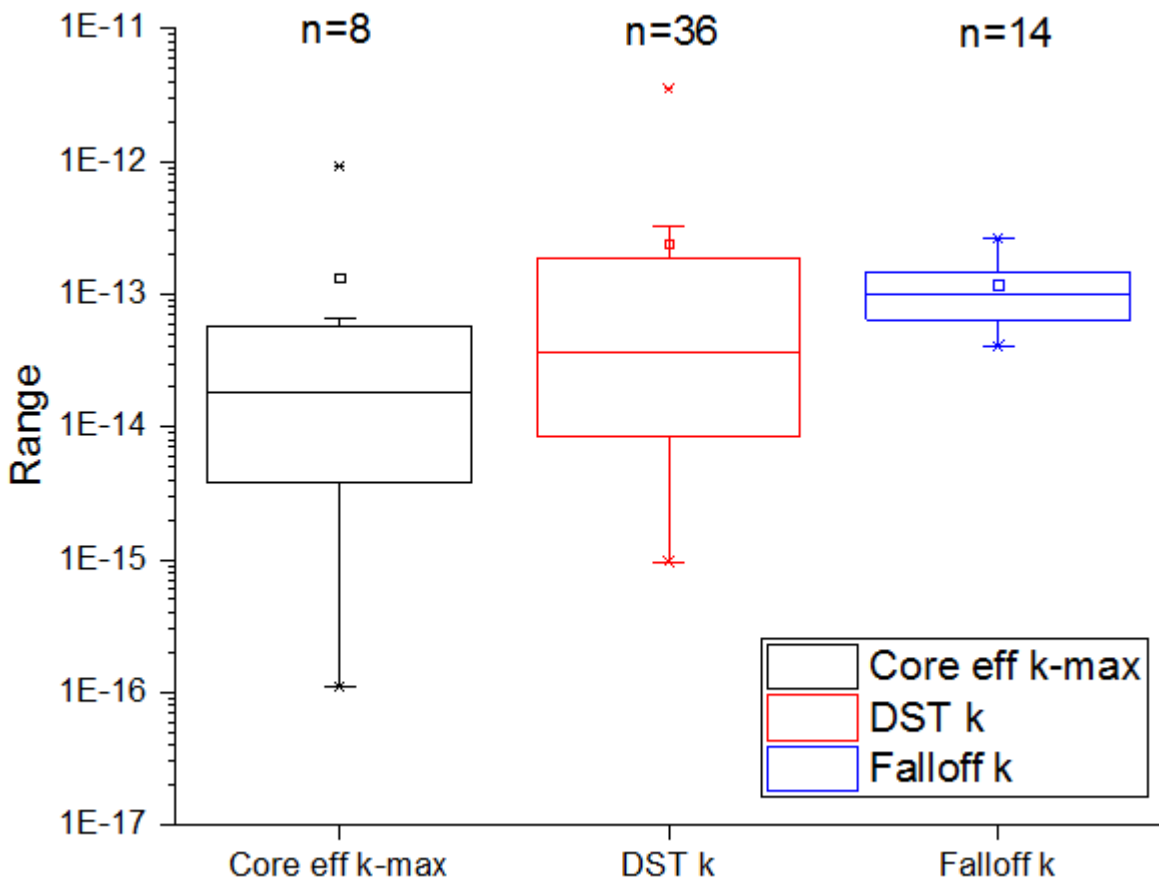
Figure 2-55: Box and whisker plot of Interlake Group DST, core and falloff test permeability, small middle box indicates mean, middle line indicates median, upper and lower bounds of large box indicate 25 and 75% quartiles, and whisker ends indicate 5 and 95% values

2.6.3.5 Interlake Group Drill Stem Test vs Radius of Investigation

In Figure 2-56 the relationship between permeability and radii of investigation in the Interlake Group is seen. Just as in the basal clastics, the higher permeability tests indicate a larger radii of investigation. The correlation of this relationship is quite strong with an R^2 value of 0.698 and a P-value of 1.16×10^{-9}.
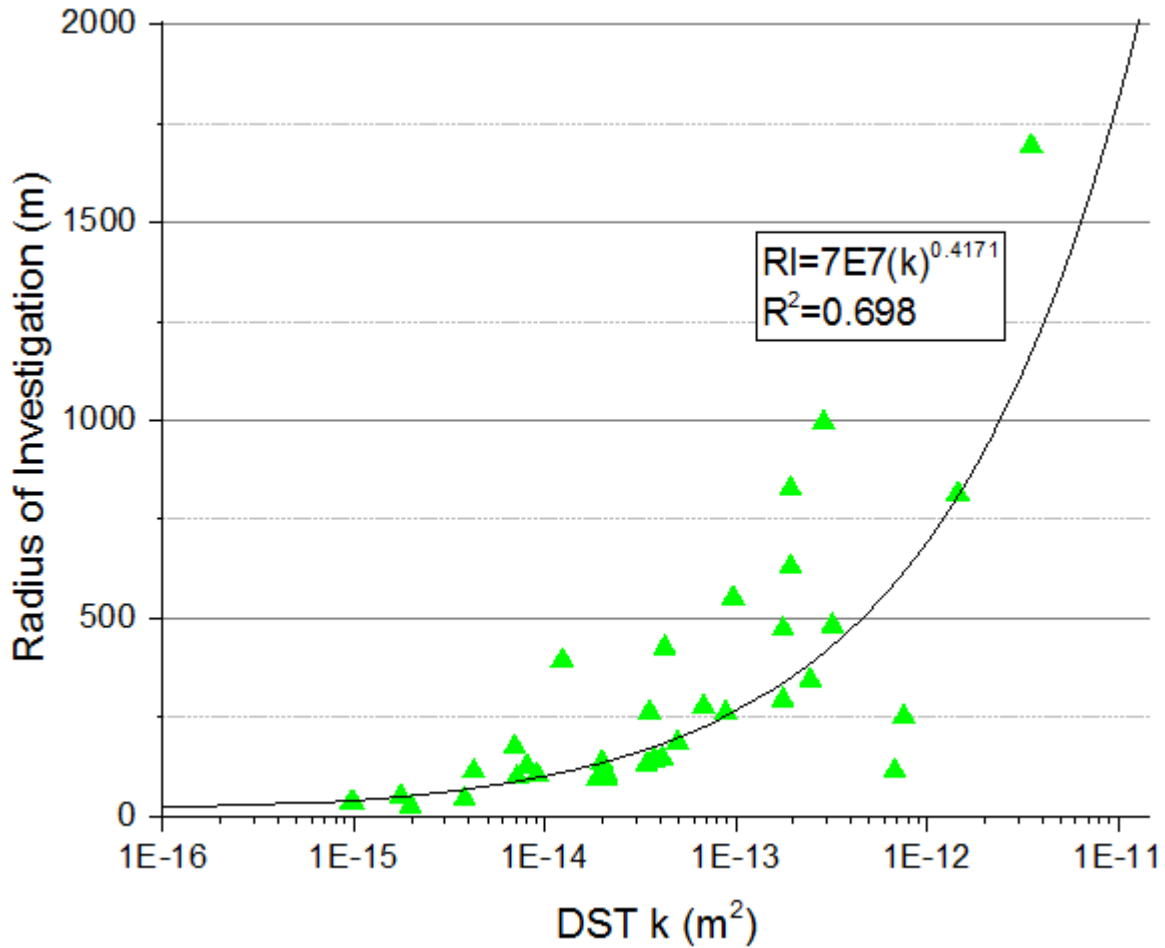
Figure 2-56: Interlake Group DST permeability vs radius of investigation, demonstrates a power relationship with an R^2 of 0.698 and a P-value of 1.16×10^{-9}, radius of investigation (RI) can be calculated using equation in figure RI=7E7(k)$^{0.4171}$

2.6.3.6 Interlake Group Compressibility vs Depth

The Interlake Group bulk compressibilities acquired from the sonic logs are relatively uniform with significantly less variability than the range seen in the basal clastics. The distribution of the compressibilities in the Interlake Group throughout the study area can be seen in Figure 2-57. Unlike the basal clastics the Interlake group does not demonstrate decreasing compressibilities with increasing depth (Figure 2-58). This is likely due to the lithological nature of the Interlake carbonates, whereby they are quite rigid and will not undergo the same degree of compaction as the sands in the Basal Clastics.
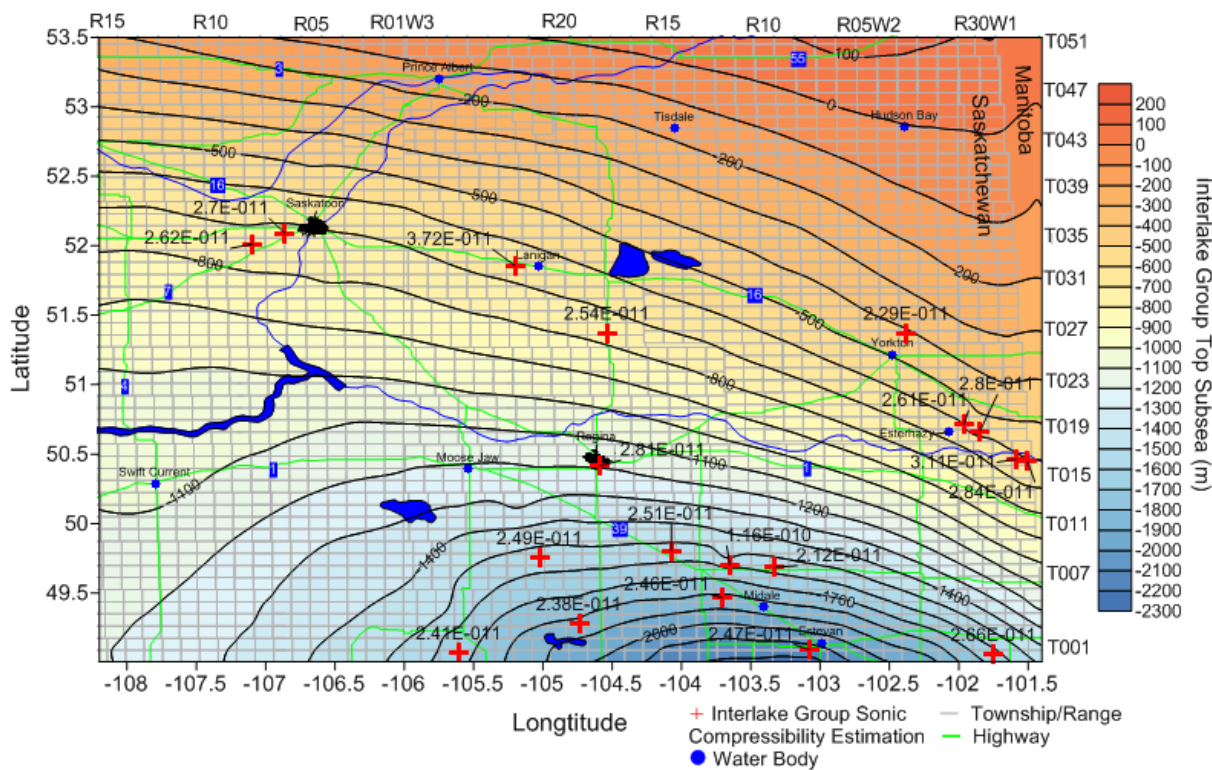
Figure 2-57: Interlake Group aquifer compressibility (Pa^{-1}) calculated from sonic logs with Interlake Group structure (metres subsea)
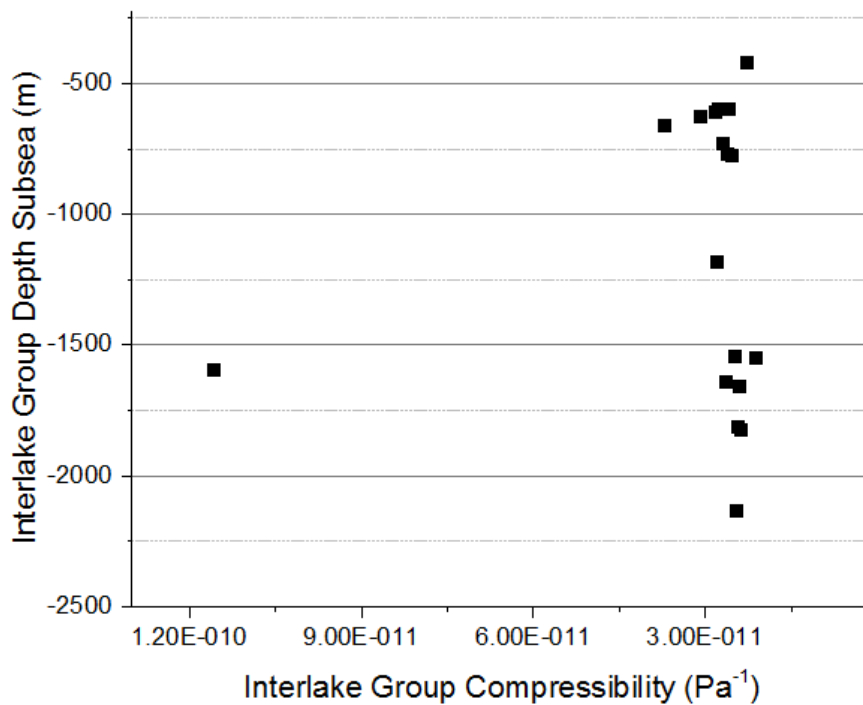
Figure 2-58: Interlake Group sonic log derived aquifer compressibility vs Interlake Group depth subsea (m)

2.7. Reservoir Characterization Discussion

2.7.1 Basal Clastics

It is apparent that there are large degrees of heterogeneity within the Winnipeg and Deadwood formations. Such variations have been observed in other studies of clastic aquifers using similar characterization techniques employed in this study. Core analysis conducted in the Wabiskaw member of the Mannville Formation (Desbarats and Bachu 1994) exhibits a transmissivity distribution highly skewed to higher values with a lower transmissivity tail, quite similar to the Deadwood Formation core permeability distribution. These similarities can be attributed to coring practices; i.e., the Wabiskaw core was preferentially sampled in high quality (i.e. permeable) sands, as is the common practice in the oil and gas industry (Desbarats and Bachu 1994), which was also the case for the core sampling in the Deadwood Formation. Core analysis conducted in the Paskapoo sandstone, a shallow groundwater aquifer in Western Alberta yields a bimodal distribution, with data largely skewed to lower hydraulic conductivities with a smaller mode at higher hydraulic conductivities (Grasby et al. 2008). This is in contrast to the core results from the Deadwood Formation. However, the Paskapoo cores were obtained throughout the formation, exhibiting alternating sequences of coarse-grained sandstones with high permeabilities, and fine-grained sandstones and mudstone with lower permeabilities (Grasby et al. 2008). These alternating sequences being characteristic of the channel deposits of the formation. The lower permeability regions sampled in the Paskapoo resulted in the skew to lower hydraulic conductivities not seen in the Deadwood Formation core due to preferential sampling in the high quality sand regions.

The pumping tests conducted in the Paskapoo Formation allow for determination of formation transmissivity in a similar manner as DSTs are able to determine permeability. The formation transmissivity distribution of the Paskapoo pumping tests appears quasi-normal bell curve with a slight skew towards lower values (Grasby et al 2008).This distribution being attributed to the variation in facies that these shallow groundwater wells are completed in, ranging from permeable channel sandstones providing good water production to mudstone dominated wells that provide poor water production. These mudstone dominated wells being drilled due to not being able to accurately predict the quality channel sand locations. In contrast, the Deadwood Formation DSTs exhibited a permeability distribution highly skewed to higher values as a result of these tests being primarily conducted in sand intervals as is the common practice for the oil and gas industry. The Winnipeg Formation DST permeability distribution was more in line with the results of the Paskapoo pumping tests due to the large influence of the low permeability sands tested in the Estevan area. The Winnipeg Formation exhibits an even larger skew to lower values than seen in the Paskapoo Formation.

The permeabilities in the Deadwood and Winnipeg formations were compared to other clastic formations throughout western Canada (Figure 2-59). The Deadwood and Winnipeg Formation sands have permeabilities that are within the same range as these other Clastic Formations. The Deadwood and to a lesser extent the Winnipeg Formation exhibited permeabilities in the same range as the Judith River and the lower end of the Paskapoo Formation, loosely consolidated shallow groundwater aquifers. Considering the Winnipeg and

Deadwood Formations are deeply buried units to have permeabilities in the same range as these shallow aquifers makes the Basal Clastics a prime target for liquid waste disposal. The Basal Sandstone unit in Alberta (equivalent to the Basal Clastic unit) exhibits considerably lower permeabilities close to what was seen in the Deadwood Formation shale. However, this study in Alberta was conducted on a limited number of cores and thus might not be representative of the formation in Alberta. The Deadwood and Winnipeg Formations have permeabilities that are considerably higher than the different facies within the Cardium Formation. The Cardium Conglomerate and Sandstone units demonstrate permeabilities within the lower end of the Winnipeg and Deadwood Formations, however the bioturbated zone within the Cardium is much tighter, requiring hydraulic fracturing to yield economic quantities of oil and gas production (Friesen et al. 2017).
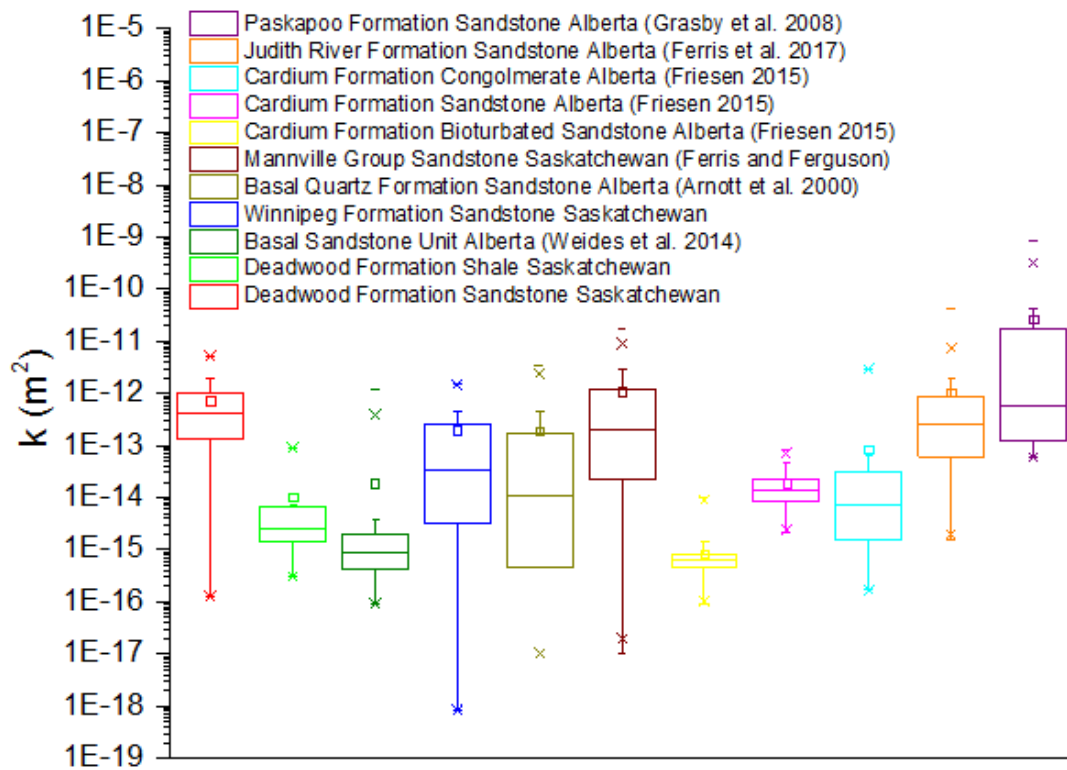
Figure 2-59: Box and whisker plot of Deadwood and Winnipeg formation permeabilities with other Clastic Formation permeabilities from core data, DSTs and pumping tests. Small middle box indicates mean, middle line indicates median, upper and lower bounds of large box indicate 25 and 75% quartiles, and whisker ends indicate 5 and 95% values

There are as well significant variations in the permeability values observed between the different methods of analysis. A great deal of the variations in permeability values from the three methods of analysis can likely be attributed to the differences in scale of measurements of the tests. The falloff tests having the largest scale of measurement, with most of the tests exhibiting a radius of investigation in the thousands of metres, while the DSTs generally had a radius of investigation of around 100-300m. The core analysis represents the smallest scale of

measurement, representing a point source scale of measurement of the aquifer. Schulz-Makuch et al. (1999) through analysis of pumping tests in heterogeneous media inferred that increased hydraulic conductivity measurements would be observed with increasing scale of measurement. It was proposed that this scaling effect was in part due to the larger scale tests encountering preferred pathways (fractures and solution conduits) that would allow faster fluid flow in the subsurface, hence larger hydraulic conductivities. The larger permeability values seen in the falloff tests compared to the DSTs and core are likely due to this effect. As well, some of the differences can be attributed to certain tests methods being biased to certain lithological facies (clean sand, dirty sand, shale). A greater proportion of a given test method being completed in a certain facies as was the case in the Estevan area where there were a disproportionate number of Winnipeg Formation DSTs (in the clean gamma ray sand) that exhibited very poor permeabilities.

From this analysis, it is apparent that the highest permeabilities in the Winnipeg and Deadwood Formations are generally located in the central regions of the province in the Saskatoon and Belle Plaine areas. These are regions with significant potash mining activity with many injection wells using the basal clastics for disposal of brine wastewater. The high permeabilities of the formations in this area has contributed to the success of these waste water disposal projects as the rocks are readily able to accept liquid wastes. The Deadwood Formation has also been used in the Kindersley area for liquid waste disposal with nine disposal wells with the oldest of these wells in service since 2010. These wells service the disposal needs of the oil and gas industry in the area. The injection rates in these wells are low generally around 500-1000 m^3/day, versus the 5000-10000 m^3/day rates seen at many of the potash mine wells. However, due to the favourable permeability values exhibited in core, the Deadwood Formation in this area is a candidate for further waste disposal, although further study of the formation through falloff test analysis in these wells would be helpful for comparison of permeabilities in these wells versus the potash mine wells.

In other areas of the province such as the Estevan and Swift Current areas, the basal clastics exhibited significantly lower permeabilities and thus the formations would be less suitable candidates for waste injection. Due to the prohibitive depths of the basal clastics, limited amounts of data are available for analysis leaving significant information gaps in providing a thorough analysis of the formation properties. Further exploratory drilling in these formations would be beneficial to provide more information on the permeability characteristics of the Winnipeg and Deadwood Formations.

2.7.2 Interlake Group

Through this analysis a wide distribution of permeability values were obtained from the Interlake Group. Unlike the Basal Clastics, there was no readily apparent regional trends in permeability. The permeabilities in the Esterhazy mine site area range from $10^{-14.4} - 10^{-12.0}$ m^2, somewhat smaller than the values seen at the mine sites utilizing the Basal Clastics which had permeabilities measuring up to $10^{-11.3}$ m^2. From this it can be inferred that the Interlake Group at the Esterhazy mine site has a lower injection capacity than the Basal Clastics do at the respective mine sites.

The Interlake Group permeabilities found in this analysis were compared to other carbonate formations (Figure 2-60). The Interlake Groups permeabilities are within the same range as these other carbonate formations. The higher permeability values seen in the Leduc Formation are due to preferential core sampling of the high porosity, high permeability dolomotized reef buildups. The lower permeability values in the Swan Hills Reef and Carbonate bank are due to the formation being un-dolomitized (Hemphill et al. 1970) as well as likely preferential sampling of the lower permeability off reef regions of the formation. The lower permeabilities observed in the Yeoman Formation are due to the lithology which is predominantly mudstone with some wackestones and packstones and the absence of high porosity reef material (Pu 2003). The Yeoman high porosity (hence permeable) zones are only seen in areas that have undergone complete dolomitization. The wide variation in permeabilities seen in the North Dakota Winnipegosis Pinnacle Reef is due to highly porous portions of the reef being sampled as well as intervals of the reef that have undergone destructive diagenesis as a result of pore plugging induced by precipitation of calcite and halite. The range in permeability values observed within the Interlake Group are likely due to varying degrees of dolomitization observed throughout the tested intervals. The intervals of the formation that have undergone greater amounts of dolomitization would exhibit higher permeabilities and would thus be more suitable candidates for liquid waste injection.
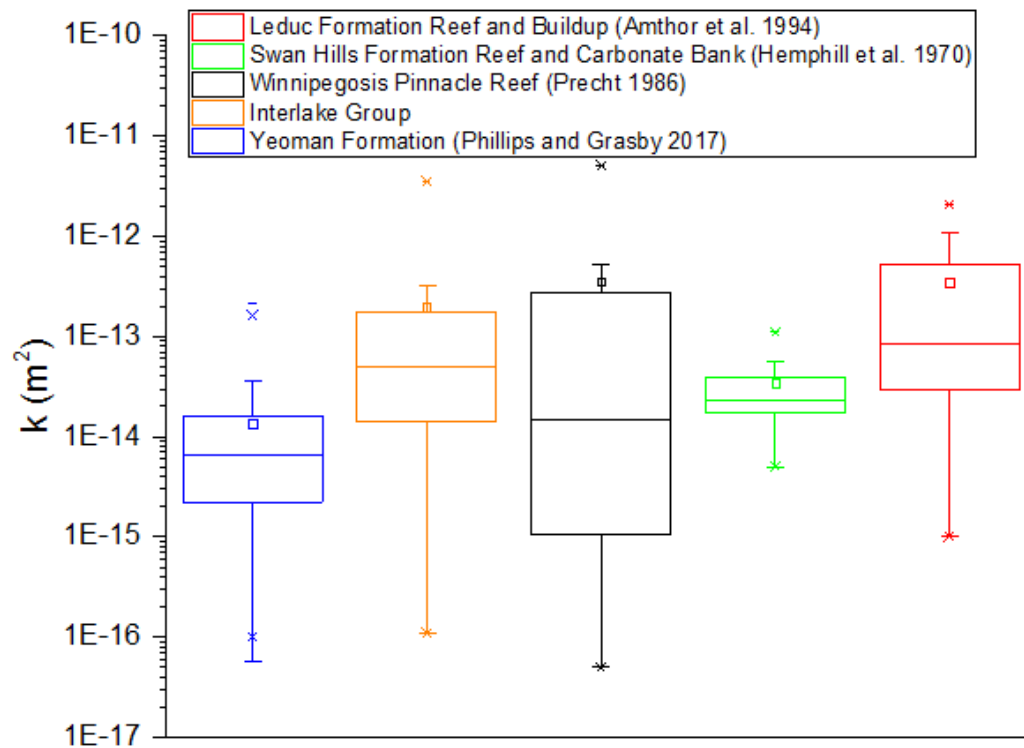
Figure 2-60: Interlake Group permeabilities with other carbonate formation permeabilities Swan Hills Reef and Carbonate Bank (Hemphill et al. 1970), Leduc Formation Reef and Buildup (Amthor et al. 1994), Winnipegosis Pinnacle Reef (Precht 1986). DST. Small middle box indicates mean, middle line indicates median, upper and lower bounds of large box indicate 25 and 75% quartiles, and whisker ends indicate 5 and 95% values

2.8 Reservoir Characterization Conclusion

It is apparent that there are large variations in permeability throughout the province in the basal clastics and the Interlake Group. In these formations it was seen that within localized areas the permeability values of the formation are strongly dependent on lithological factors observed in geophysical logs, gamma in the case of the Basal Clastics and neutron porosity in the Interlake Group. The DSTs and core within the clean sand in the Deadwood Formation having an average permeability of $10^{-12.1}$ m^2 vs $10^{-12.2}$ in dirty sands and $10^{-13.3}$ m^2 in shales. The Winnipeg Formation in core and DSTs exhibited an average permeability of $10^{-12.9}$ m^2 in clean sands and $10^{-12.50}$ m^2 in dirty sands, however the lower permeability of the clean sands were highly influenced from tests in the Estevan area that had anomalously low permeabilities within clean sands. While the average permeability values in the Interlake Group were $10^{-13.0}$ m^2 in the core and $10^{-12.6}$ m^2, significantly lower than the values seen in the sands of the Basal Clastics.

Knowing the permeability values associated with clean sand, dirty sand and shale in the Basal Clastics from the certain areas of the province, permeability values from other wells within these areas without DST or core data can be estimated from their lithological characteristics identified in geophysical logs based on the results seen in this study. While in the Interlake Group the neutron porosity values from the geophysical logs provide insights into the aquifer permeability, with low neutron porosity readings being associated with low permeabilities and higher neutron porosity reading with high permeabilities.

From the analysis of gamma ray API values and their associated permeabilities from cores and DSTs in the Basal Clastics a negative exponential relationship between the gamma ray API and permeability was identified. From the equations of these relationships permeability values can be roughly estimated based on gamma ray API values observed in geophysical logs.

3. Analytical Modelling of Potash Mine Injection Wells in Saskatchewan

3.1 Analytical Modelling Introduction

In order to gain insights into the pressure changes in the targeted aquifers (Basal Clastics and Interlake Group) brought about by large scale injection of brine waste analytical models were genereated in Aqetsolv (HydroSOLVE Inc 2016). These analytical models were constructed with data acquired from the reservoir characterization study in the previous chapter including aquifer thickness and distribution, permeability and compressibility. Numerous analytical models were generated for each of the mine sites based on different values of transmissivity (based on values obtained from DSTs, falloff tests and core obtained at each site) and storativity (based on values obtained from sonic logs, Hall (1953) correlation, and literature values of compressibility). Each of the models simulated outputs of the change in aquifer pressure over time. In order to determine which model generated the most realistic simulation outputs of pressure change, the pressure response of each model was compared to the changes in aquifer pressure measured from the falloff tests available at each injection well. The models with the pressure responses that had the best correlation with the falloff test data (lowest root mean squared error) were considered to be the most accurate. Subsequent models were developed with different values of transmissivity and storativity in order to generate simulation outputs that most closely match the observed pressure data (history-matching). These history matched models were taken as a representative model of each the mine sites, providing insights into the changes in aquifer pressure as well as the extent of the pressure propagation due to liquid waste injection. Through gaining an understanding of the aquifer response to such injection activities, future waste disposal at these sites could be better managed in order to mitigate prohibitively high increases in aquifer pressure.

The transmissivity (not to be confused with transmissibility) of an aquifer is defined as the rate of flow given a hydraulic gradient through a unit width of an aquifer of a defined thickness and is calculated with equation 3.1 (HydroSOLV Inc. 2016).

$$T_{Aquifer} = K * b \qquad\qquad (3.1)$$

Where K is the hydraulic conductivity of the aquifer $(\frac{m}{s})$, and b is the aquifer saturated thickness (m). Transmissivity is converted directly from hydraulic conductivity, while transmissibility is converted from permeability.

3.2 Data Compilation

3.2.1 Cory-Vanscoy Study Area

The Potash Corp Cory and Agrium Vanscoy mine sites (Figure 3-1) located south-west of Saskatoon were included within a single study given the close proximity of these sites. There are four injection wells in the Deadwood Formation at the Cory site and two wells at the Vanscoy site. Additionally there is a Transgas injection well (05-15) unrelated to potash mining located in the northeast of the study area. This well was briefly in operation from 2004-2007.
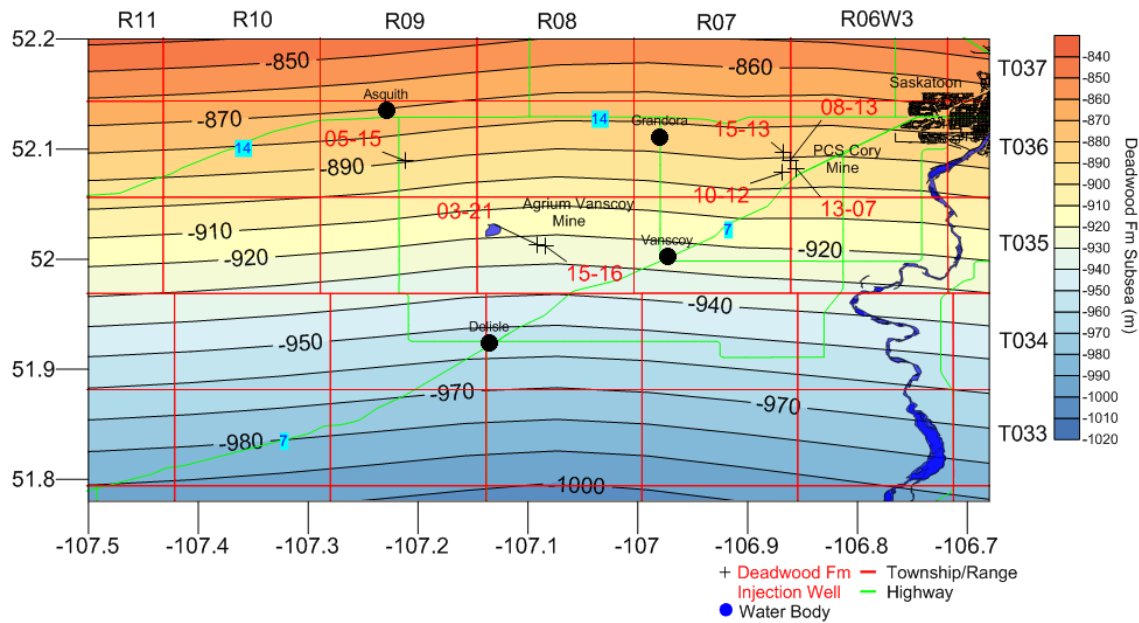
Figure 3-1: Cory and Vanscoy Mine sites with injection well locations, with Deadwood Formation structure (metres subsea)

Within the Cory-Vanscoy study area there are 7 disposal wells injecting into the Basal Clastics, falloff test records were available for 4 of these wells. Many of the tests available were unreliable and were culled. The distribution of available reliable tests in each of the wells used in this analysis is seen in Table 3-1.

Table 3-1: Falloff test distribution for Cory Vanscoy injection wells

	Cory Wells				Vanscoy Wells		Transgas Well
Year	13-07	08-13	10-12	15-13	15-16	03-21	05-15
1975		X				X	
1976		X					
1977		X				X	
1978		X				X	
1979		X				X	
1980		X				X	
1981		X				X	
1982						X	
1983		X				X	
1984						X	
1985		X				X	
1986		X					
1987		X					
1988							
1989		X					
1990		X				X	
1991		X				X	
1992		X					
1993		X					
1994		X					
1995		X					

1996		X				
1997						
1998		X				
1999	X	X				
2000	X	X				
2001	X					
2002	X	X				
2003	X	X	X			
2004	X	X	X			
2005	X		X			
2006	X	X	X			
2007	X	X	X			
2008		X	X			
2009	X	X	X			
2010	X	X	X			
2011	X	X				
2012						
2013						
2014						
2015						
Total tests	12	31	8			12

3.2.2 Allan, Patience Lake and Colonsay Study Area

The Potash Corp Allan mine, Patience Lake mine as well as the Mosaic Colonsay mine site were included in a single study as these sites are relatively close. The Allan mine site southeast of Saskatoon has two injection wells in the Deadwood Formation (Figure 3-2), 13-22 in use since July 1971 and 16-28 which was brought online in November 2006. The Patience Lake mine as well has two injection wells, 12-16 in operation intermittently since 1987, and 08-16 in use since 2008. Further to the east, the Mosaic Colonsay mine site also has two injection wells, 02-21 and 14-16 in use since 1973 and 2007 respectively.
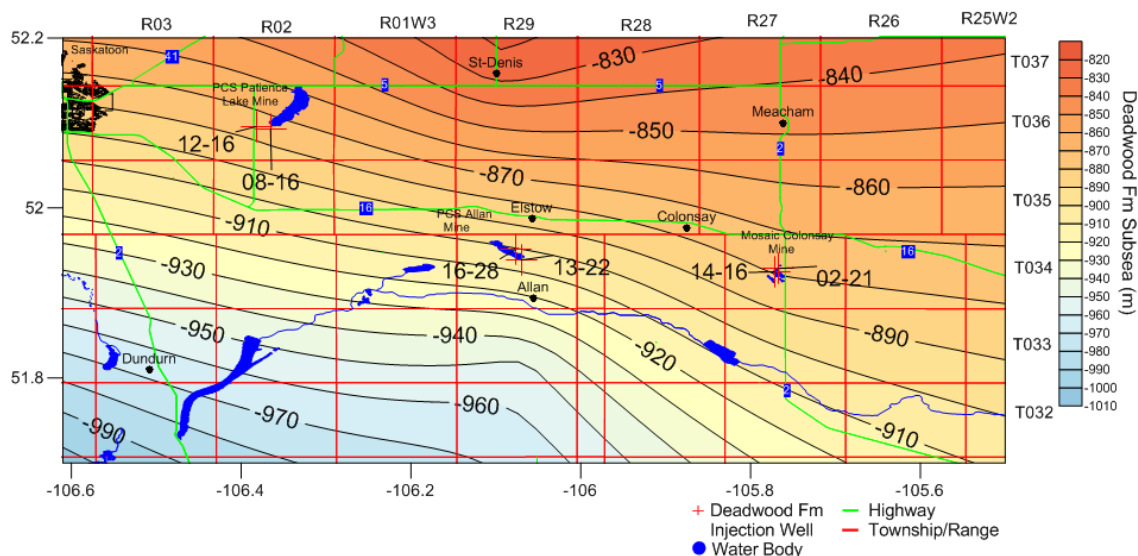
Figure 3-2: Allan, Patience Lake and Colonsay mine sites with location of injection wells within the Deadwood Formation, with Deadwood Formation structure (metres subsea)

Among the six injection wells in the Allan-Patience Lake-Colonsay area, falloff test records were available for four of the wells. The distribution of the available reliable tests in each of these four wells is seen in Table 3-2.

Table 3-2: Falloff test distribution for Allan-Patience Lake-Colonsay area injection wells

	Allan Wells		Colonsay Wells	
Year	13-22	16-28	14-16	02-21
1975				X
1976				X
1977				X
1978				
1979				
1980				
1981				
1982				
1983				
1984	X			
1985				X
1986				X
1987				X
1988				
1989				X
1990				
1991				
1992	X			X
1993				
1994				X
1995				X
1996				X
1997	X			
1998				
1999				X
2000	X			X
2001	X			X
2002				X
2003				X
2004	X			X
2005				
2006				
2007				
2008				
2009				
2010				
2011	X	X	X	X
2012	X		X	X
2013	X	X	X	X
2014	X	X	X	X
2015				
Total tests	10	3	4	21

Within this study area there were two wells with available borehole compensated sonic logs (Colonsay mine 14-16 and Patience Lake mine 08-16) that allowed for an estimation of aquifer compressibility using the relationship between shear wave and compressional wave velocity

established at the two Estevan area wells with dipole sonic logs available in the Deadwood Formation.

3.2.3 Lanigan Study Area

The Potash Corp Lanigan mine (Figure 3-3) 120 km east of Saskatoon has two wells injecting wastewater into the Deadwood Formation, 1-20 in operation since 1976 and 02-28 in use since 1995.
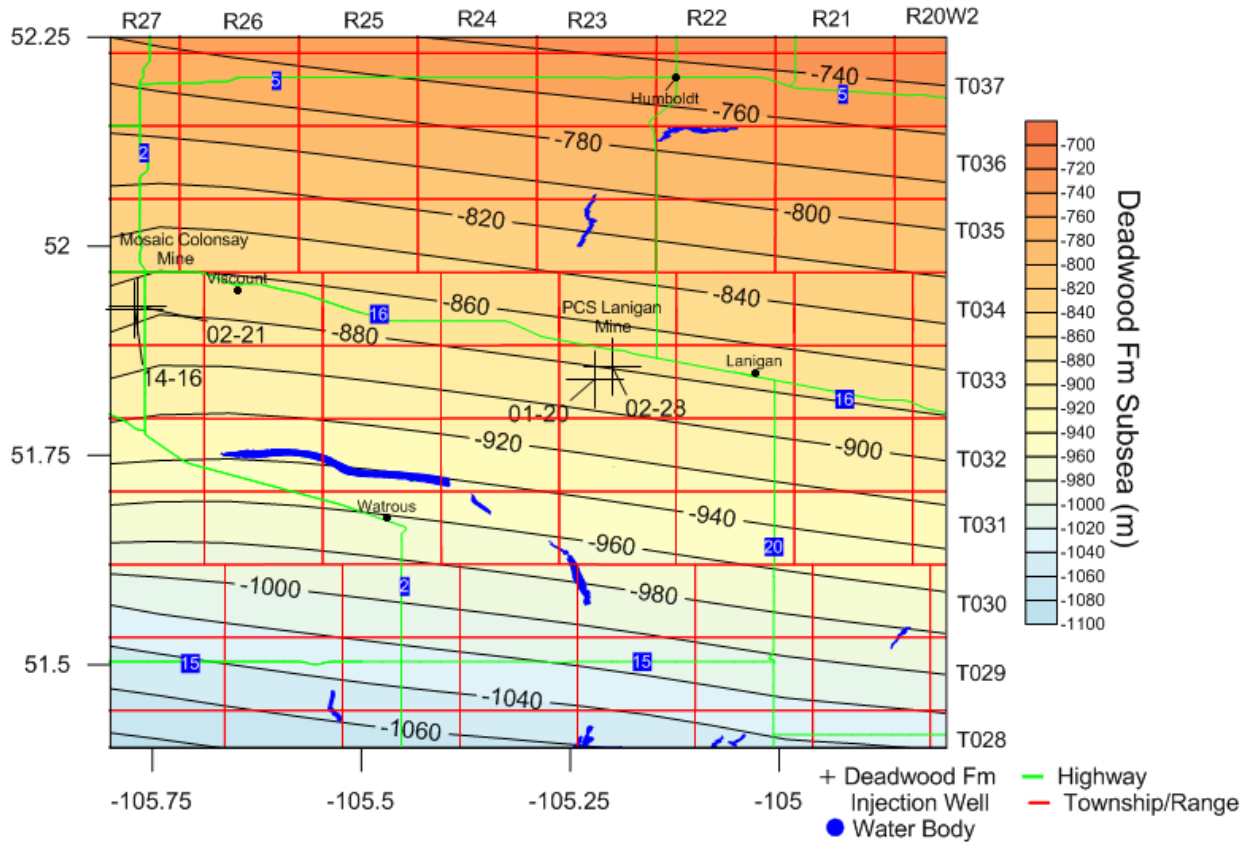
Figure 3-3: Lanigan mine site with Deadwood Formation injection well locations, with Deadwood Formation structure (metres subsea)

There are two injection wells operating at the Lanigan mine site with falloff test records available for both wells over a large time interval (Table 3-3).

Table 3-3: Falloff test distribution for Lanigan injection wells

	Lanigan Wells				
Year	01-20	02-28	Year	01-20	02-28
1977	X		1996	X	
1978			1997	X	X
1979	X		1998	X	X
1980			1999	X	X
1981	X		2000	X	X
1982			2001	X	X
1983			2002	X	X

1984			2003	X	X
1985			2004	X	X
1986			2005	X	X
1987			2006	X	X
1988			2007	X	X
1989			2008	X	X
1990			2009	X	X
1991	X		2010		
1992	X		2011	X	X
1993	X		2012	X	X
1994	X		2013	X	X
1995	X		2014	X	X
	01-20	02-28			
Total tests	26	17			

3.2.4 Esterhazy Study Area

In the Esterhazy area there are three Potash mines, the Mosaic K1 and K2 mines and the Potash Corp Rocanville Mine, making up the most densely concentrated area of potash mining in the province. Within this small area there are 32 injection wells utilizing the Interlake Group for wastewater injection (Figure 3-4).
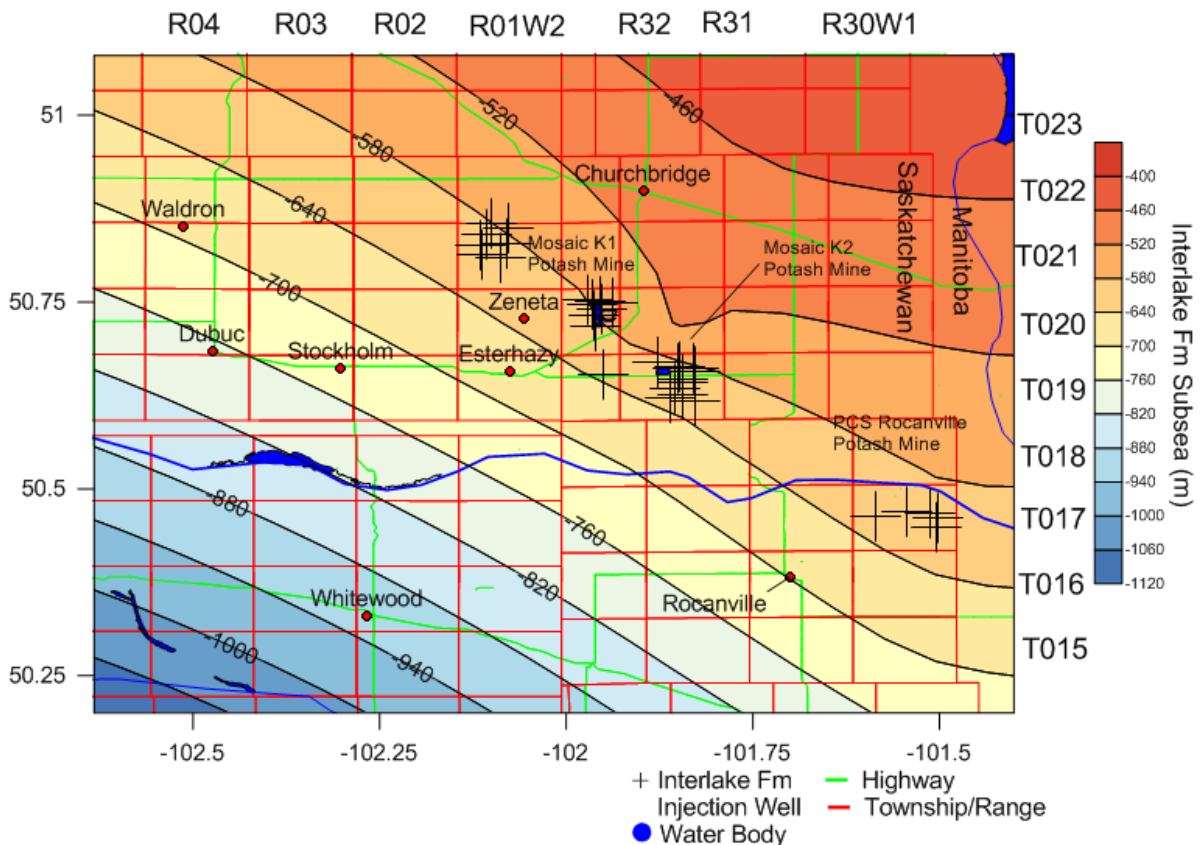
Figure 3-4: Esterhazy area mine sites with Interlake Group injection well locations, with Interlake Group structure (metres subsea)

Within the 32 injection wells disposing in the Interlake Group in the study area, falloff test records were available for 14 of these wells. The distribution of these tests can be seen in Table 3-4.

Table 3-4: Falloff test distribution for Esterhazy area injection wells

Year	Rocanville Wells				Mosaic K2					Mosaic K1				
	01-14	03-20	12-22	06-23	11-27	14-27	05-33	10-14	04-33	11-23	01-26	11-26	13-26	16-26
1975	X	X				X								
1976	X	X				X		X						
1977	X	X				X		X						
1978	X	X												
1979								X						
1980	X	X						X						
1981						X		X						
1982	X	X			X	X		X						
1983						X		X						
1984					X	X		X						
1985					X	X		X						
1986			X											
1987		X			X	X		X			X	X	X	X
1988					X	X	X		X					
1989	X	X	X		X	X	X		X					
1990	X	X		X										
1991	X	X	X	X	X	X	X		X					
1992		X		X	X	X	X		X					
1993					X	X	X		X					
1994		X	X	X										
1995		X	X	X	X	X	X	X	X	X	X	X	X	X
1996	X	X	X	X										
1997	X	X	X	X										
1998		X	X	X										
1999		X	X	X										
2000	X	X	X											
2001	X	X	X	X										
2002	X	X	X	X										
2003	X	X	X	X										
2004	X	X	X	X										
2005	X	X	X	X										
2006	X		X	X										
2007	X		X	X										
2008	X		X	X										
2009														
2010			X	X										
Total tests	20	23	19	18	10	15	6	11	6	1	2	2	2	2

3.3 Methods

Analytical modelling of the aquifer response to brine injection in the wells at each mine site was undertaken using Aqtesolv (HydroSOLVE Inc 2016). Aqtesolv is commonly used to simulate the aquifer response (drop in hydraulic head) to pumping wells, however it can also be used to model water injection. In the model, the location of each injection well was specified over a grid. The monthly injection rates for each of the wells obtained from AccuMap (AccuMap 2016) were input into the model. An average aquifer thickness for each mine site was based on

net sand thickness from gamma-ray logs. In this model the distinct sand packages within the Deadwood and Winnipeg Formations were lumped together and modelled as a single aquifer. The simulations in Aqtesolv were conducted based on the Theis equation (equation 3.2) which estimated the aquifer response to pumping (or injection) as follows (modified from Case et al. 1974):

$$s(t) = \frac{Q}{4\pi T_{Aquifer}} \int_u^\infty \frac{e^{-y}}{y} dy \qquad (3.2)$$

where
$$u = \frac{r^2 S}{4 T_{Aquifer} t_{pump}}$$

and s(t) (m) is the drawdown (or buildup) in the aquifer, Q $(\frac{m^3}{s})$ is the pumping (or injection rate), $T_{Aquifer}$ $(\frac{m^2}{s})$ is the transmissivity of the aquifer, r (m) is the distance between the pumping (or injecting) well and observation well, S is the storativity, t_{pump} (s) is the time since pumping started. The Theis equation is based on Fourier's mathematical theory of heat conduction, with this theory applied to groundwater flow (Theis 1935). The equation is able to describe groundwater flow while assuming a homogenous, isotropic aquifer with constant thickness and infinite aerial extent (McElwee 1980).

Aquifer parameters determined from the reservoir characterization study (Chapter 2), including aquifer thickness, transmissivity (converted from permeability) and storativity (converted from compressibility), were required inputs for these simulations. The transmissivity values used in the simulations were based on the permeability values interpreted at each of the mine sites from the various methods of analysis (core, DSTs and falloff tests). Additionally, aquifer storativity needed to be estimated. The storativity (S) (unit less) values were calculated with the specific storage (S_S) (m^{-1}) and aquifer thickness (b) (m) using equation 3.3 (Younger 1993)

$$S = S_s \times b \qquad (3.3)$$

The aquifer thickness was estimated based on the sand thicknesses within the injection intervals in the disposal wells at each mine site using a 75 API gamma cut-off for the basal clastics. A 6% neutron porosity reading was used as the net pay cut-off for the Interlake Group carbonates.

Specific storage (S_S) (m^{-1}) is a parameter calculated with equation 3.4 (Younger 1993)

$$S_s = \rho_w g(\alpha + \phi\beta) \qquad (3.4)$$

where ρ_w is the formation fluid density $(\frac{kg}{m^3})$, g is the acceleration due to gravity $(9.81\frac{m}{s^2})$, α is the aquifer skeleton compressibility (Pa^{-1}), ϕ is the formation porosity (unit less), and β is the compressibility of formation water (Pa^{-1}).

The aquifer skeleton compressibility was estimated using the Hall (1953) relationship of aquifer skeleton compressibility with porosity (Section 3.3.1), as well as using the relationship between compressional and shear wave velocities from dipole sonic logs (Section 3.3.2). In these two methods the bulk compressibility was estimated and substituted in place of the $(\alpha + \phi\beta)$ term of equation 3.4.

Historical injection rates for each of the wells were obtained using AccuMap (IHS AccuMap 2016). With these input parameters, Aqtesolv was used to simulate the increase in hydraulic head due to injection throughout the aquifer at each mine site. Changes in pressure heads ($\Delta\psi$) (m) were converted to simulated aquifer pressure increases (ΔP_{sim}) (Pa) using equation 3.5:

$$\Delta P_{sim} = \Delta\psi g \rho_w \qquad\qquad (3.5)$$

Where g is the gravitational acceleration constant ($9.81 m/s^2$) and ρ_w is the formation fluid density (kg/m^3).

These changes in aquifer pressure produced from the analytical models were then compared to changes in aquifer pressure estimated from the available falloff tests. In order to find the change in aquifer pressure indicated by the falloff tests, a baseline pressure at each mine site was established based on the extrapolated aquifer pressures obtained from the DSTs. This baseline pressure was then subtracted from the aquifer pressure estimates from the falloff tests in order to obtain the change in aquifer pressure ($\Delta P_{Falloff}$).

Different simulation outputs obtained using different values of transmissivity and storativity produced different aquifer pressure responses. The simulations with the strongest correlation to the falloff test results were identified as those with the lowest root mean squared error (RMSE) between the observed falloff test pressure data and the simulated aquifer pressure response. These simulations (based on particular values of transmissivity and storativity) were taken as the best representation of the aquifer at that particular mine site.

The pressure response throughout each mine site was mapped in order to gain insights into the radius of influence that these injection wells have on the aquifer. In order to provide additional insights into the distances that the pressure changes propagate through the aquifer, as well as establishing the degree of interference between the various mine sites, simulations were conducted using only a particular mine site's wells while additional simulations were conducted that included the surrounding mine sites wells while using the same aquifer parameter inputs. This analysis is useful in determining the degree of interference between the wells at the different mine sites.

Falloff Test Analysis

The analysis of the falloff tests conducted in the injection wells at the mine sites yielded valuable information including formation permeability, wellbore skin effects and radius of investigation of the tests. Additionally the static aquifer pressure was able to be estimated by extrapolating the late time pressure data to infinite shut in time ($\frac{(Tp+\Delta T)}{\Delta T}$) $= 1$ (EPA 2002) on a Horner plot (Figure 3-5). In this well (10-12) at the Cory mine this extrapolated aquifer pressure was found to be 15800 kPa at a depth of approximately 1400 m TVD. A hydrostatic pressure correction was then applied in order to account for the difference in the depth of the recorder and the mid-point injection depth. This pressure correction was calculated by multiplying the difference (m) between the recorder and mid-point injection with the pressure gradient in the area (10.0 kPa/m). The resultant corrected extrapolated aquifer pressure for this test was found to be 17200 kPa.
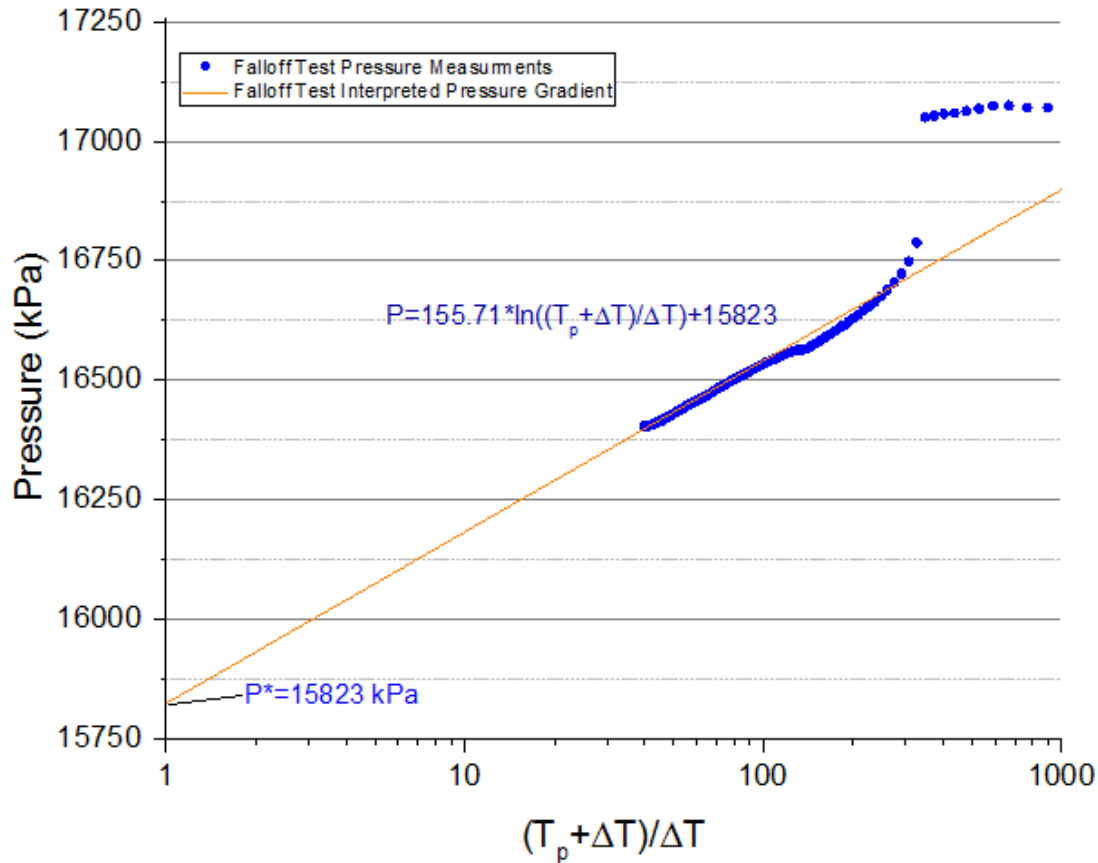
Figure 3-5: Horner plot of 2010 Falloff test data from well 10-12 (UWI 111/10-12-036-07W3) at Cory mine site, T_p=injection time since last pressure equalization, ΔT=shut in time

The difference between the aquifer pressures calculated for each falloff test and the baseline aquifer pressure at midpoint injection estimated from the DST pressure gradient yielded the change in aquifer pressure (ΔP) due to injection.

3.4 Analytical Modelling Results

3.4.1 Cory-Vanscoy Study Area

3.4.1.1 Cory-Vanscoy Aquifer Characterization

The aquifer characteristics of the Deadwood Formation at this mine site was assessed through geophysical logs, DSTs and falloff tests carried out in the injection wells. The average length of the injection wells within the Deadwood formation was 300 m. However, the thickness of the Deadwood aquifer was only 83m as much of the Deadwood Formation was dominated by thick shale sequences that would not accept injected fluids and are therefore not included in the aquifer thickness. The Deadwood Formation at this site can be considered to be comprised of several different small aquifers, with each sand package being considered an individual aquifer. The sand and shale sequences are correlatable throughout the area as determined from geophysical logs. The DST permeability values in this area were found to be higher than those

from the falloff tests. A summary of the average permeability (hence transmissivity) values can be observed in Table 3-5.

Table 3-5: Summary of average permeability (transmissivity) values determined from the various methods of analysis at the Cory-Vanscoy site.

Test Type	k (m^2)	T (m^2/s)
Core	4.87×10^{-13}	3.98×10^{-4}
Falloff Test	6.27×10^{-13}	5.13×10^{-4}
Dirty sand DST	4.84×10^{-13}	3.96×10^{-4}
Clean and dirty sand DST	1.20×10^{-12}	9.81×10^{-4}
Clean Sand DST	1.91×10^{-12}	1.57×10^{-3}

The baseline pressure established at this site is a representation of the static aquifer pressure prior to injection. In this case, the initial pressure gradient was matched to the DSTs run in 1970 as these tests preceded injection activities which began in March 1971 (Figure 3-6). The standard hydrostatic pressure gradient represents the expected increase in aquifer pressure with depth based on the fluid density of 1150 $\frac{kg}{m^3}$ of the formation fluids. This pressure gradient was found to be 11.64 $\frac{kPa}{m}$. It is apparent that the Deadwood Formation in this area is under pressured as the interpreted pressure gradient of 11.64 $\frac{kPa}{m}$ lies below the standard hydrostatic pressure gradient at this depth. The later time DSTs lie above the interpreted pressure gradient matched to the 1970 DSTs, which is due to an increase in aquifer pressure brought about by injection activities. Based on the interpreted pressure gradient and the hydrostatic pressure gradient, the aquifer pressure at a given depth (SS) as well as the expected hydrostatic pressure can be estimated using the equations in Figure 3-6.
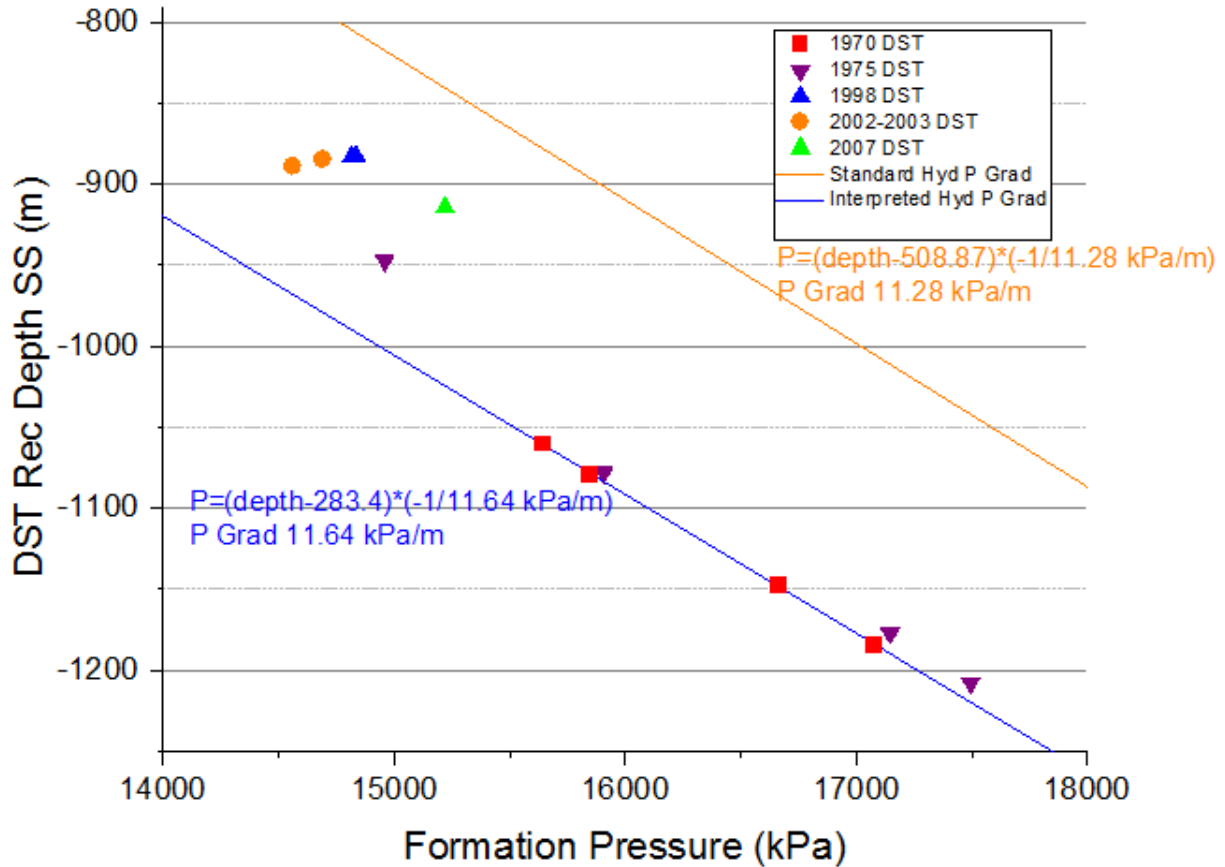
Figure 3-6: DST pressure gradient at Cory and Vanscoy mine sites, pressure at a given depth (m) can be calculated for both interpreted pressure gradient and standard hydrostatic pressure gradient based on the respective equations.

3.4.1.2 Cory-Vanscoy Analytical Modelling of Injection-Induced Pressure Change

The Cory mine well 08-13 was simulated for a variety of values of transmissivity including those derived from DSTs in clean and dirty sands, DSTs only in clean sands and falloff tests and inferred values while using a storativity value 9.84×10^{-5} derived from sonic logs in the injection wells (Figure 3-7). The higher transmissivity clean DST as well as the inferred transmissivity values resulted in the lowest simulated increase in aquifer pressure, while the lower transmissivity fall off tests indicate a significantly higher increase in aquifer pressure. These results are expected, as a higher transmissivity aquifer would more readily accept injected fluids and would more easily dissipate pressure increases into the aquifer. These analytical simulation outputs where compared to the observed changes in aquifer pressure as determined from the falloff tests. From this it became apparent which simulations (based on various values of transmissivity and storativity) produced simulation results that coincided best with the observed values from the falloff tests. The clean sand DST value of transmissivity ($T=1.57 \times 10^{-3}$ m^2/s) resulted in the best correlation with the falloff test data as it resulted in the lowest root mean square error (RMSE) between the analytical and observed data (Figure 3-7). This value of

86

transmissivity is on the higher end of the values seen in the DSTs in the area, however, as this value has the strongest correlation with the observed pressure data it is fair to infer that it is a good representation of the Deadwood Formation sands in the area. A summary of the results of these simulations can be seen in Table 3-6. An inferred transmissivity value of $1.84\times10^{-3}\,m^2$, on the higher end of the values seen in the DSTs in the area was simulated in order to determine if a higher than average transmissivity better represented the falloff test pressure data. However, the fit was found to be weaker than that found from the average values of the clean sand DSTs in the area.
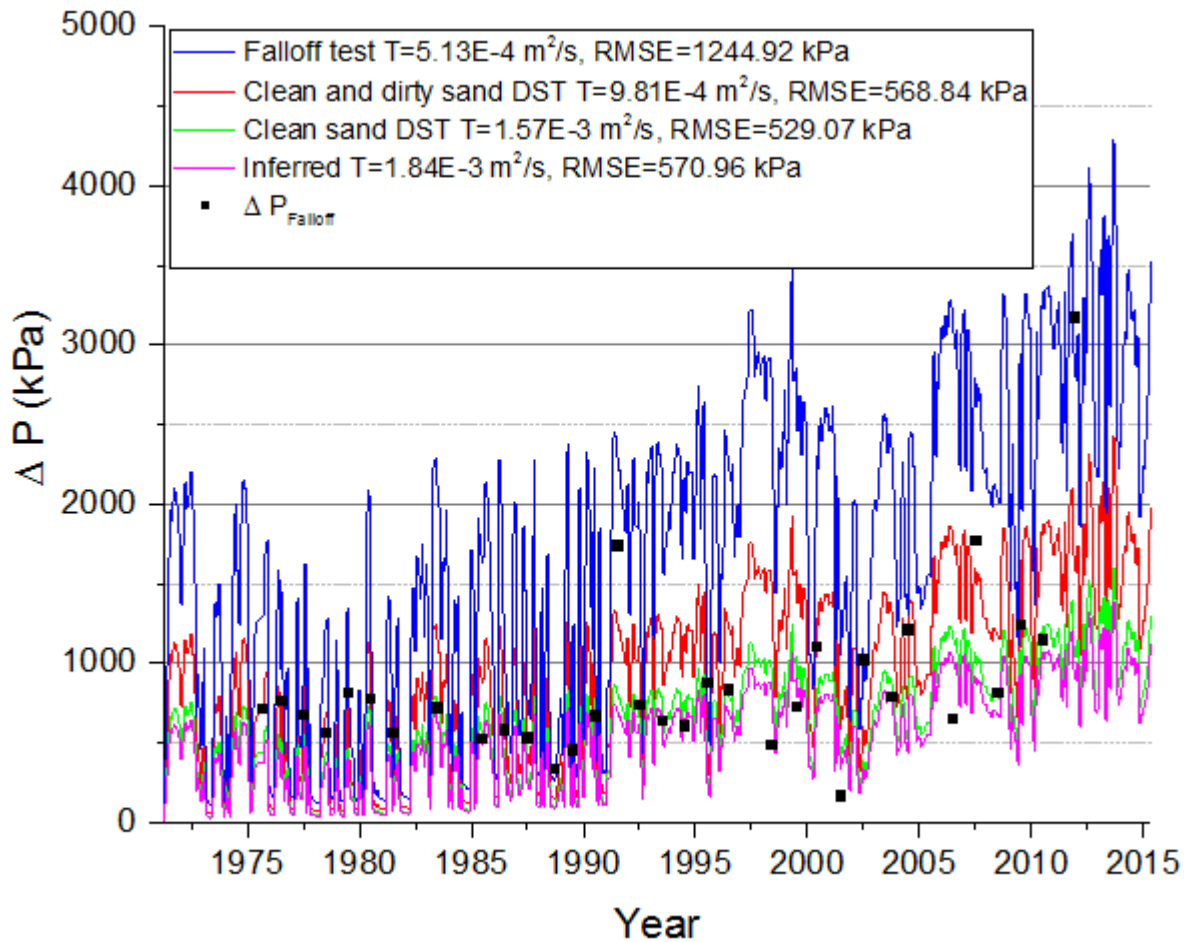
Figure 3-7: Aquifer simulation in Cory well 08-13 for varying values of transmissivity with sonic derived storativity $S=9.94\times10^{-5}$, simulation conducted with Cory and Vanscoy wells

Table 3-6: Cory and Vanscoy mine simulations with RMSE values for various values of transmissivity given sonic derived storativity ($S=9.94\times10^{-5}$).

Sim #	T (m²/s)	S	13-07 RMSE (kPa)	10-12 RMSE (kPa)	08-13 RMSE (kPa)	03-21 RMSE (kPa)	Weighte d Avg RMSE (kPa)	Description	Comments
10	9.81×10^{-4}	9.94×10^{-5}	791.87	277.63	568.84	860.27	629.85	Clean and dirty sand DST k, sonic est S	Overestimated pressure response

11	$1.57 \times x10^{-3}$	9.94×10^{-5}	734.21	212.90	529.07	890.99	596.93	Clean sand DST k, sonic est S	Most closely matched pressure response
12	5.13×10^{-4}	9.94×10^{-5}	2240.53	1872.50	1244.92	857.93	1440.54	Falloff test k, sonic est S	Significantly overestimated pressure response
45	1.84×10^{-3}	9.94×10^{-5}	714.24	186.16	570.96	913.51	614.63	Inferred k, sonic est S	Most closely matched pressure response

Additional simulations were conducted for varying values of storativity using the clean sand DST value of transmissivity (T= 1.57×10^{-3} m^2/s). The storativity values include those based on the Hall (1953) correlation of pore volume compressibility with porosity (Section 3.3.1), and the sonic log derived value of bulk compressibility (Section 3.3.2). The low and high case storativity values are based on literature values of specific storage for competent rocks (Batu 1998). The high case storativity value resulted in the lowest increase in aquifer pressure (Figure 3-8), while the sonic derived storativity resulted in the largest increase in aquifer pressure. The sonic log derived and Hall (1953) storativity value resulted in the best correlation with the observed falloff test data having the lowest RMSE, with the Hall (1953) simulation giving marginally worse results (Figure 3-8), as was the case with other wells in the study area. The sonic logs are likely the best representation of the storativity values at the mine site because this data was obtained from actual aquifer data at the mine site where the Hall (1953) approach is empirical (based on data from other study areas). A summary of the results of these simulations can be seen in Table 3-7. The RMSE values observed in all of the simulations conducted at the Cory-Vanscoy study area can be seen in Appendix I.
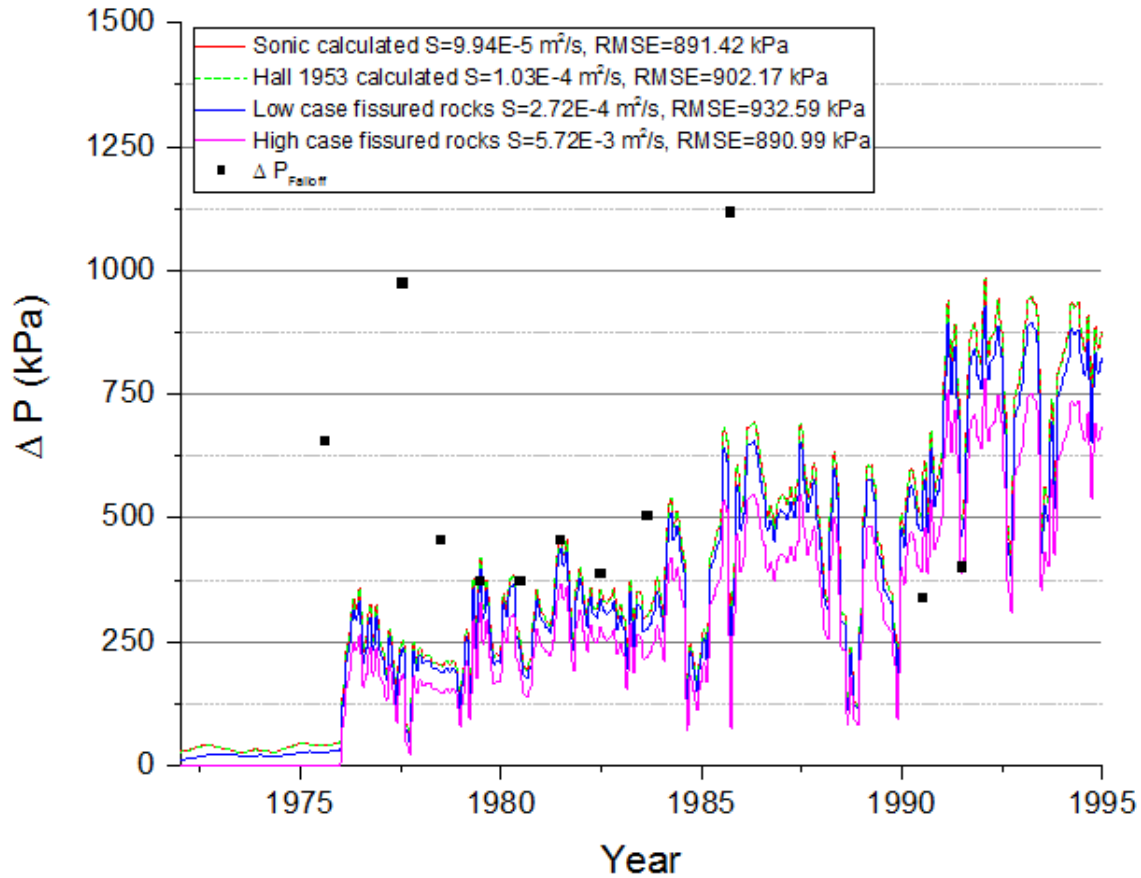
Figure 3-8: Aquifer simulation in Cory well 03-21 for varying values of storativity, using clean sand DST transmissivity (T= 1.57×10^{-3} m^2/s)

Table 3-7: Cory and Vanscoy mine simulations with RMSE values with varying values of storativity given history matched transmissivity (T=2.66×10^{-3} m^2/s)

Sim #	T (m^2/s)	S	13-07 RMSE (kPa)	10-12 RMSE (kPa)	08-13 RMSE (kPa)	03-21 RMSE (kPa)	Weighted Average RMSE (kPa)	Description	Comments
4	1.57×10^{-3}	1.03×10^{-4}	733.34	211.05	530.16	891.42	597.15	History matched k, Hall 1953 S	Corelated well with pressure response
5	1.57×10^{-3}	2.72×10^{-4}	719.01	196.38	560.61	902.17	609.59	History matched k, low end S fissured rocks	Underestimates pressure response
6	1.57×10^{-3}	5.72×10^{-3}	756.59	383.17	672.57	932.59	701.35	History matched k, high end S fissured rocks	Underestimates pressure response
11	1.57×10^{-3}	9.94×10^{-5}	734.21	212.90	529.07	890.99	596.93	History matched k, sonic est S	Most closely matched pressure response

89

Despite the large discrepancy in storativity values between the different simulations, the difference in the simulated pressure response does not vary nearly as much as in the case of varying transmissivity (Figure 3-7). However, these storativity value differences result in very large discrepancies in the distances that the pressure changes propagated through the aquifer at the mine sites. This is seen in Figure 3-9, where the scenario with a low storativity value derived from the sonic logs results in increases in hydraulic head propagating very large distances away from the mine site (up to 150km). Compared to the sonic log storativity, the high case storativity simulation hydraulic head increases where much less widespread from the mine sites (about 20 km) (Figure 3-10).
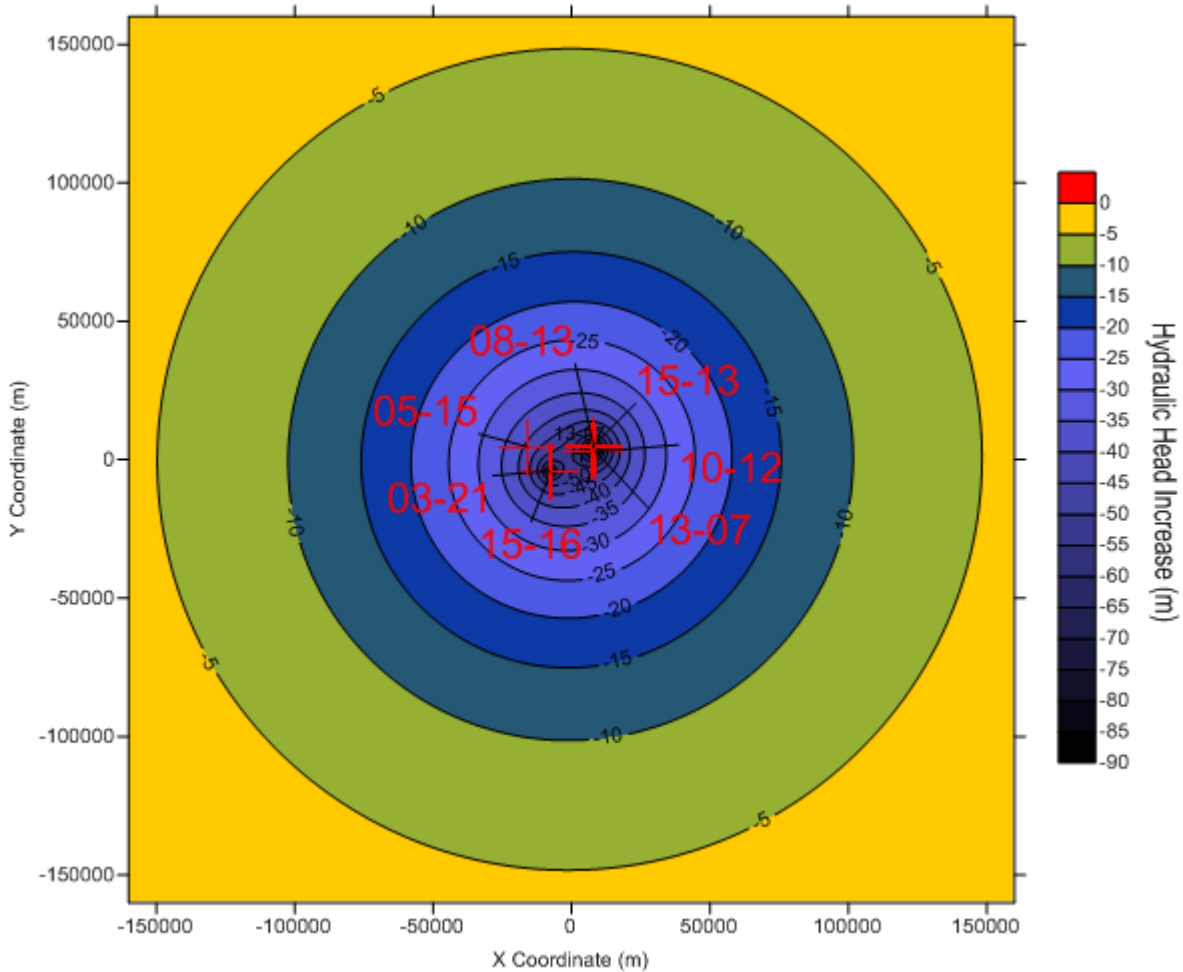
Figure 3-9: Aqtesolv simulation results for the Cory and Vanscoy mine at April 2015, using sonic estimated storativity (S=9.94×10^{-5}), and clean sand DST transmissivity (T=1.57×10^{-3} m^2/s)
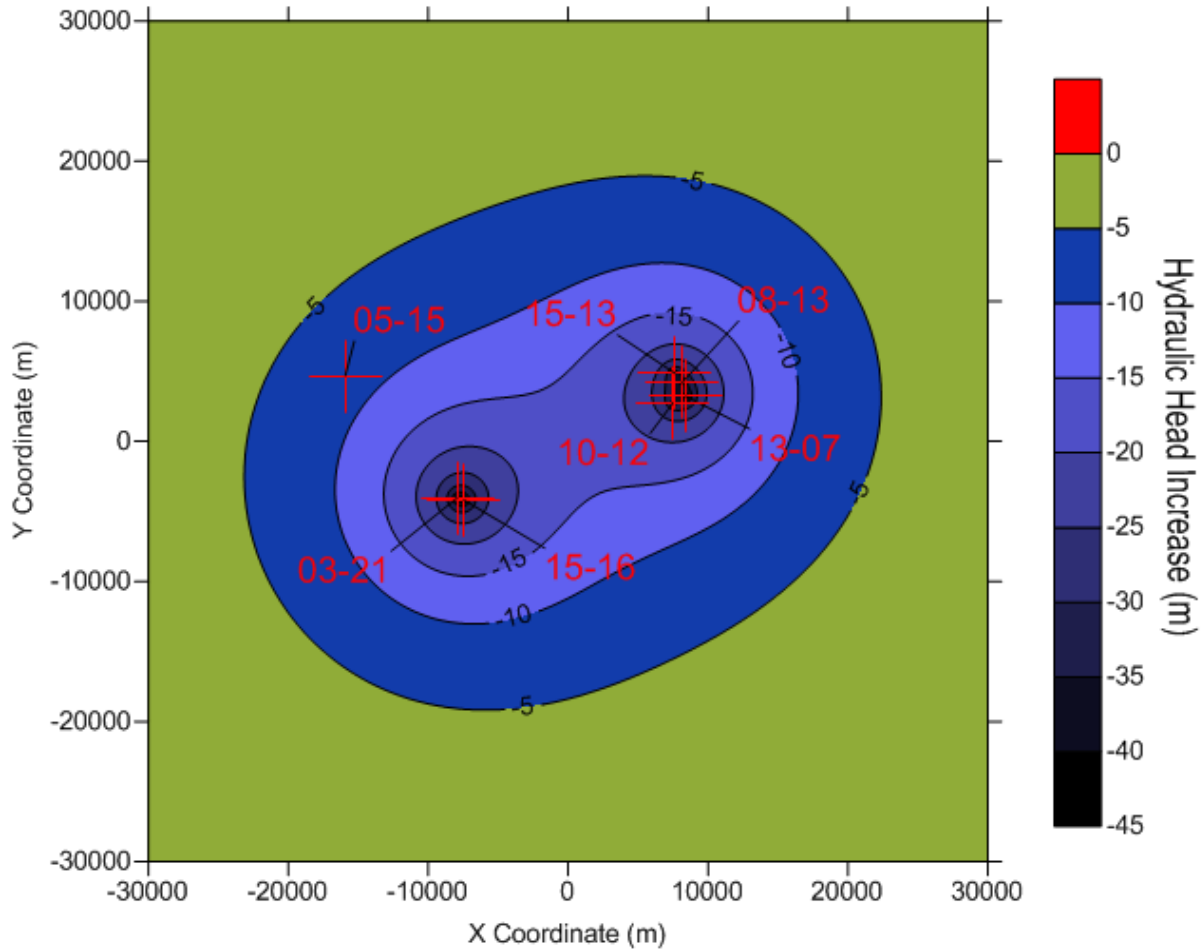
Figure 3-10: Aqtesolv simulation results for the Cory and Vanscoy mine at April 2015, using high case storativity (S=5.70×10^{-3}), and history-matched transmissivity (T=1.57×10^{-3} m^2/s)

3.4.1.3 Cory-Vanscoy Combined vs Isolated Simulation Results

The results of the isolated Cory-Vanscoy simulations were then compared to the combined simulations in order to find the effects on aquifer pressures that the Vanscoy wells had on the Cory wells (Figure 3-11). These effects were quantified with a differential pressure (kPa) between the isolated and combined simulation. The base case (resulting in the lowest RMSE with falloff test pressure data) based on the clean sand DST value of transmissivity (T=1.57×10^{-3} m^2/s) and sonic derived storativity (S=9.94×10^{-5}) results in a significantly larger differential pressure than the other simulations with higher storativity values. The differential pressure given the base case parameters was fairly significant with up to 275 kPa of pressure input from the Vanscoy and Transgas wells on the Cory mine site given that the total aquifer pressure response given these parameters in in the 1650 kPa range in certain years in the Cory 13-07 well. As well, it was observed that with the increasing injection rate input from the Vanscoy and Transgas wells the pressure differentials increase through time (Figure 3-11). Before 1976, when there were no injection wells in operation at Vanscoy, the differential pressure was zero. However when well 03-21 was brought online in 1976 a noticeable differential pressure appeared as seen in Figure 3-

12. As the production rate steadily increased in this well an increase in the differential pressure followed. Additional increases in the differential pressure where brought about by added production from the Transgas well 05-15 in 2004 and the Vanscoy well 15-16 in 2008.
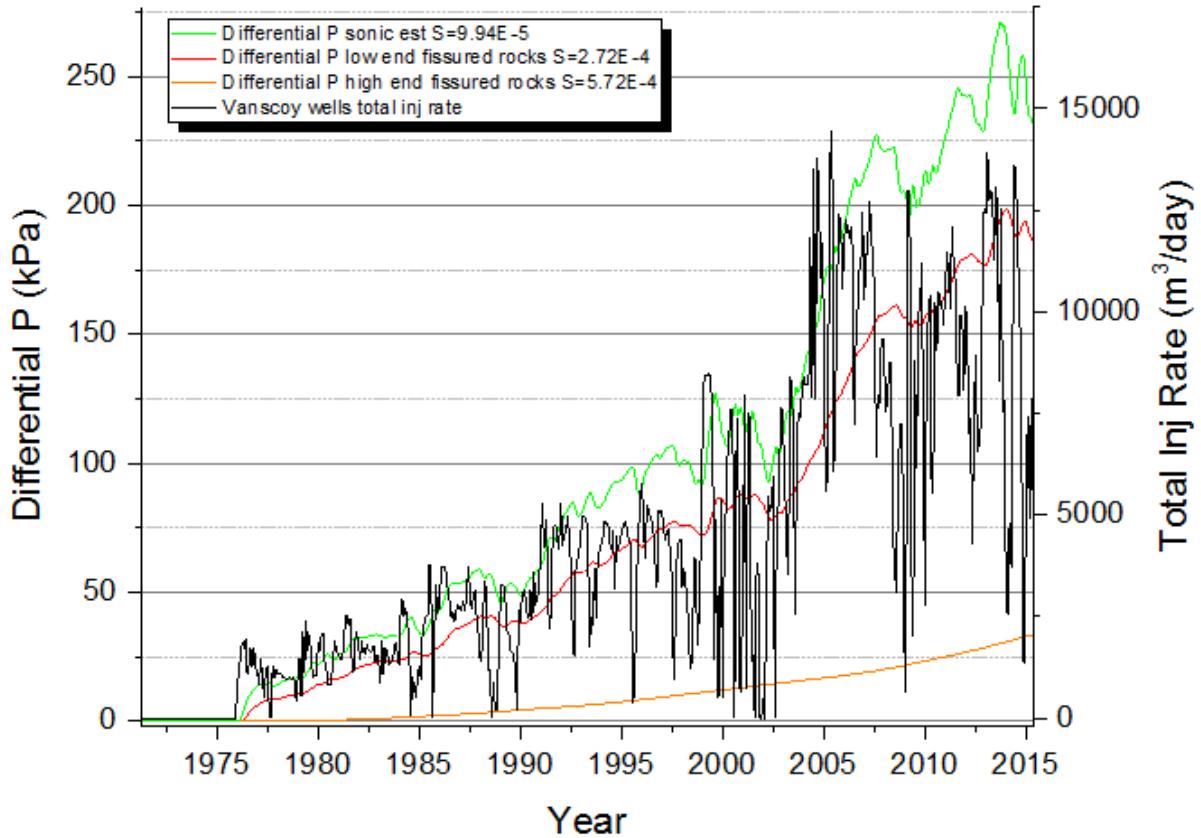
Figure 3-11: Cory well 13-07, differential pressure between Cory isolated simulation and Cory+Vanscoy combined simulation for varying storativity values with clean sand DST transmissivity (T=1.57×10^{-3} m^2/s)

Additional simulations were conducted in order to observe the differential pressure given various values of transmissivity (Figure 3-12). The inferred transmissivity values (T=1.84×10^{-3} m^2/s) resulted in the lowest differential pressure, while the lower transmissivity values given the clean sand DSTs, clean and dirty sand DSTs and falloff test result in progressively larger differential pressure given their progressively lower transmissivity values. However, due to the clean sand DST transmissivity (T=1.57×10^{-3} m^2/s) having the best fit with the observed falloff test pressure data, this simulation most likely results in the most representative differential pressure input of the Vanscoy and Transgas wells on the Cory mine site.
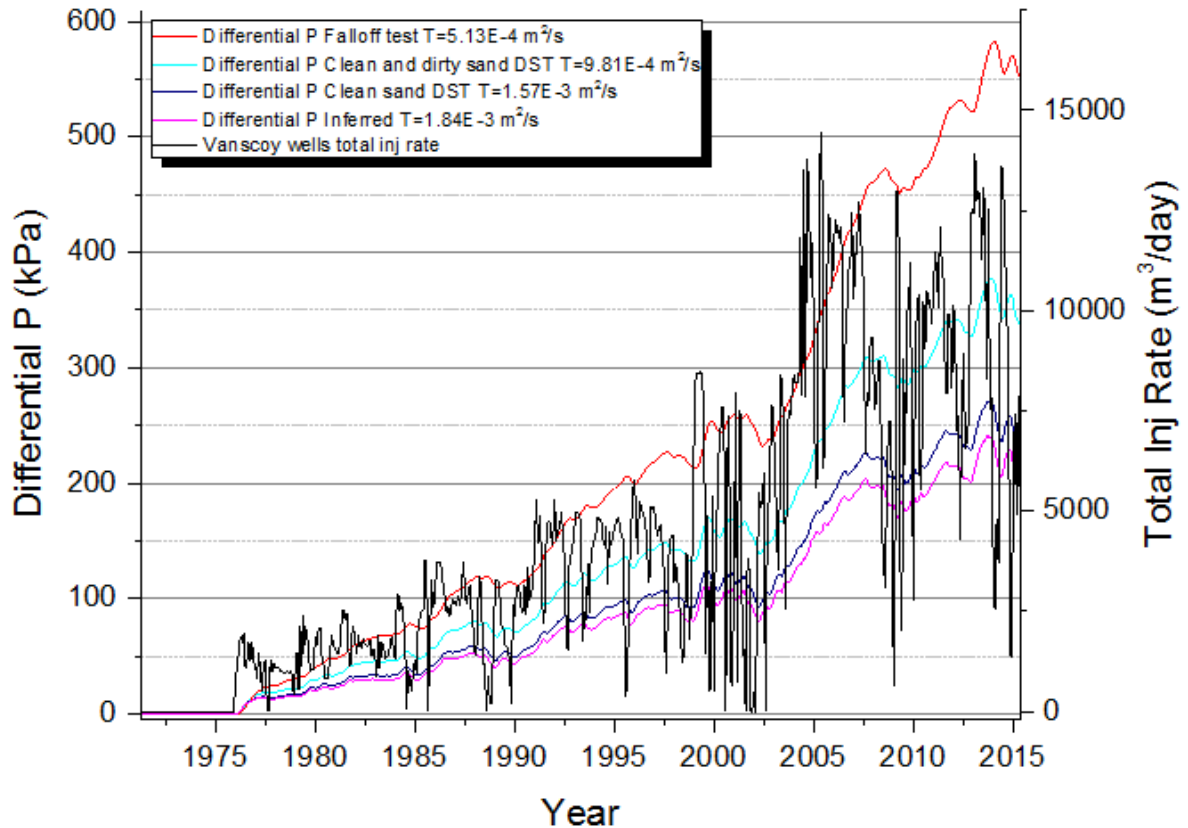
Figure 3-12: Cory well 13-07, pressure differences between Cory isolated simulation and Cory-Vanscoy combined simulation for varying transmissivity values given sonic calculated storativity ($S=9.94\times10^{-5}$)

In the Cory mine site for wells 08-13 and 13-07, both the Aqtesolv simulations and the falloff test results indicated a general increase in aquifer pressure over time due to injection activities. This increase in aquifer pressure over time is as well apparent in the plot of DST pressure gradient (Figure 3-6) where the DSTs conducted after 1971 (when injection began) appear over-pressured compared to the pressure gradient matched to the 1970's DSTs (conducted prior to injection in the area).

3.4.2 Allan, Patience Lake and Colonsay Study Area

3.4.2.1 Allan, Patience Lake and Colonsay Aquifer Characterization

The aquifer characteristics of the Deadwood Formation at this site was assessed through geophysical logs, DSTs and falloff tests from the injection wells (Table 3-8). The average aquifer thickness of the injection intervals within the Deadwood Formation was found to be 103.1 m. The average length of each of the injection wells within the Deadwood Formation is 250m, however a great deal of this is shale that is not included as net pay.

Table 3-8) Summary of average permeability (transmissivity) values determined from the various methods of analysis at the Allan-Patience Lake-Colonsay site.

Test Type	k (m^2)	T (m^2/s)
Falloff Test	1.13×10^{-12}	1.42×10^{-3}
Shale DST	2.18×10^{-14}	2.74×10^{-5}
Dirty sand DST	5.39×10^{-13}	6.78×10^{-4}
Clean and dirty sand DST	1.31×10^{-12}	1.60×10^{-5}
Clean Sand DST	2.47×10^{-12}	3.11×10^{-3}

An aquifer pressure gradient was established using DSTs in the area, with a baseline pressure gradient based on DSTs conducted in 1971/1972, prior to the onset of large-scale injection activities in the area (Figure 3-13). This pressure gradient was found to be 9.72 $\frac{kPa}{m}$, indicating an under-pressured aquifer given the hydrostatic pressure gradient of 11.3 $\frac{kPa}{m}$.
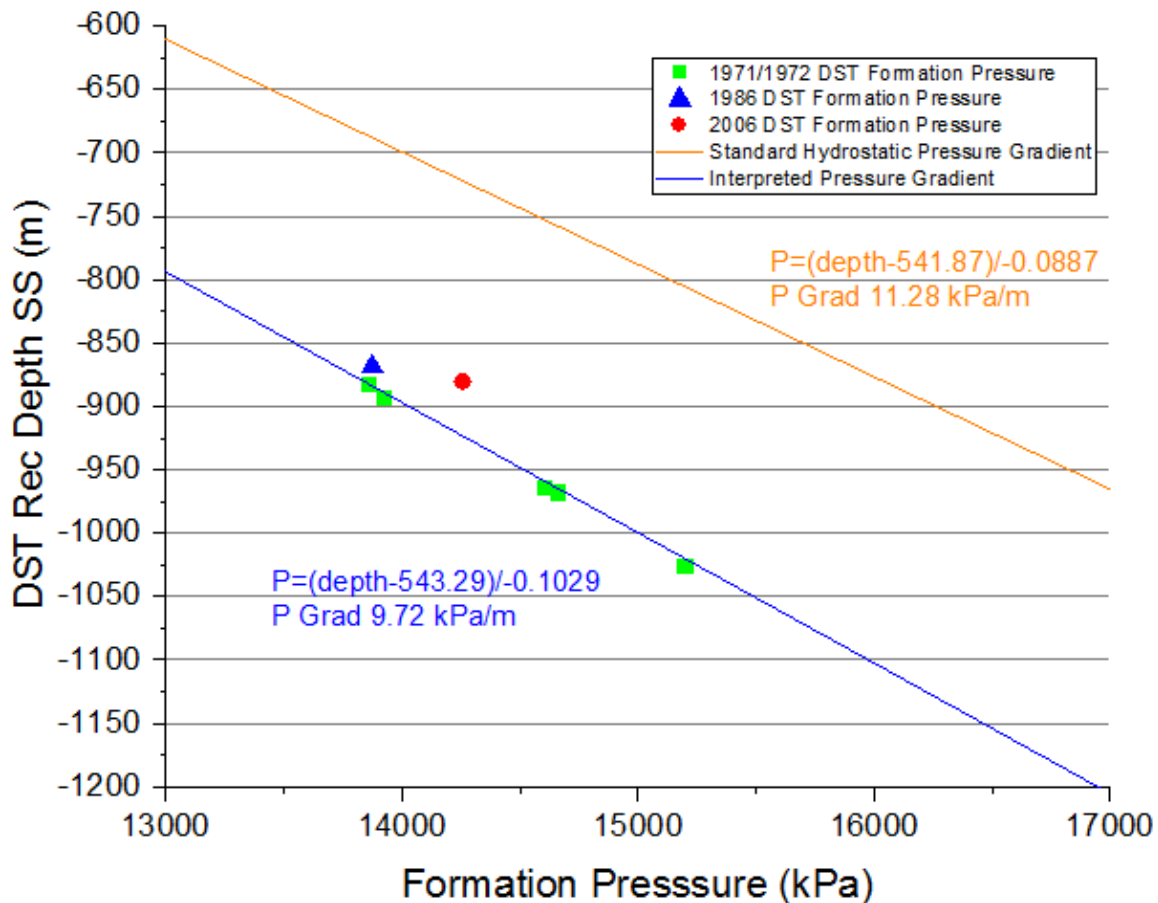
Figure 3-13: Pressure gradient at Allan, Patience Lake and Colonsay mine sites based on pre-injection 1971/1972 DSTs, pressure at a given depth (m) can be calculated for both interpreted pressure gradient and standard hydrostatic pressure gradient based on the respective equations.

3.4.2.2 Allan, Patience Lake and Colonsay Analytical Modelling of Injection-Induced Pressure Change

The change in aquifer pressure (ΔP) due to injection established from the falloff tests and baseline aquifer pressure was compared to the analytical simulation outputs from Aqtesolv. Some anomalous falloff pressure data was discounted from this comparison. In well 13-22 at the Allan site, the analytical simulation results from various values of transmissivity given sonic derived storativity ($S=1.17\times10^{-4}$) were compared to the observed pressures from the falloff test results (Figure 3-14) (Table 3-9). The dirty sand DST transmissivity ($T=6.78\times10^{-4}$ m^2/s) resulted in the largest increase in aquifer pressure, greatly exceeding the falloff test results. The falloff test transmissivity ($T=1.42\times10^{-3}$ m^2/s) as well resulted in an overestimated analytical pressure responses. The clean sand DST transmissivity ($T=3.11\times10^{-3}$ m^2/s) resulted in a significantly lower pressure response; correlating fairly well with the falloff test (significantly lower root mean square error). Further simulations were run with progressively larger transmissivity values until the optimal value with the lowest RMSE was found. The history-matched transmissivity value of 8.24×10^{-3} m^2/s was found to have the best correlation with the observed falloff test pressure data (lowest RMSE). This history-matched transmissivity ($T=8.24\times10^{-3}$ m^2/s) being considerably higher than what was observed in the well tests at these three mine sites.
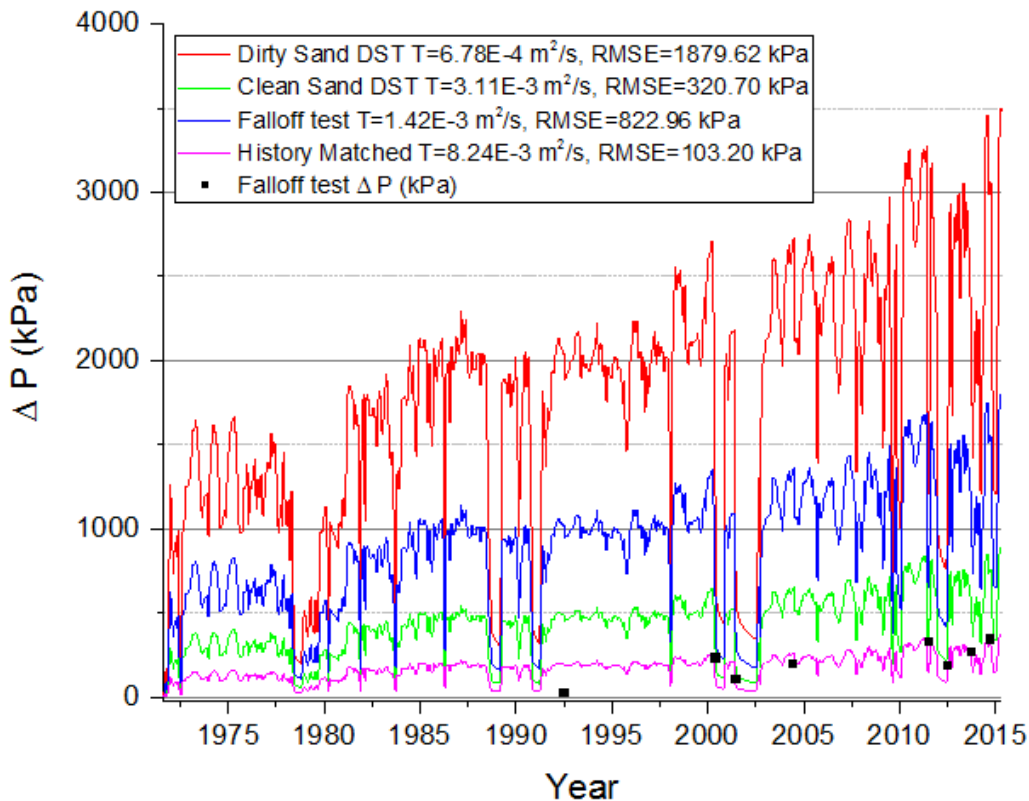
Figure 3-14: Aquifer simulation for Allan mine well 13-22 for varying values of transmissivity with sonic derived storativity ($S=1.17\times10^{-4}$), simulated with Allan, Patience Lake and Colonsay mine wells

Table 3-9: Allan, Colonsay and Patience Lake mine simulations with RMSE values for various values of transmissivity given sonic derived storativity ($S=1.17*x10^{-4}$).

Sim	T (m²/s)	S	13-22 RMSE (kPa)	16-28 RMSE (kPa)	14-16 RMSE (kPa)	02-21 RMSE (kPa)	Weighted Average RMSE (kPa)	Description	Comments
10	6.78×10^{-4}	1.17×10^{-4}	1879.62	2123.77	944.64	1531.39	1607.61	Dirty sand DST k, sonic est S	Severely overestimated pressure response
11	3.19×10^{-3}	1.17×10^{-4}	320.70	488.22	477.37	301.84	338.06	Clean sand DST k, sonic est S	Overestimated pressure response
12	1.42×10^{-3}	1.17×10^{-4}	822.96	1047.19	278.55	636.12	679.02	Falloff test k, sonic est S	Overestimated pressure response
43	8.24×10^{-3}	1.17×10^{-4}	103.20	219.49	714.17	152.08	201.39	History-matched k, sonic est S	Most closely matched pressure response

Similar results were seen in other wells in the study area, where the best correlation between the observed falloff test pressure data and the analytical aquifer simulations was established with a history-matched transmissivity significantly higher than that observed in the well tests at the mine sites. In the Colonsay mine injection well 02-21 as in the case of the 13-22 well, the same history-matched transmissivity of 8.24×10^{-3} m²/s resulted in the best correlation with the lowest RMSE (Figure 3-15).
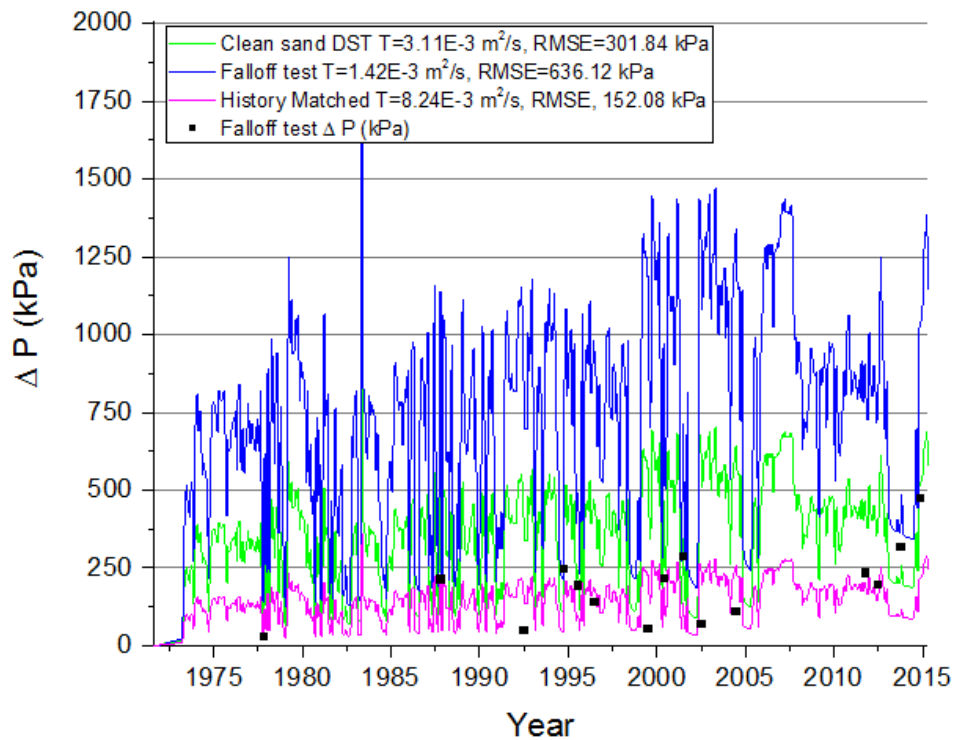
Figure 3-15: Aquifer simulation for Colonsay mine well 02-21 for varying values of transmissivity with sonic calculate storativity $S=1.17\times10^{-4}$

In one well in the study area however, the Colonsay well 14-16, the best correlation was established with the significantly lower falloff test derived transmissivity of 1.42×10^{-3} m^2/s (Figure 3-16), considerably lower than the history-matched value that correlated with the other wells. However, in this well only three reliable falloff tests were available. If more tests had been available the confidence of this correlation could more clearly established.
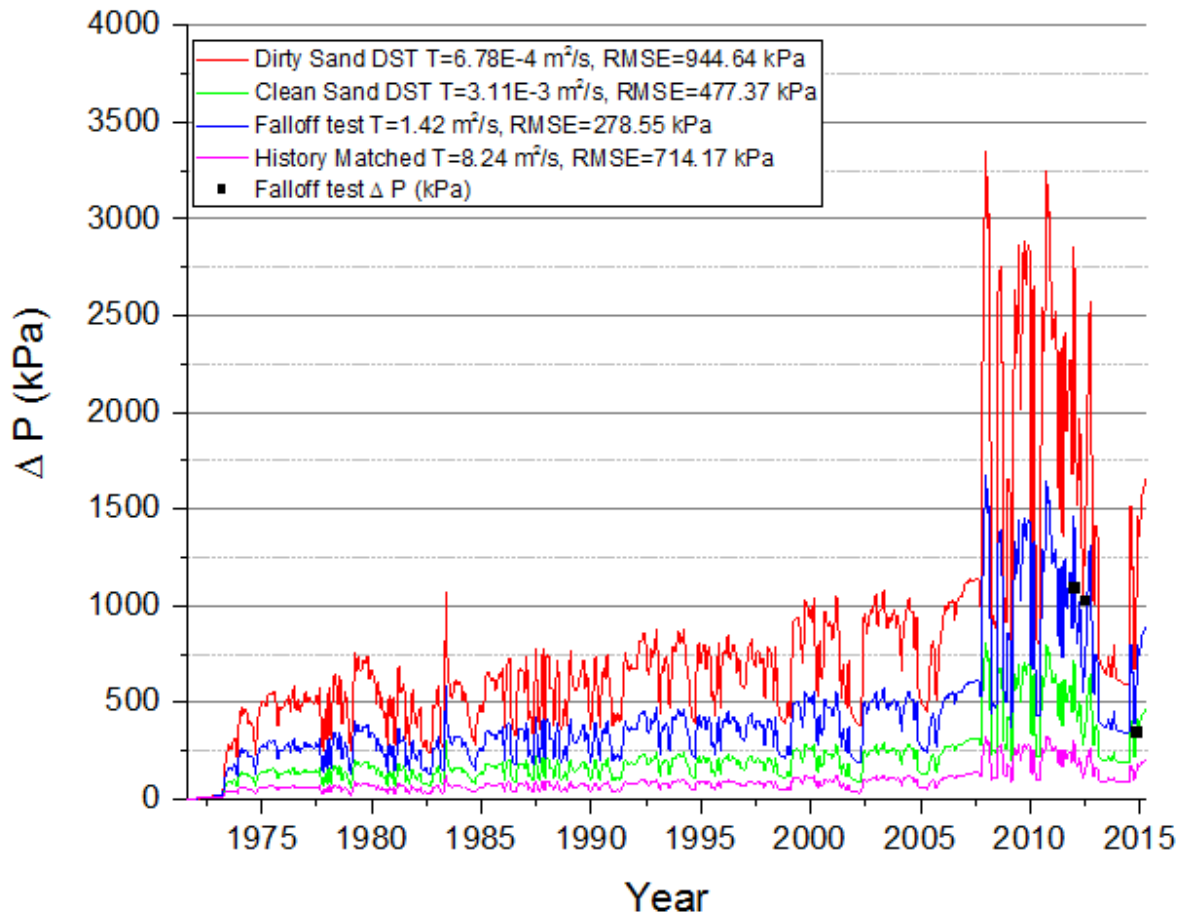
Figure 3-16: Aquifer simulation for Allan mine well 14-16 for varying values of transmissivity with sonic derived storativity (S=1.17×10^{-4})

Simulations were conducted for varying values of storativity on all of the wells in the area. As was observed at the other mine sites, varying storativity values did not have nearly as much effect on the pressure responses at injection wells as transmissivity. In this study area the strongest correlations between the analytical simulation outputs and the falloff test pressure data were observed with the sonic derived storativity. In Figure 3-17 the Allan mine well 13-22, the sonic derived storativity simulation resulted in the lowest RMSE given the history-matched transmissivity of 8.24×10^{-3} m^2/s. A summary of the results can be seen in Table 3-10. The RMSE values for all of the simulations conducted in this study area can be seen in Appendix J.
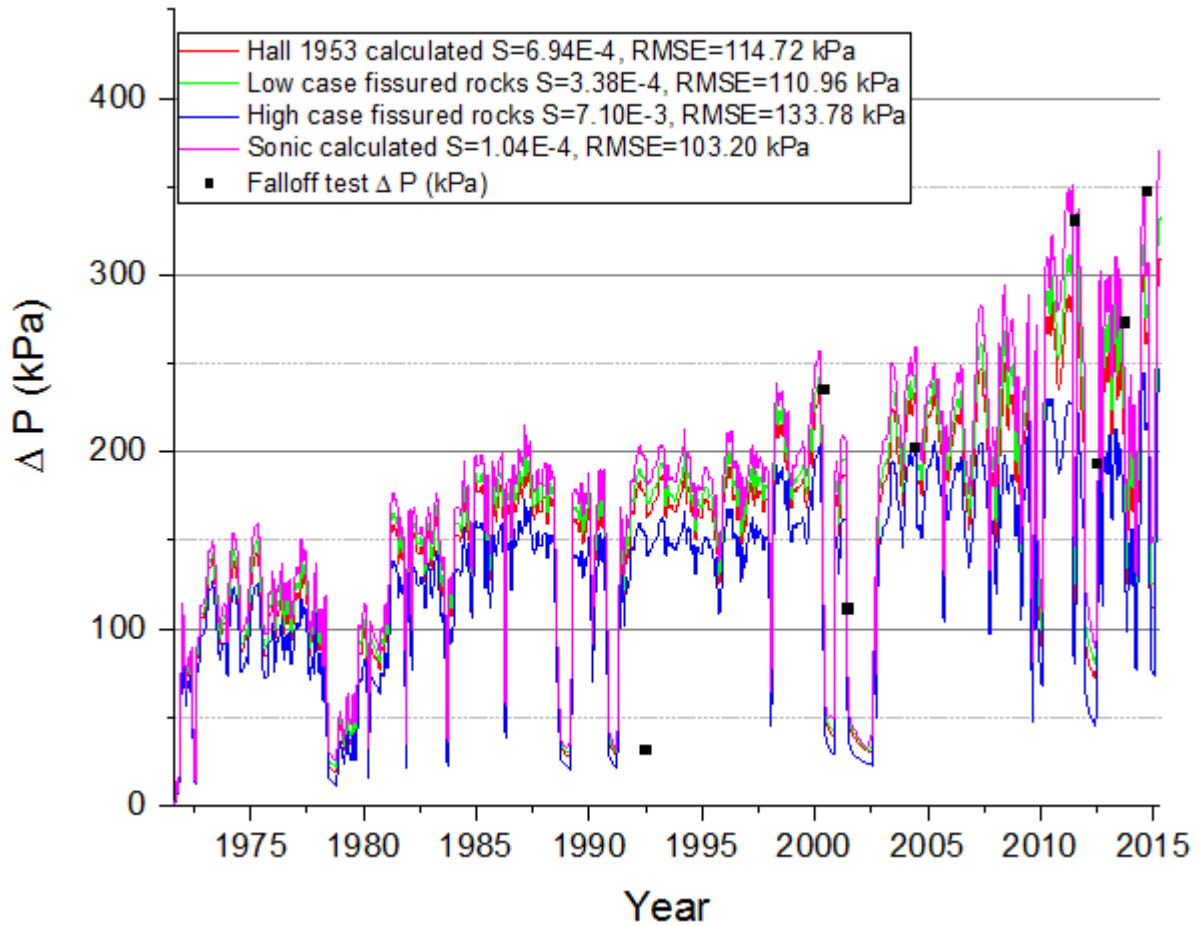
Figure 3-17: Aquifer simulation for Allan mine well 13-22 for varying values of storativity with history-matched transmissivity (T= 8.24×10^{-3} m^2/s)

Table 3-10: Allan, Colonsay and Patience Lake mine simulations with RMSE values for various values of storativity given history-matched transmissivity (T= 8.24×10^{-3} m^2/s)

Sim	T (m^2/s)	S	13-22 RMSE (kPa)	16-28 RMSE (kPa)	14-16 RMSE (kPa)	02-21 RMSE (kPa)	Weighted Average RMSE (kPa)	Description	Comments
44	8.24×10^{-3}	6.94×10^{-4}	114.72	206.57	745.70	158.84	210.67	Falloff test k, Hall 1953 est S	Underestimated pressure response
45	8.24×10^{-3}	3.38×10^{-4}	110.96	210.99	732.59	155.86	206.94	Falloff test k, low end S for fissured rocks	Underestimated pressure response
46	8.24×10^{-3}	7.10×10^{-3}	133.78	194.49	781.62	167.72	223.71	Falloff test k, high end S for fissured rocks	Significantly underestimated pressure response
43	8.24×10^{-3}	1.17×10^{-4}	103.20	219.49	714.17	152.08	201.39	Interpolated S, sonic est S	Most closely matched pressure response

Through mapping the pressure propagations at the mine sites the extent of the effects of the injection wells can be visualized. As seen in the Cory-Vanscoy area of study, the extent of the pressure propagations at the Allan, Patience Lake and Colonsay sites are highly dependent on the storativity value input in the simulation. The lower storativity inputs derived found from the sonic logs used (Figure 3-18) resulted in further pressure propagations throughout the aquifer (over 80 km) as compared to the high case storativity value in Figure 3-19 (40 km).
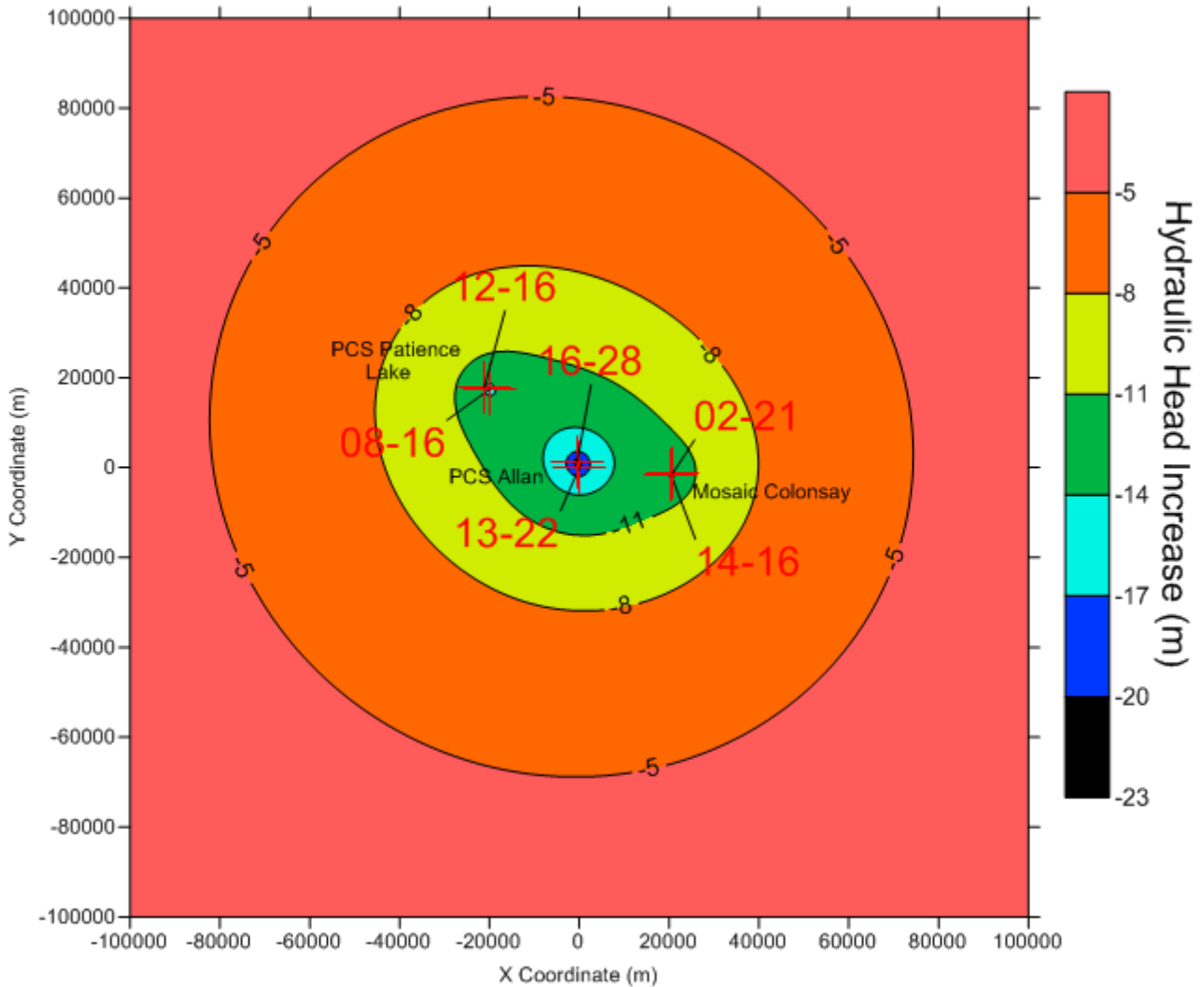
Figure 3-18: Aqtesolv simulation results for the Allan, Patience Lake and Colonsay mine site at April 2015 using interpolated T=8.24×10^{-3} m^2/s and sonic derived storativity (S=1.17×10^{-4})
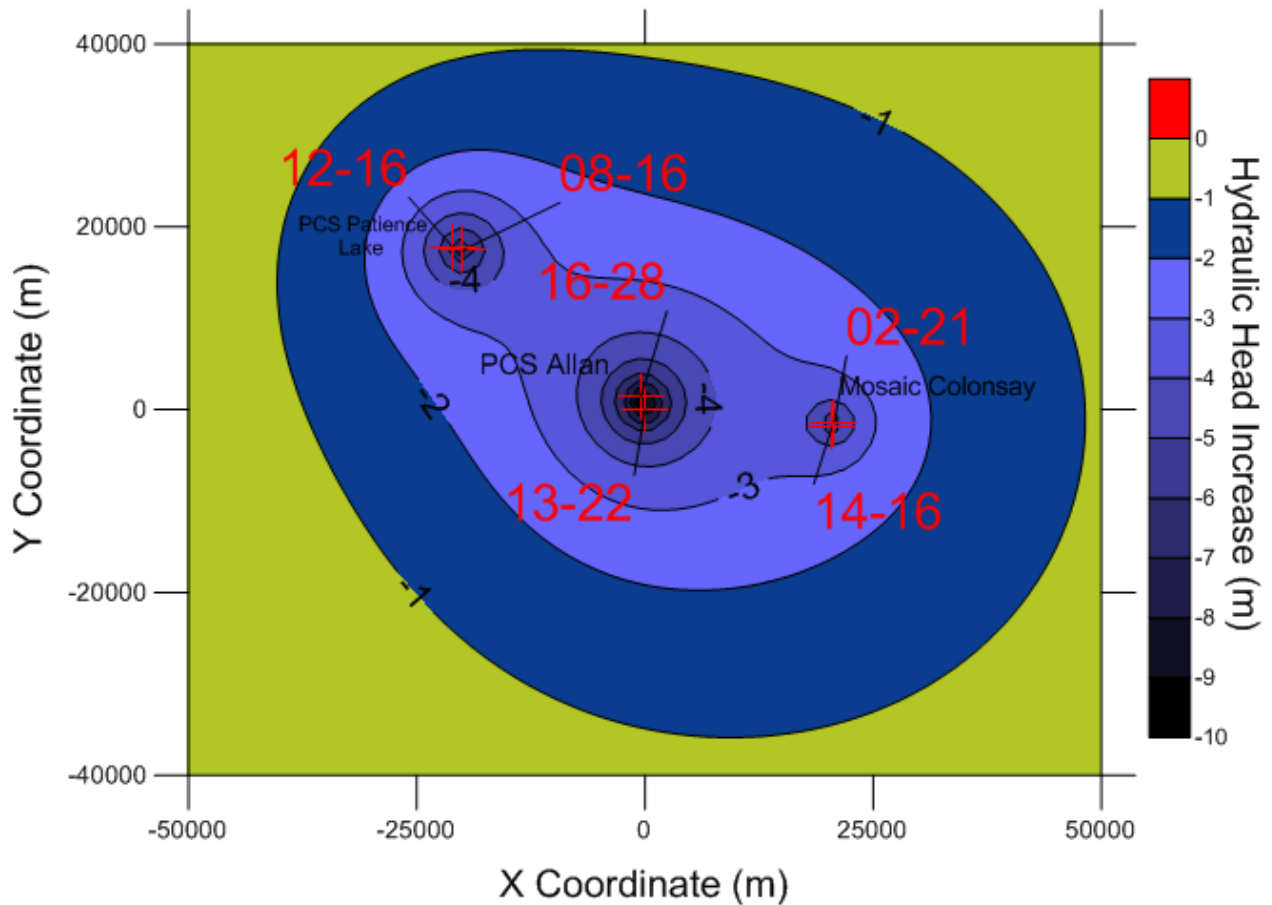
Figure 3-19: Aqtesolv simulation results for Allan, Patience Lake and Colonsay mine site at April 2015 using history-matched $T=8.24\times10^{-3}$ m^2/s and high case storativity ($S=7.10\times10^{-3}$)

3.4.2.3 Allan, Patience Lake and Colonsay Combined vs Isolated Simulation Results

Isolated simulations using only input from the Allan mine wells were conducted. These isolated simulations where then compared to the combined simulations (using injection wells from Allan, Patience Lake and Colonsay) in order to identify the effects that the neighbouring wells had on the Allan injection wells given various aquifer parameter values. In Figure 3-20 varying differential pressures over time can be observed for distinct transmissivity values given sonic calculated storativity ($S=1.17\times10^{-4}$). It can be seen that the lower transmissivity from the dirty sand DSTs resulted in the largest differential pressure, with progressively smaller differential pressures with increasing transmissivity. The most representative differential pressure is from the history-matched transmissivity ($T=8.24\times10^{-3}$ m^2/s) as this simulation has the best correlation with falloff test pressure data. Additionally, it is noted that the pressure differentials became larger over time as a result of increased injection volumes in the Patience Lake and Colonsay mine site wells (Figure 3-20). The pressure differential at the Allan well 13-22 began in 1973, when the Colonsay well 02-21 was brought online. The Patience Lake well 12-16 began injecting intermittently in 1987. A sharp increase in injection was brought about by the addition of the Colonsay well 14-16 in 2007 and the Patience Lake well 08-16 in 2008, which brought about further increases in the pressure differential.
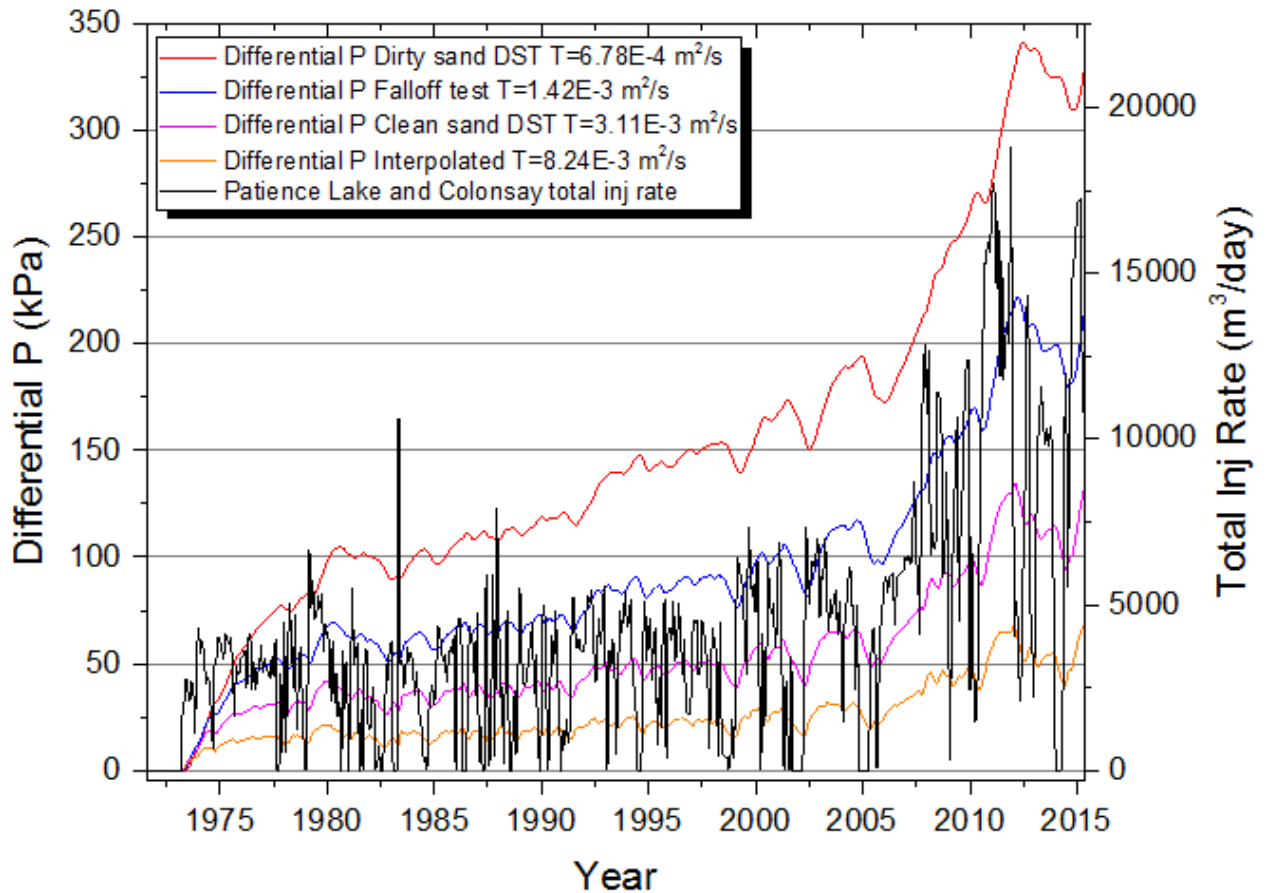
Figure 3-20: Allan mine well 13-22 pressure differential from Allan only simulation compared to Allan, Patience Lake and Colonsay simulation given different values of transmissivity given sonic calculated storativity ($S=1.17\times10^{-4}$)

The pressure differentials obtained from various values of storativity given the history-matched transmissivity ($T=8.24\times10^{-3}$ m^2/s) are seen in Figure 3-21. As was observed at the other mine sites the largest differential pressure was observed in the low value sonic calculated storativity ($S=1.17\times10^{-4}$). While the high case storativity (7.10×10^{-3}) resulted in a very low differential pressure that is practically negligible as the pressure transients are not able to propagate far enough into the formation to have a significant effect on the adjacent mine sites.
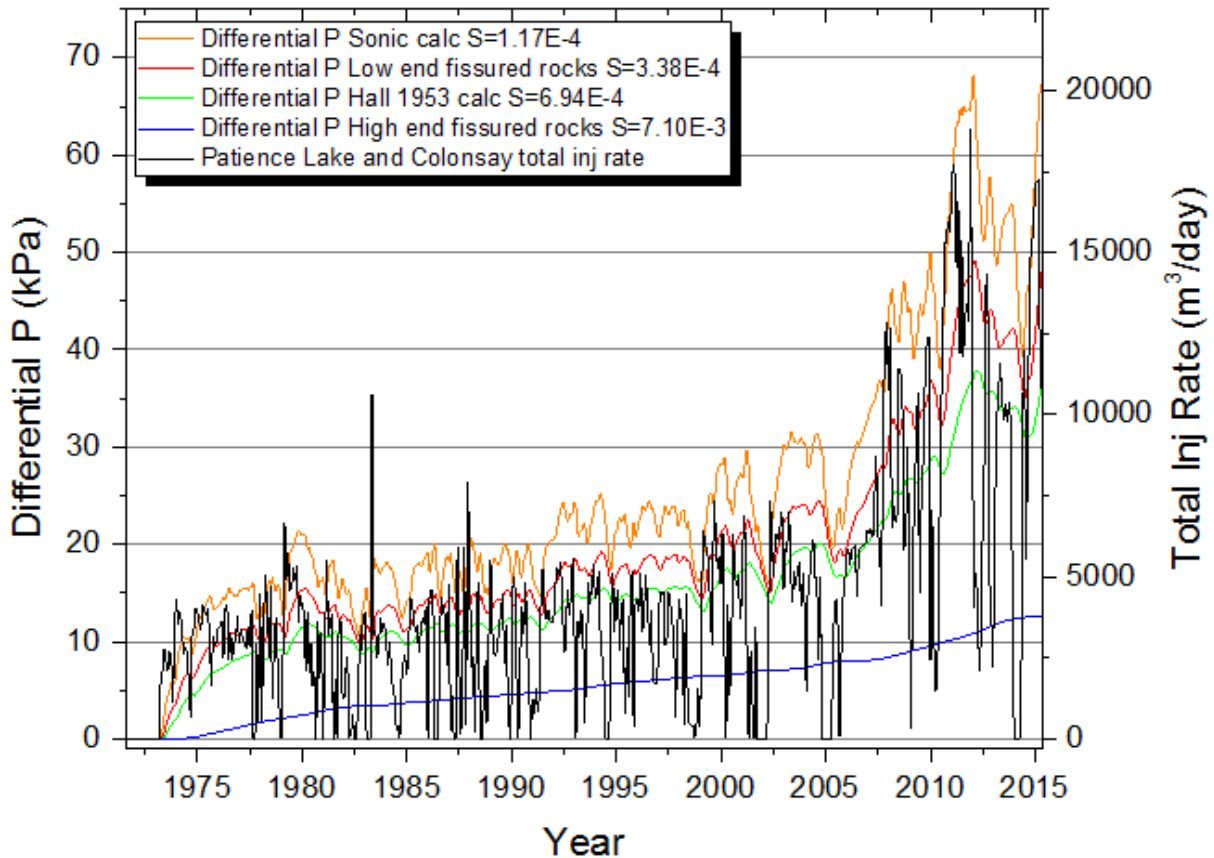
Figure 3-21: Allan mine well 13-22 differential pressure from Allan only simulation compared to Allan, Patience Lake and Colonsay simulation given different values of storativity, given base case interpolated transmissivity (T=8.24×10^{-3} m^2/s)

From the pressure differentials of the various simulations it can be seen that the Patience Lake and Colonsay wells have had a variable effect on the aquifer pressures in the Allan wells given the aquifer parameter inputs used in the Aqtesolv (HydroSOLVE Inc. 2016) simulations. The high case storativity values likely severely underestimated the pressure response while the low case sonic estimated storativity overestimated the response. Considering the history-matched transmissivity (8.24×10^{-3} m^2/s) with sonic calculated storativity (S=7.10×10^{-3}) simulation has the best correlation with the falloff test data, these aquifer parameters are likely the best representation of the aquifer, thereby providing the most accurate simulated pressure differential in this study area. Given these parameters the differential pressure is approximately 50-65 kPa at later times. Considering the total pressure response from injection at these times is around 300 kPa, this differential pressure is a significant component of the aquifer response to injection. Considering the Colonsay and Patience Lake sites are 20 and 28 km respectively away from the Allan mine site, it is reasonable to infer the injection activities at each of these three sites have noticeable effects on the aquifer conditions at the other sites.

3.4.3 Lanigan Study Area

3.4.3.1 Lanigan Aquifer Characterization

      Through analysis of the geophysical well logs the average aquifer thickness was found to be 86.3m, the average sand thickness completed within the Deadwood Formation. The sand packages within the Deadwood Formation were found to correlate across the study area.

Through Horner analysis of DSTs and falloff tests in the injection wells at the site permeability values for a variety of facies were established (Table 3-11), these values were used in the aquifer simulations at the mine site.

Table 3-11: Summary of average permeability (transmissivity) values determined from the various methods of analysis at the Lanigan site.

Test Type	k (m^2)	T (m^2/s)
Core	3.03×10^{-15}	3.31×10^{-6}
Falloff Test	6.36×10^{-13}	6.96×10^{-4}
Dirty sand low end DST	1.36×10^{-13}	1.49×10^{-4}
Dirty sand high end DST	5.32×10^{-12}	5.82×10^{-3}
Clean and dirty sand DST	1.40×10^{-12}	1.53×10^{-3}

The DSTs as well provided extrapolated aquifer pressures that allowed for a baseline aquifer pressure gradient to be established ($9.58 \frac{kPa}{m}$) using the pre-injection era DSTs (1975 DSTs) (Figure 3-22). As with the other mine sites this gradient was found to be sub-hydrostatic as the hydrostatic pressure gradient was found to be $11.3 \frac{kPa}{m}$.
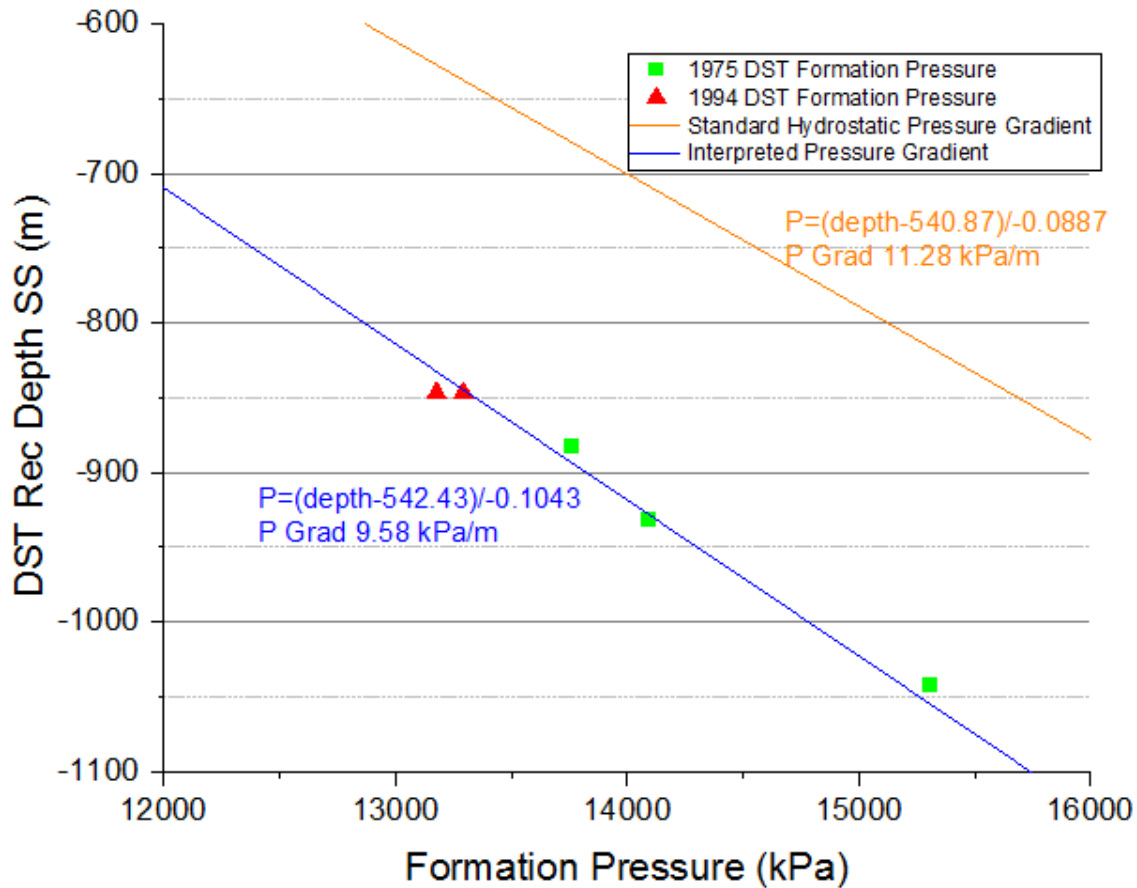
Figure 3-22: Lanigan study area pressure gradient based on pre-injection 1975 DSTs, pressure at a given depth (m) can be calculated for both interpreted pressure gradient and standard hydrostatic pressure gradient based on the respective equations.

3.4.3.2 Lanigan Analytical Modelling of Injection-Induced Pressure Change

Analytical models of the Lanigan site were created using Aqtesolv (HydroSOLVE Inc. 2016). The outputs of each of these analytical models where compared to the observed pressure responses from the falloff tests and the difference between the results was quantified with root mean square error (RMSE) (Appendix K). The history-matched transmissivity of 2.02×10^{-3} m^2/s was found to have the strongest correlation with the falloff test data with the lowest RMSE values (Figures 3-23 and 3-24). The very low transmissibilities of the low end of the dirty sand DSTs grossly overestimated the aquifer pressure responses with a very large RMSE, while the falloff tests transmissivity overestimated the responses to a less severe degree. The clean and dirty sand DST along with the high end dirty sand DST transmissivity values provide fairly good correlations with the observed data however the history-matched value which lies between these values provided a better correlation. A summary of the RMSE values observed from the varying transmissivity simulations can be seen in Table 3-12.
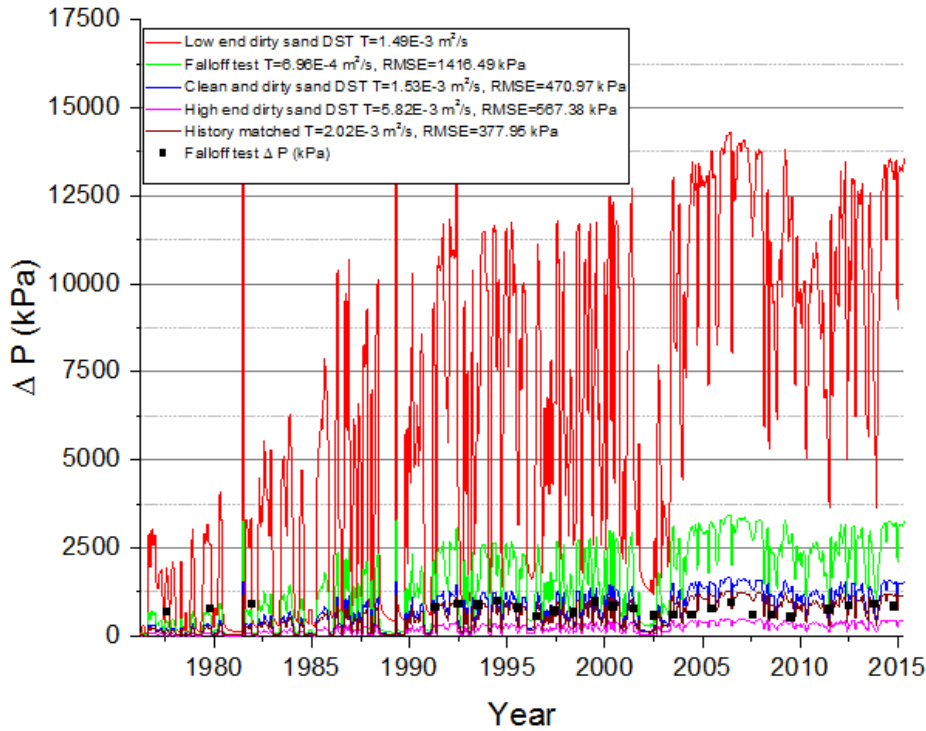
Figure 3-23: Aquifer simulation for Lanigan mine well 01-20 with varying values of transmissivity with sonic calculated storativity S=9.90×10^{-5}
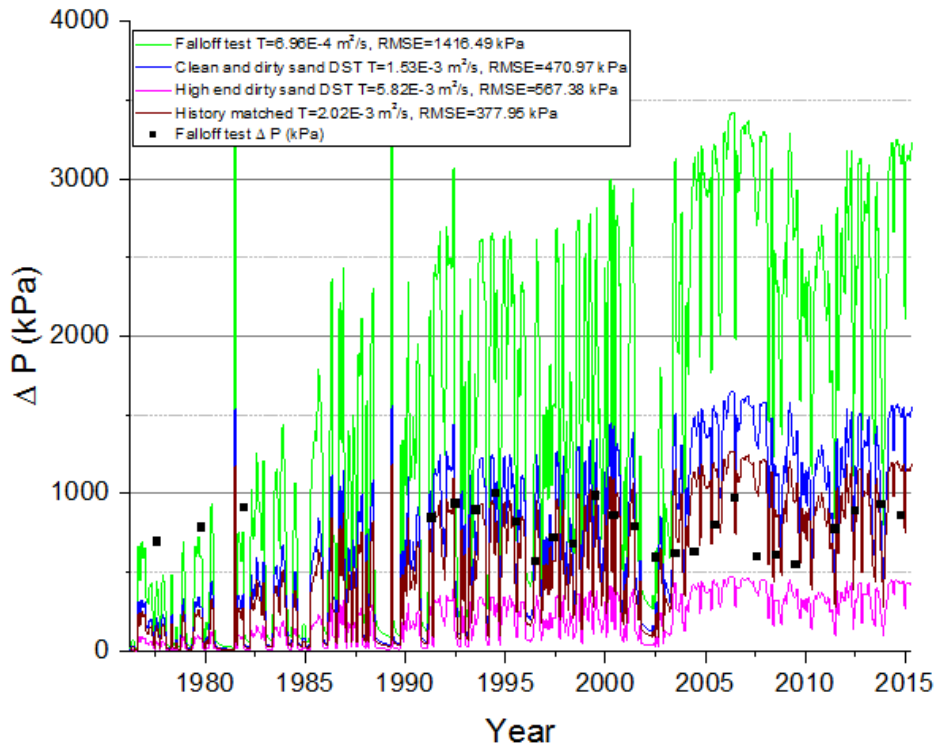
Figure 3-24: Aquifer simulation for Lanigan mine well 01-20 with varying values of transmissivity (without low end dirty sand DST) with sonic calculated storativity (S=9.90×10^{-5})

Table 3-12: Lanigan mine simulations with RMSE values for various values of transmissivity given sonic derived storativity (S=9.90×10^{-5}).

Sim	T (m^2/s)	S	01-20 RMSE (kPa)	02-28 RMSE (kPa)	Weighted Average RMSE (kPa)	Description	Comments
14	1.49×10^{-4}	9.90×10^{-5}	8178.17	9894.98	8779.06	Low end dirty sand T, sonic calc S	Grossly overestimated pressure response
16	6.96×10^{-4}	9.90×10^{-5}	1416.49	1844.99	1566.47	Falloff test T, sonic calc S	Overestimated pressure response
13	1.53×10^{-3}	9.90×10^{-5}	470.81	572.41	572.41	Clean and dirty sand DST T, sonic calc S	Slightly overestimated pressure response
44	2.02×10^{-3}	9.90×10^{-5}	377.95	564.03	443.08	History matched T, sonic calc S	Most closely matched pressure response
15	5.82×10^{-3}	9.90×10^{-5}	567.38	398.29	508.20	High end T dirty sand DST, sonic calc S	Underestimated pressure response

In the Lanigan injection well 02-28, the observed pressure responses from the falloff tests were slightly lower than those observed in the 01-20 well, as a result the high end dirty sand transmissivity simulation had the strongest correlation with the falloff test data (Figure 3-25).
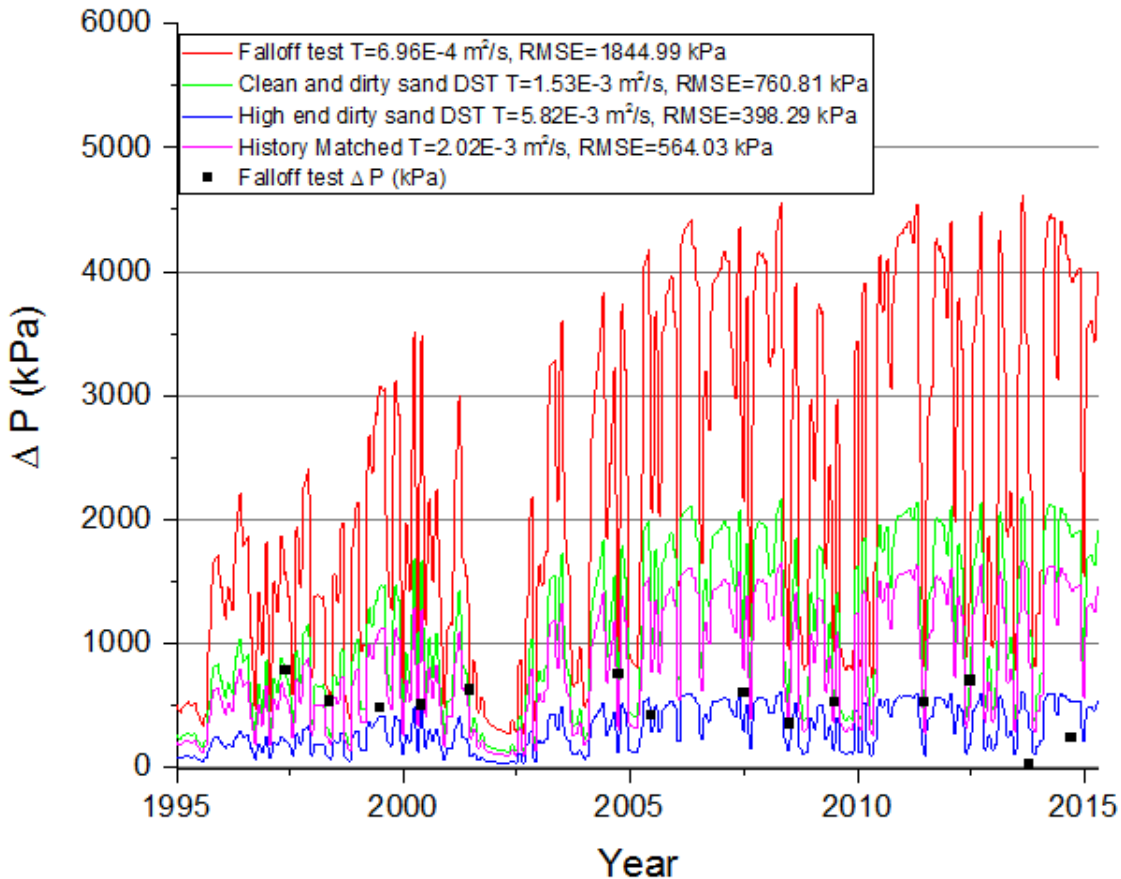
Figure 3-25: Aquifer simulation for Lanigan mine well 02-28 with varying values of transmissivity (without low end dirty sand DST) with sonic calculated storativity (S=9.90×10^{-5})

Simulations conducted for varying values of storativity yielded an array of analytical pressure responses, however the RMSE between these simulations were quite similar (Figure 3-26). The Hall (1953) produced the simulation with the lowest RMSE by a thin margin (Table 3-13). Due to the very similar RMSE between the simulations it cannot be determined with great confidence which parameter best represents the true aquifer storativity. However, the sonic derived storativity is the best representation as it was determined from actual aquifer data.
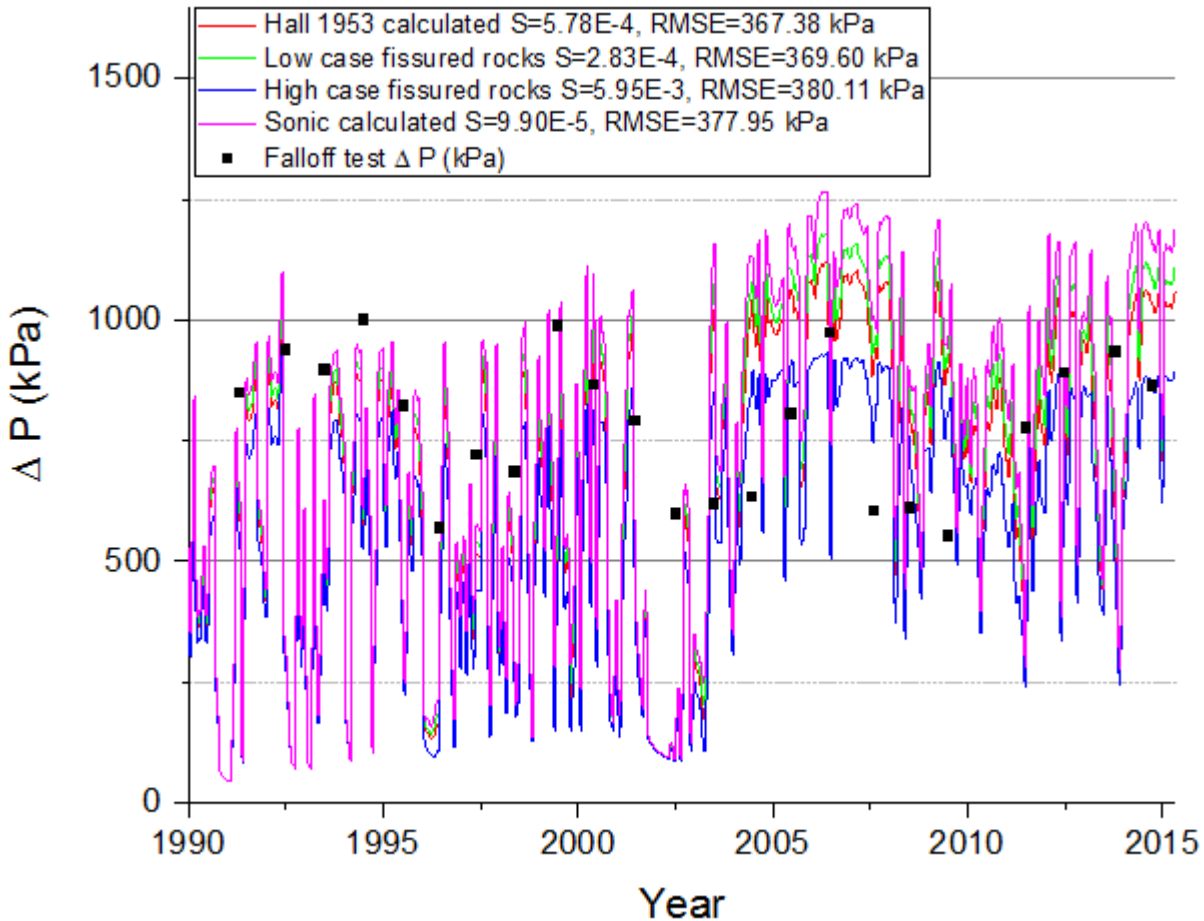
Figure 3-26: Aquifer simulation for Lanigan mine well 01-20 with varying values of storativity with history matched transmissivity ($T=2.02\times10^{-3}$ m^2/s)

Table 3-13: Lanigan mine simulations with RMSE values for various values of storativity given history matched transmissivity ($T=2.02\times10^{-3}$ m^2/s).

Sim	T (m^2/s)	S	01-20 RMSE (kPa)	02-28 RMSE (kPa)	Weighted Average RMSE (kPa)	Description	Comments
41	2.02×10^{-3}	5.78×10^{-4}	367.38	516.36	419.53	History matched T, Hall 1953 S	Most closely matched pressure response
42	2.02×10^{-3}	2.83×10^{-4}	369.60	534.78	427.41	History matched T, low end S fissured rocks	Slightly overestimated pressure response

43	2.02×10^{-3}	5.95×10^{-3}	380.11	466.33	410.28	History matched T, high end S fissured rocks	Slightly underestimated pressure response
44	2.02×10^{-3}	9.90×10^{-5}	377.95	564.03	443.08	History matched T, sonic est S	Slightly overestimated pressure response

Through mapping the aquifer pressure responses at the mine site, the extent of the pressure propagations given could be seen. As with the other mine sites the most distant pressure propagations were seen in the low value sonic derived storativity values (Figure 3-27) with increases in hydraulic head occurring over 100 km away from the mine site. The least distant were seen in the high storativity case (Figure 3-28) with pressure propagations only extending 15 km away.
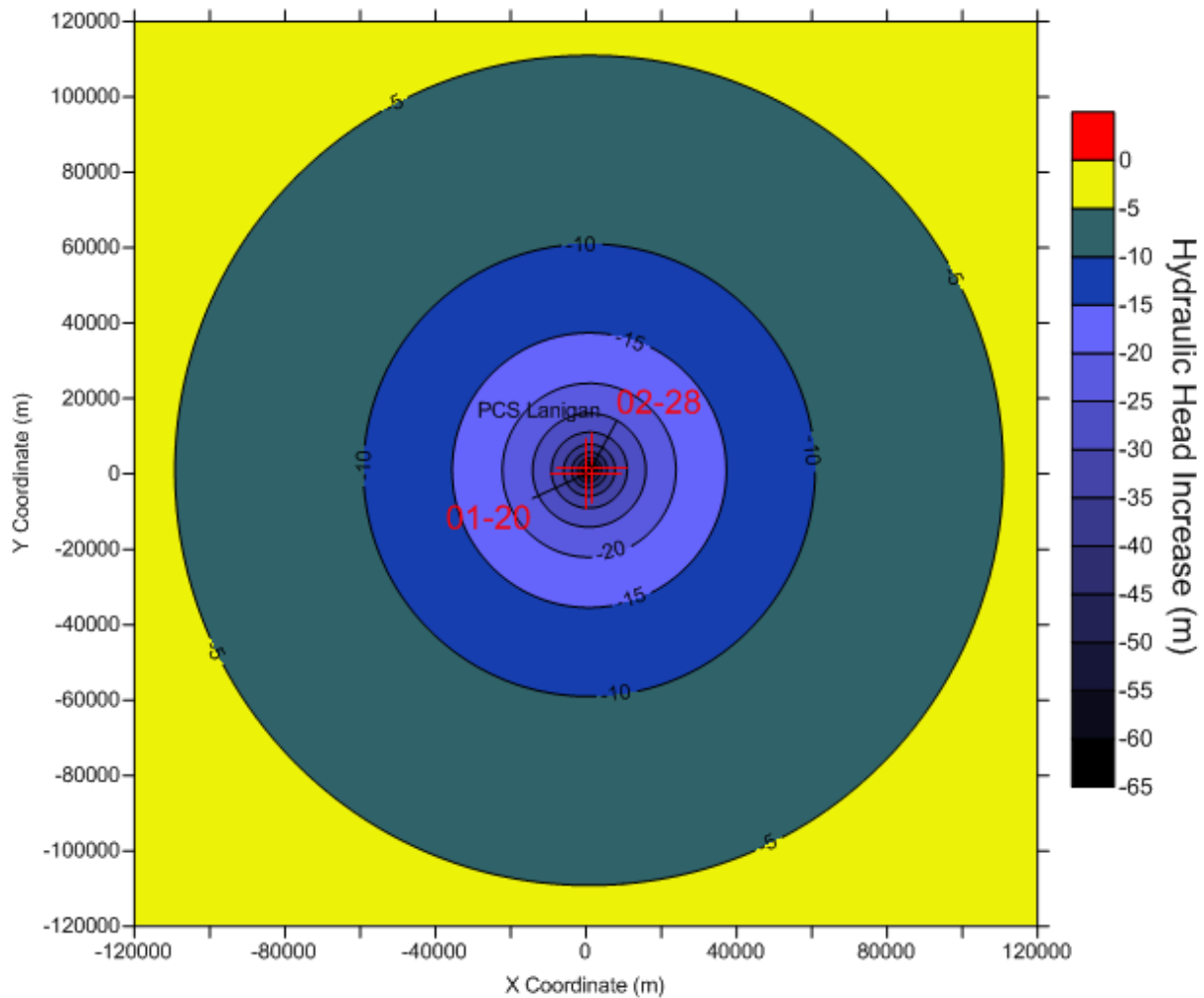
Figure 3-27: Aqtesolv simulation results for the Lanigan mine site at April 2015, using sonic calculated storativity S=9.90×10^{-5} and interpolated T=2.02×10^{-3} m^2/s
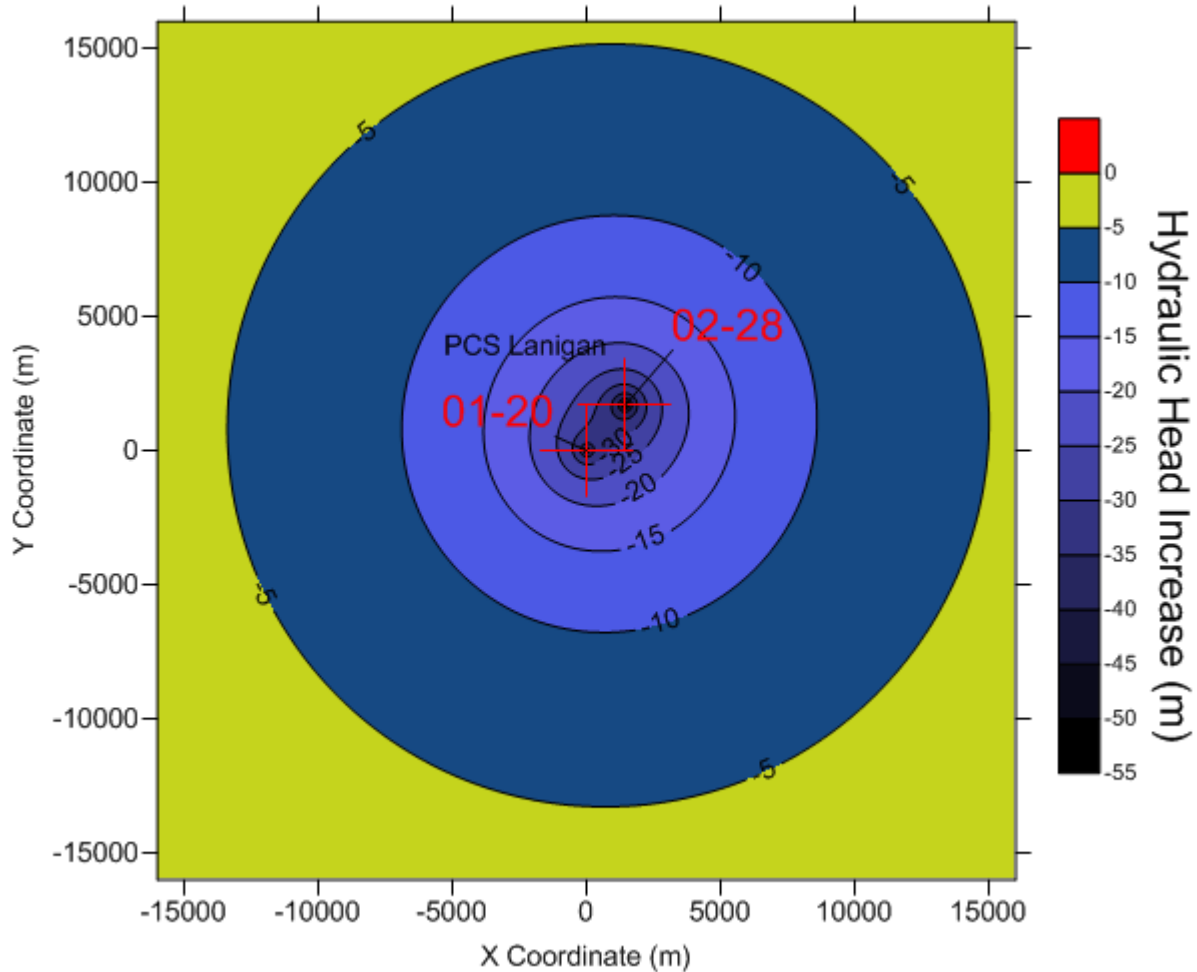
Figure 3-28: Aqtesolv simulation for the Lanigan mine site at April 2015, using high end storativity (S=5.95×10^{-3}) and interpolated T=2.02×10^{-3} m^2/s

3.4.3.3 Lanigan Combined vs Isolated Simulation Results

To simulate the effects that the Colonsay injection wells had on the Lanigan mine site, the two Lanigan injection wells were simulated both with and without the two Colonsay mine injection wells using a variety of aquifer parameters (Figure 3-29 and 3-30). As was observed in the other mine sites, the pressure differential between the two mine sites is highly dependent on the aquifer parameters. The high end storativity resulted in the smallest pressure differentials which are nearly negligible (Figure 3-29). The low value sonic derived storativity resulted in some of the largest pressure differentials, as in these cases the pressure transients are able to propagate much further into the aquifer away from the injection wells.
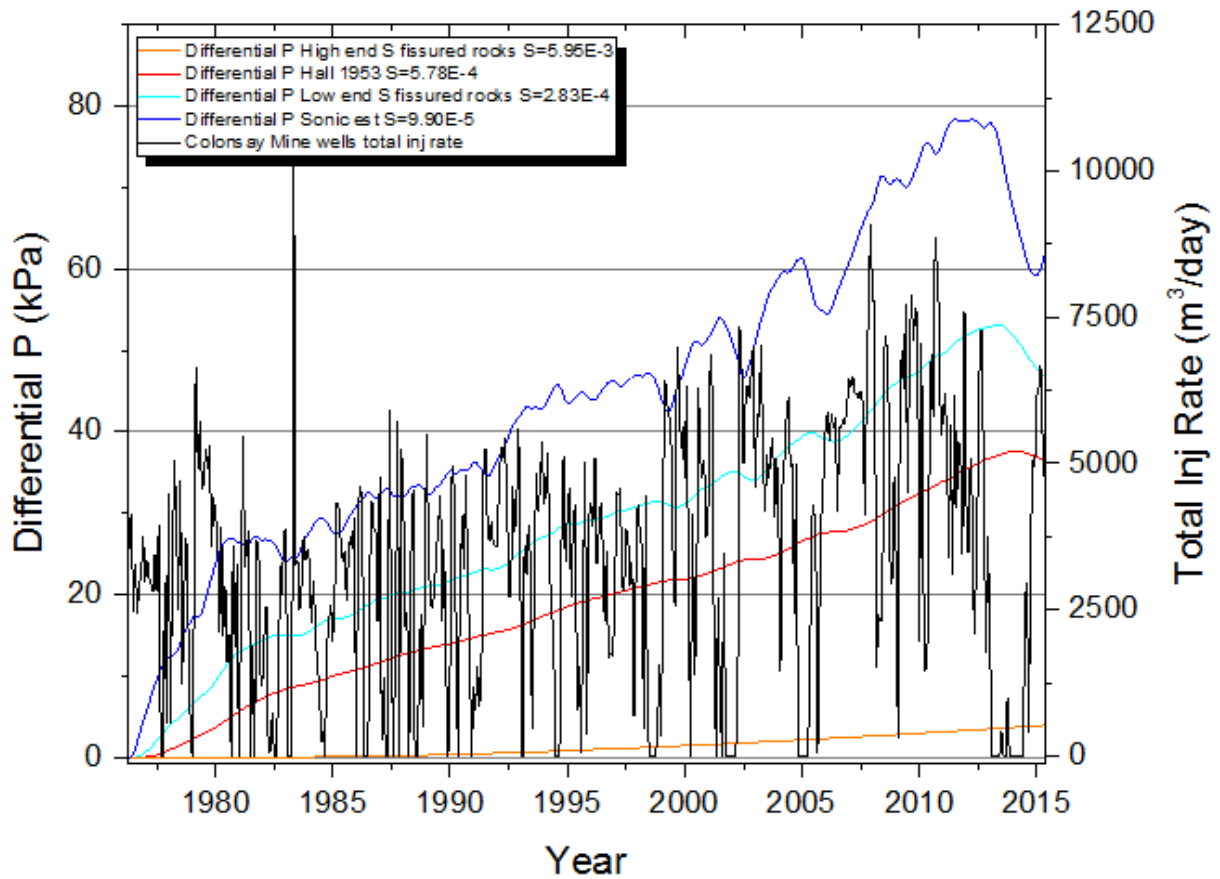
Figure 3-29: Lanigan well 01-20, pressure differences between Lanigan isolated simulation and Lanigan+Colonsay combined simulation with total production rates from Colonsay wells based on different values of storativity given history matched transmissivity (T=2.02×10^{-3} m^2/s)

The analysis of pressure differential given differing values of transmissivity is seen in Figure 3-30. It can be seen that the low transmissivity values obtained from the falloff tests resulted in the highest pressure differential, while the high transmissivity high end dirty sand DST resulted in the lowest pressure differential given the sonic derived value of storativity.
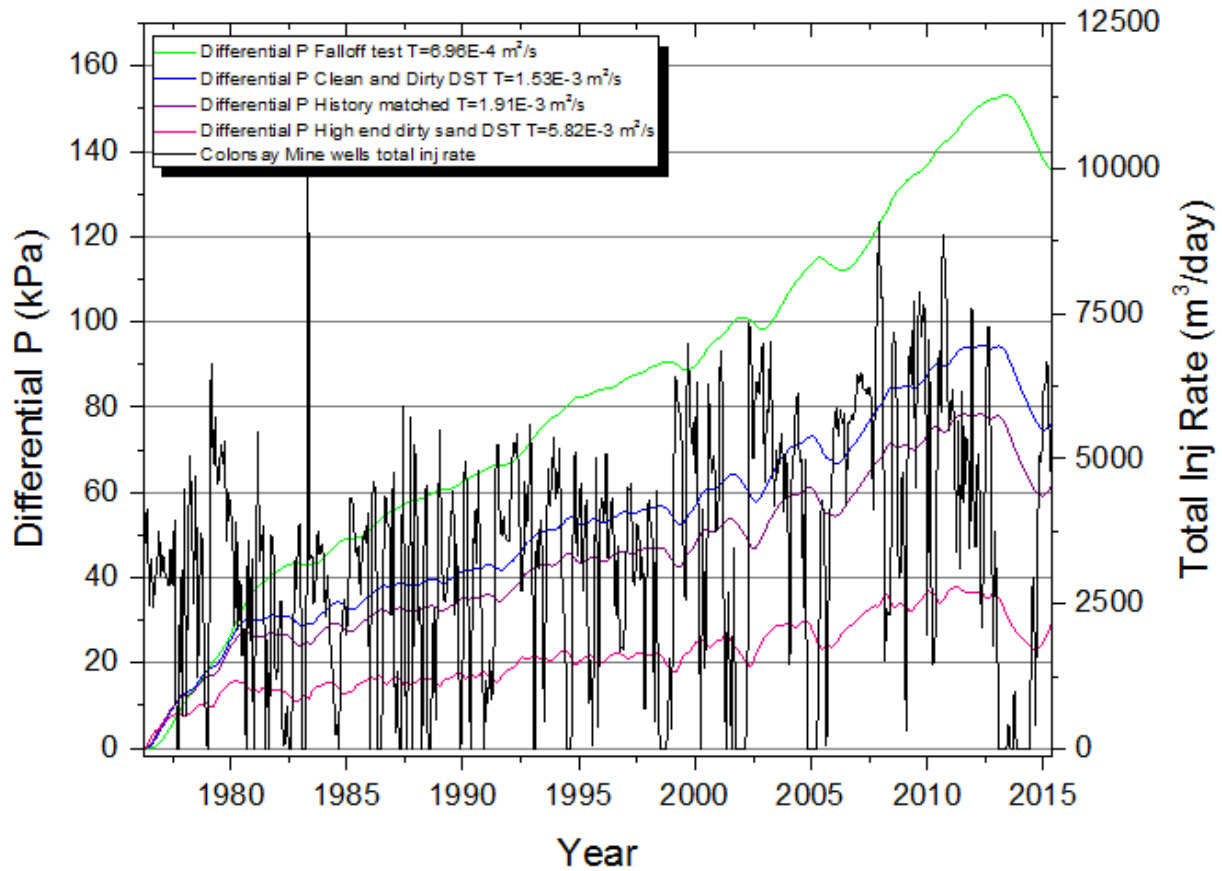
Figure 3-30: Lanigan well 01-20, pressure differences between Lanigan isolated simulation and Lanigan+Colonsay combined simulation with total production rates from Colonsay wells based on different values of transmissivity given sonic derived storativity (S=9.90×10^{-5})

The large discrepancies between the pressure differential responses between the Colonsay and Lanigan mine sites due to different input parameters of transmissivity and especially storativity give insights into the degree of interconnectivity between the two mine sites. Given that these mine sites are 40 km apart, significantly further than the spacing between other pairs of mine sites in the province the degree of interference would be expected to be lower. This was confirmed from the pressure differential simulation where the low value sonic derived storativity along with the history matched transmissivity only resulted in a maximum differential pressure of 80 kPa compared to over 175 kPa seen between Cory and Vanscoy in a simulation based on the same parameters.

The simulation that is the best representation of the true aquifer conditions would be that based on the history matched transmissivity (T=2.02×10^{-3} m^2/s) and sonic derived storativity (S=9.90×10^{-5}). This simulation resulted in an 80 kPa pressure differential, inferring a moderate level of interference between the Lanigan and Colonsay injection wells.

3.4.4 Esterhazy Study Area

3.4.4.1 Esterhazy Aquifer Characterization

Through analysis of DSTs, core, falloff tests and geophysical logs the aquifer characteristics of the Interlake Group at the Esterhazy mine sites were established. The average net pay of the injection wells was found to be 105 m based on the completed intervals of the Interlake Group with greater than 6% neutron porosity. The permeability values obtained from the various methods of analysis (Table 3-14) were significantly lower than those seen in the Basal Clastics at the other mine sites, with a DST average permeability of only 1.26×10^{-13} m^2 and a core permeability of 9.13×10^{-13} m^2.

Table 3-14) Summary of average permeability (transmissivity) values determined from the various methods of analysis at the Esterhazy study area

Test Type	k (m^2)	T (m^2/s)
Core	9.13×10^{-13}	9.82×10^{-4}
DST	1.26×10^{-13}	1.35×10^{-4}
Falloff Test	1.18×10^{-13}	1.27×10^{-4}

Aquifer pressures obtained from the DSTs at the mine site allowed for a baseline pressure gradient to be established. The 1971-1972 DSTs conducted before large scale injection activities in the Interlake Group in the area were used to establish this baseline aquifer pressure (Figure 3-31). As was observed at the mines sites utilising the Basal Clastics for waste disposal, the Interlake Group in the Esterhazy area exhibited a sub-hydrostatic pressure gradient with a pressure gradient of 9.27 $\frac{kPa}{m}$. The hydrostatic pressure gradient is 11.3 $\frac{kPa}{m}$ based on an aquifer fluid density of 1150 $\frac{kg}{m^3}$.
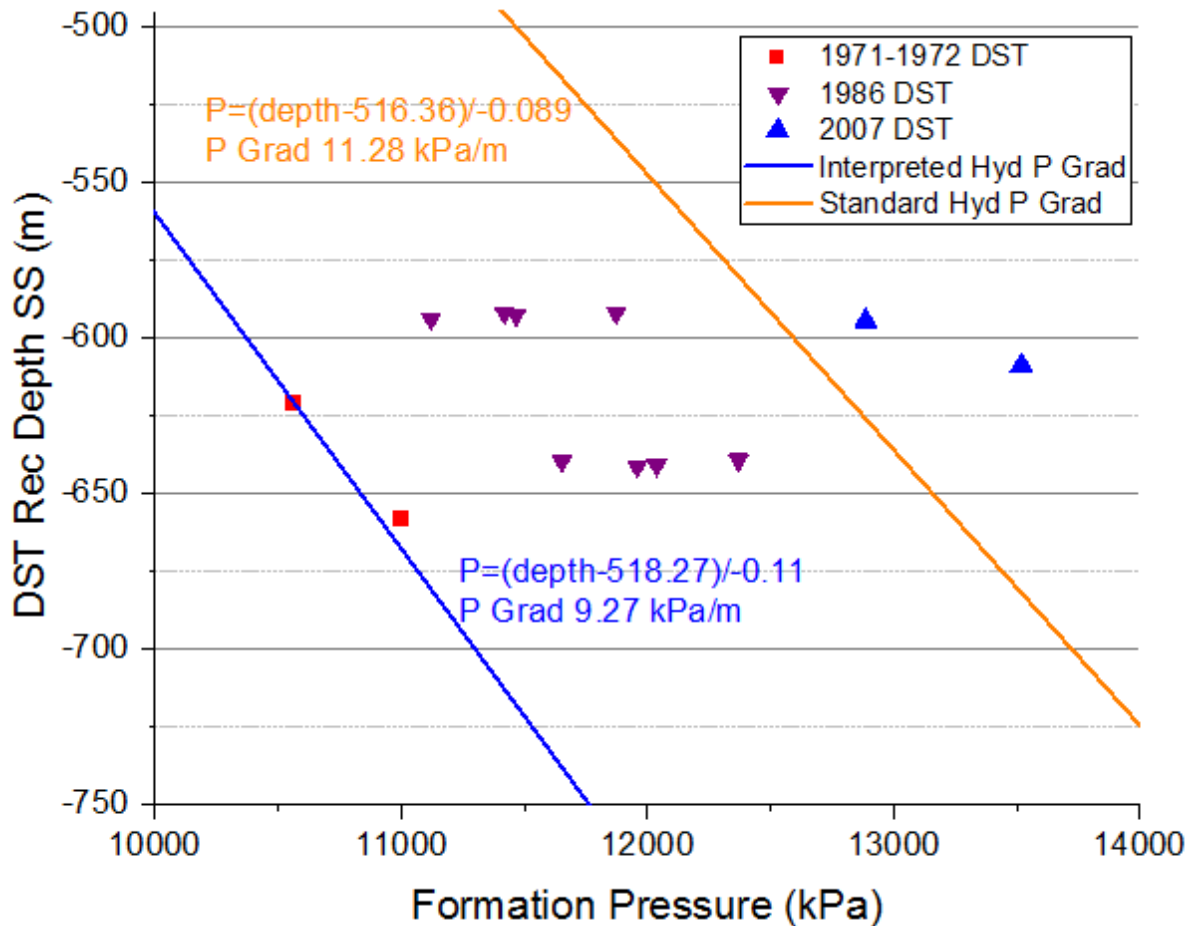
Figure 3-31: DST Pressure Gradient at Esterhazy mine site based on pre-injection 1971/1972 DSTs, pressure at a given depth (m) can be calculated for both interpreted pressure gradient and standard hydrostatic pressure gradient based on the respective equations.

3.4.4.2 Esterhazy Analytical Modelling of Injection-Induced Pressure Change

Analytical models where generated in Aqtesolv to model the changes in aquifer pressure as a result of injection activities in the Esterhazy study area based on various values of transmissivity and storativity. These results where then compared to the pressure data obtained from the falloff tests in the injection wells. In the PCS Rocanville mine well 12-22 given the sonic derived storativity ($S=3.73\times10^{-5}$), the analytical simulation outputs obtained from the DST transmissivity overestimated the pressure response with respect to the falloff tests (Figure 3-32), while the core derived transmissivity slightly underestimated the response. The history-matched value of 7.53×10^{-4} m^2/s (in between the core and DST values) was found to have the strongest correlation with the falloff test data (lowest RMSE). Additionally, this history-matched transmissivity was found to have the overall best correlation with all of the injection wells with falloff tests available, whereby the overall weighted average RMSE value was the lowest for this value of transmissivity given sonic derived storativity (Table 3-15).

113
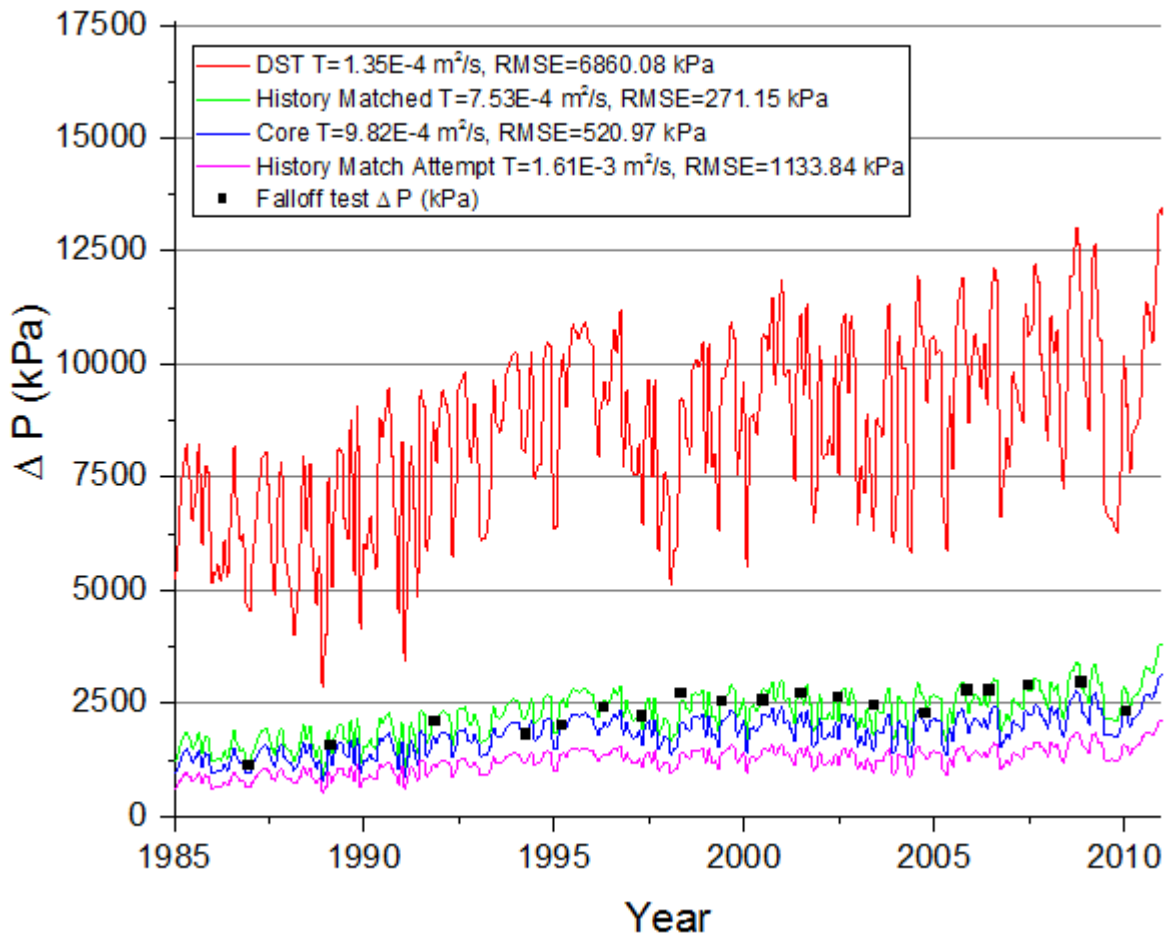
Figure 3-32: Aquifer simulation for PCS Rocanville mine injection well 12-22 for varying values of transmissivity with sonic derived storativity (S=3.73×10^{-5}), simulated using all Esterhazy injection wells

Table 3-15: Esterhazy study area simulations with RMSE values for various values of transmissivity given sonic derived storativity (S=3.73×10^{-5}).

Sim	Transmissivity (m^2/s)	Storativity	Weighted Average RMSE (kPa)	Description	Comments
4	1.35×10^{-4}	3.73×10^{-5}	7583.19	DST k, sonic est S	Severely overestimated pressure response
44	7.53×10^{-4}	3.73×10^{-5}	826.80	History-matched k, sonic est S	Most closely matched pressure response
8	9.82×10^{-4}	3.73×10^{-5}	930.64	Core k, sonic est S	Underestimated pressure response
12	1.61×10^{-3}	3.73×10^{-5}	1361.40	History-match attempt k, sonic est S	Underestimated pressure response

In other wells in the study area similar results were seen. In the PCS Rocanville well 06-23, where a history-matched value of transmissivity resulted in the lowest RMSE with the falloff test data. However in this well the history-matched transmissivity (6.99×10^{-4} m^2/s) was found to have

114

a slightly stronger correlation than the history-matched value that had the best correlation with the majority of the wells in the area (T=7.53×10^{-4} m^2/s) (Figure 3-33).
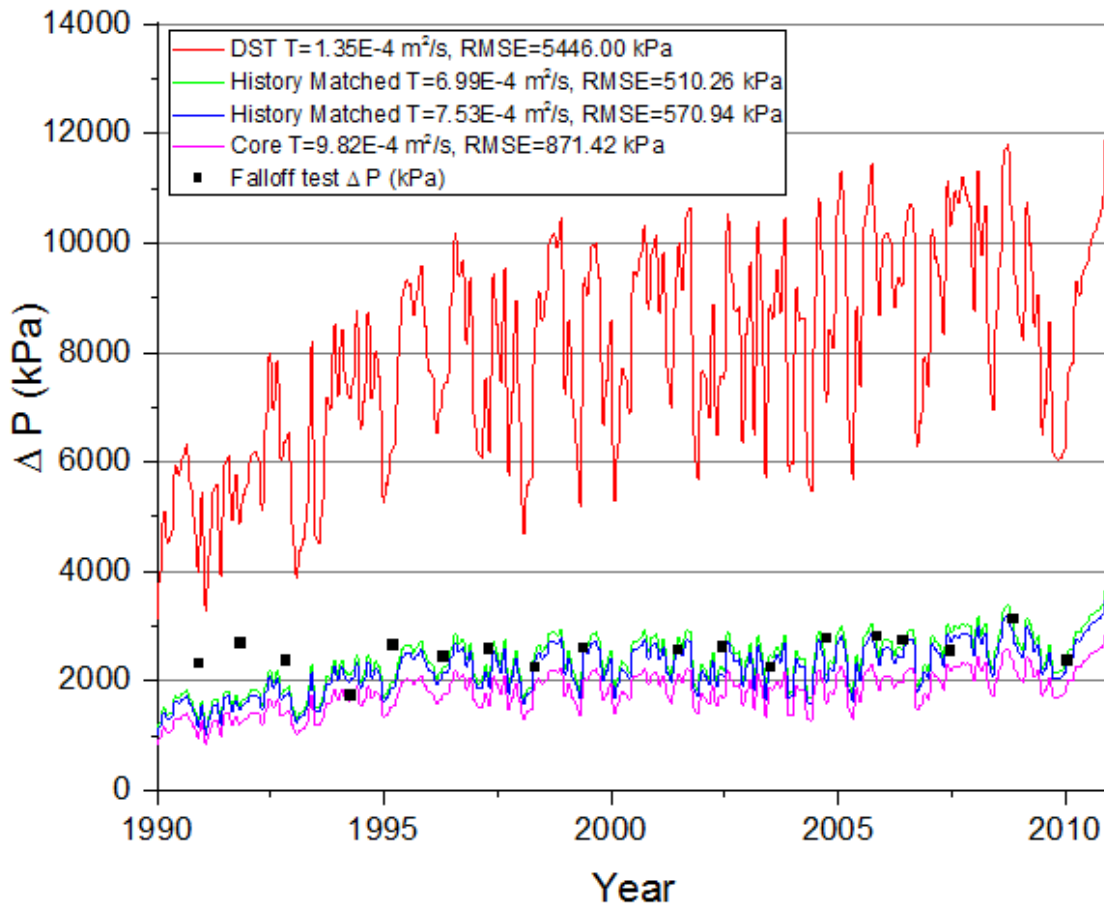
Figure 3-33: Aquifer Simulation for PCS Rocanville mine injection well 06-23 for varying values of transmissivity with sonic derived storativity (S=3.73×10^{-5}), simulated using all Esterhazy injection wells

Aquifer simulations were as well conducted for varying values of storativity while using a constant transmissivity. In Figure 3-34 it is evident in the Rocanville mine well 01-14 that the best correlation between the analytical pressure response and the observed falloff test pressure data is achieved with the sonic calculated storativity. Furthermore, given the history-matched transmissivity (T=7.54×10^{-4} m^2/s) the sonic derived storativity (S=3.73×10^{-5}) produced results that had the best overall correlation with all of the wells with falloff tests available, whereby the weighted average RMSE for the wells with available tests was the lowest (RMSE=826.80 kPa) (Table 3-16). A summary of all of the RMSE values for all of the simulations can be seen in Appendix L.
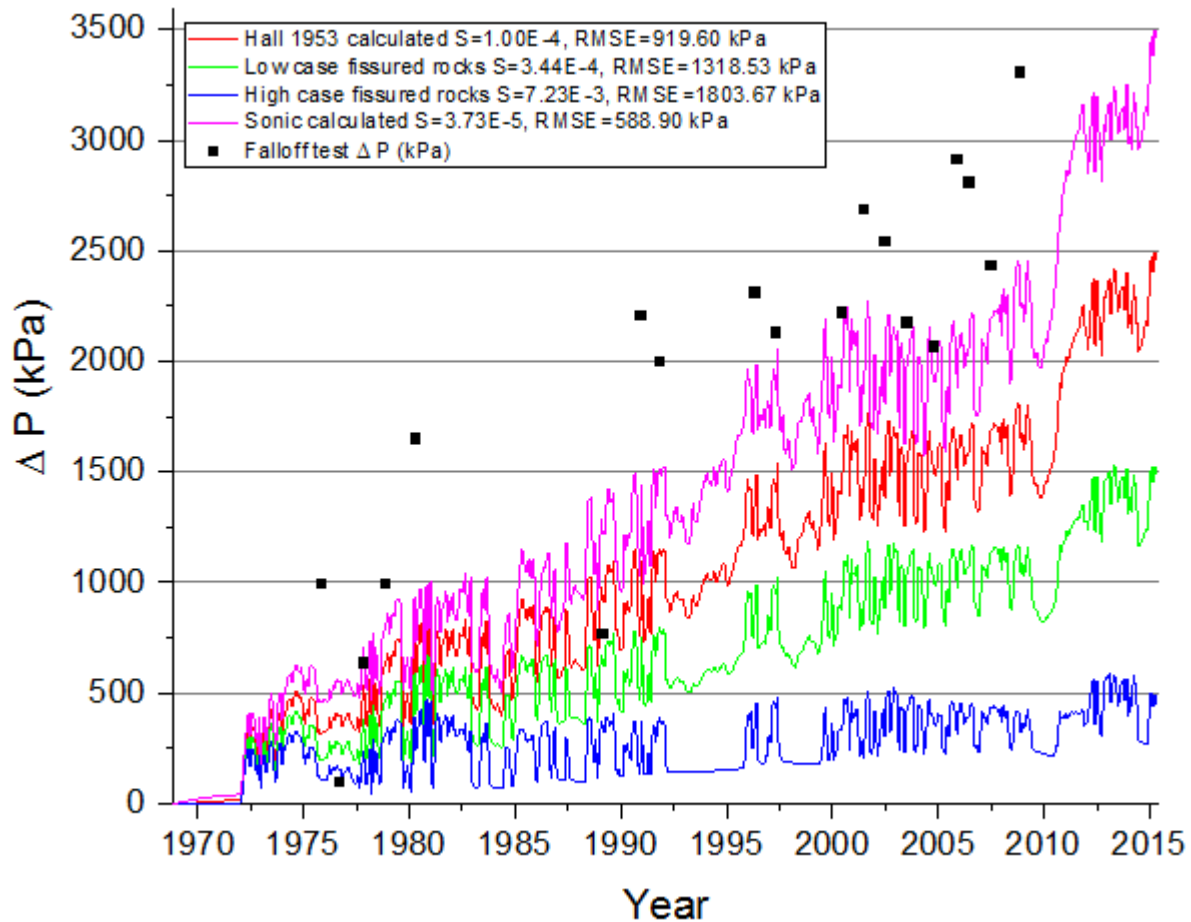
Figure 3-34: Aquifer simulation for Rocanville well 01-14 for varying values of storativity given history-matched transmissivity (T=7.53×10^{-4} m^2/s)

Table 3-16: Esterhazy study area simulations with RMSE (weighted average RMSE, wells with higher number of falloff tests given more weight) values for various values of storativity given history matched transmissivity (T=7.53×10^{-4} m^2/s)

Sim	Transmissivity (m^2/s)	Storativity	Weighted Average RMSE (kPa)	Description	Comment
41	7.53×10^{-4}	1.01×10^{-4}	975.49	History-matched k, Hall 1953 S	Underestimated pressure response
42	7.53×10^{-4}	3.44×10^{-4}	1239.31	History-matched k, low end S for fissured rocks	Underestimated pressure response
43	7.53×10^{-4}	7.23×10^{-3}	1748.19	History-matched k, high end S for fissured rocks	Underestimated pressure response
44	7.53×10^{-4}	3.73×10^{-5}	826.80	History-matched k, sonic est S	Most closely matched pressure response

It is evident that the three separate mine sites within the Esterhazy study area, (PCS Rocanville, Mosaic K1 and K2) have different pressure responses from injection, observed in both the analytical simulations outputs and the falloff test data. In Figure 3-35 it is seen that the Rocanville wells have a lower pressure response than the K1 and K2 wells which have nearly

116

double the simulated increase in pressure as well as significantly higher observed falloff test pressure change. This discrepancy can be attributed to the well density at the mine sites. At Rocanville there is a much lower well density than the K1 or K2 sites with only 5 wells compared to the 13 wells each at K2 and 14 at K1 (Figure 3-4). This higher well density would be injecting an overall greater volume of wastewater and thereby result in larger increases in aquifer pressures over time.
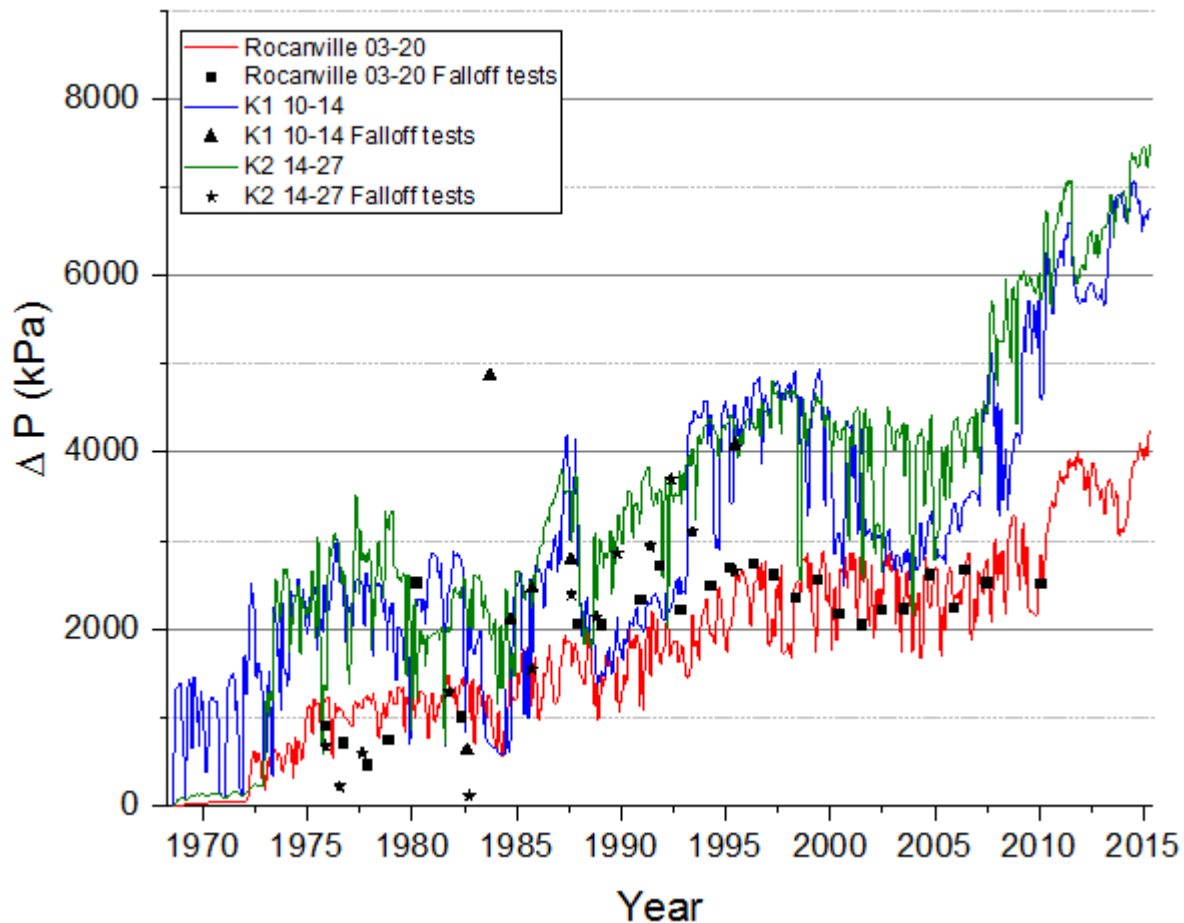
Figure 3-35: Simulation with history-matched transmissivity (T=7.53×10^{-4} m^2/s), sonic derived S=3.73×10^{-5}, with Rocanville, K1 and K2 wells pressure responses

3.4.4.3 Esterhazy Combined vs Isolated Simulation Results

The degree of interference between the wells at the three separate mines within the Esterhazy study area was simulated by running the simulations with all of the wells at the three mines and then again with only the wells at the K1 and K2 mine sites. The difference between the results provides the degree of influence that injection activities at the Rocanville site have on the K1 and K2 sites. Figures 3-36 and 3-37 illustrates this degree of interference while accounting for variations in the parameters of transmissivity and storativity. As in the cases of the Deadwood Formation wells it was found that the lower storativity simulations based on the

117

sonic log bulk compressibility resulted in larger pressure differentials in the wells (larger degree of interference) (Figure 3-36). Additionally the low permeability simulations resulted in larger pressure differentials as seen in Figure 3-37, where based on sonic storativity (S=3.73×10^{-5}) the low transmissivity DST simulation (T=1.35×10^{-4} m^2/s) resulted in a significantly larger pressure differential than the higher value history-matched and core derived transmissibilities. Additionally it can be seen (Figure 3-36 and 3-37) that with increasing injection rates (as a result of the addition of new wells) from the Rocanville wells over time the pressure differential increases. This is expected as increased injection rates would result in larger interferences between the mine sites.
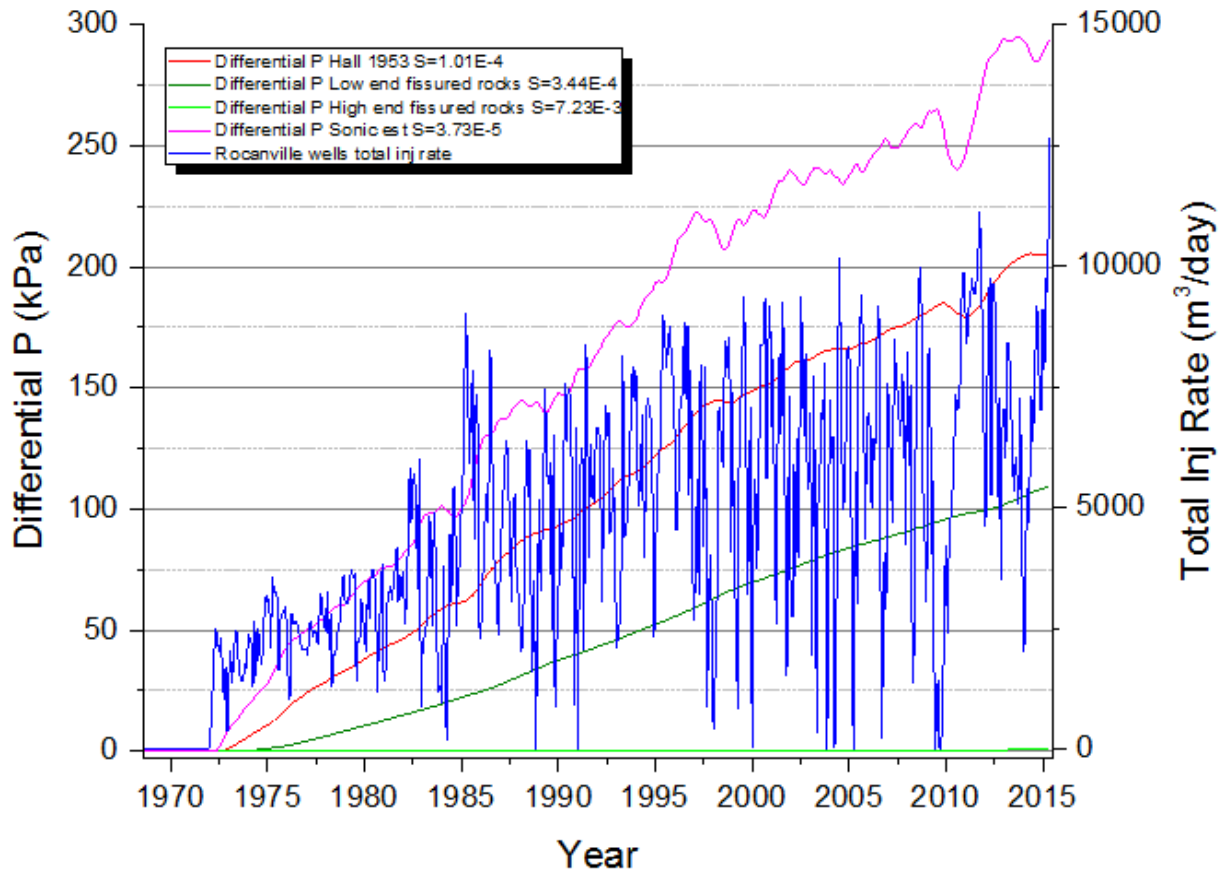
Figure 3-36: Mosaic K1 mine well 10-14 pressure differential from Esterhazy combined simulation compared to Esterhazy K1 and K2 mine wells only for varying values of storativity given history-matched transmissivity (T=7.53×10^{-4} m^2/s)
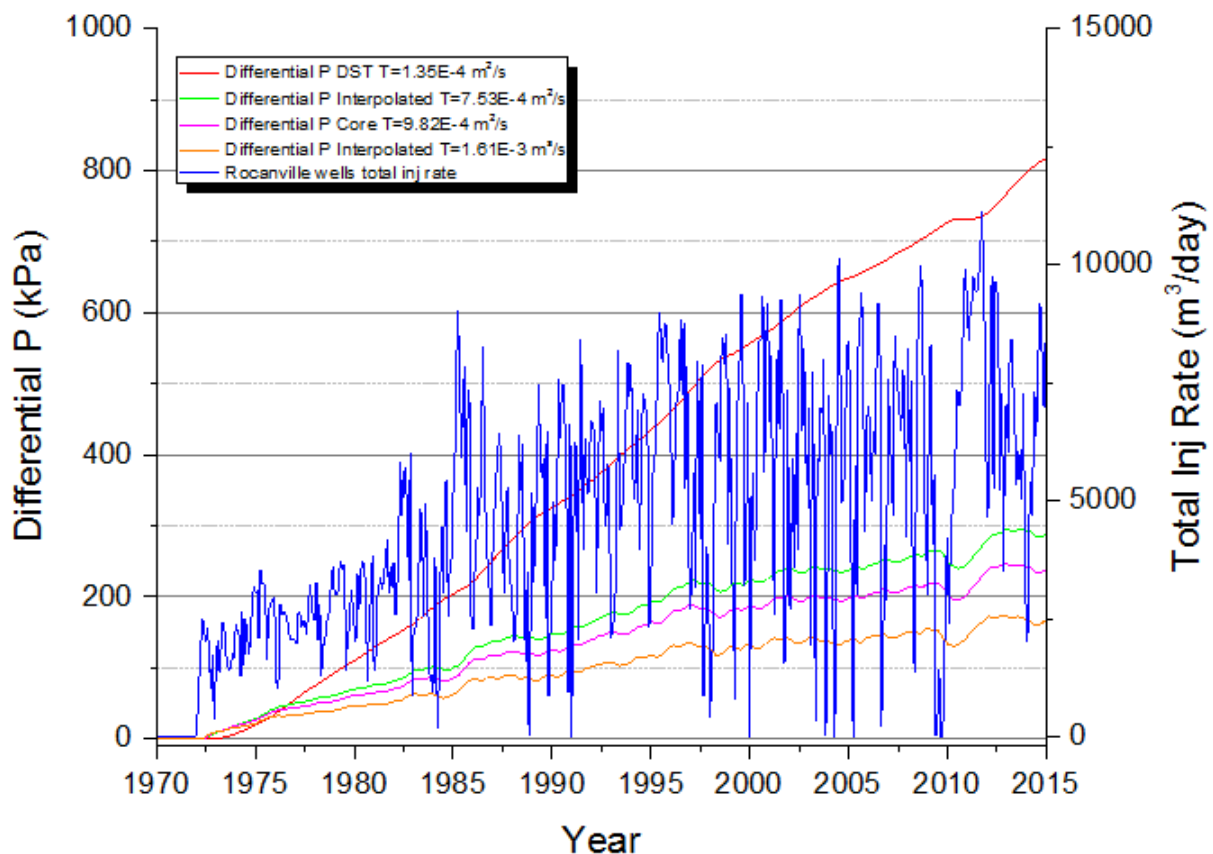
Figure 3-37: Mosaic K1 mine well 10-14 pressure differential from Esterhazy combined simulation compared to Esterhazy K1 and K2 mine wells only for varying values of transmissivity with sonic derived storativity (S=3.73×10^{-5})

The extent of the pressure propagations within the Interlake Group at the Esterhazy mine site brought about by injection is illustrated in Figure 3-38 and 3-39. As observed in the mine sites utilizing the Basal Clastics for waste disposal, the extent of the pressure propagations into the formation is highly dependent on the storativity value input in the simulation. The small sonic derived storativity (3.73×10^{-5}) resulted in much further pressure propagations (over 300 km) (Figure 3-38) as compared to the higher end storativity of fissured rocks (7.23×10^{-3}) in Figure 3-39, where the pressure propagations are only around 40 km.

The distances of these pressure propagation were somewhat higher than observed in the Basal Clastics injection sites, where around 80-150 km of propagation were observed with the sonic derived storativity. However, the sonic derived compressibilities were found to be considerably higher in the Basal Clastics (~1.06×10^{-10} Pa^{-1}) relative to the Interlake Group carbonates (~3.14×10^{-11} Pa^{-1}) , thereby resulting in larger storativities and less distant pressure propagations for these simulations.
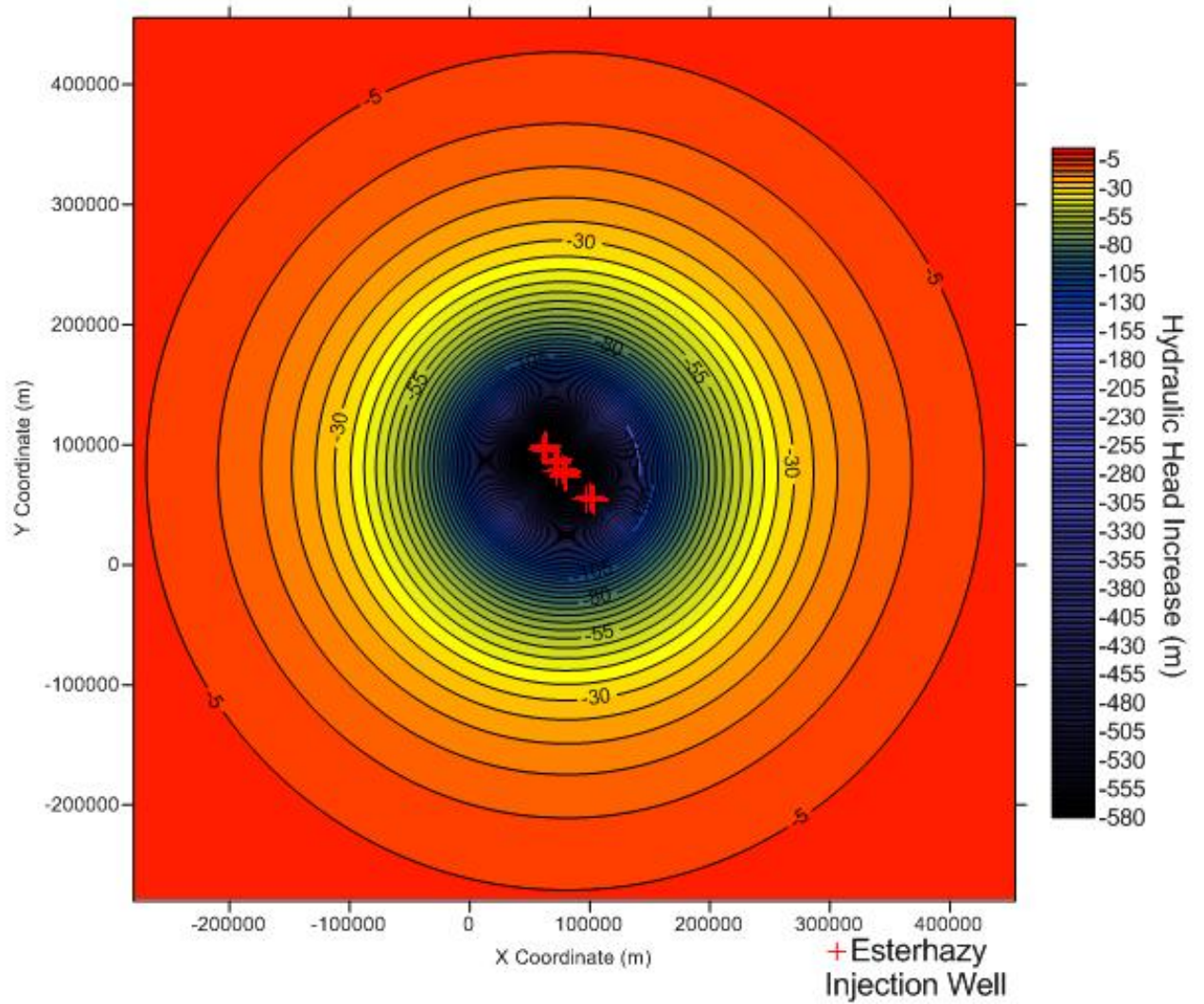
Figure 3-38: Aqtesolv simulation results for the Esterhazy Mine site at April 2015 based on history-matched transmissivity (T=7.53×10^{-4} m^2/s) and sonic estimated storativity (S=3.73×10^{-5})
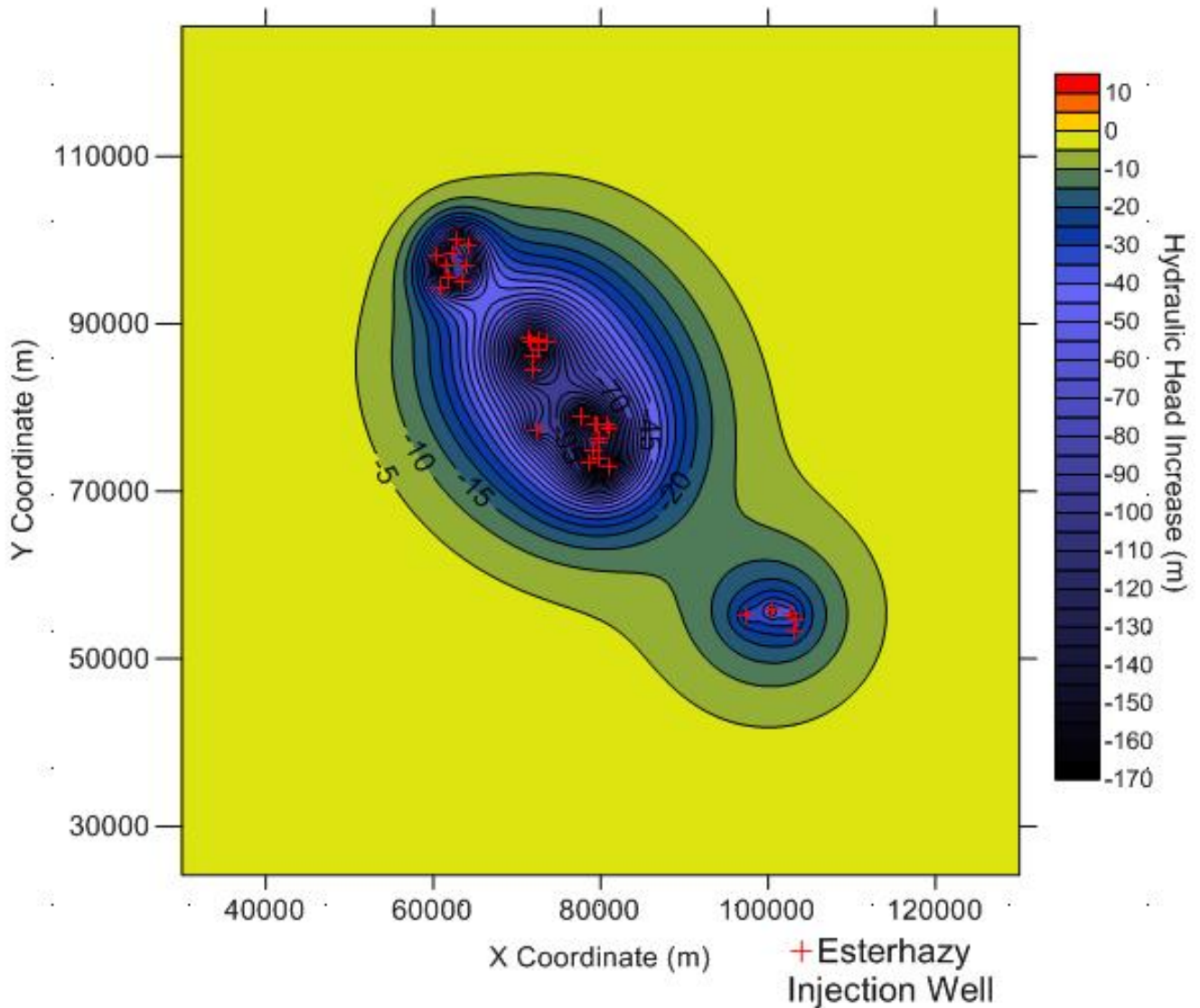
Figure 3-39: Aqtesolv simulation results for the Esterhazy Mine site at April 2015 based on history-matched transmissivity (T=7.53×10^{-4} m^2/s) and high case storativity for fissure rocks (S=7.23×10^{-3})

3.5 Overall Analytical Modelling Results

Through conducting history matching with falloff test pressure data, the Aqtesolv analytical models for each mine site provide a representative model (lowest RMSE between analytical simulation outputs and falloff test pressure data) best depicting real world conditions. Representative aquifer parameters of transmissivity (permeability) and storativity (aquifer compressibility) were ascertained for each site through these models. The history-matched values of transmissivity (permeability) were typically somewhat higher than those obtained from well tests and core at each site (Table 3-17).

121

Table 3-17: Average values of permeability obtained from various methods of analysis at each mine site

	Cory-Vanscoy	Allan, Patience Colonsay	Lanigan	Esterhazy
Core k (m^2)	4.87×10^{-13}	NA	3.03×10^{-15}	9.13×10^{-13}
DST k (m^2)	1.20×10^{-12}	1.31×10^{-12}	1.40×10^{-12}	1.26×10^{-13}
Falloff Test DST k (m^2)	6.27×10^{-13}	1.13×10^{-12}	6.36×10^{-13}	1.18×10^{-13}
History Matched k (m^2)	2.25×10^{-12}	6.75×10^{-12}	1.85×10^{-12}	7.00×10^{-13}

In addition to the permeability input into the models, the results of the simulation outputs were as well highly dependent on the injection rates the mine sites were subjected to. The overall injection rates of all of the wells in each study area were compiled. In Figure 3-40 it can be seen that the Esterhazy study area has undergone much higher overall injection rates as compared to the sites utilizing the Basal Clastics with upwards of three times the volumes of fluid being disposed of. These higher volumes are due to the much larger number of wells in the Esterhazy area (32) as compared to the 2-7 wells at the other sites.
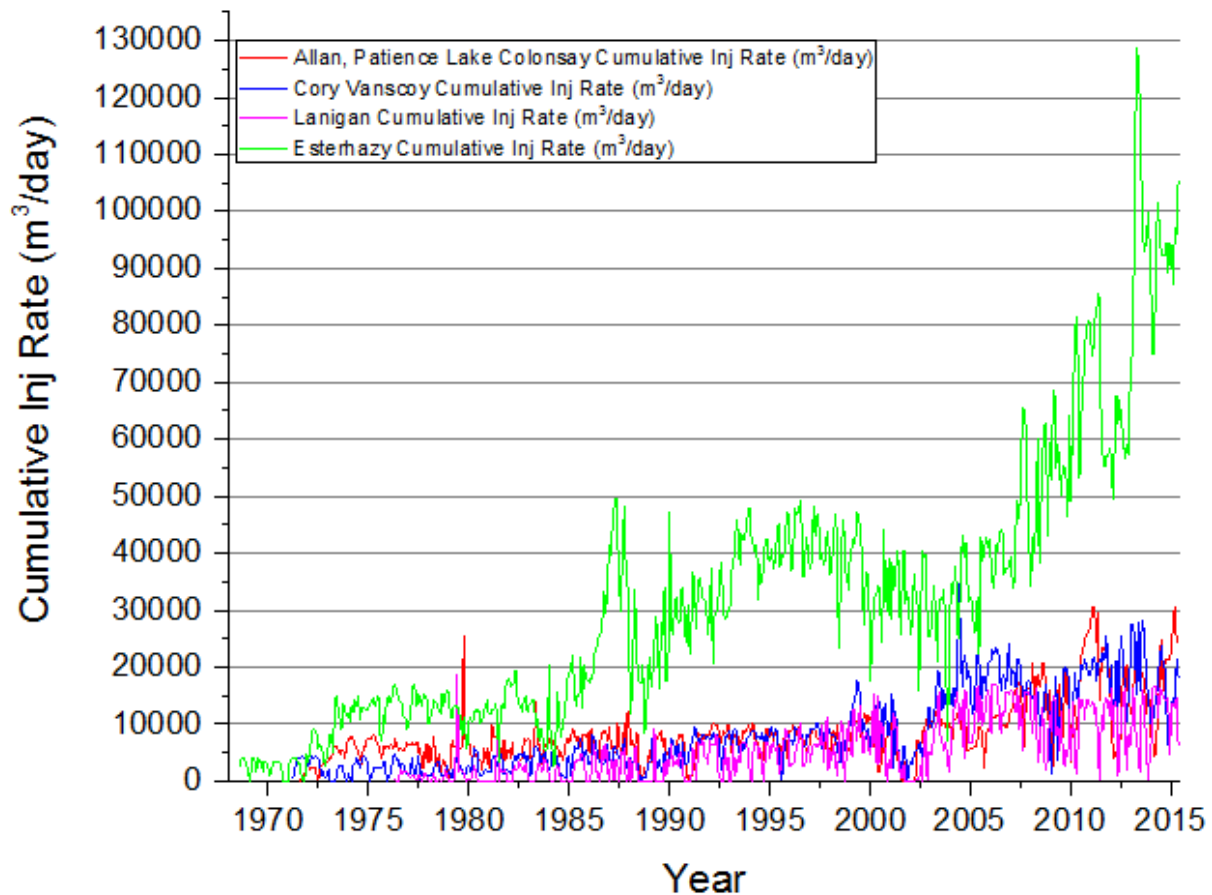
Figure 3-40: Cumulative injection rates for each respective mine site

A typical aquifer response at each mine site based on the history-matched parameters of each respective site is illustrated in Figure 3-41. The aquifer pressure response is higher at the Esterhazy site as compared to the sites utilizing the Basal Clastics (Cory-Vanscoy, Allan Patience Colonsay, and Lanigan). The pressure response in the Esterhazy K2 well is nearly five times greater than that from the Basal Clastic sites (Figure 3-41). Within the Esterhazy study area, the Rocanville site had a significantly lower pressure response than the K1 or K2 sites.
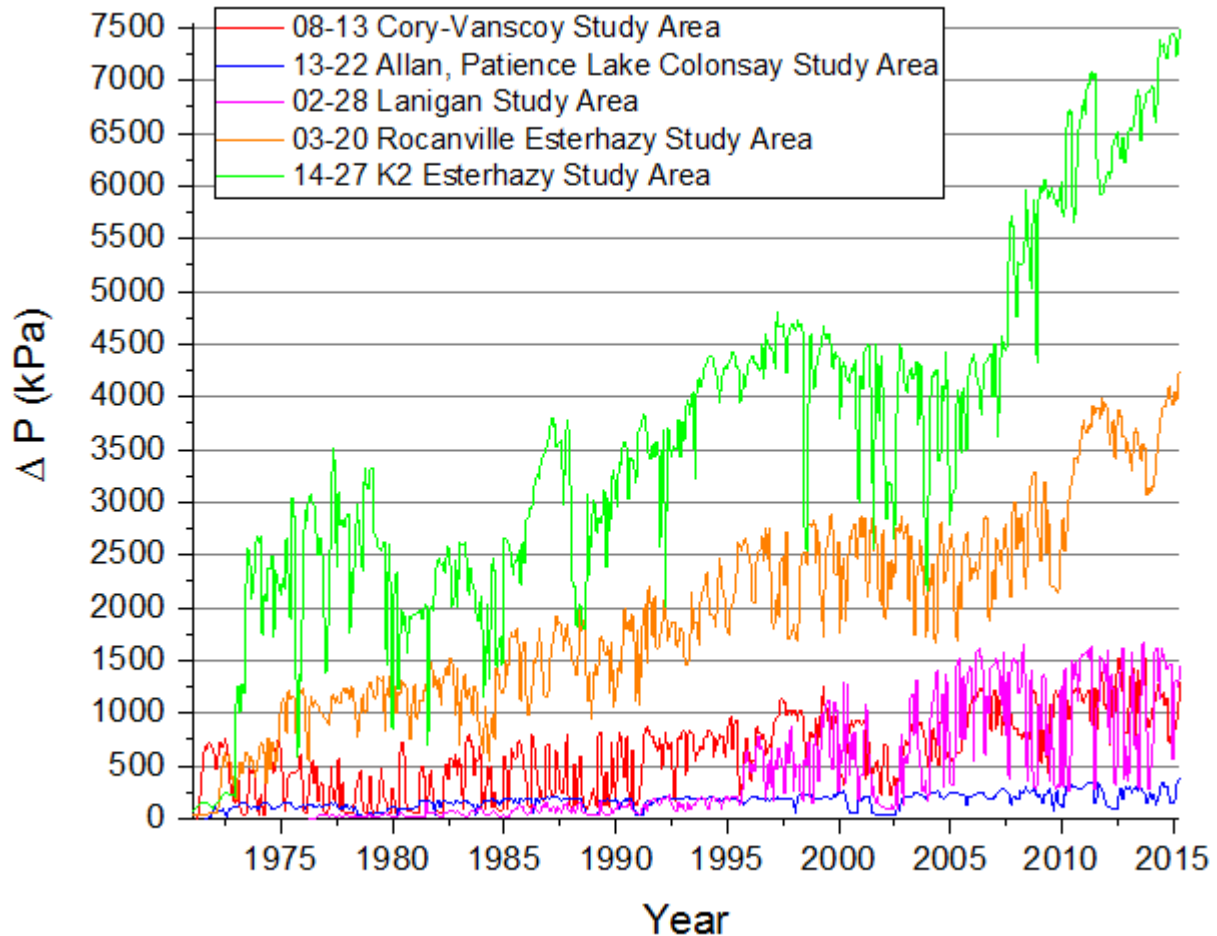
Figure 3-41: Typical simulated aquifer response for a representative well at each respective mine site based on the representative history matched transmissivity for each site with sonic derived storativity for each site

Through the Aqtesolv models insights were able to be gained into the extent of the injection-induced pressure propagations at each of the mine sites. The extent of these pressure propagations was found to be highly dependent on the aquifer storativity (aquifer compressibility) input in the simulation. The low storativity values calculated from the dipole sonic logs resulted in the furthest pressure propagations while the simulations using the high case storativity for fissured rocks resulted in the least distant (Table 3-18). The sonic estimated storativity simulations which were found to have the best correlation in history-matching as well

as being based on actual field data (rather than empirical correlations) provide the best representation of the pressure prorogation in the aquifer.

Table 3-18: Summary of injection-induced pressure propagations (km's) at mine sites based on different storativity values and history-matched transmissivity

	Cory-Vanscoy	Allan, Patience Colonsay	Lanigan	Esterhazy
Sonic estimated S	150	80	110	300
High case S for fissured rocks	22	40	15	30

3.6 Analytical Modelling of Injection Wells Discussion

The representative aquifer permeabilities calculated through history-matching were found to be considerably larger than those obtained from well tests and core at each of the study areas, this was likely due to scaling effects where the tests conducted over a larger area were more likely to encounter preferential flow pathways within the aquifer. History-matched permeabilities represent the largest scale of measurement, as these models are conducted based on data throughout the entire mine site, while the DSTs and falloff tests are investigating 10's to 100's of metres into the aquifer and the core data is only a point source representation of the aquifer.

Through the analytical models and the falloff test data it was apparent that the pressure response at the Esterhazy site was much greater than that seen at any of the Basal Clastics sites both in terms of increases in aquifer pressure as well as the distance of pressure propagation. A great deal of this difference can be attributed to the fluid volumes injected at each of the sites, where the overall injection rates at the Esterhazy site were considerably higher than any of the Basal Clastic sites (over three times higher). Although the injection rates in the Esterhazy wells are generally lower than those at the Basal Clastic sites, the sheer number of injection wells in the Esterhazy area (32) resulted in a very large quantity of fluid disposed of in the Interlake Formation in a relatively small geographical area. This higher quantity of fluid resulted in larger increases in aquifer pressure. However, the larger volume of fluid disposed of at the Esterhazy site was not the only factor at play resulting in the larger pressure buildup. The permeabilities in the Interlake Formation at the Esterhazy site from the various methods of analysis were found to be considerably smaller than those observed at the Basal Clastic sites. The lower permeabilities of the Interlake Formation in this area means the aquifer is less readily able to accept injected fluids that resulted in a larger increase in pressure buildup from injection activities.

Within the Esterhazy study area the pressure response from the K1 and K2 mine sites was found to be somewhat higher than the Rocanville mine. This can as well be attributed to well density where the Rocanville site has a lower well density than the K1 or K2 sites and thus the Interlake Formation is more readily able to dissipate the pressure transients from a lower volume of injected fluids.

The more distant pressure propagations found in the history-matched models at the Esterhazy site can be attributed to the larger fluid volumes injected into the aquifer as well as the lower sonic log derived storativity in the Interlake Formation at this site. The larger quantities of fluids injected would require more space to propagate outward into the formation. The aquifer compressibility (hence storativity) was found to be significantly less in the Interlake Formation at the Esterhazy site than the Deadwood Formation at the Basal Clastic sites. The Interlake Formation being composed of stiff incompressible carbonates has a much lower compressibility than the sands of the Basal Clastics.

The very distant pressure propagations predicted in history-matched models for each of the study areas would result in interference between neighboring mine sites that are often only 10's of kilometres apart. This interference was confirmed through modelling isolated models where neighboring mine wells were not taken into account and then again with the combined models to see the difference in the aquifer response. At each of the sites significant pressure differentials were determined from this analysis (for models based on history-matched parameter inputs), confirming that wells at neighboring mine sites (such as the Cory and Vanscoy mine sites) had a substantial effect on the pressure response of each other.

3.7 Analytical Modelling Conclusion

Through generating analytical models at each of the potash mine sites in Saskatchewan insights were gained into changes in aquifer pressures that have occurred over time as a result of injection of brine waste. Through conducting history-matching with the falloff test pressure data representative models for each mine site were generated that provided the most realistic simulation outputs of aquifer pressure. From these history-matched models it was observed that the Esterhazy site utilizing the Interlake Group for waste disposal has undergone much larger increases in aquifer pressures than the sites utilizing the Basal Clastics. Where at the Esterhazy site utilizing there has been upwards of 7000 kPa increases in aquifer pressure compared to the 400-1500 kPa increase in the Basal Clastic sites. It is reasonable to assume that the lower aquifer permeabilties as well as the higher volumes of fluid disposed of at the Esterhazy site are responsible for these much larger increases in aquifer pressure. Additionally the distances of the pressure propogations were found to be much greater at the Esterhazy site (300 km) compared to the Basal Clastic sites (80-150 km) this being due to the lower compressibility (storativity) of the Interlake Group carbonates as compared to the sand units in the Basal Clastics.

4. Conclusion

Through conducting a large-scale reservoir characterization study the permeabilities of both the basal clastics and the Interlake Group were able to be estimated throughout the study area. It was apparent that there are large differences in permeability both spatially and with respect to lithology in these aquifers. As well, the permeabilities in these aquifers at the potash mine sites were ascertained. Through knowing the permeabilities at each of the mine sites, the suitability for injection of these aquifers was could be determined, with higher permeability values being more suitable for injection.

Through detailed reservoir characterization, the Basal Clastics were identified to have the largest permeabilities in the Saskatoon area, an area where the Basal Clastics are utilized extensively for wastewater injection at the Potash mines. In other areas of the province, the permeabilities in the Basal Clastics were somewhat lower. There are, however, large data gaps where no information is available as there are no wells drilled into the Basal Clastics, the permeabilities in these areas could lay anywhere within the extensive range seen throughout the study area. Further exploratory drilling in these areas of low well density is necessary in order to better assess these areas.

Within the Interlake Group there were no readily apparent regional trends in permeability, as well the range of permeability values observed was considerably smaller than in the Basal Clastics. In the Esterhazy area where the Interlake Group is utilized for potash mine waste injection, the permeabilities were considerably lower than those observed in the Basal Clastics at the respective mine sites where this formation is utilized.

The permeability distributions mapped in various parts of the province in this study will aid in future developments of the Basal Clastics and Interlake Group by providing a general overview of the location of the most suitable areas for brine injection. However, further study is needed in order to determine the lithological factors that are responsible for controlling permeability within the basal clastics and Interlake Group. Petrographic analysis of core from these formations could help identify lithological controls on permeability. Additionally, further exploratory drilling would be beneficial to provide a complete picture of the permeability characteristics of these formations throughout Saskatchewan.

Analytical models of the injection activities at each mine site offered insight into the changes in aquifer pressures. These models were constructed with data acquired from the reservoir characterization component of this study including the aquifer permeability and compressibility, reservoir thickness and reservoir heterogeneities. Through the use of different input values of aquifer permeability and compressibility (observed in the reservoir characterization study) in the Aqtesolv analytical models various simulation outputs were generated. It was observed that the changes in aquifer pressure were most dependent on the formation transmissivity (permeability) input, with larger increases in formation pressure observed with smaller permeabilities. The extent of the pressure propagations at the mine sites was found to be most dependent on the aquifer storativity (compressibility). Smaller storativities were found to result in further pressure propagations into the aquifer.

History-matching in the analytical models was conducted whereby the aquifer pressure simulation outputs were compared to falloff test pressure data. Successive iterations were run in the models with various input values of transmissivity and storativity until simulation outputs were produced that most closely matched the falloff test pressure data. The history-matched values of permeability (transmissivity) were generally found to be somewhat higher than the values obtained from core and well tests at the mine sites. This can likely be attributed to scaling effects where the radius of investigation of the core and well tests is much smaller than that of the history-matched models. The larger scale of investigation in the models would more likely encounter high permeability preferential flow paths.

The outputs of the history-matched models provide the most accurate insights into the real world conditions at the various mine sites. These models illustrate the best estimate of the rise in aquifer pressure brought about by the injection activities, as well as the extent of these pressure propagations through the aquifer. Different pressure responses were observed for the history-matched models at each of the mine sites. These differences were in part the result of variations in aquifer permeabilities between each of the sites. Higher pressure responses were observed in mine sites with lower aquifer permeabilities, as these aquifers are less readily available to accept injected fluid and as a result pressures build up. Additionally, different overall injection rates from all of the wells at each of the mine sites were responsible for a great deal of the difference in the pressure responses. Higher overall injection rates resulted would result in a larger increase in aquifer pressure. In the case of the Interlake Formation at the Esterhazy site, the lower aquifer permeabilities observed as well as the substantially higher overall injection rates resulted in very large increases in aquifer pressure over time, significantly higher than those seen at any of the Basal Clastic mine sites.

The pressure responses produced from the analytical models at each of the mine sites will be of assistance for future planning of injection activities. Through knowing the aquifer response at each site based on past injection rates, future predictions of aquifer responses will be possible and future injection activities at these respective sites will be able to be better managed.

Future research at each of these mine sites into the link between the injection activities and seismicity would be beneficial. The pressure responses simulated at each of the mine sites in this study would provide an excellent comparison to the seismic data in order to provide a link between how the changes in aquifer pressure have effected seismicity.

REFERENCES

Amthor JE, Mountjoy EW and Machel HG (1994) Regional-scale porosity and permeability variations in Upper Devonian Leduc buildups: implications for reservoir development and prediction in carbonates. AAPG bulletin, 78(10):1541-1558

Anderson TC (1982) Exploration history and hydrocarbon potential of the Ordovician Winnipeg Formation in the Southern Williston Basin. Fourth International Williston Basin Symposium October 5, 1982:19-25

Al-Fattah S M and Al-Marhoun MA (1994) Evaluation of empirical correlations for bubble point oil formation volume factor. Journal of Petroleum Science and Engineering, 11(4):341-350

Arnott RWC, Zaitlin BA, and Potocki, DJ (2000) Geological controls on reservoir distribution in the Lower Cretaceous Basal Quartz, Chin Coulee–Horsefly Lake area, south-central Alberta. Bulletin of canadian petroleum geology, 48(3):212-229

Arps JJ and Roberts TG (1955) The effect of the relative permeability ratio, the oil gravity, and the solution gas-oil ratio on the primary recovery from a depletion type reservoir. Trans. AIME, 204:120-127

Alley WM, Scott Bair E, and Wireman M (2013) "Deep" groundwater. Groundwater, 51(5):653-654

Bachu S and Hitchon B (1996) Regional-scale flow of formation waters in the Williston Basin. AAPG bulletin, 80(2):248-264

Bansal RK (2010) A textbook of strength of materials. Laxmi Publications.

Batu V (1998) Aquifer hydraulics: a comprehensive guide to hydrogeologic data analysis (Vol. 1). John Wiley & Sons.

Beggs HD and Robinson JR (1975) Estimating the viscosity of crude oil systems. Journal of Petroleum technology, 27(09):1-140

Benn AA and Rostron BJ (1998) Regional hydrochemistry of Cambrian to Devonian aquifers in the Williston basin, Canada-USA. Eighth International Williston Basin Symposium, Saskatchewan Geological Society Special Publication No. 13. 238-246

Black WM (1956) A review of drill-stem testing techniques and analysis. Journal of Petroleum Technology 8(6):21-30. http://dx.doi.org/10.2118/589-G
Borah I (1992) Drill stem testing. Development Geology Reference Manual. AAPG Methods in Exploration Series 10:131-137

Borah I (1992) Drill stem testing. Development Geology Reference Manual. AAPG Methods in Exploration Series 10:131-137

Bredehoeft JD (1965) The drill-stem test: the petroleum industry's deep-well pumping test. Ground Water 3(3):31-36. doi: 10.1111/j.1745-6584.1965.tb01218.x

Brown RH (1953) Selected procedures for analyzing aquifer test data. Journal (American Water Works Association), 45(8):844-866

Case CM, Pidcoe WW and Fenske PR (1974) Theis equation analysis of residual drawdown data. Water Resources Research, 10(6):1253-1256.

Chierici GL (2012) Principles of petroleum reservoir engineering (Vol. 2). Springer Science & Business Media.

Crawford GE, Pierce AE, and McKinley RM (1977) Type curves for Mckinley analysis of drill-stem test data. SPE Annual Fall Technical Conference and Exhibition. Society of Petroleum Engineers.

Dake (1978) Fundamentals of reservoir engineering. Vol 8. Elsevier Science BV.

Dixon J (2008) Stratigraphy and facies of Cambrian to Lower Ordovician strata in Saskatchewan. Bulletin of Canadian Petroleum Geology, 56(2):93-117

Desbarats AJ and Bachu S (1994) Geostatistical analysis of aquifer heterogeneity from the core scale to the basin scale: A case study. Water Resources Research, 30(3):673-684

Dolan JP, Einarsen CA, Hill GA (1957) Special applications of drill-stem test pressure data. Society of Petroleum Engineers. Petroleum Transactions, 210:318-324

Environmental Protection Agency (2002) EPA region 6 UIC pressure falloff testing guideline third revision. United States Environmental Protection Agency:1-9: 5-6, A-10-14.

Ferguson G and Grasby SE (2014) The geothermal potential of the basal clastics of Saskatchewan, Canada. Hydrogeology Journal 22(1):143-150. doi: 10.1007/s10040-013-1061-5

Ferguson G (2015) Deep injection of waste water in the western Canada sedimentary basin. Groundwater, 53(2):187-194.

Ferris D, Lypka M, and Ferguson G (2017) Hydrogeology of the Judith River Formation in southwestern Saskatchewan, Canada. Hydrogeology Journal, 25(7):1985-1995

Friesen OJ (2015) Permeability Heterogeneity in Bioturbated Strata, Cardium Formation, Pembina Field, and the Identification of Potential Waterflood Opportunities (Doctoral dissertation, Science:).

Friesen OJ, Dashtgard SE, Miller J, Schmitt L, and Baldwin C (2017) Permeability heterogeneity in bioturbated sediments and implications for waterflooding of tight-oil reservoirs, Cardium Formation, Pembina Field, Alberta, Canada. Marine and Petroleum Geology, 82, 371-387.

geoLOGIC systems Ltd. (2016) geoSCOUT

Grasby SE, Chen Z, Hamblin AP, Wozniak PR, and Sweet AR (2008) Regional characterization of the Paskapoo bedrock aquifer system, southern Alberta Geological Survey of Canada Contribution 2008-0479. Canadian Journal of Earth Sciences, 45(12):1501-1516

Greggs DH and Hein FJ (2000) The sedimentology and structure of the lower Paleozoic Deadwood Formation of Saskatchewan. Summary of Investigations 1:2000-2004

Haidl F, Nimegeer A and Marsh A (2006) Stratigraphy and Hydrocarbon Potential of Silurian Interlake Strata, Southeastern Saskatchewan. Geology of giant petroleum fields: AAPG Memoir, 14, 50-90.

Hall HN (1953) Compressibility of reservoir rocks. Journal of Petroleum Technology, 5(01):17-19.

Hemphill CR, Smith RI and Szabo F (1970) Geology of Beaverhill Lake reefs, Swan Hills area, Alberta

Hongkui G, Yingsong L, Shanzhou M and Lili S O N G (2001) Difference of rock elastic parameters under static and dynamic loading. Frontiers of Rock Mechanics and Sustainable Development in the 21st Century. Taylor and Francis, 69-71.

HydroSOLVE Inc (2016) Aqtesolv

IHS AccuMap (2016) AccuMap

Kazemi H, Merrill LS, Jargon JR (1972) Problems in interpretation of pressure fall-off tests in reservoirs with and without fluid banks. Journal of Petroleum Technology 24(9):1-147. http://dx.doi.org/10.2118/3696-PA pp 1147-1153.

Kent DM (1994) Paleogeographic Evolution of the Cratonic Platform – Cambrian to Triassic; Geological Atlas of the Western Canada Sedimentary Basin, Ch. 7.

Kessler LG (1991) Subsidence controlled stratigraphic sequences and the origin of shelf sand ridges, Winnipeg Group (Middle Ordovician) Manitoba, Saskatchewan, North Dakota. In: Christopher, J.E., Haidl, F.M. (Eds.), Eighth International Williston Basin Symposium, Saskatchewan Geological Society Special Publication, 11:1–3

Kestin J, Khalifa HE, Correia RJ (1981) Tables of the dynamic and kinematic viscosity of aqueous NaCl solutions in the temperature range 20-150 °C and the pressure range 0.1-35 MPa. Journal of Physical and Chemical Reference Data 10(1):71-88. http://dx.doi.org/10.1063/1.555641

Khatchikian A (1996) Deriving reservoir pore-volume compressibility from well logs. SPE Advanced Technology Series, 4(01), 14-20

Lehr JH (1986) Underground injection: a positive advocate. Proceedings of the International Symposium on the Subsurface Injection of Liquid Wastes, New Orleans, 51–56

Lee AL, Gonzalez MH and Eakin BE (1966) The viscosity of natural gases. Journal of Petroleum Technology, 18(08), 997-1.

LeFever RD (1996) Sedimentology and stratigraphy of the Deadwood-Winnipeg Interval (Cambro-Ordovician), Williston Basin. In: Longman, M.W., Sonnenfeld, M.D. (Eds.), Paleozoic Systems of the Rocky Mountain Region. Rocky Mountain Section, Society for Sedimentary Geology. 11–28

Lohman SW, Bennett RR, Brown RH, Cooper HH Jr, Drescher WJ, Ferris JG, Johnson AI, McGuinness CL, Piper AM, Rorabaugh M I , Stallman RW, and Theis CV (1970), Definitions of selected ground-water terms revisions and conceptual refinements: U.S. Geological Survey Open-File Report, 1-21

Maier LF (1962) Recent developments in the interpretation and application of DST data. Journal of Petroleum Technology 14(11):1-213

Martindale W, and Larson BW (2003) Interlake Facies & Reservoir, Bryant and Adjacent areas, Southeast Saskatchewan.

Matthews CS, and Russell DG (1967) Pressure buildup and flow tests in wells (Vol. 1). Dallas, TX: Society of petroleum engineers of AIME.

McAlister JA, Nutter BP, Lebourg M. (1965) A new system of tools for better control and interpretation of drill-stem tests. Journal of Petroleum Technology 17(2):207-214

McCain WD Jr. (1990) The Properties of petroleum fluids second edition, PennWell Publishing Company, 1-489

McCain WD Jr, (1991) Reservoir-fluid property correlations-state of the art (includes associated papers 23583 and 23594). SPE Reservoir Engineering 6(02):266-272

McElwee CD (1980) The Theis Equation: Evaluation, Sensitivity to Storage and Transmissivity, and Automated Fit of Pumptest Data (No. 3). Kansas Geological Survey.

Megathan ER (1987) Silurian Interlake Group: A Sequence of Cyclic Marine and Freshwater Carbonate Deposits in the Central Williston Basin. Williston Basin Symposium.

Mckinley RM, Vela S, Carlton LA (1968) A field application of pulse testing for detailed reservoir description. Journal of Petroleum Technology 20(3):313-321. http://dx.doi.org/10.2118/1822-PA

Microsoft Office (2013)

National Earthquake Database, Government of Canada
http://www.earthquakescanada.nrcan.gc.ca/

Nowak TJ and Lester GW (1955) Analysis of pressure fall-off curves obtained in water injection wells to determine injective capacity and formation damage. Petroleum Transactions, AIME 204:96-102. 97-98.

Nimegeers A (2000) An Allostratigraphic Analysis of the Middle Ordovician Winnipeg Group in Southern Saskatchewan, unpublished B.Sc. Honours Thesis. University of Regina, Regina

Nygaard R (2010) Geomechanical Analysis: Wabamun Area CO2 Sequestration Project (WASP). Energy and Environmental Systems Group, University of Calgary.

Palombi D and Rostron B (2006) Regional Hydrochemistry of Lower Paleozoic Aquifers in the Northern Portion of the Williston Basin, Saskatchewan-Manitoba. Saskatchewan and Northern Plains Oil and Gas Symposium 2006. 201-209

Paterson DF (1988) Review of regional stratigraphic relationships of the Winnipeg Group (Ordovician), the Deadwood Formation (Cambro-Ordovician) and underlying strata in Saskatchewan. Summary of Investigations 88(4):224-225

Prasad RK (1975) Pressure transient analysis in the presence of two intersecting boundaries. Journal of Petroleum Technology, 27(01):89-96

Precht WF (1986) Reservoir development and hydrocarbon potential of Winnipegosis (Middle Devonian) pinnacle reefs, southern Elk Point Basin, North Dakota. Carbonates and Evaporites, 1(1):83-99.

Pu R (2003) Pool characterization of Ordovician Midale field: Implication for Red River play in northern Williston basin, southeastern Saskatchewan, Canada. AAPG bulletin, 87(11):1699-1715.

Rostron B, White D, Hawkes C, Chalaturnyk R (2014) Characterization of the aquistore CO_2 project storage site, Saskatchewan, Canada, Energy Procedia 63:2977-2984. doi:10.1016/j.egypro.2014.11.320
State Water Resources Control Board Division of Water Quality GAMA Program (2016) Groundwater information sheet – Salinity.

Saskatchewan Ministry of Energy Resources (2011) Stratigraphic correlation chart. Saskatchewan Ministry of Energy Resources, Regina, SK. http://www.er.gov.sk.ca/stratchart

Schulze-Makuch D, Carlson DA, Cherkauer DS and Malik P (1999) Scale dependency of hydraulic conductivity in heterogeneous media. Ground Water, 37(6):904-919

Seibel C (2002) An Examination of the Source Rock Potential of the Deadwood and Winnipeg Formations of Southern Saskatchewan. Unpublished M.Sc. Thesis, University of Regina. Regina, 1–140.

Slind OL, Andrews GD, Murray DL, Norford, BS, Paterson DF, Salas CJ and Tawadros EE (1994) Middle Cambrian to Lower Ordovician strata of the Western Canada Sedimentary

Basin. Geological Atlas of the Western Canada Sedimentary Basin. Edited by G. Mossop and I. Shetsen. Canadian Society of Petroleum Geologists and Alberta Research Council, Special Report, 4:87-108

Sloss LL (1963) Sequences in the cratonic interior of North America. Geological Society of America Bulletin 74:93–110

Smith M, Bend S (2004) Geochemical analysis and familial association of Red River and Winnipeg reservoired oils of the Williston Basin, Canada. Organic geochemistry 35(4):443-452. http://dx.doi.org/10.1016/j.orggeochem.2004.01.008

Sutton RP (1985) Compressibility factors for high-molecular-weight reservoir gases. SPE Annual Technical Conference and Exhibition. Society of Petroleum Engineers. 1-6.

Theis CV (1935) The relation between the lowering of the Piezometric surface and the rate and duration of discharge of a well using ground-water storage. Eos, Transactions American Geophysical Union, 16(2): 519-524.

Tsang CF and Niemi A (2013) Deep hydrogeology: a discussion of issues and research needs. Hydrogeology Journal, 21(8):1687-1690

Warner JH and Lehr DL (1981) Subsurface wastewater injection: the technology of injecting wastewater into deep wells for disposal, Premier Press.

Weides S, Moeck, I, Majorowicz J, and Grobe M (2014) The Cambrian Basal Sandstone Unit in central Alberta—an investigation of temperature distribution, petrography, and hydraulic and geomechanical properties of a deep saline aquifer. Canadian Journal of Earth Sciences, 51(8), 783-796.

White R K and Mohsenin NN (1967) Apparatus for determination of bulk modulus and compressibility of materials. Transactions of the ASAE, 10(5), 670-0671.

Whittaker S, Worth K (2011) Aquistore: A fully integrated demonstration of the capture, transportation and geologic storage of CO_2, Energy Procedia 4:5607-5614. doi:10.1016/j.egypro.2011.02.550

Vazquez M, Beggs HD (1980) Correlations for fluid physical property prediction. Journal of Petroleum Technology 32(06):968-970. http://dx.doi.org/10.2118/6719-PA

Vigrass LW (1971) Depositional framework of the Winnipeg Formation in Manitoba and eastern Saskatchewan. Geological Association of Canada Special Paper No 9:225– 234

Younger PL (1993) Simple generalized methods for estimating aquifer storage parameters. Quarterly Journal of Engineering Geology and Hydrogeology, 26(2):127-135.

Appendix A

Skin Effects for a Drill Stem Test (Borah 1992).

To quantify the effects that the filter cake in the wellbore would have on reducing fluid production during a drill stem test the concept of skin effect was developed (Bredehoeft 1965). The larger the skin effect, the more influence the wellbore skin has on the DST.

Skin values for drill stem tests typically are positive or close to zero, whereas a negative skin is indicative of stimulation, as a well has not been stimulated during a drill stem test such a value is likely erroneous (Borah 1992).

$$s' = 1.151 \left(\frac{p_i - p_{wf}}{m} - \log\left(\frac{kt}{\phi\mu c_t r_w^2}\right) + 3.23 \right)$$

p_i=Initial Static Reservoir Pressure (psi)   m= Slope of Line on DST Plot Over 1 Log Cycle (psi/cycle)

p_{wf}= Bottom Hole Flowing Pressure (psi)   k=Permeability (mD)

t= Flowing Time (min) ϕ=Porosity (fraction)

μ=Viscosity (cp) c_{bulk}=Bulk Compressibility (psi^{-1})

r_w=Wellbore Radius (ft)

Skin Factor of a Falloff Test (EPA 2002)

$$s = 1.1513\left(\frac{P_{1hr} - P_{wf}}{m}\right) - \log\left(\frac{k}{(t_p + 1)\phi\mu c_t r_w^2}\right) + 3.23)$$

s=skin factor (dimensionless)

P_{1hr}=Pressure intercept along semi-log straight line at shut in time of 1 hr (psi)

P_{wf}=Injection Pressure Prior to Shut In (psi) μ=Viscosity at Reservoir Conditions (cp)

m=Slope of Semi-log Straight Line (psi/cycle)   k=Permeability (mD)

ϕ=Porosity (Fraction) c_t=Total Compressibility (psi^{-1})

r_w=Wellbore Radius (ft) t_p=Injection Time (hrs)

Appendix B

Gas Formation Volume Factor Calculation

The gas formation volume factor is a representation of the change in volume of a unit of gas from reservoir conditions to surface conditions whereby (Dake 1978)

$$B_g = \frac{V_{RES}}{V_{SC}}$$

B_g= Gas Formation Volume Factor

V_{RES}= Volume of Gas at Reservoir Conditions

V_{SC}=Volume of Gas at Surface Conditions

The gas formation volume factor is able to be calculated with the known reservoir temperature and pressure using the equation (Modified from Dake 1978)

$$B_g = \frac{0.351ZT}{P_{res}}$$

B_g= Gas Formation Volume Factor (rcm/stcm)

Z= Gas compressibility Factor

T= Reservoir Temperature (°K)

P_{Res}= Reservoir Pressure (kPa)

The Gas compressibility factor (Z) can be found through the use of the Standing-Katz chart, once the pseudo-reduced pressure and temperature are known (Modified from Dake 1978)

$$P_{PR} = \frac{P_{RES}}{P_{CRIT}}$$

$$T_{PR} = \frac{T_{RES}}{T_{CRIT}}$$

P_{PR}= Pseudo-Reduced Pressure T_{PR}= Pseudo-Reduced Temperature

P_{RES}=Reservoir Pressure (kPa) T_{RES}=Reservoir Temperature (°K)

P_{CRIT}=Critical Pressure (kPa) T_{CRIT}=Critical Temperature (°K)

The critical temperatures and pressures can be found using the equations (Modified from Sutton 1985)

$$T_{CRIT}= 94.0+194.2\gamma_g-41.1\gamma_g{}^2$$

$$P_{CRIT}=5220-903.3\gamma_g-24.7\gamma_g{}^2$$

γ_g=Gas Gravity

The gas gravity was able to be obtained from AccuMap (HIS AccuMap 2016) whereby chemical analysis on the gas samples from the drill stem test yielded the elemental composition of the gases and the corresponding specific gravity and molecular weight of the gas.

Once the critical temperature and pressure are calculated the Standing-Katz chart is used to find the gas compressibility factor Z.

Oil Formation Volume Factor

The formation volume factor for oil (B_O) is somewhat more complicated to analyse as it is representative of the volume occupied in the reservoir of oil and dissolved solution gas of one standard unit of oil at standard conditions (Al-Fattah and Al-Marhoun 1994). In order to find B_O the solution gas ratio (R_S) must be found (Al-Fattah and Al-Marhoun 1994). R_S is defined as the amount of gas in standard volumes that will dissolve into one stock tank volume of oil at reservoir temperature and pressures (Arps and Roberts 1955). R_S was estimated from the volumes of gas vs oil that flowed during the drill stem tests. In order to calculate B_O, the bubble point pressure was first required to be found.

Bubble point pressure was estimated from (McCain 1991)

$$p_b = 18.2(C_{pb} - 1.4)$$

Where

$$C_{pb} = \left(\frac{R_s}{\gamma_g}\right)^{0.83} \times 10^{0.00091T_{Res}-0.0125API}$$

R_S=Solution gas ratio (scf/STB)   T=Reservoir Temperature (°F)

γ_g=Gas specific gravity   API=Oil Gravity (API)

As well before calculating bubble point pressure the γ_{gs} or gas specific gravity at reference separator conditions of 100 psi needed to be calculated (Vasquez and Beggs 1980). This was required as the equations for bubble point pressure were dependent on this calibration. As the separator temperature and pressure conditions were not available they were assumed to be at standard condition for this calculation (personal communication Professor Hawkes). γ_{gs} was able to be found from (Vasquez and Beggs 1980).

$$\gamma_{gs} = \gamma_{gp}\left(1 + 5.912 \times 10^{-5}(API) \times Tlog\left(\frac{p}{114.7}\right)\right)$$

γ_{gp} =Gas Gravity Obtained at Separator Conditions   API=Oil Gravity (API)

p= Separator Pressure (assumed standard conditions (14.504 psi)

T= Temperature (assumed standard conditions 77°F)

Where below bubble point pressure the formation volume factor of oil (B_O) was able to be determined through (Vasquez and Beggs 1980).

$$B_O = 1 + C_1 R_s + C_2(T - 60)\left(\frac{API}{\gamma_{GS}}\right) + C_3 R_s(T - 60)\left(\frac{API}{\gamma_{GS}}\right)$$

Where the coefficients

Coefficient	Oil Gravity <= 30 API	Oil Gravity > 30 API
C_1	4.677×10^{-4}	4.67×10^{-4}
C_2	1.751×10^{-5}	1.1×10^{-5}
C_3	-1.811×10^{-8}	1.337×10^{-9}

At reservoir pressures above the bubble point pressure, the oil formation volume would shrink as a result of compression as shown by the equation (Vasquez and Beggs 1980).

This oil compressibility was able to be found from (Vasquez and Beggs 1980).

$$c_O = \frac{-1433 + 5R_s + 17.2T - 1180\gamma_{GS} + 12.61API}{p \times 10^5}$$

C_o=Oil compressibility (psi^{-1})

T=Reservoir Temperature (°F)   API= Oil Gravity (API)

γ_{gs}=Gas Specific Gravity at Reference Conditions (100psi)

The B_O was then able to be found by calculating the B_O at bubble point pressure using the previous equation and then using this value in the equation (Vasquez and Beggs 1980).

$$B_O = B_{OB}\text{expIC}_o(p - p_b)$$

B_{OB}= Oil Formation Volume Factor at Bubble Point Pressure (bbl/STB)

p=Reservoir Pressure (psi) p_b=Bubble Point Pressure (psi)

Appendix C

Density of Formation Water (Chierici 1994)

$\rho_w 730.6 + 2.025\text{T} - 3.8 \times 10^{-3}T^2 + [2.362 + 1.197 \times 10^{-2}T + 1.835 \times 10^{-5}T^2] + [2.374 - 1.024 \times 10^{-2}T + 1.49 \times 10^{-5}T^2 - 5.1x10^{-4}P]C$

ρ_w=Formation Water Density (kg/m3)

P=Pressure (Mpa) – Valid from 0-50 Mpa

T_{Res}= Reservoir Temperature (°K) – Valid from 293-373 °K

C=Concentration of total dissolved solids (g/L)

Viscosity of Formation Water Table (Kestin et al. 1981)

Use tables to correlate viscosity μ from formation pressure, temperature and formation water salinity.

T=Temperature (°C)

P_s=Static formation pressure, found from DST plot at infinite time where log[(t+Δt)/Δt]=1 (Warner and Lehr 1981).

C=Concentration of sodium chloride in solution (mol/kg)

Water saturation is 100% in an aquifer, may be between 10-50% in an oil reservoir, if gas present will have large effect on compressibility as c_g are much higher than other fluids.

Appendix D

<u>Oil Viscosity</u> (Beggs and Robinson 1975)

$$\mu_{go} = A\mu_{OD}^{B}$$

A=10.715(R_S+100)$^{-0.515}$

μ_{OD}= Viscosity of Gas Free Oil (cp)

B=5.44(R_S+150)$^{-0.338}$

μ_{go}= Viscosity of Gas Saturated Oil (cp)

R_S=Solution Gas Ratio (scf/STB)

$$\mu_{OD} = 10^{X} - 1$$

X=y$T^{-1.163}$

Y=10^{Z}

Z=3.3024-0.02023 (API)

T_{res}= ReservoirTemperature (°F)

API= Oil Gravity (°API)

<u>Gas Viscosity</u> (Lee et al. 1966)

$$\mu_g = \frac{Y1\exp(Y5)}{10000}$$

$$Y1 = \frac{\left(22.65 + 0.03873MW_g\right)T^{1.5}}{(209.2 + 19.26MW_g + 1.8T)}$$

$$Y2 = 3.448 + \frac{548}{T} + 0.01009MW_g$$

$$Y3 = 2.447 - 0.2224Y2$$

$$Y4 = \frac{0.4222MW_g}{10000B_g}$$

$$Y5 = Y2(Y4^{Y3})$$

MW_G=Molecular Weight of Gas (dimensionless)

B_g=Gas Formation Volume Factor ($\frac{rcm}{stcm}$)

T_{res}= Reservoir Temperature (°K)

μ_g=Gas Viscosity (cp)

Appendix E

High Confidence Horner Plot
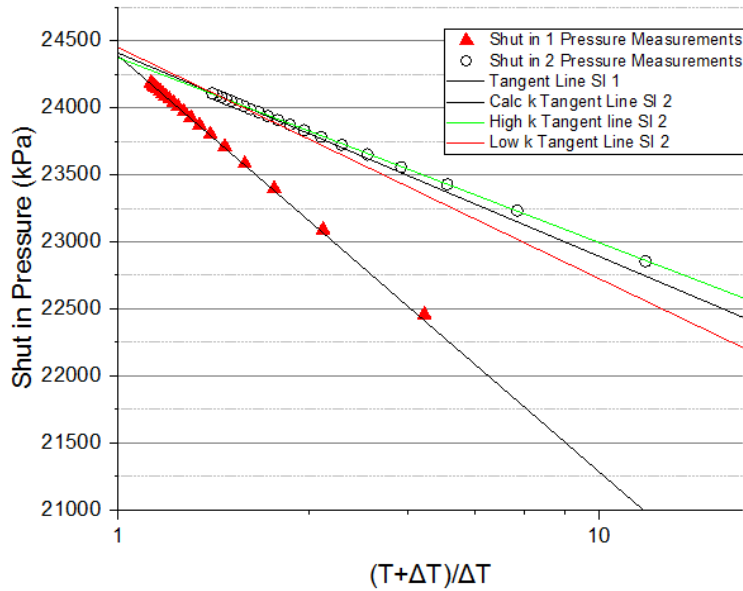
DST 2 from 131/06-18-009-06W2 conducted in clean Winnipeg Formation sands. Shut in period 2 measurements used for permeability analysis follow a smooth trend with no erratic measurements allowing for accurate line fitting. There is little variation for slope interpretation as can be seen in the tangent lines for the low and high permeability interpretation. In this was only a 13.5 and 16.8 % variation from the calculated value of the low and high permeability interpretations respectively.

Medium Confidence Horner Plot
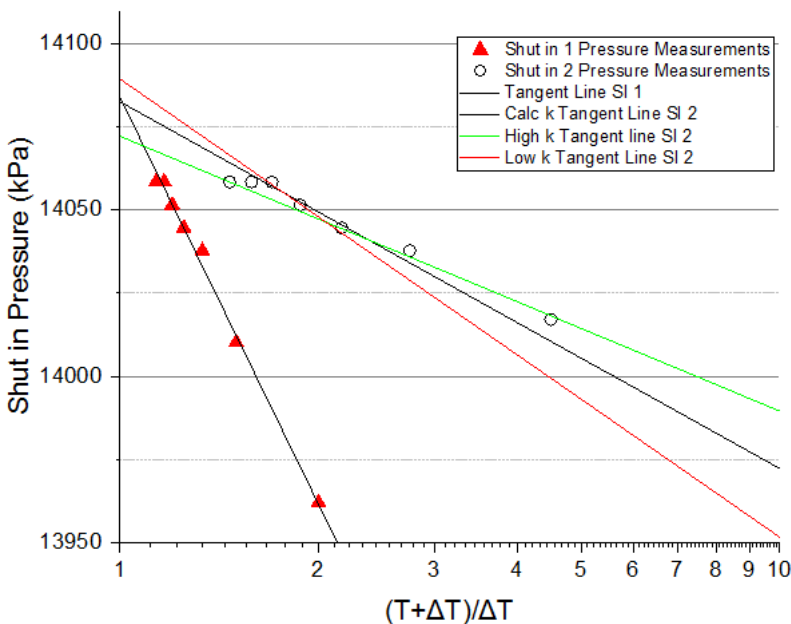
DST 2 from 131/01-20-033-23W2 conducted in dirty Deadwood Formation sands at the PCS Lanigan potash mine. In this example there are few pressure measurements, thereby not allowing a highly accurate line fitting to be conducted. As well the pressure measurements are somewhat erratic as well as flat at late times. The result of this is low and high permeability cases that deviate 20.00 and 33.33 % from the calculated value respectively.

Low Confidence Horner Plot
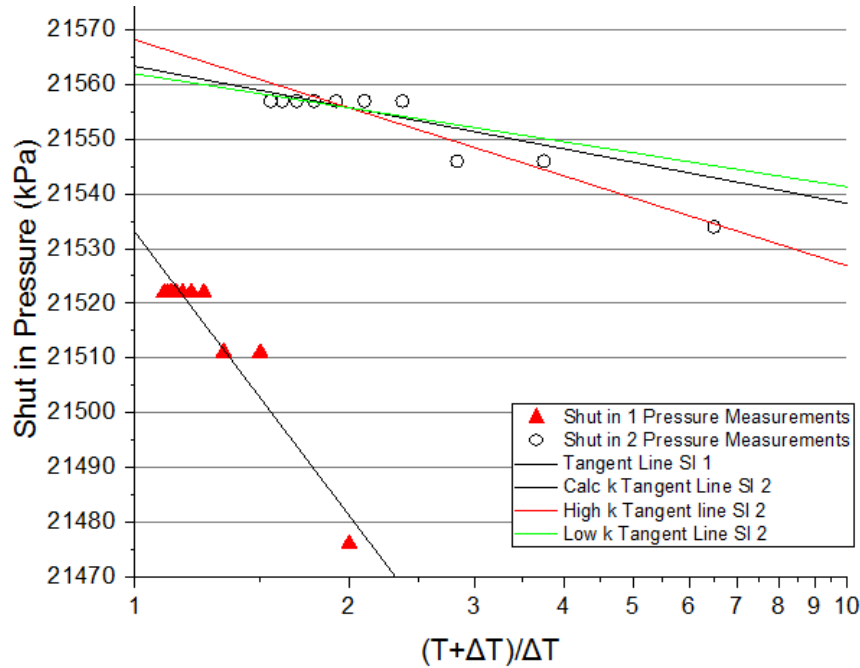
In DST 2 from 131/03-08-017-19W2 conducted in clean Winnipeg Formation sands there are very limited pressure measurements taken. Additionally, the late time data is completely flat and thus the less representative early time data is used for analysis. There is considerable variation in how the line fitting can be undertaken resulting in a low and high permeability case that vary 39.33 and 21.33% from the calculated value respectively. A DST of this quality would normally be discarded, however the permeability results of the interpretation were within the range of values seen in other wells in the area and thus this test was included.

Appendix F

Table 1) Deadwood Formation DST and core wells, with assigned well number and calculated permeability values

UWI	Well #	DST #	Horner Match Conf	DST k log(m²)	Sensit Low k log(m²)	Sensit High k log(m²)	Sen Low %	Sen High %		Core eff k-Max log(m²)
Clean Low Gamma Ray Sand										
Midale Area										
111/16-23-002-01W2/00	42									-13.0
141/04-16-006-13W2/00	43									-13.3
131/04-01-009-13W2/02	44	4	High	-15.9	-15.9	-15.9	-2.1	0		
142/12-01-010-09W2/00	45									-12.7
131/01-33-014-12W2/00	46									-13.5
Average				-15.9						-13.0
Bengough Area										
121/15-23-009-23W2/00	47	3	Med	-11.9	-12.0	-11.8	-20.0	25.0		
Belle Plain Area										
131/03-08-017-19W2/00	48	3	Med	-12.3	-12.4	-12.3	-20.0	23.1		-13.0
191/04-24-017-24W2/00	49	1	Med	-12.3	-12.4	-12.3	-9.0	18.3		
191/04-24-017-24W2/00	49	2	Med	-12.5	-12.5	-12.4	-6.3	6.7		
191/08-14-017-24W2/00	69								-12.3	
101/02-11-015-26W2/00	50									-12.9
Average				-12.4					-12.3	-12.9
Saskatoon Area										
111/13-07-036-06W3/00	51	1	High	-11.7	-11.8	-11.6	-15.8	31.0	-12.1	
111/08-13-036-07W3/00	52	3	Med	-11.6	NA	NA	NA	NA	-12.2	
	52	4	Med	-11.6	NA	NA	NA	NA		
131/01-20-033-23W2/00	53	1	Med	-12.7	-12.8	-12.6	-17.1	-11.5	-12.1	
UWI	Well #	DST #	Horner Match Conf	DST k log(m²)	Sensit Low k log(m²)	Sensit High k log(m²)	Sen Low %	Sen High %		Core eff k-Max log(m²)
	53	3	Med	-11.9	-12.0	-11.8	-11.1	33.3		
141/02-28-033-23W2/00	54	2	Med	-13.0	NA	NA	NA	NA	-12.0	
131/02-21-034-27W2/00	55	1	Med	-11.5	-11.5	-11.3	-17.1	31.8	-12.5	
	55	3	High	-11.9	-11.9	-11.8	-4.8	5.3		

UWI	Well #	DST #	Horner Match Conf	DST k log(m²)	Sensit Low k log(m²)	Sensit High k log(m²)	Sen Low %	Sen High %		Core eff k-Max log(m²)
191/14-16-034-27W2/00	70								-12.0	
111/16-28-034-01W3/00	72								-11.8	
121/03-21-035-08W3/00	56	1	Med	-12.3	-12.3	-12.2	-10.0	20.0	-12.4	
	56	2	Med	-12.0	-12.1	-12.0	-19.2	16.7		
	56	3	Med	-12.4	-12.6	-12.2	-34.3	53.3		
	56	7	Med	-11.7	-11.8	-11.7	-16.8	12.9		-12.3
191/15-16-035-08W3/00	57								-12.0	
Average				-11.8					-12.1	-12.3
Kindersley Area										
121/12-03-031-20W3/00	58									-12.6
141/04-05-035-26W3/00	59									-12.0
141/03-18-036-25W3/00	60									-12.0
101/16-36-036-25W3/00	61									-12.5
Average										-12.2
				)						
Prince Albert Area										
101/11-15-046-01W3/00	62									-12.3
121/12-30-049-27W3/00	63									-11.9
101/08-11-062-22W3/00	64									-12.2
Average										-12.1
Other										
101/10-03-005-08W3/00	65									-12.3
Dirtier Higher Gamma Ray Sands										
Midale Area										
131/11-34-006-11W2/02	66	1	High	-13.7	-13.7	-13.6	-10.3	25.0		
111/09-18-007-11W2/00	67	1	Med	-13.8	-13.9	-13.7	-20.0	33.3		
Average				-13.7						
Belle Plaine Area										
191/04-04-018- 19W2/00	68									-13.2
UWI	Well #	DST #	Horner Match Conf	DST k log(m²)	Sensit Low k log(m²)	Sensit High k log(m²)	Sen Low %	Sen High %		Core eff k-Max log(m²)
191/08-14-017-24W2/00	69	2	High	-12.7	-12.8	-12.7	-4.8	5.3	-12.3	
Saskatoon Area										
131/01-20-033-23W2/00	53	2	Med	-11.3	-11.4	-11.2	-20.0	33.3	-12.1	

UWI	Well #	DST #	Horner Match Conf	DST k log(m²)	Sensit Low k log(m²)	Sensit High k log(m²)	Sen Low %	Sen High %	Falloff Test k log(m²)	Core eff k-Max log(m²)
141/02-28-033-23W2/00	54	1	Med	-12.9	NA	NA	NA	NA	-12.0	-14.5
131/02-21-034-27W2/00	55	2	Med	-12.7	-12.7	-12.6	-13.4	21.2	-12.5	
UWI	Well #	DST #	Horner Match Conf	DST k log(m²)	Sensit Low k log(m²)	Sensit High k log(m²)	Sen Low %	Sen High %	Falloff Test k log(m²)	Core eff k-Max log(m²)
191/14-16-034-27W2/00	70								-12.0	
141/13-22-034-01W3/00	71	1	Low	-11.9	-12.1	-11.7	-41.2	66.7	-11.9	
111/16-28-034-01W3/00	72	1	Med	-13.1	NA	NA	NA	NA	-11.8	
121/03-21-035-08W3/00	56								-12.4	
191/15-16-035-08W3/00	57								-12.0	
111/13-07-036-06W3/00	51	2	High	-12.8	-12.8	-12.7	-5.6	6.3	-12.1	
111/08-13-036-07W3/00	52	2	Med	-11.8	NA	NA	NA	NA	-12.2	
	52	5	Med	-12.4	NA	NA	NA	NA		
111/10-12-036-07W3/00	73	1	High	-13.3	-13.3	-13.2	-10.9	13.9	-12.6	
111/05-15-036-09W3/00	74	1	High	-13.0	-13.1	-13.0	-16.7	24.9		
Average				-12.0					-12.1	-14.5
Kindersley Area										
101/15-34-034-27W3/00	75									-12.7
102/12-21-031-21W3/00	76	5	Med	-11.8	-11.9	-11.7	-12.5	31.3		
Swift Current Area										
101/08-17-018-14W3/00	77	3	Med	-15.3	-15.3	-15.3	-2.1	5.6		
101/01-09-017-14W3/00	78									-13.5
101/09-27-014-10W3/00	79									-14.0
Average				-15.3						-13.7
Other										
101/12-10-005-08W3/00	80	4	Low	-12.4	-12.6	-12.3	-33.3	33.3		
Shales										
Bengough Area										
131/06-02-003-21W2/02	81	3	High	-14.2	-14.3	-14.2	-9.1	11.1		
Swift Current Area										
101/03-10-017-14W3/00	82									-15.5
UWI	Well #	DST #	Horner Match Conf	DST k log(m²)	Sensit Low k log(m²)	Sensit High k log(m²)	Sen Low %	Sen High %		Core eff k-Max log(m²)
	82	1	High	-14.6	-14.7	-14.6	-10.0	10.7		-14.4
	82	2	High	-14.8	-14.8	-14.8	-4.5	7.7		-14.8
	82	3	High	-14.9	-15.0	-14.9	-6.7	7.7		-14.8
111/11-03-017-14W3/00	83									-14.7

121/07-09-017-14W3/00	84								-15.2
101/05-07-014-10W3/00	85								-15.3
102/05-07-014-10W3/00	85								-14.2
Average				-14.8					-14.7
Saskatoon Area									
141/13-22-034-01W3/00	71	2	High	-13.6	-13.7	-13.6	-10.0	5.9	
Kindersley Area									
101/13-20-030-14W3/00	86	8	High	-14.3	-14.3	-14.3	-5.4	9.4	
Prince Albert Area									
101/01-25-054-26W3/00	87								-13.0
101/12-04-058-19W3/00	88	1	Med	-12.1	-12.2	-12.0	-6.2	22.0	

Appendix G Winnipeg Formation DST and core wells, with assigned well number and calculated permeability values

UWI	Well #	DST #	Horner Match Conf	k DST log(m^2)	Sensit Low k log(m^2)	Sensit High k log(m^2)	Sen Low %	Sen High %	K Falloff test log(m^2)	Core eff kmax log(m^2)
Clean low gamma ray sand										
Estevan Area										
141/16-19-001-32W1/00	30									-14.0
101/01-06-002-04W2/00	1	5	Med	-14.6	-14.7	-14.5	-11.1	23.1		
111/14-06-006-06W2/00	2	2	High	-14.8	-14.9	-14.8	-21.1	11.9		
131/08-16-006-11W2/02	31									-14.3
111/16-20-006-11W2/00	32									-15.0
101/03-16-002-10W2/00	3	1	Med	-15.7	-15.8	-15.9	-17.7	21.7		
131/08-34-006-11W2/00	4	3	Med	-14.5	-14.6	-14.4	-15.0	27.5		
141/04-35-006-11W2/03	5	2	Med	-15.8	-15.9	-15.8	-13.6	10.0		-13.7
141/07-24-008-09W2/02	6	2	Med	-14.5	-14.5	-14.3	-6.3	66.7		
UWI	Well #	DST #	Horner Match Conf	k DST log(m^2)	Sensit Low k log(m^2)	Sensit High k log(m^2)	Sen Low %	Sen High %	K Falloff test log(m^2)	Core eff kmax log(m^2)
131/06-18-009-06W2/00	7	2	High	-14.0	-14.1	-14.0	-12.0	10.6		
121/06-20-006-13W2/00	8	1	Med	-18.1	-18.1	-17.0	-6.3	11.1		-14.8
131/02-32-008-10W2/00	9	8	High	-14.4	-14.5	-14.4	-18.2	12.5		
141/07-02-009-13W2/00	34									-13.9
141/07-28-010-10W2/02	10	1	High	-13.4	-13.4	-13.3	-12.3	22.8		
		5	High	-15.0	-15.0	-15.0	-3.7	10.0		
191/08-06-010-15W2/02	11	3	High	-14.7	-14.7	-14.6	-2.3	15.9		
132/07-02-010-09W2/00	35									-13.4
131/07-04-011-09W2/00	12	3	High	-12.7	-12.8	-12.6	-14.6	17.1		
101/03-27-011-09W2/00	33									-13.3
121/06-28-013-11W2/00	13	1	High	-14.0	-14.1	-14.0	-7.3	16.9		
131/01-33-014-12W2/00	36									-13.6
Average				-13.7						-13.7
Milestone Area										
101/16-26-013-27W2/00	14	2	Med	-12.3	-12.4	-12.2	-16.7	25.0		
Belle Plaine Area										
131/03-08-017-19W2/02	15	2	Med	-11.8	-12.1	-11.8	-39.3	21.3		
191/08-14-017-24W2/00	16	1	High	-12.5	-12.5	-12.4	-7.7	20.0	-12.3	
101/08-17-023-20W2/00	17	3	Med	-12.2	-12.2	-12.1	-10.2	25.7		
Average				-12.1					-12.3	

UWI	Well #	DST #	Horner Match Conf	k DST log(m²)	Sensit Low k log(m²)	Sensit High k log(m²)	Sen Low %	Sen High %	K Falloff test log(m²)	Core eff kmax log(m²)
Bengough Area										
101/12-33-005-23W2/00	18	6	Med	-13.4	-13.5	-13.4	-12.0	22.2		
133/03-06-005-21W2/00	19	3	Med	-13.5	-13.7	-12.7	-37.5	525.0		
		5	Med	-14.1	-14.1	-14.0	-5.0	5.6		
131/06-02-003-21W2/02	20	1	High	-14.2	-14.3	-14.2	-7.1	8.3		-13.1
121/08-06-007-15W2/05	37									-14.0
Average				-13.7						-13.3
Esterhazy Area										
121/01-14-017-30W1/00	38									-13.1
111/14-27-019-32W1/00	22	3	Med	-12.9	-13.0	-12.8	-17.8	23.3		
101/04-22-021-02W2/02	39									-12.9
101/04-10-022-32W1/00	23	2	Med	-12.1	-12.2	-12.0	-20.0	25.0		
Average				-12.3						-13.0
UWI	Well #	DST #	Horner Match Conf	k DST log(m²)	Sensit Low k log(m²)	Sensit High k log(m²)	Sen Low %	Sen High %	K Falloff test log(m²)	Core eff kmax log(m²)
Dirtier Higher Gamma Ray Sand										
Milestone Area										
141/03-11-010-16W2/00	24	1	High	-13.4	-13.5	-13.4	-7.9	16.00		-13.2
121/06-36-012-15W2/02	25	1	High	-13.3	-13.4	-13.3	-14.3	11.11		
111/06-24-012-26W2/00	26	2	Med	-12.6	-12.6	-12.5	-16.7	25.00		
101/08-02-012-27W2/00	27	4	Low	-12.6	-12.7	-12.4	-20.0	60.00		
Average				-12.8						-13.2
Bengough Area										
101/11-34-007-25W2/00	21	4	Med	-14.0	-14.1	-14.0	-7.7	20.0		
Belle Plaine Area										
131/03-08-017-19W2/02	15	1	Med	-12.9	-13.1	-12.8	-31.8	25.0		
Esterhazy Area										
121/03-20-017-30W1/00	28	4	Med	-12.1	-12.2	-12.1	-10.5	13.3		
121/10-14-020-33W1/00	40									-12.7
Other Areas										
101/08-36-016-06W2/00	29	1	Low	-12.1	-12.4	-12.0	-40.0	40.0		
101/02-05-061-24W2/00	41									-12.0

Appendix H Interlake Group DST and core wells, with assigned well number and calculated permeability values

UWI	Well #	DST #	Horner Match Conf	DST k log(m²)	Sensit Low k log(m²)	Sensit High k log(m²)	Sen Low %	Sen High %	Falloff Test k log(m²)	Core eff k-Max log(m²)
131/09-34-003-04W2/00	122									
101/09-05-003-28W2/00	96	5	Med	-13.0	-13.1	-12.9	-16.7	25.0		
101/02-04-004-11W2/00	90	5	Med	-13.9	-14.0	-13.8	-10.0	18.4		
101/03-26-004-20W2/00	95	6	High	-14.4	-14.4	-14.3	-7.7	9.1		
191/04-11-004-21W2/00	94	1	High	-12.7	-12.8	-12.6	-16.7	25.0		
111/03-01-004-25W2/00	97	8	High	-14.2	-14.2	-14.1	-10.0	12.5		
131/11-04-005-07W2/04	123									-14.8
101/15-05-005-07W2/00	124									-13.2
101/12-10-005-08W3/00	116	1	Med	-13.4	-13.3	-14.3	-20.0	36.4		
UWI	Well #	DST #	Horner Match Conf	DST k log(m²)	Sensit Low k log(m²)	Sensit High k log(m²)	Sen Low %	Sen High %	Falloff Test k log(m²)	Core eff k-Max log(m²)
101/11-34-007-25W2/00	98	2	Med	-13.5	-13.5	-13.3	-14.3	50.0		
101/14-19-008-32W1/00	125									-14.2
101/08-30-008-33W1/00	126									-13.7
111/03-27-008-13W2/00	91	3	Med	-11.5	-11.5	-11.4	-11.1	14.3		
131/06-32-008-16W2/00	127									-16.0
101/12-12-010-14W2/00	92	9	Med	-11.8	-11.9	-11.7	-16.7	25.0		
192/08-06-010-15W2/00	93	1	Med	-12.7	-12.8	-12.6	-25.0	25.0		
131/01-32-014-30W1/00	99	3	High	-14.4	-14.5	-14.4	-8.3	10.0		
141/08-20-014-31W1/00	100	1	High	-14.5	-12.6	-12.4	-11.1	23.1		
121/03-20-017-30W1/00	139								-12.6	
121/12-22-017-30W1/00	130								-13.0	
141/06-23-017-30W1/00	134								-13.2	
131/11-27-019-32W1/00	131								-13.1	
131/07-22-019-32W1/02	103	3	Med	-12.8						
131/10-22-019-32W1/02	104	3	Med	-13.7						
111/14-27-019-32W1/00	105	1	Med	-13.1	-13.1	-13.0	-14.3	20.0	-12.7	
191/05-33-019-32W1/00	132								-13.2	
142/04-33-019-32W1/00	135								-13.1	
111/01-26-020-33W1/00	106	3	Med	-12.1	-12.2	-12.0	-13.0	33.3	-12.8	
		4	High	-13.7	-13.7	-13.6	-12.5	16.7		
111/11-23-020-33W1/00	136								-13.4	
121/11-26-020-33W1/00	107	3	High	-13.5	-13.5	-13.4	-11.1	14.3	-12.9	
		4	High	-13.7	-13.8	-13.7	-15.0	13.3		

UWI	Well #	DST #	Horner Match Conf	DST k log(m²)	Sensit Low k log(m²)	Sensit High k log(m²)	Sen Low %	Sen High %	Falloff Test k log(m²)	Core eff k-Max log(m²)
141/13-26-020-33W1/00	108	3	High	-12.6	-12.7	-12.6	-20.0	14.3	-12.6	
		4	High	-13.7	-13.7	-13.6	-8.3	15.8		
121/16-26-020-33W1/00	109	3	High	-13.4	-13.4	-13.4	-10.0	8.0	-13.0	
		4	High	-13.4	-13.5	-13.4	-10.0	12.5		
121/10-14-020-33W1/00	133								-12.9	
101/08-17-023-20W2/00	112	2	Med	-13.7	-13.7	-13.7	-7.7	13.2		
101/01-32-027-11W3/00	117	7	Med	-14.0	-14.1	-14.0	-7.9	16.7		
121/03-24-028-08W2/00	110	4	Med	-12.5						
101/13-22-030-16W2/00	113	2	Med	-13.2	-13.2	-13.1	-10.0	12.5		
101/13-20-030-14W3/00	118	6	Med	-15.0	-15.1	-15.0	-16.7	11.1		
101/09-21-033-15W3/00	119	2	Med	-14.1	-14.2	-14.1	-5.6	21.4		
191/01-27-035-09W2/00	111	1	Med	-12.2	-12.3	-12.1	-16.7	25.0		
121/03-21-035-08W3/00	121	8	Med	-12.8	-13.0	12.6	-46.7	60.0		
101/07-02-038-01W3/00	120	2	Med	-14.8	-14.8	-14.7	-6.7	7.7		
UWI	Well #	DST #	Horner Match Conf	DST k log(m²)	Sensit Low k log(m²)	Sensit High k log(m²)	Sen Low %	Sen High %	Falloff Test k log(m²)	Core eff k-Max log(m²)
101/16-09-043-21W2/00	115	2	Med	-14.1	-14.2	-14.0	-12.5	16.7		
101/01-32-047-19W2/00	128									-13.9

Appendix I Cory and Vanscoy mine simulations with RMSE values

Sim #	T (m²/s)	S	13-07 RMSE (kPa)	10-12 RMSE (kPa)	08-13 RMSE (kPa)	03-21 RMSE (kPa)	Weighted Average RMSE (kPa)	Description
1	9.81×10^{-4}	1.033×10^{-4}	1038.2	662.9	550.2	829.8	710.7	Clean and dirty sand DST k, Hall 1953 S
2	9.81×10^{-4}	2.72×10^{-4}	933.2	505.5	529.1	840.5	662.4	Clean and dirty sand DST k, low end S fissured rocks
3	9.81×10^{-4}	5.72×10^{-3}	760.9	256.0	575.0	871.7	626.4	Clean and dirty sand DST k, high end S fissured rocks
10	9.81×10^{-4}	9.94×10^{-5}	791.9	277.6	568.8	860.3	629.9	Clean and dirty sand DST k, sonic est S
38	1.23×10^{-3}	1.03×10^{-4}	838.2	397.2	502.9	858.2	621.0	Inferred k, Hall 1953 S
39	1.23×10^{-3}	2.72×10^{-4}	781.7	290.9	516.5	869.5	605.6	Inferred k, low end S fissured rocks
40	1.23×10^{-3}	5.72×10^{-3}	732.5	287.8	614.4	902.0	650.2	Inferred k, high end S fissured rocks
41	1.23×10^{-3}	9.94×10^{-5}	840.9	402.0	502.7	857.7	621.9	Inferred k, sonic est S
46	1.43×10^{-3}	1.03×10^{-4}	758.9	261.6	514.3	879.6	598.4	Inferred k, Hall 1953 S
47	1.43×10^{-3}	2.72×10^{-4}	731.4	207.9	540.8	890.7	601.5	Inferred k, low end S fissured rocks
48	1.43×10^{-3}	5.72×10^{-3}	743.8	346.7	561.2	922.1	681.8	Inferred k, high end S fissured rocks
49	1.43×10^{-3}	9.94×10^{-5}	760.3	264.78	513.34	879.2	598.5	Inferred k, sonic est S
50	1.52×10^{-3}	1.03×10^{-4}	740.8	226.1	524.1	887.4	596.7	Inferred k, Hall 1953 S
51	1.52×10^{-3}	2.72×10^{-4}	722.4	197.4	553.4	898.2	606.1	Inferred k, low end S fissured rocks
52	1.52×10^{-3}	5.72×10^{-3}	751.8	369.9	665.2	929.0	694.4	Inferred k, high end S fissured rocks
53	1.52×10^{-3}	9.94×10^{-5}	781.9	228.37	523.1	886.9	604.3	Inferred k, sonic est S
4	1.57×10^{-3}	1.03×10^{-4}	733.3	211.0	530.12	891.4	597.12	Clean sand DST k, Hall 1953 S
5	1.57×10^{-3}	2.72×10^{-4}	719.0	196.4	560.6	902.2	609.6	Clean sand DST k, low end S fissured rocks
6	1.57×10^{-3}	5.72×10^{-3}	756.6	383.2	672.6	932.6	701.4	Clean sand DST k, high end S fissured rocks
11	1.57×10^{-3}	9.94×10^{-5}	734.2	212.9	529.1	891.0	596.9	Clean sand DST k, sonic est S
7	5.13×10^{-4}	1.03×10^{-4}	2229.3	1859.4	1238.3	857.34	1433.4	Falloff test k, Hall 1953 S
8	5.13×10^{-4}	2.72×10^{-4}	1964.2	1548.4	1085.8	846.2	1266.2	Falloff test k, low end S fissured rocks
9	5.13×10^{-4}	5.72×10^{-3}	1348.6	821.3	796.3	824.4	910.0	Falloff test k, high end S fissured rocks
12	5.13×10^{-4}	9.94×10^{-5}	2240.5	1872.5	1244.9	857.9	1440.5	Falloff test k, sonic est S
13	1.64×10^{-3}	1.03×10^{-4}	723.9	193.1	541.2	898.1	599.8	Inferred k, Hall 1953 S
14	1.64×10^{-3}	2.72×10^{-4}	716.6	200.9	573.0	908.6	617.0	Inferred k, low end S fissured rocks
15	1.64×10^{-3}	5.72×10^{-3}	765.3	402.4	684.7	938.4	712.5	Inferred k, high end S fissured rocks
16	1.64×10^{-3}	9.94×10^{-5}	724.5	194.0	540.0	897.6	599.4	Inferred k, sonic est S
17	2.05×10^{-3}	1.03×10^{-4}	718.6	219.1	602.6	927.5	637.9	Inferred k, Hall 1953 S
18	2.05×10^{-3}	2.72×10^{-4}	311.1	282.3	635.8	936.8	586.4	Inferred k, low end S fissured rocks
19	2.05×10^{-3}	5.72×10^{-3}	813.5	492.0	739.5	963.3	764.8	Inferred k, high end S fissured rocks
20	2.05×10^{-3}	9.94×10^{-5}	718.2	216.9	601.3	927.1	636.8	Inferred k, sonic est S
21	2.46×10^{-3}	1.03×10^{-4}	745.5	304.8	656.2	949.2	684.4	Inferred k, Hall 1953 S
22	2.46×10^{-3}	2.72×10^{-4}	768.2	368.8	687.1	957.6	713.7	Inferred k, low end S fissured rocks
Sim #	T (m²/s)	S	13-07 RMSE (kPa)	10-12 RMSE (kPa)	08-13 RMSE (kPa)	03-21 RMSE (kPa)	Weighted Average RMSE (kPa)	Description
23	2.46×10^{-3}	5.72×10^{-3}	915.3	589.5	787.3	960.5	819.5	Inferred k, high end S fissured rocks
24	2.46×10^{-3}	9.94×10^{-5}	744.7	302.3	655.0	948.9	683.3	Inferred k, sonic est S
33	2.66×10^{-3}	1.03×10^{-4}	762.2	344.7	679.2	958.1	705.7	Inferred k, Hall 1953 S
34	2.66×10^{-3}	2.72×10^{-4}	786.7	405.8	708.8	966.0	734.1	Inferred k, low end S fissured rocks
35	2.66×10^{-3}	5.72×10^{-3}	875.0	583.1	797.1	988.1	821.1	Inferred k, high end S fissured rocks
36	2.66×10^{-3}	9.94×10^{-5}	761.3	342.23	678.1	957.8	704.6	Inferred k, sonic est S

25	2.87×10^{-3}	1.03×10^{-4}	779.2	380.8	699.9	965.9	725.2	Inferred k, Hall 1953 S
26	2.87×10^{-3}	2.71×10^{-4}	804.5	438.7	728.0	973.3	752.6	Inferred k, low end S fissured rocks
27	2.87×10^{-3}	5.72×10^{-3}	891.8	605.9	811.8	994.4	835.7	Inferred k, high end S fissured rocks
28	2.87×10^{-3}	9.94×10^{-5}	778.3	378.5	698.8	965.6	724.1	Inferred k, sonic est S
29	3.28×10^{-3}	1.03×10^{-4}	811.8	442.2	735.1	979.0	759.0	Inferred k, Hall 1953 S
30	3.28×10^{-3}	2.72×10^{-4}	837.3	494.0	760.7	985.7	784.3	Inferred k, low end S fissured rocks
31	3.28×10^{-3}	5.72×10^{-3}	680.9	643.7	836.4	1004.7	814.4	Inferred k, high end S fissured rocks
32	3.28×10^{-3}	9.94×10^{-5}	810.8	440.1	734.1	978.7	758.0	Inferred k, sonic est S

Appendix J Allan, Colonsay and Patience Lake mine simulations with RMSE values

Sim	T (m²/s)	S	13-22 RMSE (kPa)	16-28 RMSE (kPa)	14-16 RMSE (kPa)	02-21 RMSE (kPa)	Weighted Average RMSE (kPa)	Description
1	6.78×10^{-4}	6.94×10^{-4}	1606.6	1779.8	661.3	1326.3	1366.2	Dirty sand DST k, Hall 1953 est S
2	6.78×10^{-4}	3.38×10^{-4}	1711.7	1911.8	757.5	1404.5	1457.3	Dirty sand DST k, high end S for fissured rocks
3	6.78×10^{-4}	7.10×10^{-3}	1332.0	1432.8	471.1	1123.7	1135.0	Dirty sand DST k, high end S for fissured rocks
10	6.78×10^{-4}	1.17×10^{-4}	1879.6	2123.8	944.6	1531.4	1607.6	Dirty sand DST k, sonic est S
4	3.19×10^{-3}	6.94×10^{-4}	267.0	412.1	552.0	267.9	307.0	Clean sand DST k, Hall 1953 est S
5	3.19×10^{-3}	3.38×10^{-4}	287.5	440.9	522.4	280.5	318.5	Clean sand DST k, low end S for
6	3.19×10^{-3}	7.10×10^{-3}	212.8	331.3	629.1	234.8	276.2	Clean sand DST k, high end S for fissure rocks
11	3.19×10^{-3}	1.17×10^{-4}	320.7	488.2	477.4	301.8	338.1	Clean sand DST k, sonic est S
7	1.42×10^{-3}	6.94×10^{-4}	871.6	874.4	300.3	609.7	668.2	Falloff test k, Hall 1953 est S
8	1.42×10^{-3}	3.38×10^{-4}	742.0	940.6	276.1	652.3	658.0	Falloff test k, low end S for fissured rocks
9	1.42×10^{-3}	7.10×10^{-3}	551.3	695.7	399.9	514.8	525.5	Falloff test k, high end S for fissured rocks
12	1.42×10^{-3}	1.17×10^{-4}	823.0	1047.2	278.6	636.1	679.0	Falloff test k, sonic est S
13	3.78×10^{-3}	6.94×10^{-4}	189.6	345.7	609.5	223.2	262.3	Falloff test k, Hall 1953 est S
14	3.78×10^{-3}	3.38×10^{-4}	204.5	368.2	578.2	231.1	269.1	Falloff test k, low end S for fissured rocks
15	3.78×10^{-3}	7.10×10^{-3}	155.1	282.6	670.6	203.0	243.7	Falloff test k, high end S for fissured rocks
16	3.78×10^{-3}	1.17×10^{-4}	229.3	405.3	535.5	245.5	282.0	Falloff test k, sonic est S
17	4.41×10^{-3}	6.94×10^{-4}	153.4	303.4	639.4	204.7	242.3	Falloff test k, Hall 1953 est S
18	4.41×10^{-3}	3.38×10^{-4}	163.2	321.4	616.7	218.5	251.5	Falloff test k, low end S for fissured rocks
19	4.41×10^{-3}	7.10×10^{-3}	133.9	253.1	698.7	184.2	228.3	Falloff test k, high end S for fissured rocks
20	4.41×10^{-3}	1.17×10^{-4}	181.2	351.4	582.7	211.2	251.1	Falloff test k, sonic est S
21	5.03×10^{-3}	6.94×10^{-4}	130.6	273.4	666.9	179.2	222.7	Falloff test k, Hall 1953 est S
Sim	T (m²/s)	S	13-22 RMSE (kPa)	16-28 RMSE (kPa)	14-16 RMSE (kPa)	02-21 RMSE (kPa)	Weighted Average RMSE (kPa)	Description
22	5.03×10^{-3}	3.38×10^{-4}	136.3	287.9	646.6	183.3	225.5	Falloff test k, low end S for fissured rocks
23	5.03×10^{-3}	7.10×10^{-3}	124.0	233.1	720.3	186.4	227.6	Falloff test k, high end S for fissured rocks
24	5.03×10^{-3}	1.17×10^{-4}	148.4	312.3	616.4	188.6	230.3	Falloff test k, sonic est S
25	6.29×10^{-3}	6.94×10^{-4}	111.7	470.8	706.6	164.7	227.3	Falloff test k, Hall 1953 est S
26	6.29×10^{-3}	3.38×10^{-4}	110.7	244.7	689.8	163.7	209.1	Falloff test k, low end S for fissured rocks
27	6.29×10^{-3}	7.10×10^{-3}	122.0	209.7	751.3	168.4	18.7	Falloff test k, high end S for fissured rocks
28	6.29×10^{-3}	1.17×10^{-4}	112.9	261.0	665.5	163.9	208.4	Falloff test k, sonic est S
41	6.92×10^{-3}	1.17×10^{-4}	105.6	244.0	684.0	157.8	203.8	Interpolated S, sonic est S
29	7.55×10^{-3}	6.94×10^{-4}	111.4	214.1	734.0	159.5	209.4	Falloff test k, Hall 1953 est S
30	7.55×10^{-3}	3.38×10^{-4}	107.0	220.0	735.8	156.9	207.4	Falloff test k, low end S for fissured rocks
31	7.55×10^{-3}	7.10×10^{-3}	129.0	198.2	772.5	167.2	221.4	Falloff test k, high end S for fissured rocks

32	7.55×10^{-3}	$1.17^*\times10^{-4}$	102.8	230.7	699.6	154.	201.7	Interpolated S, sonic est S
42	8.18×10^{-3}	1.17×10^{-4}	103.1	220.4	712.9	152.2	201.7	Interpolated S, sonic est S
44	8.24×10^{-3}	6.94×10^{-4}	114.7	206.6	745.7	158.8	210.7	Falloff test k, Hall 1953 est S
45	8.24×10^{-3}	3.38×10^{-4}	111.0	211.0	732.6	155.9	206.9	Falloff test k, low end S for fissured rocks
46	8.24×10^{-3}	7.10×10^{-3}	133.8	194.5	781.6	167.7	223.7	Falloff test k, high end S for fissured rocks
43	8.24×10^{-3}	1.17×10^{-4}	103.2	219.5	714.2	152.1	201.4	Interpolated S, sonic est S
33	8.81×10^{-3}	6.94×10^{-4}	118.1	201.8	754.0	159.0	212.2	Falloff test k, Hall 1953 est S
34	8.81×10^{-3}	3.38×10^{-4}	112.3	205.3	741.7	155.7	207.8	Falloff test k, low end S for fissured rocks
35	8.81×10^{-3}	7.10×10^{-3}	204.7	192.4	788.0	168.5	244.2	Falloff test k, high end S for fissured rocks
36	8.81×10^{-3}	1.17×10^{-4}	105.4	212.3	724.5	151.4	202.2	Interpolated S, sonic est S
37	1.01×10^{-2}	6.94×10^{-4}	126.4	194.6	769.4	160.5	216.4	Falloff test k, Hall 1953 est S
38	1.01×10^{-2}	3.38×10^{-4}	120.3	196.5	758.6	156.9	211.8	Falloff test k, low end S for fissured rocks
39	1.01×10^{-2}	7.10×10^{-3}	146.0	189.6	799.8	170.7	230.3	Falloff test k, high end S for fissured rocks
40	1.01×10^{-2}	1.17×10^{-4}	112.2	200.8	743.7	151.9	205.6	Interpolated S, sonic est S

Appendix K) Lanigan mine simulations with RMSE values

Sim	T (m^2/s)	S	01-20 RMSE (kPa)	02-28 RMSE (kPa)	Description
4	1.49×10^{-4}	5.78×10^{-4}	7178.2	7998.9	Low end dirty sand k, Hall 1953 calc S
5	1.49×10^{-4}	2.83×10^{-4}	7652.3	7739.9	Low end dirty sand k, low end S fissured rocks
6	1.49×10^{-4}	5.95×10^{-3}	5946.5	6734.3	Low end dirty sand k, high end S fissured rocks
14	1.49×10^{-4}	9.90×10^{-5}	8178.2	9895.0	Low end dirty sand k, sonic calc S
10	6.96×10^{-4}	5.78×10^{-4}	1215.1	1635.2	Falloff test k, Hall 1953 calc S
11	6.96×10^{-4}	2.83×10^{-4}	1300.2	1721.3	Falloff test k, low end S fissured rocks
12	6.96×10^{-4}	5.95×10^{-3}	944.0	1377.1	Falloff test k, low end S fissured rocks
16	6.96×10^{-4}	9.90×10^{-5}	1416.5	1845.0	Falloff test k, sonic calc S
1	1.53×10^{-3}	5.78×10^{-4}	409.8	681.6	Clean and dirty sand DST k, Hall 1953 calc S
2	1.53×10^{-3}	2.83×10^{-4}	432.4	712.9	Clean and dirty sand DST k, low end S fissured rocks
Sim	T (m^2/s)	S	01-20 RMSE (kPa)	02-28 RMSE (kPa)	Description
3	1.53×10^{-3}	5.95×10^{-3}	362.0	589.4	Clean and dirty sand DST k, high end S fissured rocks
13	1.53×10^{-3}	9.90×10^{-5}	470.8	572.4	Clean and dirty sand DST k, sonic calc S
33	1.64×10^{-3}	5.78×10^{-4}	386.9	631.3	Interpolated k, Hall 1953 calc S
34	1.64×10^{-3}	2.83×10^{-4}	403.7	659.2	Interpolated k, low end S fissured rocks
35	1.64×10^{-3}	5.95×10^{-3}	358.5	550.7	Interpolated k, high end S fissured rocks
36	1.64×10^{-3}	9.90×10^{-5}	433.9	721.8	Interpolated k, sonic calc S
37	1.91×10^{-3}	5.78×10^{-4}	366.7	542.6	Interpolated k, Hall 1953 calc S
38	1.91×10^{-3}	2.83×10^{-4}	372.3	563.3	Interpolated k, low end S fissured rocks
39	1.91×10^{-3}	5.95×10^{-3}	370.9	484.9	Interpolated k, high end S fissured rocks
40	1.91×10^{-3}	9.90×10^{-5}	386.0	596.1	Interpolated k, sonic calc S
41	2.02×10^{-3}	5.78×10^{-4}	367.4	516.4	Interpolated k, Hall 1953 calc S
42	2.02×10^{-3}	2.83×10^{-4}	369.6	534.8	Interpolated k, low end S fissured rocks
43	2.02×10^{-3}	5.95×10^{-3}	380.1	466.3	Interpolated k, high end S fissured rocks
44	2.02×10^{-3}	9.90×10^{-5}	378.0	564.0	Interpolated k, sonic calc S
17	2.19×10^{-3}	5.78×10^{-4}	373.6	484.9	Interpolated k, Hall 1953 calc S
18	2.19×10^{-3}	2.83×10^{-4}	372.3	501.9	Interpolated k, low end S fissured rocks
19	2.19×10^{-3}	5.95×10^{-3}	395.5	445.1	Interpolated k, high end S fissured rocks
20	2.19×10^{-3}	9.90×10^{-5}	394.4	524.6	Interpolated k, sonic calc S
29	2.46×10^{-3}	5.78×10^{-4}	425.5	471.1	Interpolated k, Hall 1953 calc S
30	2.46×10^{-3}	2.83×10^{-4}	386.7	456.5	Interpolated k, low end S fissured rocks
31	2.46×10^{-3}	5.95×10^{-3}	422.9	441.0	Interpolated k, high end S fissured rocks
32	2.46×10^{-3}	9.90×10^{-5}	381.4	474.5	Interpolated k, sonic calc S
25	2.73×10^{-3}	5.78×10^{-4}	414.6	421.8	Interpolated k, Hall 1953 calc S
26	2.73×10^{-3}	2.83×10^{-4}	406.7	429.0	Interpolated k, low end S fissured rocks
27	2.73×10^{-3}	5.95×10^{-3}	450.7	405.8	Interpolated k, high end S fissured rocks
28	2.73×10^{-3}	9.90×10^{-5}	397.5	441.0	Interpolated k, sonic calc S
21	3.28×10^{-3}	5.78×10^{-4}	458.4	421.3	Interpolated k, Hall 1953 calc S
22	3.28×10^{-3}	2.83×10^{-4}	448.9	399.4	Interpolated k, low end S fissured rocks
23	3.28×10^{-3}	5.95×10^{-3}	493.5	395.9	Interpolated k, high end S fissured rocks
24	3.28×10^{-3}	9.90×10^{-5}	436.5	405.3	Interpolated k, sonic calc S
7	5.82×10^{-3}	5.78×10^{-4}	585.6	407.3	
8	5.82×10^{-3}	2.83×10^{-4}	578.2	403.5	High end k dirty sand DST, low end S fissured rocks
9	5.82×10^{-3}	5.95×10^{-3}	610.9	421.3	High end k dirty sand DST, high end S fissured rocks
15	5.82×10^{-3}	9.90×10^{-5}	567.4	398.3	High end k dirty sand DST, sonic calc S

Appendix L) Esterhazy mine simulations with RMSE values

Sim	T (m²/s)	S	Weighted Avg RMSE (kPa)	Description
1	1.35×10^{-4}	1.01×10^{-4}	5742.4	DST k, Hall 1953 S
2	1.35×10^{-4}	3.44×10^{-4}	4125.2	DST k, low end S for fissure rocks
3	1.35×10^{-4}	7.23×10^{-3}	2367.1	DST k, high end S for fissured rocks
4	1.35×10^{-4}	3.73×10^{-5}	7583.2	DST k, sonic est S
25	5.38×10^{-4}	1.01×10^{-4}	944.2	History-matched k, Hall 1953 S
26	5.38×10^{-4}	3.44×10^{-4}	1114.1	History-matched k, low end S for fissured rocks
27	5.38×10^{-4}	7.23×10^{-3}	1542.0	History-matched k, high end S for fissured rocks
28	5.38×10^{-4}	3.73×10^{-5}	1119.7	History-matched k, sonic est S
33	6.99×10^{-4}	1.01×10^{-4}	946.7	History-matched k, Hall 1953 S
34	6.99×10^{-4}	3.44×10^{-4}	1202.1	History-matched k, low end S for fissured rocks
35	6.99×10^{-4}	7.23×10^{-3}	1704.0	History-matched k, high end S for fissured rocks
36	6.99×10^{-4}	3.73×10^{-5}	841.4	History-matched k, sonic est S
41	7.53×10^{-4}	1.01×10^{-4}	975.5	History-matched k, Hall 1953 S
42	7.53×10^{-4}	3.44×10^{-4}	1239.3	History-matched k, low end S for fissured rocks
43	7.53×10^{-4}	7.23×10^{-3}	1748.2	History-matched k, high end S for fissured rocks
Sim	T (m²/s)	S	Weighted Avg RMSE (kPa)	Description
44	7.53×10^{-4}	3.73×10^{-5}	826.8	History-matched k, sonic est S
45	7.80×10^{-4}	1.01×10^{-4}	991.3	History-matched k, Hall 1953 S
46	7.80×10^{-4}	3.44×10^{-4}	1259.9	History-matched k, low end S for fissured rocks
47	7.80×10^{-4}	7.23×10^{-3}	1768.7	History-matched k, high end S for fissured rocks
48	7.80×10^{-4}	3.73×10^{-5}	828.6	History-matched k, sonic est S
29	8.07×10^{-4}	1.01×10^{-4}	1008.6	History-matched k, Hall 1953 S
30	8.07×10^{-4}	3.44×10^{-4}	1282.2	History-matched k, low end S for fissured rocks
31	8.07×10^{-4}	7.23×10^{-3}	1788.2	History-matched k, high end S for fissured rocks
32	8.07×10^{-4}	3.73×10^{-5}	835.1	History-matched k, sonic est S
37	9.14×10^{-4}	1.01×10^{-4}	1082.9	History-matched k, Hall 1953 S
38	9.14×10^{-4}	3.44×10^{-4}	1368.2	History-matched k, low end S for fissured rocks
39	9.14×10^{-4}	7.23×10^{-3}	1857.5	History-matched k, high end S for fissured rocks
40	9.14×10^{-4}	3.73×10^{-5}	887.1	History-matched k, sonic est S
5	9.82×10^{-4}	1.01×10^{-4}	1136.3	Core k, Hall 1953 S
6	9.82×10^{-4}	3.44×10^{-4}	1418.7	Core k, low end S for fissured rocks
7	9.82×10^{-4}	7.23×10^{-3}	1895.2	Core k, high end S for fissured rocks
8	9.82×10^{-4}	3.73×10^{-5}	930.6	Core k, sonic est S
21	1.08×10^{-3}	1.01×10^{-4}	1209.7	History-matched k, Hall 1953 S
22	1.08×10^{-3}	3.44×10^{-4}	1482.6	History-matched k, low end S for fissured rocks
23	1.08×10^{-3}	7.23×10^{-3}	1940.1	History-matched k, high end S for fissured rocks
24	1.08×10^{-3}	3.73×10^{-5}	995.8	History-matched k, sonic est S
17	1.18×10^{-3}	1.01×10^{-4}	1289.2	History-matched k, Hall 1953 S
18	1.18×10^{-3}	3.44×10^{-4}	1557.0	History-matched k, low end S for fissured rocks
19	1.18×10^{-3}	7.23×10^{-3}	1985.0	History-matched k, high end S for fissured rocks
20	1.18×10^{-3}	3.73×10^{-5}	1079.8	History-matched k, sonic est S
13	1.34×10^{-3}	1.01×10^{-4}	1393.4	History-matched k, Hall 1953 S
14	1.34×10^{-3}	3.44×10^{-4}	1634.2	History-matched k, low end S for fissured rocks
15	1.34×10^{-3}	7.23×10^{-3}	2040.1	History-matched k, high end S for fissured rocks
16	1.34×10^{-3}	3.73×10^{-5}	1197.3	History-matched k, sonic est S
9	1.61×10^{-3}	1.01×10^{-4}	1536.4	History-matched k, Hall 1953 S
10	1.61×10^{-3}	3.44×10^{-4}	1747.5	History-matched k, low end S for fissured rocks
11	1.61×10^{-3}	7.23×10^{-3}	2110.1	History-matched k, high end S for fissured rocks
12	1.61×10^{-3}	3.73×10^{-5}	1361.4	History-matched k, sonic est S